Gas Condensate Flow Behavior and Sampling

by

Øivind Fevang

A Dissertation for the Partial Fulfillment
of Requirements for the
Degree of Doktor Ingeniør

Division of Petroleum Engineering
and Applied Geophysics
The Norwegian Institute of Technology
University of Trondheim

October 1995

To my father and mother
who encouraged me to start this study

Acknowledgement

I wish to express my sincerest thanks to my advisor Curtis Whitson for excellent guidance and encouragement through many fruitful discussions. I am also indebted to Mike J. Fetkovich for the technology he has provided me (and the industry) through his invaluable publications, discussions, and lectures in gas technology, well performance, and general reservoir engineering. Sincere thanks goes to Michael Golan for many useful discussions, and the suggestions he made during the final stages of the thesis. I would also like to thank Andreas Haldoupis, Lars Høier, and my other fellow students at the institute for positive feedback, and many interesting discussions.

I would like to thank Professor Jan Reffstrup from the Technical University of Denmark, Professor Ole Torsæter from University of Trondheim, and Dr. Aaron Zick from Zick Technologies for serving in my graduate committee.

The study was financed by The Norwegian Institute of Technology Scholarship Fund. Support from Arnfinn and Lise Heies Fund, and The Norwegian Institute of Technology Travel Fund made it possible to participate in several international conferences.

Last, but not least, I am indebted to my wife, Tove, for her patience and support during the course of this work.

Preface

This dissertation summarizes and concludes my dr.ing research work. The main objective of this research was to develop improved methods for treating gas condensate reservoir and well behavior.

Chapters 1 and 2 discuss reservoir fluid flow behavior in gas condensate reservoirs. This work has lead to the development of a new and apparently accurate method for modeling gas condensate well deliverability. Furthermore, a new laboratory procedure has been designed to obtain relative permeability data needed specifically for treating reservoir well deliverability.

I have chosen to include a general discussion on gas reservoirs in Chapter 1. The topics that are summarized here reflect some of my "along-the-way" research work -- work that paved the way towards my understanding of the issues involved, and setting the stage for the development of measures needed to treat some rather complex problems in gas condensate reservoirs. I hope that including this background material will help convey the message that engineering of gas condensate reservoirs is merely an extension of traditional "dry" gas reservoir engineering.

Before starting my work on the three specific gas condensate topics covered in this thesis, I had the opportunity to work with my advisor on several other research projects in the more general field of gas and gas condensate reservoir engineering. Some of the more interesting were:

- *Rate-Time-Superposition.*
  Development of the theory and a Fortran program for analyzing the production performance of wells producing from low-permeability, layered no-crossflow gas reservoirs.

- *Cumulative Effective Compressibility in Gas-Water Systems.*
  Development of the methods and a spreadsheet program for computing gas-water PVT properties and cumulative effective compressibilities required for proper treatment of water expansion and water influx terms found in the Fetkovich material balance for high-pressure gas reservoirs.

- *EOS Fluid Characterizations of Gas Condensates.*
  Analysis of several gas condensate reservoir fluids from around the world (North Sea, Pakistan, Philippines, U.S.A., and Middle East). These studies included detailed data integrity checks, EOS predictions with different

methods, and tedious EOS tuning to match the experimental data.

- *Compositional Reservoir Simulation Studies*.
  Use of several compositional and black-oil reservoir simulators (Intera's ECL100 and ECL300, and RSRC's MORE-EOS and MORE-BlackOil) for studying compositionally-sensitive reservoir processes: miscible and immiscible gas injection studies; single-well and full-field performance studies of gas condensate reservoirs.

- *Production Monitoring of Gas Condensate Well Behavior*.
  Collection and analysis of daily and monthly production data on several gas condensate reservoirs, and interpretation of multirate well test data.

Looking back on this considerable work (related but not included in my dissertation), I realize that it was necessary to have a clear overall picture of gas (condensate) reservoir and well behavior before having the necessary insight to solve the specific problems that are presented in my final thesis.

Most of the results presented in Chapters 1 and 2 are presented in two SPE papers:

- Fevang, Ø. and Whitson, C.H.: "Modelling Gas Condensate Well Deliverability," paper SPE 30714, presented at the 1995 SPE Annual Technical Conference & Exhibition, Oct. 22-25 (1995)

- Fevang, Ø. and Whitson, C.H.: "Accurate Insitu Compositions in Petroleum Reservoirs," Paper SPE 28829 presented at the 1994 EUROPEC meeting (Oct. 25-27) (1994)

The papers are included as appendices to the thesis.

The first paper (SPE 30714) is discussed in detail in Chapters 1 and 2 of the thesis. The second paper (SPE 28829) describes an experimental procedure for determining accurate estimates of original insitu oil and gas compositions. The results of this second paper are not covered separately in the text of the thesis because I feel that the paper stands alone and is sufficiently complete (with a level of detail that will preclude its publication in any SPE journal).

Trondheim, October 1995
Øivind Fevang

Summary

The three main issues addressed in my research work, as presented in this thesis, are:

- Gas Condensate Well Deliverability
- Gas Condensate Relative Permeability
- Representivity of Gas Condensate Samples

Each subject is summarized below.

Gas Condensate Well Deliverability
Chapter 1 discusses a method for modeling well deliverability of gas condensate wells. A new method is proposed for practical and accurate deliverability modeling. Well deliverability is calculated using a modified form of the classical Evinger-Muskat[1] pseudopressure approach, originally proposed for solution gas drive oil wells. The reservoir information needed to apply the proposed method includes the producing *gas-oil ratio* (GOR), PVT properties (black-oil or an EOS model), and gas-oil relative permeabilities. The proposed method is successfully tested by detailed numerical simulations using radial, vertical fracture, and horizontal well geometries.

It is shown that single-well simulations can be reproduced almost exactly by the proposed simple rate equation using an appropriate pseudopressure function. The key issue is knowing the producing GOR accurately. Effects related to near-wellbore damage, vertical fracture, or flow improvement due to horizontal well trajectory are incorporated in the rate equation by a constant skin term.

The effect of gas-oil relative permeability on well deliverability is studied. The conclusion of this work is that well deliverability impairment due to condensate "blockage" depends mainly on the relative permeabilities within a narrow and well-defined range (usually $1<k_{rg}/k_{ro}<50$). This normally corresponds to gas relative permeabilities ranging from 0.05 to 0.3. Relative permeabilities at low oil saturations ($k_{rg}>0.3$) only have a second-order effect on deliverability for rich gas condensates.

A key observation and conclusion from this study is that critical oil saturation has *no* direct effect on well deliverability. It is also shown that the effect of *gas-oil interfacial tension* (IFT) on relative permeability has little or no effect on gas condensate well performance (e.g. length of plateau production). These observations are radically different from traditional thinking.

The most important application of the proposed pseudopressure method is to provide a simple method for calculating *bottomhole flowing pressure* (BHFP) in coarse-grid models. It is shown that the proposed pseudopressure method is readily calculated for each well grid cell, based on grid cell pressure and producing GOR only. Consequently, the cumbersome procedure of local grid refinement near wells is not necessary, and relatively large well grid cells can be used, while still providing an accurate description of well deliverability.

Gas Condensate Relative Permeability

Chapter 2 presents an experimental procedure for measuring relative permeabilities, designed specifically for modeling well deliverability. The proposed laboratory procedure is based on the simple but relatively accurate model of three distinct flow regions surrounding a gas condensate well. In particular, the procedure is geared to providing data to compute the large effect of condensate blockage in the near-wellbore Region 1.

The proposed experimental procedure for measuring relative permeabilities uses a steady-sate method under conditions that mimic flow in the reservoir during depletion. The fundamental relationship $k_{rg}=f(k_{rg}/k_{ro})$ is established by flowing different gas-oil mixtures through the core. The different mixtures are obtained using equilibrium gas taken from stages of a *constant volume depletion* (CVD) experiment. The gas is flowed through a choke or a backpressure regulator before it enters the core, reducing the flowing pressure to a relatively low value (as would be expected in the near-wellbore region when pressure constraints force a well on decline).

Both reservoir fluid and laboratory-mixed synthetic gas condensates can be used to perform the relative permeability measurements. It is shown that using actual reservoir fluid has the added advantage of eliminating uncertainties in viscosities when calculating relative permeabilities from the steady-state flow rates and pressure drops.

It is shown that saturation measurements are not needed for each steady-state experiment. Accordingly, it is suggested to simplify (reduced costs) by measuring the oil saturation for only one steady-state experiment. This additional saturation data helps to convert the function $k_{rg} = f(k_{rg}/k_{ro})$ to a saturation-dependent relation that is a needed as input to a reservoir simulator. It is recommend to measure saturations for the highest k_{rg}/k_{ro} ratio, mainly because this data (together with k_{rg} measurements at immobile oil saturations) provide the necessary $k_{rg}(S_o)$ information for the outer Region 2 where only gas is flowing.

A novel procedure is proposed for measuring oil saturation following a steady-state flow test. Equilibrium gas (injected at an elevated pressure) is used to displace the

gas/oil mixture in the core into a receiving container. The receiving container is disconnected from the core and brought to the pressure conditions that existed in the core during the steady-state experiment. The oil volume is measured, where it is easily shown that this volume corresponds to the average oil saturation in the core multiplied by the pore volume.

Representivity of Gas Condensate Samples (Appendix B)
This paper describes experimental procedures for determining accurate estimates of original insitu reservoir oil and gas compositions. The proposed *equilibrium contact mixing* (ECM) method can be used with samples which are clearly *not* representative of insitu fluids (e.g. due to near-wellbore multiphase behavior, reservoir depletion, or separator sampling problems). ECM procedures are recommended for saturated, undersaturated, and depleted reservoirs.

Examples are given for reservoir fluids ranging from lean-gas/black-oil systems to highly volatile gas/oil systems. Furthermore, it is shown that the proposed ECM method can be used to obtain estimates of depth-weighted average insitu compositions in reservoirs with gravity-induced vertical compositional gradients.

The Peng-Robinson (PR) and Soave-Redlich-Kwong (SRK) equations of state (EOS) are used in calculations, with extensive characterization of the C_{7+} fractions. Static PVT experiments and radial 1D/2D compositional simulations of typical fluid-sampling conditions are used to verify the proposed methods.

Partly due to the success of the ECM method, the traditional definition of a "representative" sample is reconsidered, and a more general definition is recommended. The general definition ("*reservoir-representative*") is any uncontaminated sample produced from a reservoir, where the measured composition and PVT properties are of good quality. The traditional definition ("*insitu representative*") is a special case where the sample represents an insitu reservoir composition at a specific depth (or an average composition for a depth interval).

Separator sampling of gas condensate and volatile oil reservoirs is widely used. The paper presents an analysis of traditional separator sampling methods, potential errors in separator sampling, and a critical evaluation of the "isokinetic" sampling method. Isokinetic sampling is currently used to sample separator gas streams when separator liquid "carryover" is suspected. Problems with the isokinetic method are discussed, and suggestions are made for field and laboratory measurements which are needed to confirm the validity of isokinetic sampling.

References
1. Evinger, H.H. and Muskat, M.: "Calculation of Theoretical Productivity Factor," *Trans.*, AIME (1942) **146**, 126-139.

Contents

Acknowledgement i

Preface iii

Summary v

1. Gas Condensate Well Deliverability 1
   1.1. Introduction 1
   1.2. Gas Condensate Reservoir Performance 5
      1.2.1. Dry Gas Material Balance - Reservoir Depletion Characteristics 5
      1.2.2. Gas Condensate Material Balance 9
   1.3. Gas Rate Equations 10
   1.4. Proposed Gas Condensate Rate Equation 16
      1.4.1. Flow Regimes and Primary Flow Behavior 18
      1.4.2. Coexistence of Flow Regions 23
      1.4.3. Calculating Pseudopressure 24
   1.5. Verification of Proposed Rate Equation 28
   1.6. Multiphase Treatment of Wells In Coarse Grid Simulation 38
      1.6.1. Description of The Proposed Multiphase Pseudopressure Method 38
      1.6.2. Verification of Coarse Grid Simulation Using Pseudopressure . 40
      1.6.3. Discussion of Coarse Grid Simulation Using Pseudopressure . . . 44
   1.7. Compositional vs. Black-Oil PVT Formulation 44
   1.8. Relative Permeability Effects 47
      1.8.1. Primary Functional Relationship $k_{rg} = f(k_{rg}/k_{ro})$ 47
      1.8.2. Critical Oil Saturation 52
      1.8.3. Gas-Oil Interfacial Tension Effect's on Well Deliverability 56
   1.9. Conclusions 60
   1.10. References 61

2. Gas-Condensate Relative Permeability 65
   2.1. Introduction 65
   2.2. Gravity Segregation 69
   2.3. Effect on Well Deliverability 72
      2.3.1. Flow Regimes and Primary Flow Behavior 72
      2.3.2. Critical Oil Saturation (S_{oc}) 80
      2.3.3. Interfacial Tension (IFT) 81
      2.3.4. Velocity/IFT Effect (Capillary Number N_c) 86
   2.4. Proposed Experimental Procedure 93

2.4.1. General Description 93
2.4.2. Choosing the Fluid System 98
2.4.3. Interpreting Laboratory Results 99
2.4.4. Boundary Effects 102
2.5. Conclusions 106
2.6. References 107

Nomenclature 111

Appendix A
Accurate Insitu Compositions in Petroleum Reservoirs (SPE 28829)

Appendix B
Modeling Gas Condensate Well Deliverability (SPE 30714)

Chapter 1.

Gas Condensate Well Deliverability

1.1. Introduction

Gas condensate reservoirs are characterized by production of both surface gas and varying quantities of stock-tank oil (STO). The STO is commonly referred to as "condensate" or "distillate". Typical condensate surface yields range from 10 to 300 STB/MMscf. The added economic value of produced condensate, in addition to gas production, makes the recovery of condensate a key consideration in developing gas condensate reservoirs. In the extreme case of a non-existent gas market, producible condensate is the only potential source of income.

At reservoir conditions, a gas condensate reservoir contains single phase gas. As the gas flows through the reservoir, through the production tubing, and finally through the surface separator, liquid condenses from the gas. Isothermal condensation of liquids in the reservoir, as pressure drops below the dewpoint pressure, constitutes the process of retrograde condensation. Liquids condensed in the reservoir are, for the most part, "lost" or unrecoverable.

A main difference between a "gas" reservoir and a "gas condensate" reservoir is that a gas reservoir will not experience two hydrocarbon phases at reservoir conditions, and hence there will be no liquid condensation ("condensate loss") in the reservoir. On the other hand, a gas reservoir won’t have significant condensible surface liquids to "loose" due to retrograde condensation. This leads to the apparent contradiction that the leaner the gas condensate, the higher the condensate recovery (as a percent of initial in place).

The second important difference between gas and gas condensate reservoirs is the loss in well deliverability experienced by gas condensate reservoirs due to the buildup of significant liquid saturations near the wellbore. Gas reservoirs will not experience such deliverability loss because liquids do not condense at reservoir temperature. Well deliverability loss due to condensation and accumulation of liquids near the wellbore in gas condensate reservoirs is the main subject of this chapter. It is also the starting point for discussions on relative permeability measurements in the second chapter.

When bottomhole flowing pressure (BHFP) drops below the dewpoint pressure a

region of relatively high liquid saturation forms close to the wellbore. This high liquid saturation results in reduced gas relative permeability and lowered well deliverability. The effect of reduced gas permeability close to the wellbore is often called "condensate blockage."

Well deliverability is the relation defining a well's production rate as a function of some constraining pressure. Strictly speaking, this rate-pressure relation should be defined at the *wellhead*, and so defined the well deliverability relation includes *all* sources for pressure loss from the reservoir to the surface separators (bulk reservoir, near wellbore, tubing, and gathering lines). A less useful but commonly used definition of well deliverability considers only the pressure losses in the reservoir ("wellbore" deliverability). Because gas is always sold at the surface, deliverability calculations (and rate-time production forecasts) should always be based on the well(head) deliverability relation.

The contribution of the different sources of pressure loss on well deliverability will depend primarily on reservoir permeability. For reservoirs with a permeability higher than about 200 md, the reservoir pressure losses are usually negligible compared to the total pressure loss. For example, reduced deliverability due to condensate blockage might have a pronounced effect on the wellbore deliverability, but almost no effect on wellhead deliverability (because tubing pressure losses are dominant). For reservoirs with "lower" permeability (<50 md) the reduced reservoir deliverability due to condensate blockage can have a significant effect on well(head) deliverability.

The effect of condensate blockage depends on (1) relative permeabilities, (2) PVT properties, and (3) how the well is being produced (constant rate vs. constant BHFP). Furthermore, the reduced wellbore deliverability due to condensate blockage is *only* important when BHFP reaches a minimum (dictated by surface pressure constraints) and the well is forced to go on decline.

When this research began in 1990, the flow behavior of gas condensates from the reservoir to the wellbore was not well understood. Calculation of gas condensate well(bore) deliverability has in fact been a long-standing problem.

Muskat[1] addresses the condensate blockage problem in his discussions of gas cycling, where he introduces a simple method for estimating the radius of condensate blockage as a function of time, gas rate, and reservoir rock and fluid properties. Fetkovich[2] uses Muskat's results to derive a rate- and time-dependent blockage skin for use in the standard gas rate equation.

Kniazeff and Naville[3] and Eilerts et al.[4,5] were the first to numerically model radial gas condensate well deliverability. These studies show radial saturation and pressure profiles as a function of time and other operational variables, confirming that condensate blockage reduces well deliverability. Kniazeff and Naville also study the

effect of non-Darcy flow (in the gas phase) on well deliverability.

Gondouin et al.[6] make a significant contribution towards the fundamental understanding of gas condensate well deliverability. Through radial black-oil simulations, they extend the work by Kniazeff and Naville, showing the importance of condensate blockage and non-Darcy flow effects on backpressure performance. They also give experimental procedures and measurements that quantify the effects of relative permeability and *multiphase* non-Darcy flow.

O'Dell and Miller[7] present the first gas rate equation using a pseudopressure function to describe the effect of condensate blockage. The equation is valid when (1) produced wellstream is the original reservoir gas, and (2) the blockage radius is relatively small (i.e. the reservoir pressure is significantly above the dewpoint). From their results, it is clear that well deliverability can be significantly reduced even for small regions of condensate blockage.

Fussell[8] presents EOS compositional simulations of radial gas condensate wells producing by pressure depletion below the dewpoint. He shows that the effect of condensate accumulation on well productivity and that O'Dell-Miller equation (with a small correction to account for gas dissolved in the flowing oil phase) dramatically overpredicts the deliverability loss due to condensate blockage, compared with simulation results. He also evaluates the effect of phase behavior and relative permeability characteristics on production performance.

Jones and Raghavan[9,10] treat, for the most part, transient pressure behavior (drawdown and buildup) of radial wells. They use EOS compositional simulation with simple three-component (C_1-C_4-C_{10}) gas condensate mixtures. The key observation made concerning long-term ("boundary-dominated") well deliverability, is that the pseudopressure function presented by Fussell is accurate at all times during depletion. The integral must be evaluated using pressures and saturations known as a function of radius at a given time in depletion ("reservoir integral pseudopressure"). However, as they point out themselves, this isn't very helpful because they have to do compositional simulation to know the pressures and saturations at a given time in depletion. In this chapter it is shown how to easily get the pressures and saturations from the instantaneous producing GOR (i.e. the producing wellstream composition).

A review of dry gas and gas condensate reservoir performance is presented in the first section. It presents the dry gas material balance equation in the form of a traditional straight line relationship between p/z and G_p (cumulative gas production) for volumetric reservoirs. A "volumetric" reservoir is defined as one where hydrocarbon pore volume (HCPV) is invariant during pressure depletion. The most common reasons for deviation from the straight line relationship between p/z and G_p are discussed. Furthermore it is shown that the straight line relationship between p/z and G_p can also be used for gas condensate reservoirs. Cumulative gas

production G_p must then be modified to include the effect of produced condensate. Additionally, the "two-phase" z-factor is used (instead of single phase z-factor) when the average reservoir pressure drops below the dewpoint pressure.

Section 2 reviews the gas rate equation. It describes the rate equation and shows that it consists of a productivity factor and a pressure dependent fluid (potential) integral. The productivity factor includes basic reservoir properties and a skin factor. The skin factor includes both a constant skin term and a rate dependent skin term. The consequences of using rate dependent skin factor is discussed. Furthermore, the general gas rate equation is compared with the "back-pressure" equation. A discussion is also given of how well deliverability can be determined from production tests.

The fluid flow from the reservoir to the wellbore in gas condensate reservoirs is analyzed in Section 3. It is shown that gas condensate wells producing with BHFP below the dewpoint have up to three flow regions. *Region 1* is closest to the wellbore and has, for all practical purposes, a constant flowing composition (GOR), where both oil and gas flow. *Region 2* is a region where condensate accumulates, but the oil mobility is practically zero. *Region 3* is the outer region where reservoir pressure is greater than the dewpoint and only (original) gas flows. Based on observations of the three flow regions (when and how they develop) a simple rate equation is proposed for gas condensate wells.

Section 4 verifies the proposed gas condensate rate equation. Simulated rate-time performance using a numerical reservoir simulator is compared with calculated rate-time performance using the proposed gas condensate rate equation. The rate-time performance is compared for two different gas condensate fluids with radial, vertically fractured, and horizontal well geometries.

Application of the proposed rate equation in numerical reservoir simulators are examined in Section 5. It examines the possibility of using the proposed rate equation in coarse-grid, full-field models to correctly convert the well grid-cell pressure to BHFP. Examples are given for radial, vertically fractured, and horizontal wells.

Section 6 examines why black-oil and compositional formulations often yield noticeable differences in well deliverability, and investigate if this problem can be reduced using a modified $\mu_o(p)$ relationship in the simulator.
Relative permeability effects on well deliverability are discussed in Section 7. It is shown that the main component of deliverability loss occurs in Region 1, and that the deliverability loss is dictated by the relationship $k_{rg}=f(k_{rg}/k_{ro})$. The effect of critical oil saturation on well deliverability is investigated, as well as the effect of gas-oil interfacial tension (IFT) on relative permeabilities.

1.2. Gas Condensate Reservoir Performance

1.2.1. Dry Gas Material Balance - Reservoir Depletion Characteristics

Based on the real gas equation of state (pV=znRT), where z is only pressure dependent (in an isothermal reservoir), it can be shown that a simple material balance relation exists for a volumetric dry gas reservoir depletion[11]:

$$\frac{p}{z} = \left(\frac{p}{z}\right)_i (1 - G_p/G) \qquad \textbf{(l.1)}$$

where p_i is initial pressure, z_i is initial gas compressibility factor, G is initial in-place gas (IGIP), p is current average reservoir pressure, z is current gas compressibility factor, and G_p is the cumulative produced gas. Gas reserves for a dry gas reservoir are conventionally predicted using the graphical solution of this simple material balance. As shown by **Eq. (l.1),** p/z should be linear with G_p, and the IGIP is obtained when p/z is extrapolated to zero.

Deviations from a linear relationship between p/z and G_p are due to violations of the constant-HCPV assumption used in the simple material balance. The deviations are usually caused by one or more of the following phenomena:

- Water influx
- Rock and water compressibilities
- Changing drainage areas (for p/z vs. G_p on a well basis)
- Non-communicating commingled units

These non-idealities are discussed below.

Water Influx

When an aquifer is in pressure communication with a gas reservoir, water may encroach into the reservoir as pressure declines. A p/z vs. G_p plot will not extrapolate to the IGIP because the HCPV is being reduced as water encroaches (**Fig.l.1**). Bruns et al.[12] show that the effect of an aquifer depends mainly on the aquifer permeability, aquifer size, initial reservoir pressure, water and rock compressibilities.

The theoretical encroachable water (W_{ei}) is the maximum volume of water that can enter the reservoir if average reservoir pressure reaches minimum BHFP (and rate approaches zero),

$$W_{ei} = c_{aq} V_{aq} (p_i - p_{wfmin}) \qquad \textbf{(l.2)}$$

c_{aq} is total cumulative aquifer (water+rock) compressibility, V_{aq} the aquifer volume, p_i is initial reservoir pressure, and p_{wfmin} is minimum BHFP. Both the size of the aquifer and the initial pressure are important to determine the maximum encroachable water. Aquifer compressibility is also important to know, but fortunately c_{aq} is relatively constant for most reservoirs and relatively easy to obtain.

The best method to estimate the potential effect of an aquifer is to compute the volume ratio W_{ei}/HCPV. This ratio determines the maximum fraction of the HCPV that can be filled with water if the reservoir is depleted to the minimum BHFP. A ratio greater than one indicates that the entire reservoir will water out prior to the average reservoir pressure reaching p_{wfmin}.

The maximum encroachable water $W_e(p_R)$ at any depletion stage, as a function of the prevailing average reservoir pressure p_R is given by

$$W_e(p_R) = W_{ei} \frac{p_i - p_R}{p_i - p_{wfmin}} \qquad \textbf{(l.3)}$$

The fraction of $W_e(p_R)$ that actually enters the reservoir is mainly dependent on the aquifer permeability and time. The effect of permeability can be conceptualized by analogy to a choke separating two sealed bottles where gas is withdrawn from one of the bottles. A high-permeability aquifer is equivalent to a large choke opening, and a low-permeability aquifer is equivalent to a small choke opening. A high-permeability aquifer responds fast to a reduction in reservoir pressure, and has therefore about the same pressure at any given time as the reservoir. This type of aquifer is called a "pot" aquifer. The amount of encroached water in a pot aquifer is independent of time and is determined accurately using **Eq. (l.3)**.

For low-permeability aquifers a time delay is seen in depletion between the reservoir and the aquifer. Methods to calculate the water influx from aquifers with low to intermediate permeabilities include the rigorous van Everdingen-Hurst[13] method which is based on the method of superposition, and the simplified Fetkovich pseudosteady state method[14]. A reservoir with an aquifer with a permeability less than about 1 md behaves practically as a constant-volume reservoir, independent of the aquifer size, because only a small fraction of W_{ei} actually enters the reservoir during the lifetime of the field.

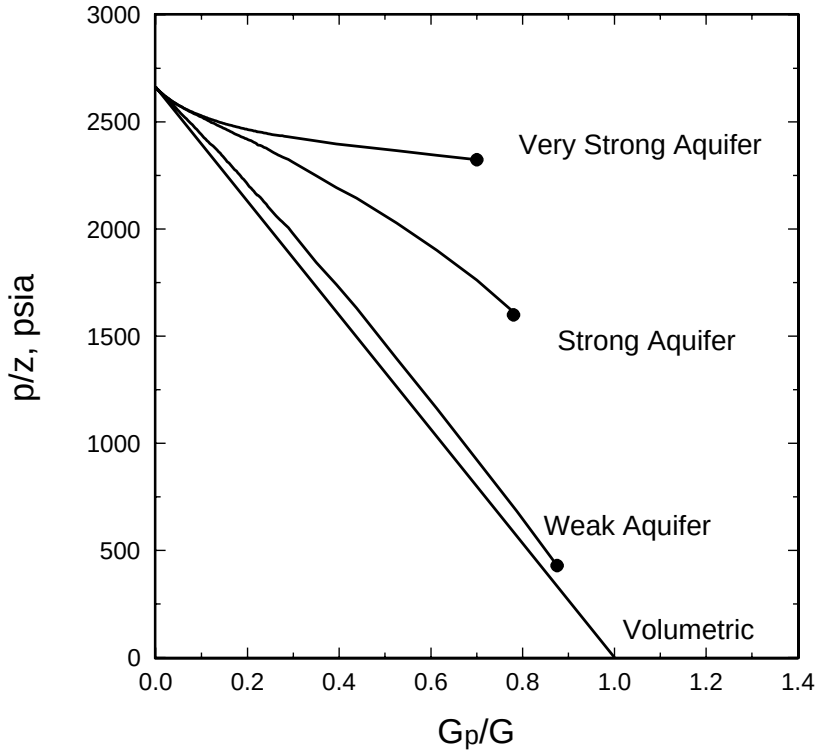

Fig l.1 The effect of water influx on a p/z vs. G_p/G (after Golan and Whitson[23]).

Fig. l.1 shows the effect that water influx has on a plot of p/z vs. G_p. Note that if early production data is used to determine IGIP by extrapolation, even a weak aquifer may lead to a dramatic over-estimation of IGIP.

The recovery from volumetric gas reservoirs is usually more than 80% of the IGIP. Gas reservoirs with an active aquifer usually have lower ultimate recoveries, because the encroached water displaces only 70-80% of the gas. About 20-30% the IGIP is trapped behind the water. This trapped gas is usually unrecoverable. The trapped gas saturation depends on rock properties, usually correlated with a trapping constant C_t and the initial water saturation[15].

Rock and Water Compressibilities

For high pressure gas reservoirs Fetkovich et al.[16] show the importance of including all sources for pressure support, e.g. rock and water compressibility of net and non-net pay zones, small aquifers (pot aquifers), and normal aquifers. Furthermore, they show the importance of using the *cumulative compressibility* $[\bar{c}(p)]$ in material balance calculations. The cumulative compressibility $\bar{c}(p)$ is defined as:

$$\bar{c}(p_R) = \frac{1}{V_i}\left[\frac{V_i - V(p_R)}{p_i - p_R}\right] \qquad \textbf{(l.4)}$$

where V_i is initial volume and V(p) is the volume at the current pressure.

Fetkovich et al.[16] have shown that the material balance for gas reservoirs, when accounting for all sources for pressure support can be written as,

$$(p/z)[1-\bar{c}_e(p)(p_i-p)] = (p/z)_i\left[1-\frac{G_p}{G}+\frac{W_e}{GB_g}\right] \qquad \textbf{(l.5)}$$

where

$$\bar{c}_e = \frac{S_{wi}\bar{c}_{tw}+\bar{c}_f+\frac{V_{pNNP}}{V_{pR}}(\bar{c}_{tw}+\bar{c}_f)}{1-S_{wi}} \qquad \textbf{(l.6)}$$

S_{wi} is initial water saturation, $\bar{c}_{tw}$ is cumulative water compressibility ,$\bar{c}_f$ is cumulative formation compressibility, V_{pNNP} is total pore volume of all non-net pay zones, V_{pR} is reservoir pore volume, and B_g is gas formation volume factor. This material balance equation [**Eq. (l.5)**] results in straight line $(p/z)[1-\bar{c}(p)(p_i-p)]$ vs. G_p. It will only extrapolate to G at zero $(p/z)[1-\bar{c}(p)(p_i-p)]$ for reservoirs without "normal" aquifers (W_e=0 throughout depletion).

Changing Drainage Areas (Per Well)

When p/z vs. G_p plot is made on a well by well basis and there are several wells producing from a common reservoir, the extrapolation of p/z to zero determines the initial gas in-place allocated for each well. The "instantaneous" ratio of the reserves of a particular well to the total reserves is equal to production rate from that well divided by the total production rate from the reservoir[17]. Any time-dependent change in the fraction of a particular well's production rate of the total rate (e.g. due to adding new wells, or stimulation only some wells) results in a change in the drainage volume allocated to the well. The p/z vs. G_p plot, for a single well in a multi-well reservoir exhibits a straight line segment for each period where the rate fraction of the well is constant. However, the total reservoir p/z vs. G_p plot will be a straight line (assuming the reservoir behaves "volumetrically").

Non-Communicating Commingled Units

Fetkovich et al.[18] show that in many cases, the deviation from straight line p/z vs. G_p behavior, occurs in wells penetrating and producing commingled from several non-communicating layers. Reservoirs with commingled production from non-communicating reservoir units usually experience differential depletion. The degree of differential depletion is dictated by the depletion ratios of the non-communicating layers[18,19]. The *depletion ratio* is defined as the production rate from a layer divided by that layer's IGIP. Rapid pressure drop occurs in layers with high depletion ratios, typically layers with high permeability and low volumes.

The p/z vs. G_p plot has a very characteristic behavior for layered no-cross flow reservoirs experiencing differential depletion. The p/z drops rapidly and then flattens at a value close to the BHFP. The reason is that when the well is shutin late in depletion, the high-pressure layer produces into the low-pressure layer through the wellbore (backflow). The wellbore pressure measured during a build-up test is dominated by (and therefore close) to the average reservoir pressure of the most depleted layer.

Early rate decline behavior is dictated by layers with high depletion ratios, while late time behavior is dictated by layers with low depletion ratios. The transition from early to late rate-decline behavior is smooth and will practically never show "double depletion". Rate decline behavior wells producing from non-communicating multi-layer reservoir are characterized by high Arp's[20,21] exponents in the range of 0.5-0.9.

1.2.2. Gas Condensate Material Balance

Case I - Reservoir Pressure above Dewpoint Pressure
The p/z vs. G_p form of the material balance is used also for gas condensate reservoirs when reservoir pressure is above the dewpoint. The cumulative gas production is modified to include the condensate production. This gas is called "wet" gas. The produced condensate quantity is converted to its gas equivalent (GE) by assuming that the condensate can be expressed in terms of an ideal gas,

$$GE = V = \frac{nRT_{sc}}{p_{sc}} = \frac{a_2 N_p \rho_o}{M_o} \frac{RT_{sc}}{p_{sc}} \qquad \textbf{(I.7)}$$

where a_2=5.615 ft^3/bbl for field units and a_2=1 for pure SI units. R is the universal gas constant, T_{sc} is temperature at standard conditions, p_{sc} is pressure at standard conditions, N_p is cumulative STO produced, ρ_o and M_o are the density and molecular weight, respectively, of the produced condensate.

In summary, the material balance for a volumetric gas condensate reservoir above the dewpoint is,

$$\frac{p}{z} = \left(\frac{p}{z}\right)_i (1 - G_{pw}/G_w) \qquad \textbf{(I.8)}$$

where G_w is initial wet gas in place, and G_{pw} produced wet gas.

Case II - Reservoir Pressure Below Dewpoint Pressure
When the reservoir pressure drops below the dewpoint pressure, condensate drops out of the reservoir gas. This violates several of the basic assumptions implicit in the traditional gas material balance equation.

A solution to the problem was to design a laboratory experiment to duplicate or

model closely the reservoir depletion of a volumetric gas condensate reservoir. The experiment is a constant volume depletion experiment (CVD)[22]. A sample of the original reservoir fluid sample is placed in a high-pressure PVT cell at reservoir temperature and dewpoint pressure. The pressure is reduced stepwize in the PVT cell by expanding the cell volume until the pressure reaches a predetermined value. At constant pressure equilibrium gas is removed to return the PVT cell volume to the initial dewpoint volume. A typical CVD experiment consists of 7-10 pressure steps.

The CVD experiment provides data that can be used directly by the reservoir engineer. From the data obtained, a so called *two-phase z-factor (z_2)* is *calculated* assuming that the gas condensate reservoir depletes according to the material balance of a gas condensate reservoir above the dewpoint. The p/z_2 vs. G_{pw} for a volumetric gas condensate reservoir is a straight line obtained from the gas material balance:

$$\frac{p}{z_2} = \left(\frac{p}{z}\right)_i (1 - G_{pw}/G_w) \qquad \textbf{(I.9)}$$

It is assumed in **Eq.(I.9)** that the oil that condenses from the reservoir gas does not flow into the wellbore. This is a probably a valid approximation even for rich gas condensates. Close to the wellbore some of the oil dropping out of the reservoir gas will flow into the wellbore, but this phenomenon has marginal effect on the overall reservoir performance.

The producing gas-oil ratio (R_p) from a gas condensate reservoir changes as a function of average reservoir pressure when the reservoir pressure is below the dewpoint pressure. R_p is close to the inverse of solution oil-gas ratio at the prevailing average reservoir pressure, $1/r_s(p_R)$. As reservoir gas flow towards the well some of the condensate originally dissolved in the reservoir gas drops out as liquid because of the pressure drop associated with the flow. Only the condensate that drops out of the gas close to the wellbore reaches high enough saturation (and thus mobility) to flow into the wellbore. The condensate dropping out further out in the reservoir is immobile. The outward condensation region is called the condensate buildup region. Immobile condensate buildup in this region is the cause of the difference between R_p and $1/r_s(p_R)$. The difference between R_p and $1/r_s(p_R)$ is negligible in the calculation of reservoir recoveries, but is very important for well deliverability calculations (as demonstrated later in this chapter).

1.3. Gas Rate Equations

The general gas rate equation for a dry gas well in pseudosteady state for any geometry (e.g. radial, vertically fractured or horizontal well) is,

$$q_g = C \int_{p_{wf}}^{p_R} \frac{1}{\mu_g B_g} dp$$

or **(l.10)**

$$q_g = C^* \int_{p_{wf}}^{p_R} \frac{p}{\mu_g z} dp$$

where,

$$C = \frac{2\pi a_1 k h}{\ln(r_e/r_w) - 0.75 + s'}$$

$$C^* = C \frac{T_{sc}}{p_{sc} T_R} \quad \textbf{(l.11)}$$

$$s' = s + Dq$$

and $a_1=1/(2\pi \cdot 141.2)$ for field units, and $a_1=1$ for pure SI units.

The pressure integral includes only fluid properties: gas viscosity μ_g, gas formation volume factor B_g (or, equivalently, gas compressibility factor z). The constant C includes basic reservoir properties such as permeability k, thickness h, drainage radius r_e, and wellbore radius r_w.

The total effective skin s´ is the sum of a constant skin s, and a rate dependent skin Dq_g. D is the coefficient of the rate dependent skin. The constant skin s is a composite factor that accounts for non-ideal flow conditions such as formation damage, stimulation, partial pay zone penetration, perforation restriction, and non radial drainage geometry. The traditional approach for estimating[23] or measuring[24] composite skin for a well producing single-phase fluid can be used to determine skin.

The constant skin and the rate-dependent skin can be found by plotting s´ vs. q_g for different test rates. This should result in a straight line with a slope D, and the constant skin may be found by extrapolating the line to zero flow rate. This analysis is only valid if the k·h product and other constants in the constant C are kept constant for all production rates.

The gas rate equation [**Eq.(l.10)**] changes from the simple linear rate-pressure relationship of Darcy's law to the quadratic Forchheimer model[23,25] if a rate dependent skin is used. The general gas rate equation written in terms of the Forchheimer model is,

$$\int_{p_{wf}}^{p_R} \frac{1}{B_g \mu_g} dp = A q_g + B q_g^2 \qquad \textbf{(l.12)}$$

where

$$A = \frac{\ln(r_e/r_w) - 0.75 + s}{2\pi a_1 k h}$$
$$\textbf{(l.13)}$$
$$B = \frac{D}{2\pi a_1 k h}$$

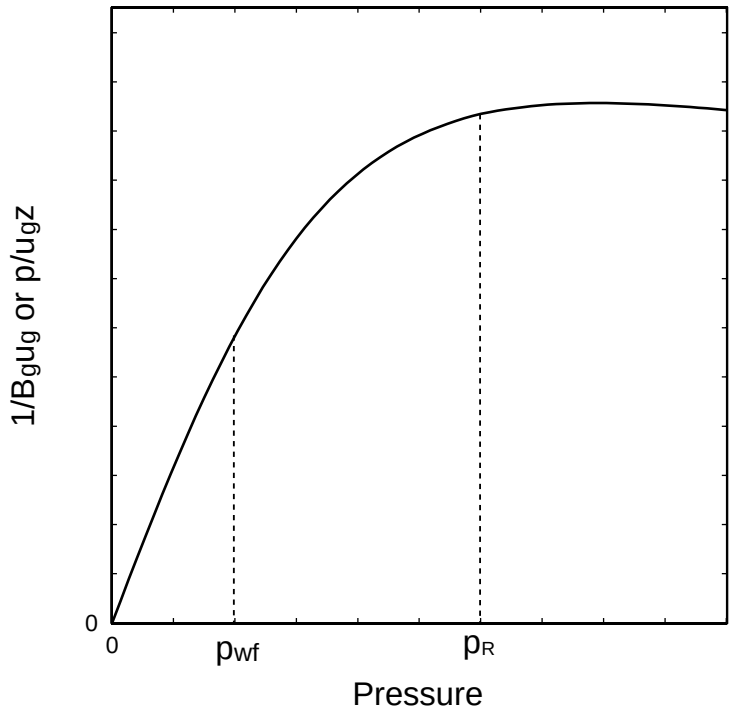

Fig. l.2 A typical plot of the gas pressure function vs. pressure. The area under the curve between p_R and p_{wf} represents the integral in **Eq.(l.10)**.

The pressure integral in the gas rate equation has been given a special name, pseudopressure (Al-Hussainy et al.[26]), designated here using the current SPE symbol $p_p(p)$, and defined

$$p_p(p) = 2\int_0^p \frac{1}{B_g \mu_g} dp$$
$$\textbf{(l.14)}$$
$$p_p(p) = \frac{2T_{sc}}{p_{sc} T_R} \int_0^p \frac{p}{\mu_g Z} dp$$

Substituting p_p in the gas rate equation gives

$$q = \frac{C}{2}[p_p(p_R) - p_p(p_{wf})] \quad \textbf{(l.15)}$$

The pressure function plotted in **Fig. l.2** exhibits three distinct regions. The *low-pressure region* has a straight line relationship between $p/\mu_g z$ and pressure. This behavior usually exits for pressures below 2000 psia. The second region has a curved relationship between $p/\mu_g z$ and pressure. This region usually exists between 2000 psia and 3000-5000 psia. The upper pressure limit of the second region depends mainly on the reservoir temperature (high reservoir temperature results in a higher upper pressure limit of the second region). The third high-pressure region has a pressure function $p/\mu_g z$ that is nearly constant (or slightly decreasing) for pressures higher than 3000-5000 psia.

The low pressure behavior of $p/\mu_g z$ yields a simple analytical solution to the pressure integral in **Eq.(l.10)**:

$$2\int_0^p \frac{p}{\mu_g z}\,dp = \frac{p_R^2 - p_{wf}^2}{\mu_g z} \quad \textbf{(l.16)}$$

The solution of the pressure integral takes into account the fact that the $1/\mu_g z$ is essentially constant in the low pressure region, and can therefore be evaluated at any pressure below 2000 psia. When substituting the solution of the pressure integral the gas rate equation at low pressures becomes

$$q_g = C^{**}(p_R^2 - p_{wf}^2) \quad \textbf{(l.17)}$$

where $C^{**} = C^*/(2\mu_g z)$.

At high pressures where $p/\mu_g z$ is nearly constant, the fluid integral has a simple analytical solution. However, this solution is not useful in rate-time forecasting because it requires a p_{wf} higher than 3000-5000 psia.

Backpresssure Equation

In 1936 Rawlins and Snellhardt[27] developed the classical backpressure equation relating gas rate to BHFP,

$$q_g = C_{bp}(p_R^2 - p_{wf}^2)^n \quad \textbf{(l.18)}$$

The equation was developed after interpreting several hundred multirate gas tests. Originally, the equation was proposed based on empirical observation, without suggestion as to why pressure squared should be used, or why the exponent n had to range between 0.5 and 1. Today it is known that the "pressure squared" behavior in the backpressure equation accounts for the pressure dependence of the pseudopressure integral, while the backpressure exponent n accounts for varying

degrees of high-velocity (non-Darcy) flow.

The backpressure rate equation is the most commonly used gas rate equation, probably because it is accurate enough for many practical applications, and it has a simple straight-line relationship between Δp^2 and rate when plotted on a log-log backpressure plot. The slope of rate vs. Δp^2 on such a plot is equal to 1/n. C_{bp} is then readily calculated from any point on the curve. If the average reservoir pressure is larger than about 2500 psia then pseudopressure function Δp_p can be used instead of Δp^2.

Estimating Well Deliverability

Several testing procedures can be used to determine the backpressure relation of a well[28]. They involve flowing the gas well at a sequence of rates while measuring the corresponding flowing and buildup pressures, and plotting the result as q_g vs. $\Delta p^2=p_R{}^2-p_{wf}{}^2$ (or Δp_p) on a backpressure plot. The test should be performed with rates in a range similar to the expected rates during production. Note that the backpressure relation obtained from a test is completely dependent of time ("stabilized") if the production time for each rate reaches pseudosteady state flow conditions.

The most common method to find the parameters A and B in Forchheimer's model [**Eq. (l.12)**] is a plot $\Delta p^2/q_g$ vs. q_g on cartesian graph paper. This should give a straight line with slope B and an intercept (zero flow rate) equal to A. Another method is to match the production data to the dimensionless backpressure type curve, as suggested by Whitson[29,30].

The backpressure equation and the general gas rate equation calculates identical values for Darcy flow (n = 1), and when non-Darcy flow effects totally dominate (n = 0.5). For intermediate n values ($0.5 < n < 1$) the two rate equations are not equal for the entire range of valid flowing pressures. However, over a limited range of production rates (the range experienced during the life of a well), the two gas rate equations can provide practically "identical" description of the rate-pressure relationship. That is, the curvature predicted by the Forchheimer model on a backpressure plot is generally small within the range of gas production rates of interest. The initial gas rate and gas rate at abandonment bound the range of gas rates of interest. The difference between upper and lower rate is usually only one or (at most) two log cycles.

Stimulation Representing a Constant Skin

Low permeability ($k < 1$ md) gas wells are usually stimulated upon initial completion. The main objective with stimulation is to increase production capacity. Two types of stimulation exist: matrix acidizing and fracturing. The first method primarily improves the permeability in the vicinity of the wellbore. The second one creates a thin but highly conductive vertical fracture extending from the wellbore into the reservoir. The fracture length can range from 10 ft to 1000 ft; design fracture lengths are usually 100 to 500 ft.

It can be shown that the general gas rate equation can be used for stimulated wells. The improved capacity due to stimulation can be accounted for by a constant negative skin in the rate equation. A matrix acidizing job which improves the permeability around the wellbore to k_a in a cylinder shape from r_w to a radius r_a can be expressed as a skin factor s_a[23],

$$s_a = [k/k_a - 1] \ln(r_a/r_w) \quad \textbf{(l.19)}$$

where k is the reservoir permeability. The improved capacity for fractured wells can also be accounted for by a constant skin term s_f[23],

$$s_f = -\ln(\frac{x_f}{2r_w}) \quad \textbf{(l.20)}$$

where x_f is equal to the distance from the wellbore to one fracture tip. The constant 2 in **Eq. (l.20)** is normally used for fractures with infinite conductivity. For fractures with a finite conductivity the constant is higher, resulting in a lower improvement in well deliverability. It may be useful to work with an apparent wellbore radius r_{wa} instead of fracture half length or skin, particularly for rate-time production forecasting with type curves based on dimensionless rate and time.

The total skin of a well be can by obtained (approximately) by adding the different skin factors, in a manner that corrects for convergence effects of partially penetrated well configurations.

Transient Rate Decline

When a shutin well is opened for production it disturbs the pressure equilibrium in the reservoir. The pressure disturbance propagates away form the wellbore. Before the pressure distribution reaches the reservoir boundaries, the production conditions will tend to change rapidly. Production during this period is referred to as transient (or infinite-acting) production. After the pressure disturbance reaches the entire reservoir boundary the production conditions at the wellbore tend to stabilize; subsequent changes in pressure and/or rate are more gradual and are dictated primarily by pressure depletion of the entire reservoir. Production in this period is referred to as pseudosteady state production. The rate of pressure decline during pseudosteady state depletion is the same throughout the reservoir when the production rate is constant (assuming a homogeneous, uniform distribution of rock properties).

Two methods of transient production are usually considered when testing or interpreting production data: constant BHFP and constant rate. A constant BHFP implies that p_{wf} is held constant, resulting in a gradual decrease in production rate. This type of transient production occurs when a well is put on production and is constrained by a constant pipeline backpressure, resulting in a near-constant BHFP. A constant production rate implies that p_{wf} is gradually decreasing to keep the production rate constant. The pressure transient during constant rate production is mainly used for well testing purposes. However, the BHFP decline in a constant-rate

well behaves similarly and is controlled by the same mechanisms causing rate decline in a well producing with constant BHFP.

For engineering analysis, the transient production period can be considered as a series of discrete steady-state production periods with increasing reservoir drainage radius. The general gas rate equations for constant wellbore pressure production is

$$q_g(t) = C(t) \int_{p_{wf}}^{p_R} \frac{1}{B_g \mu_g} dp \qquad \textbf{(I.21)}$$

where

$$C(t) = \frac{2\pi a_1 k h}{\ln(r_e(t)/r_w) - 0.75 + s'} \qquad \textbf{(I.22)}$$

The problem of quantifying $r_e(t)$ and $q_g(t)$ has received extensive mathematical treatment. The solution is usually given in the form of a relationship between a dimensionless rate q_D and a dimensionless time t_D. The relationship q_g vs. t for a particular well can be calculated from the general relationship q_D vs. t_D, including information about permeability-thickness, skin (effective wellbore radius), and drainage area.

A generalized graphical presentation of q_D vs. t_D based on analytical and empirical (Arps) relationships was first given by Fetkovich[23,24,31] . For computing purposes Edwardson et al.[23,32] gives a set of equations that approximate the infinite-acting $q_D(t_D)$ solution.

An interesting observation is that the time to the end of transient behavior is independent of the skin factor and thus, independent on the type of well (radial vertically fractured or horizontal). Transient production is an important issue in low-permeability reservoirs where the time to reach pseudosteady state may be from months to years if the permeability is very low. To reduce the time of transient production or transient rate decline in tight reservoirs the well spacing (and thus the drainage boundaries) must be reduced.

1.4. Proposed Gas Condensate Rate Equation

The general volumetric rate equation for a gas condensate well of any geometry (e.g. radial, vertically fractured, or horizontal) is, for a *compositional formulation*,

$$q_g = C\left(\frac{RT_{sc}}{p_{sc}}\right)\beta_s \int_{p_{wf}}^{p_R} \left(\frac{\rho_g k_{rg}}{M_g \mu_g} + \frac{\rho_o k_{ro}}{M_o \mu_o}\right) dp \qquad \textbf{(I.23)}$$

The constant C is the same as for the traditional gas rate equation. (RT_{sc}/p_{sc})

converts the wellstream from a molar basis to a standard-gas-volume basis. β_s determines the molar fraction of the wellstream that is gas after surface separation. The integral represents the pseudopressure on a molar basis for the total *producing wellstream* (multiplication by β_s yields surface gas rate q_g). The first part of the integral represents the pseudopressure contribution from the flowing reservoir gas phase to the pseudopressure of the producing wellstream. The second part of the integral represents the pseudopressure contribution from the flowing reservoir oil phase to the pseudopressure of the producing wellstream. The contribution to the pseudopressure from the reservoir oil phase is generally negligible except for near critical gas condensates.

In terms of *black-oil PVT* parameters, the rate equation for gas condensates is

$$q_g = C \int_{p_{wf}}^{p_R} \left(\frac{k_{rg}}{B_{gd}\mu_g} + R_s \frac{k_{ro}}{B_o \mu_o} \right) dp \qquad \textbf{(l.24)}$$

where

$$C = \frac{2\pi a_1 k h}{\ln(r_e/r_w) - 0.75 + s} \qquad \textbf{(l.25)}$$

a_1 and C are the same as for the general gas rate equation [**Eq. (l.10)**]. Relative permeabilities k_{rg} and k_{ro} are defined relative to *absolute permeability*, and *not* relative to permeability at irreducible water saturation. This distinction is particularly important when correlating relative permeability data.

In **Eq. (l.24)**, the constant C is the same as for the general rate equation. The integral represents the pseudopressure for the *surface gas*. The first part of the integral represents the pseudopressure contribution from the flowing reservoir gas phase. The second part of the integral represents the pseudopressure contribution from the flowing reservoir oil phase. The contribution to the pseudopressure from the reservoir oil phase is generally negligible except for near-critical gas condensates.

As for the dry-gas rate equation, skin s is a composite factor that includes non-ideal flow effects such as damage, stimulation, drainage geometry, and partial penetration. The pseudopressure integral is for practical purposes independent of well geometry. This greatly simplifies the treatment of gas condensate well deliverability.

The effect of a rate-dependent skin Dq_g term is not included in this study. The rate dependent skin is zero for all of the examples in this chapter. Realistically, the effect of a non-Darcy flow might not be completely accounted for by a simple rate-dependent skin because non-Darcy effects will also be a function of relative permeabilities and or saturations, and therefore should be treated accordingly.

The deliverability loss due to condensate blockage is particularly important in reservoirs where the main part of the total well pressure drop (reservoir to separator) occurs in the reservoir (usually low-permeable reservoirs). The production rate from wells producing from low-permeability reservoirs is usually so low that the pressure drop caused by non-Darcy flow effects can be neglected. Furthermore, wells producing from low permeability gas condensate reservoirs are usually fractured which often eliminates non-Darcy flow effects.

However, for reservoirs in low-permeability reservoirs (and consequently where reservoir deliverability limits the production rate), condensate blockage will be of primary importance.

Note that the only difference between the general rate equation for a dry gas and the proposed rate equation for a gas condensate is the inclusion of relative permeabilities in the pseudopressure integral. The condensate blockage effect is, with this formulation, automatically included in the pseudopressure integral in terms of relative permeability. It has been suggested in the past to include the condensate blockage effect as a skin factor that should change as a function of time. This is not recommended because it makes well performance monitoring more difficult; the skin due to condensate blockage is time and rate dependent, and therefore not constant throughout depletion.

1.4.1. Flow Regimes and Primary Flow Behavior

Fluid flow towards a gas condensate well producing from a reservoir undergoing depletion can be divided into three main flow regions, extending from the wellbore outward.

Region 1: An inner near-wellbore region saturated with oil and gas which *both* are flowing simultaneously.

Region 2: A region of condensate buildup where the liquid condensate is (practically) immobile and only gas is flowing.

Region 3: A region containing single phase (original) reservoir gas.

For a given producing condition, one, two, or all three regions may exist. The three flow regions develop after reaching a kind of pseudosteady state (not related to the transient-flow definition). The flow-region pseudosteady state conditions, after being established, will change only gradually with time (as a series of steady state conditions).

The three regions are illustrated in **Fig. l.3**, as calculated for a particular case (Lean Gas B). The fluid properties for Lean Gas B are given in **Figs. l.6-l.9**, the reservoir

properties this example are given in **Tables 2 and 3**, and the relative permeabilities are shown in **Fig. l.10**.

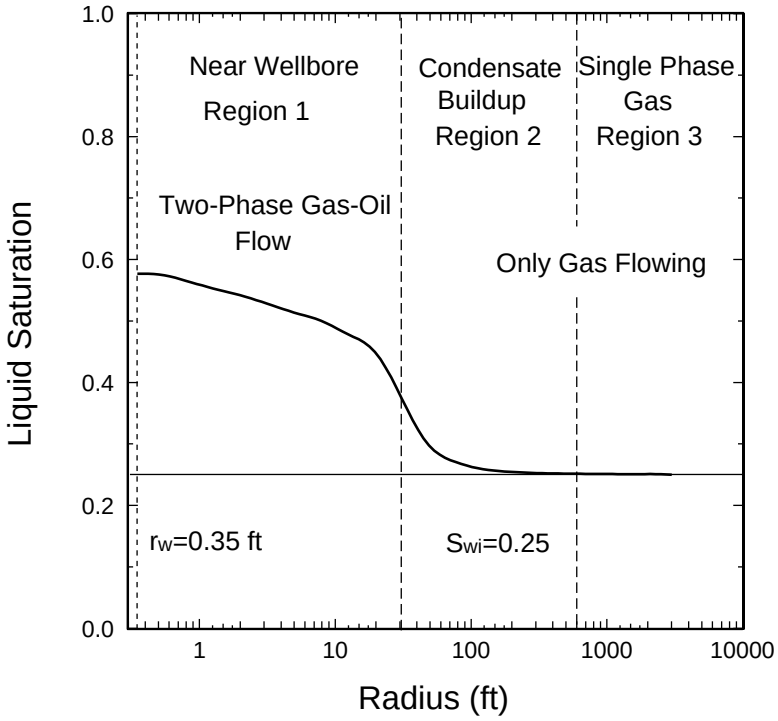

Fig. l.3 Flow regions for a radial well producing from a gas condensate reservoir (Lean Gas B).

Near Well Region (Region 1)

The *flowing* composition (GOR) within Region 1 is constant throughout. That means that the single-phase gas entering Region 1 has the same composition as the produced wellstream mixture. Conversely, if we know the producing wellstream, then we know the flowing composition within Region 1. Furthermore, the dewpoint of the producing wellstream mixture equals the reservoir pressure at the outer edge of Region 1.

Region 1 is the main source of flow resistance, and thus deliverability loss in gas condensate wells. The deliverability loss depends mainly on gas relative permeability in Region 1, and the size of Region 1.

The gas relative permeability in Region 1 is mainly a function of liquid saturation distribution. The liquid saturation that develops will depend on the richness of the flowing wellstream, and the PVT properties of the reservoir gas entering Region 1. The steady-state saturation distribution in Region 1 is determined (as a function of radius) *specifically* to ensure that all liquid condensing from the single-phase gas entering Region 1 has sufficient mobility to flow through and out of Region 1 without any net accumulation.

The size of Region 1 increases gradually with time. The Region 1 growth is mainly a function of the PVT properties of the original reservoir gas and the production rate. The characteristics of Region 1 will be illustrated henceforth through several simulated examples.

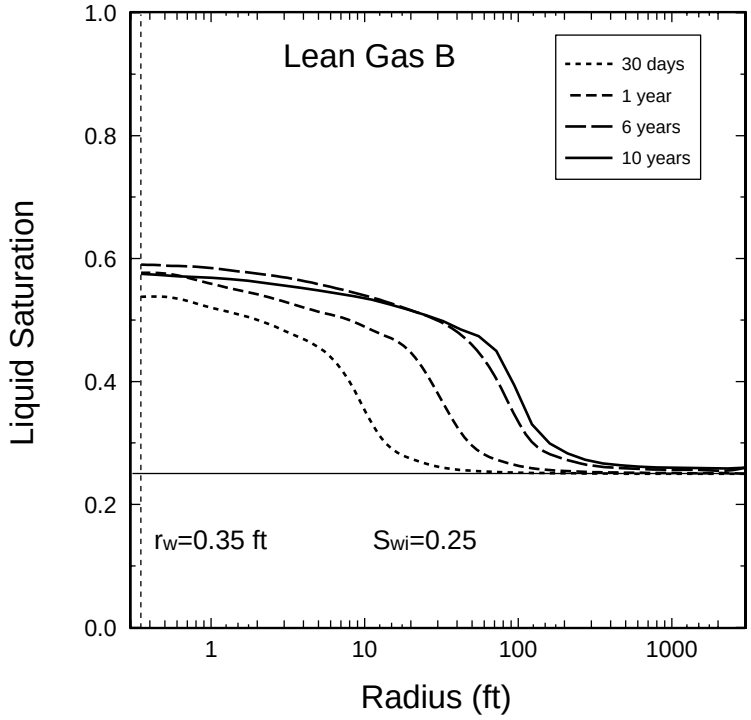

Fig. l.4 Liquid saturation as a function of radius in different stages of depletion, for a radial well producing from a reservoir with Lean Gas B.

Fig. l.4 shows the saturation distribution as a function of time for a radial well producing from a reservoir with lean gas B. Region 1 is the part of the reservoir with a liquid saturation larger than about 35%. Condensate saturation within Region 1 varies both with time and pressure because it depends on the amount of condensate flowing in Region 1. The amount of condensate flowing at each radial distance in Region 1 is equal to the difference in solution oil-gas ratio (OGR), Δr_s, between the gas entering Region 1 and the gas flowing at a given radial distance. Because the solution OGR decreases with pressure the condensate saturation increases towards the wellbore.

Region 1 increases as a function of time, and its outer boundary moves gradually outward. The liquid saturation close to the wellbore first increases upon initiation of production and early depletion stages but starts to decrease later in depletion. The increase in oil saturation close to the wellbore early in depletion occurs because BHFP in this simulated example decreases during the first 3.5 years. However, late in depletion when production starts to decline the condensate saturation close to the

well decreases because the gas entering Region 1 is becoming leaner as the reservoir depletes.

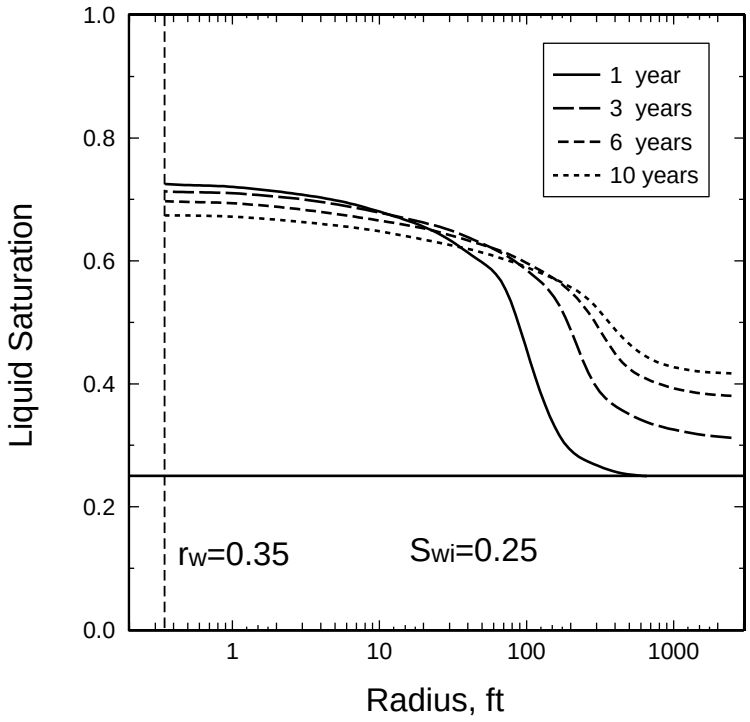

Fig. l.5 Liquid saturation as a function of radius in different stages of depletion, for a radial well producing from a reservoir with Rich Gas A.

Fig. l.5 shows the saturation distribution as a function of time for another example (Rich Gas A). The fluid properties for Rich Gas A are given in **Figs. l.6-l.9**. The reservoir properties are given in **Tables 2 and 3**, and relative permeabilities are shown in **Fig. l.10**. The difference in the condensate saturation between **Fig. l.4** and **Fig. l.5** is caused only by the difference in richness of the original reservoir gas. Region 1 is, in this case, the part of the reservoir with a liquid saturation higher than about 50%. The well deliverability loss in Region 1 is so high for this richer gas that rate starts to decline immediately. Consequently, the liquid saturation in Region 1 decreases throughout depletion. The size of Region 1 after 10 years of production is about 300 ft with Rich Gas A and about 100 ft with Lean Gas B.

Note the saturation as a function of radius at the outer edge of Region 1 is "smeared" out in **Figs. l.4-l.5**, due to simulation grid effects. It would have been steeper if a higher grid resolution had been used (though the effect on well deliverability using finer gridding would have been negligible).

The Condensate Buildup Region (Region 2)

Region 2 defines a region of net accumulation of condensate. The condensate formed in this region has zero or very low mobility. Effectively, only gas is flowing

in Region 2.

The buildup of condensate is caused by two mechanisms: (a) the condensate dropping out of the reservoir gas due to pure decline in the bulk of the reservoir, and (b) the condensate dropout due to the pressure gradient imposed on the flowing reservoir gas within Region 2.

The condensate saturation caused by pure pressure depletion is easily calculated from the liquid dropout curve from a constant volume depletion (CVD) experiment[33], corrected for water saturation. The condensate saturation caused by the gas flowing through Region 2 is more complicated to calculate. For radial flow assuming zero oil mobility and a "black-oil" type model, Muskat[1] gives an expression that can be used to compute the saturation profile,

$$S_o(r,t) = \int_0^t \frac{q_g}{2\pi r \phi} \frac{dp}{dr} \frac{dr_s}{dp} B_o \, dt \qquad \textbf{(l.26)}$$

The condensate saturation coming from the gas flowing through Region 2 increases towards the well because pressure decreases radially inward, the pressure gradient increases, and the flow area decreases.

The condensate saturation in a small cylindrical volume element in Region 2 increases until the saturation is so high that the condensate dropping out of the gas in the volume element has enough mobility to flow out of the volume element; the volume element now becomes the outer limit of Region 1. Thus, Region 1 increases as a function of time because Region 2 is decreasing (Region 1 expands into Region 2). The size of Region 2 is largest just after the reservoir pressure drops below the dewpoint. It decreases in size with time because Region 1 expands. The size and importance of Region 2 is greatest for lean gas condensates (see **Figs. l.4-l.5**).

For well deliverability calculations, the condensate saturations in Region 2 can be approximated by the liquid dropout curve from a CVD experiment, corrected for water saturation (as shown later in this chapter).

The important consequence of Region 2 is that producing wellstream composition (GOR) is leaner than calculated by a simple volumetric material balance (e.g. CVD measurements). Incorrect use of material balance GORs in the calculation of the pseudopressure significantly overestimates deliverability loss in Region 1, especially at early times in depletion just after reservoir pressure drops below the dewpoint. The well deliverability loss is much larger in Region 1 than in Region 2 because oil saturation is much greater in Region 1. The GOR calculated from a simple volumetric material balance indirectly implies that Region 2 does not exist because the producing composition is equal the gas composition at the average reservoir pressure. The effect of the size of Region 2 (producing GOR) on well deliverability is discussed in detail in a subsequent section.

Even though Region 2 has a big influence on well deliverability, it has only a small effect on net condensate recovery. The effect is small on oil recovery calculations because of the relatively small difference between the producing oil-gas ratio ($r_p=1/R_p$) and solution oil-gas ratio r_s of the producing wellstream (evaluated at average reservoir pressure).

The Single Phase Gas Region (Region 3)
Region 3 will always (and only) exist in a gas condensate reservoir that is currently undersaturated. The standard treatment[26] of single phase gas flow is used to quantify the contribution of Region 3 to well deliverability. Composition is constant in Region 3, equal to the original reservoir gas.

1.4.2. Coexistence of Flow Regions

The following observations have been made regarding the coexistence of the three flow regions.

Region 1 will always (and only) exist when BHFP is below the dewpoint. A short transition period is required to build up steady-state saturations in Region 1. The buildup period is longer for a vertically fractured well because of linear flow close to the well, compared with radial or horizontal wells with radial convergent flow near the well. Furthermore, linear flow close to a vertically fractured well reduces the near-wellbore pressure gradients and increases the initial buildup region.

Region 2 will always exist together with Region 1 after reservoir pressure drops below the dewpoint. In this case, Region 3 will vanish. It is not possible for Regions 2 and 3 to exist in the absence of Region 1 (after steady-state conditions are reached).

All three regions exist for slightly undersaturated reservoirs with BHFP less than the dewpoint. Region 2 may "disappear" or have negligible effect for highly undersaturated reservoirs.

For a very rich (near-critical) gas condensate, Region 1 may exist *throughout* the drainage area (in the absence of Regions 2 and 3), after the reservoir pressure drops below the dewpoint. This requires that the condensate saturation calculated from the CVD liquid dropout curve is sufficiently higher than critical oil saturation.

Table 1 Summarizes the existence conditions of the different flow regions.

Table 1 Coexistence of Flow Regions			
	$p_{wf}>p_d$	$p_R < p_d$	$p_{wf} < p_d$ and $p_R > p_d$
Region 1		X	X
Region 2		(X)	(X)
Region 3	X		X
X exist (X) may exist			

1.4.3. Calculating Pseudopressure

Based on observations of the three flow regions for many gas condensate systems, a simple method to accurately calculate the pseudopressure integral in **Eqs. (l.23) and (l.24)** has been developed. The approach is an extension of the pseudopressure method proposed originally by Evinger and Muskat[34] for solution gas drive oil wells.

First the pseudopressure integral is broken into three parts, corresponding to the three flow regions discussed above.

$$\underline{\text{Total}} \qquad \Delta p_p = \int_{p_{wf}}^{p_R} \left(\frac{k_{rg}}{B_{gd}\mu_g} + \frac{k_{ro}}{B_o\mu_o} R_s\right) dp =$$

$$\underline{\text{Region 1}} \qquad \int_{p_{wf}}^{p^*} \left(\frac{k_{rg}}{B_{gd}\mu_g} + \frac{k_{ro}}{B_o\mu_o} R_s\right) dp \quad + \qquad \textbf{(l.27)}$$

$$\underline{\text{Region 2}} \qquad \int_{p^*}^{p_d} \frac{k_{rg}}{B_{gd}\mu_g} dp \quad +$$

$$\underline{\text{Region 3}} \qquad k_{rg}(S_{wi}) \int_{p_d}^{p_R} \frac{1}{B_{gd}\mu_g} dp$$

An important observation in connection with the pressure integral is that only the producing GOR (R_p), BHFP (p_{wf}) and current average reservoir pressure (p_R) are needed to determine the pressure limits for each of the integrals in **Eq. (l.27)**.

Region 1 Pressure Limits

The flowing wellbore pressure p_{wf} determines the lower limit for the pressure integral in Region 1. The external region boundary pressure p* determines the upper limit of the pressure integral in Region 1. Since only single phase gas flows into Region 1, the dewpoint pressure of the gas entering Region 1 must equal p*. Furthermore, p* must be equal the dewpoint of the producing wellstream, since the flowing composition in Region 1 is constant. Using a black-oil PVT approach (with r_s data known as a function of pressure), we locate the pressure in the PVT table where $r_s=1/R_p$, this pressure defining p*. In a compositional treatment, the dewpoint of the producing wellstream composition is defined as p*.

If $p^*>p_R$, then integration of the Region 1 pressure function should be only from p_{wf} to p_R; in this case, Regions 2 and 3 don't exist. In this case ($p^*>p_R$), the proposed pseudopressure is almost identical to the pseudopressure concept proposed by Evinger and Muskat[34] for solution gas drive oil wells (the only difference being that oil dissolved in reservoir gas is considered in the present formulation).

Region 2 Pressure Limits

The calculated pressure p* determines the lower pressure limit for the pressure integral in Region 2. The upper pressure limit of the pressure integral is equal to initial dewpoint pressure p_d if $p_R > p_d$, or it equals average reservoir pressure p_R if $p_R < p_d$.

Region 3 Pressure Limits

Region 3 is the single phase gas region. This pressure integral exists only if the reservoir pressure is greater than the dewpoint pressure. The lower pressure limit of Region 3 pressure integral is the initial dewpoint pressure and the upper pressure limit is the current average reservoir pressure.

The following sections describe procedures for calculate the pressure integral for each region based on PVT properties of the reservoir fluid, relative permeabilities, producing GOR R_p, FBHP p_{wf} and average reservoir pressure p_R.

Region 1

The Region 1 pseudopressure integral is solved using the modified Evinger-Muskat approach. At pressures $p < p^*$ the PVT properties R_s, B_o, r_s, B_{gd}, μ_o, and μ_g are found directly from black-oil PVT data. Next, the equation defining producing GOR for a system with known producing GOR R_p[35],

$$R_p = R_s + \left(\frac{k_{rg}}{k_{ro}}\right)\left(\frac{\mu_o B_o}{\mu_g B_{gd}}\right)(1 - r_s R_p) \qquad \textbf{(l.28)}$$

is rearranged and solved for k_{rg}/k_{ro}. This expression gives the ratio k_{rg}/k_{ro} as a function of pressure, with all PVT variables on the right-hand side known as a function of pressure.

$$\frac{k_{rg}}{k_{ro}}(p) = \left(\frac{R_p - R_s}{1 - r_s R_p}\right)\frac{\mu_g B_{gd}}{\mu_o B_o} \qquad \textbf{(l.29)}$$

It is readily shown[9,36] that **Eq. (l.29)** can be expressed in terms of the oil relative volume of the producing wellstream during a constant composition expansion, $V_{roCCE}=V_o/(V_g+V_o)$,

$$\frac{k_{rg}}{k_{ro}}(p) = \left(\frac{1}{V_{roCCE}} - 1\right)\frac{\mu_g}{\mu_o} \qquad \textbf{(l.30)}$$

The relative oil volume V_{roCCE}, can be expressed in terms of black-oil PVT properties by combining **Eqs. (l.29) and (l.30)**, which for any producing GOR, R_p, gives

$$V_{roCCE}(p) = \left[1 + \left(\frac{R_p - R_s}{1 - r_s R_p}\right)\frac{B_{gd}}{B_o}\right]^{-1} \qquad \textbf{(l.31)}$$

As shown by Evinger and Muskat[34], relative permeabilities k_{rg} and k_{ro} can each be expressed directly as a function of the ratio k_{rg}/k_{ro} when both phases are mobile. For a given R_p, relative permeabilities k_{rg} and k_{ro} in Region 1 can be evaluated directly as a function of pressure, $k_{rg}(p) = f[k_{rg}/k_{ro}(p)]$, and $k_{ro}(p) = f[k_{rg}/k_{ro}(p)]$, using **Eq. (l.29)**. The pressure integral for Region 1 is now easily computed because it contains only pressure-dependent PVT variables.

The contribution of gas dissolved in oil $[R_s k_{ro}/(\mu_o B_o)]$ to the pseudopressue integral is negligible except for near-critical gas condensates. It is included here merely to generalize the treatment and to keep the pseudopressure integral valid for all types of reservoir fluids. It also helps to emphasis that both fluids (gas and oil) are flowing in Region 1.

Region 2

When Region 2 exists ($R_p > 1/r_s$, with r_s evaluated at p_R), the Region 2 pressure integral is evaluated using $k_{rg}(S_o)$, where oil saturation S_o is estimated as a function of pressure from CVD experiments. The relative oil volumes $V_{roCVD}(p)=V_o(p)/V_d$, corrected for initial water saturation, yields the saturation-pressure relationship $S_o(p)=[V_{roCVD}(p)](1-S_w)$, If V_{roCVD} values are not known for the black-oil PVT data set, they can be calculated using the following equations,

$$(V_{roCVD})_k = \frac{N_{CVD,k-1} - G_{CVD,k-1}(r_s)_k}{1-(r_s R_s)_k}(B_o)_k$$

$$N_{CVD,k-1} = \left(\frac{V_{roCVD}}{B_o} + \frac{1-V_{roCVD}}{B_{gd}} r_s\right)_{k-1} \qquad \textbf{(l.32)}$$

$$G_{CVD,k-1} = \left(\frac{V_{roCVD}}{B_o} R_s + \frac{1-V_{roCVD}}{B_{gd}}\right)_{k-1}$$

where subscript k represents the current pressure stage, k-1 represents the previous pressure stage, and $(V_{roCVD})_0 = 0$.

The above equations [**Eqs. (l.32)**] calculate the CVD liquid dropout curve from black-oil PVT properties. The **Eqs. (l.32)** are developed using black-oil gas and oil material balance equations to "simulate" the CVD experiment.
The following equations can be used to evaluate the amount stock tank oil ($N_{CVD,k-1}$) and gas ($G_{CVD,k-1}$) at the end of the previous depletion stage (initial PVT-cell volume is set to 1),

$$N_{CVD,k-1} = \left(\frac{V_{roCVD}}{B_o} + \frac{1-V_{roCVD}}{B_{gd}} r_s\right)_{k-1} \qquad \textbf{(l.33)}$$

$$G_{CVD,k-1} = \left(\frac{V_{roCVD}}{B_o} R_s + \frac{1-V_{roCVD}}{B_{gd}}\right)_{k-1}$$

The amount of surface oil and gas after the pressure in the PVT-cell is reduced (by increasing the cell volume), including the removed equilibrium gas, is equal to the amount of surface oil and gas in the PVT-cell at the end of the previous depletion stage. Thus the amount of stock tank oil at the end of the previous pressure stage can also be evaluated from

$$(N_o)_{CVD,k-1} = \left(\frac{V_{roCVD}}{B_o}\right)_k + [G_{CVD,k-1} - \left(\frac{V_{roCVD}}{B_o}\right)_k (R_s)_k]\,(r_s)_k \qquad \textbf{(l.34)}$$

Everything in **Eq. (l.34)** is known except for V_{roCVD}. Rearranging and solving **Eq. (l.34)** for V_{roCVD} results in the first equation in **Eqs. (l.32)**.

Region 3
Only PVT properties are found in the Region 3 integral. The traditional single-phase gas pseudopressure function can be used.

1.5. Verification of Proposed Rate Equation

The rate equation has been developed based on a physical understanding of flow conditions in the three flow regions. The accuracy of this relatively simple model is verified by numerical simulation of two reservoir fluid systems with three different well geometries.

Production by pressure depletion is simulated using a conventional numerical reservoir simulator. The production rates from the simulator are then compared with the production rates calculated from **Eq. (l.24)** using the proposed method outlined above.

The two fluids are:

Rich Gas A, an undersaturated gas condensate with 175 STB/MMscf and a maximum CVD liquid dropout of 23%.

Lean Gas B, a slightly undersaturated gas condensate with 45 STB/MMscf and a maximum CVD liquid dropout of 2%.

PVT properties are calculated with an EOS using methods proposed by Whitson[33], and are shown for the two fluids in **Figs. l.6-l.9**. The reservoir properties are given **Tables 2 and 3**. The gas-oil relative permeability data are calculated using a Corey equation[37] [**Eq. (l.35)**]. Set A curves are shown in **Fig. l.10**. Unless otherwise stated, these curves are used in all calculations. The numerical grids used for the different well geometries are given in **Table 4.**

$$k_{ro} = k_r(S_{wi})\,(S_o*)^2\,\left(\frac{S_o}{1-S_{wi}}\right)^{(2+\lambda)/\lambda} \qquad \textbf{(l.35)}$$

$$k_{rg} = k_r(S_{wi})\,(S_g*)^2\,[1-(1-S_g*)^{(2+\lambda)/\lambda}]$$

where

$$S_o* = \frac{S_o - S_{oc}}{1 - S_{wi} - S_{oc}} \qquad \textbf{(l.36)}$$

$$S_g* = \frac{S_g}{1 - S_{wi}}$$

$k_r(S_{wi})$ is relative permeability at interstitial water saturation, λ is pore size distribution parameter, and S_{oc} is critical oil saturation. $k_r(S_{wi}) = 0.8$, $\lambda = 2$, and $S_{oc} = 0.1$ is used to generate Set A curves (**Fig. l.10**).

TABLE 2 RESERVOIR PROPERTIES USED IN SIMULATIONS

Water Compressibility, psi^{-1}	$2.67 \cdot 10^{-6}$
Rock Compressibility, psi^{-1}	$5.00 \cdot 10^{-6}$
Reservoir Height h, ft	200
Porosity ϕ, %	30
Absolute (horizontal) Permeability k, md	6
Relative Permeability at S_{wi}	0.8
Irreducible Water Saturation S_{wi}, %	25
Reservoir Area, acres	650
Gas Plateau Rate, MMscf/D	40
Minimum BHFP p_{wfmin}, psia	1500

TABLE 3 KEY RESERVOIR FLUID PROPERTIES

	Rich Gas A	**Lean Gas B**
Initial Reservoir Pressure, psia	6500	5500
Initial Reservoir Temperature, ^oF	266	315
Dewpoint Pressure, psia	5900	5400
Maximum CVD Liquid Dropout V_{roCVD}, %	24	2
Initial Solution OGR r_{si}, STB/MMscf	175	45
STO API Gravity, ^oAPI	55	45

Separator conditions. Stage 1 p = 375 psia and T = 108^{o}F, Stage 2 p = 14.7 psia and T = 60^{o}F.

TABLE 4 NUMERICAL MODEL GRID DATA.

Grid Description		Grid Dimension, ft
Radial Well Grid		
Radial coordinates. Total radius r_e = 3000 ft. Skin s = 0 in **Eq. (l.25)**, used in **Eqs. (l.23)-(l.24)**.		0.53 0.89 1.39 2.15 3.35 5.20 8.07 12.53 19.46 30.23 36.94 72.9 113.2 175.01 273.01 423.97 658.41 1022.49 1587.88 2465.9
Vertically Fractured Well Grid		
Cartesian coordinates. One quarter of the well simulated. Equal model width and length of 2658.5 ft. Fracture grid k = 10,000 md. Skin s = -4 in **Eq. (l.25)**, used in **Eqs. (l.23)-(l.24)**.	Δx	2*15 7*10 2*50 3*100 100 100 15*137.2
	Δy	3 0.83 1.53 2.81 5.15 9.44 17.31 58.24 106.82 195.92 359.34 659.06 1207.8
Horizontal Well Grid		
Cartesian coordinates. One eighth of the well simulated (1/2 reservoir height and 1/4 area). Equal model width and length of 2658.5; model height of 100 ft. Skin s = -4 in **Eq. (l.25)**, used in **Eqs. (l.23)-(l.24)**.	Δx	100 2*50 8*10 2*100 2*200 300 400 500 458
	Δy	3 0.83 1.53 2.81 5.15 9.44 17.31 58.24 106.82 195.92 359.34 659.06 1207.8
	Δz	3 0.83 1.53 2.81 5.15 9.44 17.31 31.75 28.18

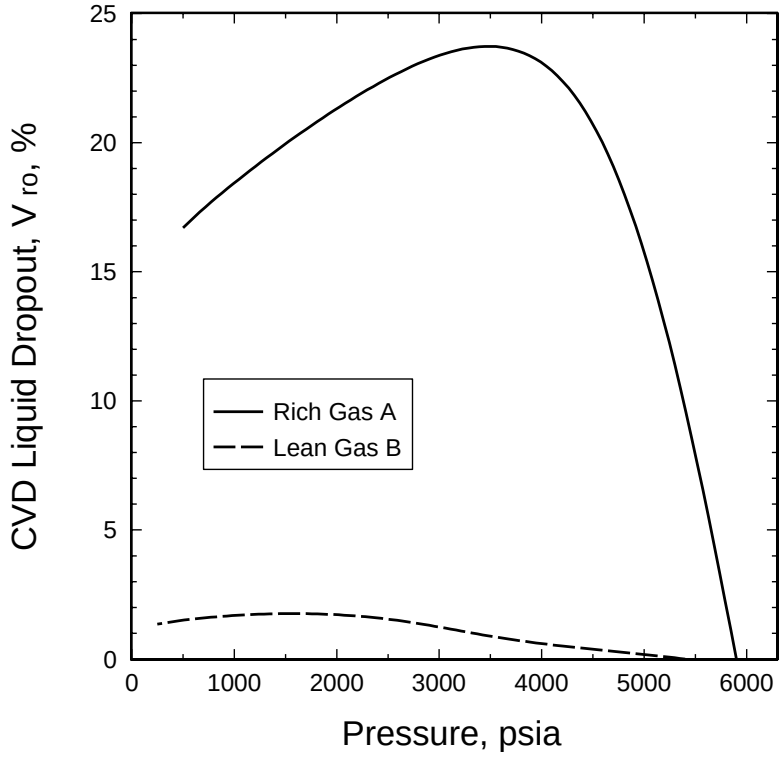

Fig.l.6 CVD liquid dropout curves for reservoir fluids Rich Gas A and Lean Gas B.

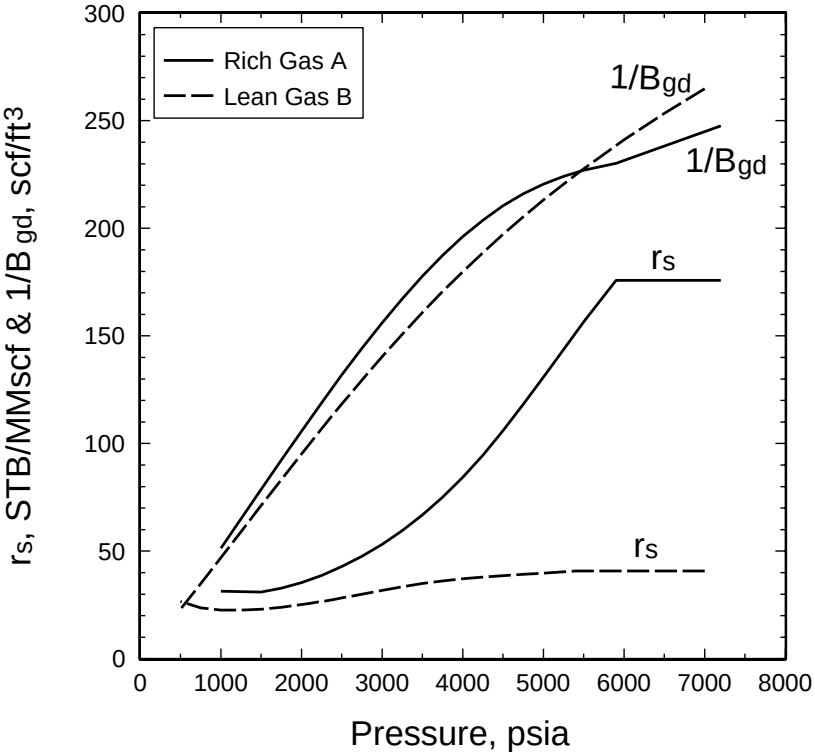

Fig. l.7 Black-oil PVT data for Rich Gas A and Lean Gas B. Gas phase properties r_s and B_{gd}.

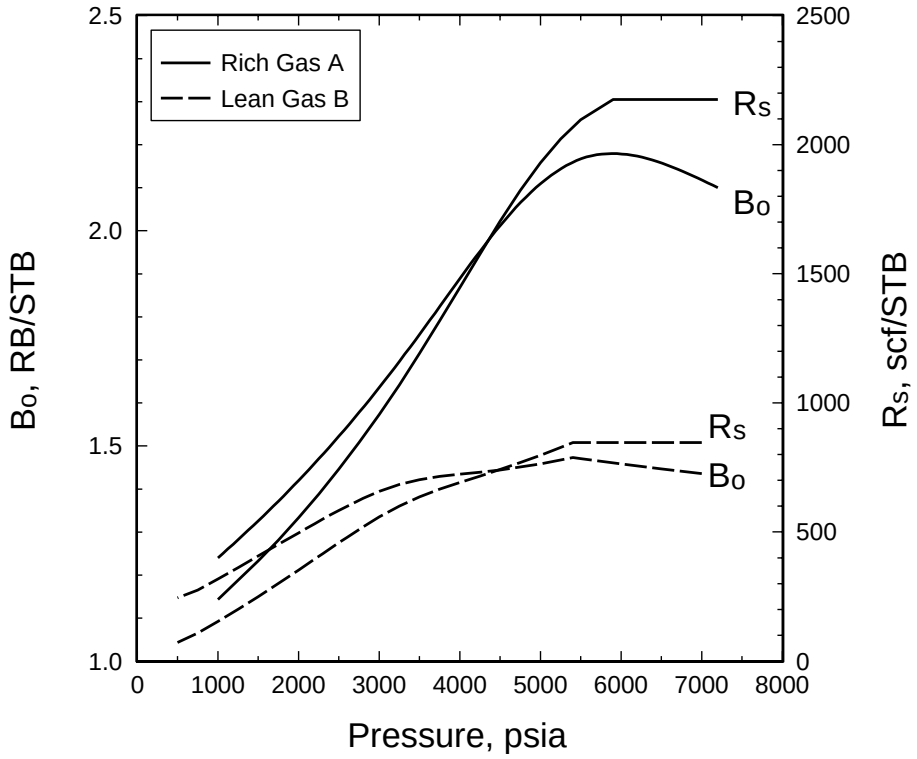

Fig. l.8 Black-oil PVT data for Rich Gas A and Lean Gas B. Oil phase properties R_s and B_o.

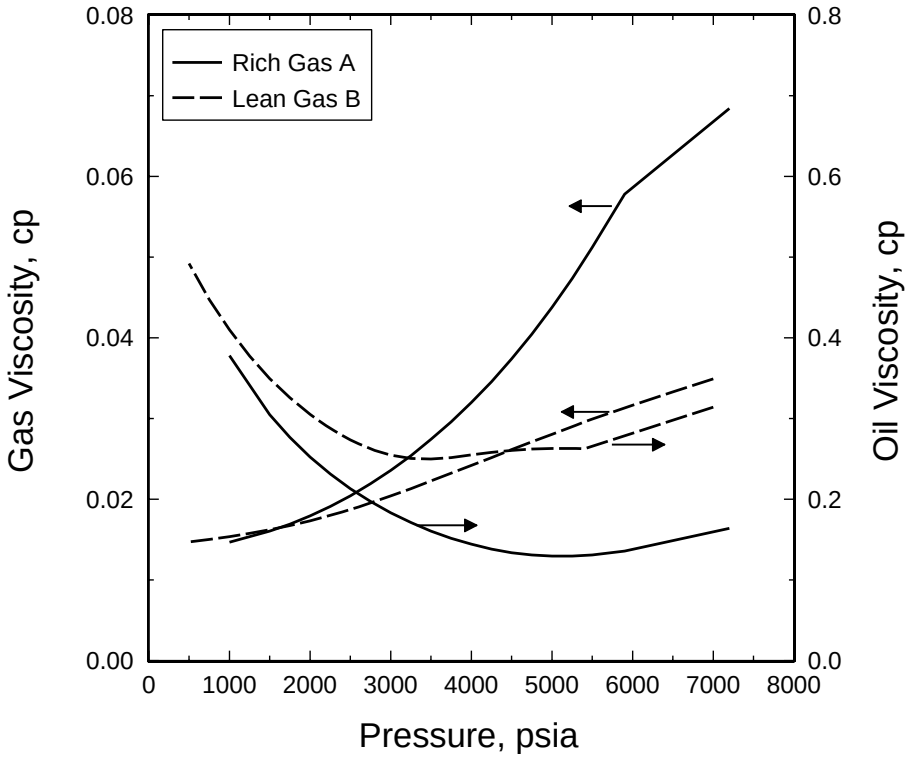

Fig. l.9 Black-oil PVT data for Rich Gas A and Lean Gas B. Gas and oil phase viscosities.

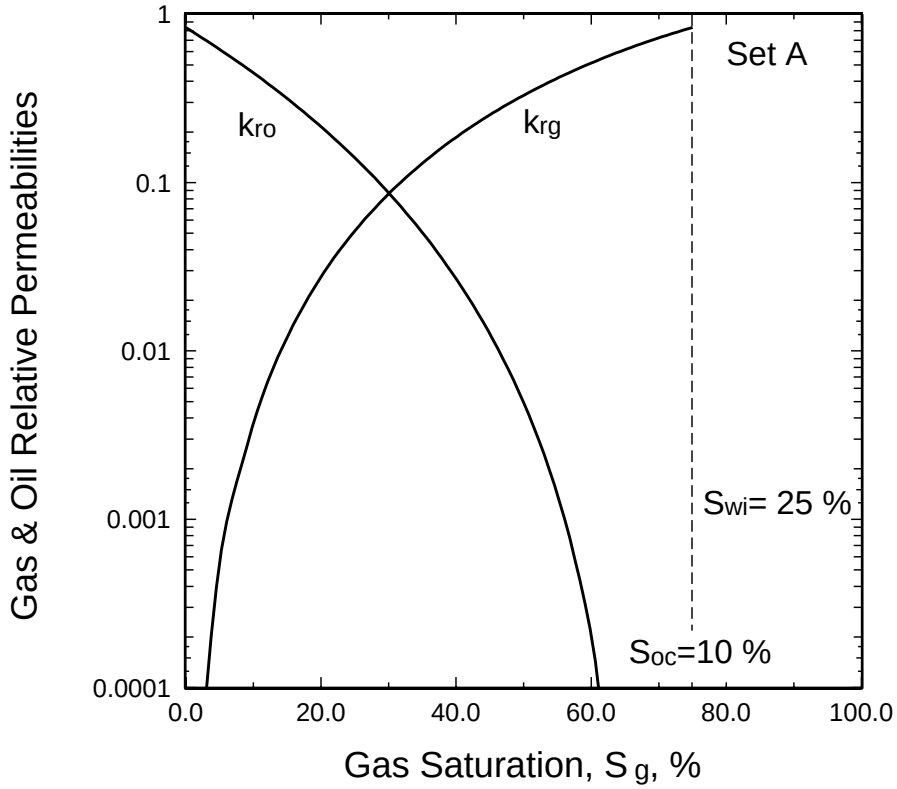

Fig. l.10 Set A gas and oil relative permeability curves used in simulations.

Calculating Pseudopressure

Gas rate is calculated with the analytical gas flow equation using the using the method proposed here (*"Proposed Method"*) for determining pseudopressure in **Eq. (l.24)**. It uses the same black-oil PVT data as used in the simulation. The producing GOR, BHFP, and average reservoir pressure as a function of time are taken from the results obtained by the simulator.

To demonstrate the effect that Region 2 has on well deliverability, gas rate is also calculated using producing GOR equal to $1/r_s$ (r_s evaluated at p_R). The same method is used to determine the pseudopressure. This approach represents a simplified model where only Region 1 and Region 3 exist when the average reservoir pressure is above the dewpoint pressure, and only Region 1 exists when the average reservoir pressure is below the dewpoint. For these calculations, BHFP and average reservoir pressure as a function of time are taken from the simulator. This calculation approach is equivalent to using a material balance method based on a simple CVD depletion process (*"CVD MB Method"*), which also implies that Region 2 doesn't exist.

Radial Well - Lean Gas B

The production forecast for a radial well producing Lean Gas B is shown in **Fig. l.11**. The circles represent simulation results. The solid line represents the gas rate

calculated with the Proposed Method to evaluate the pseudopressure integral. The productivity index (PI) constant C that multiplies the pseudopressure function in the rate equation is calculated from **Eq. (l.25)**, with skin equal to zero.

The dashed line represents the results of the case where $R_p = 1/r_s(p_R)$ is used to evaluate the pseudopressure integral ("CVD MB Method"). Note that the difference in the producing GOR for the two methods is small, while the difference in production rate is large (**Fig. l.11**). The dot-dashed line also represents results using the "CVD MB Method", but with BHFP p_{wf} = 1500 psia (constant for all times).

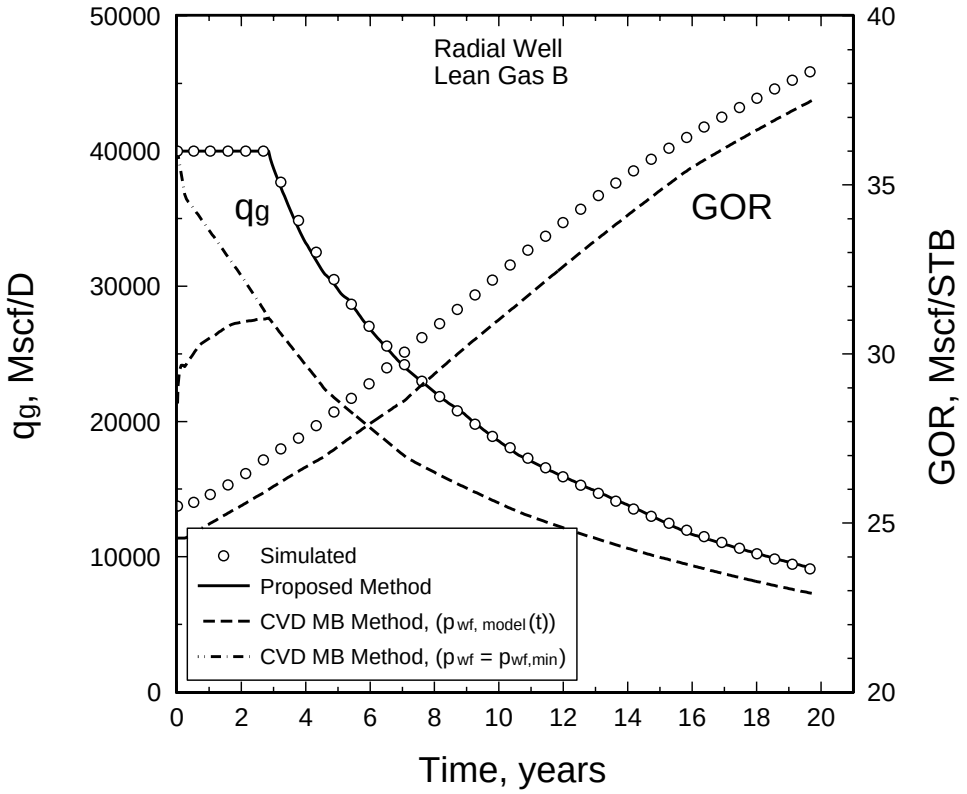

Fig. l.11 Well performance for a radial well with Lean Gas B. Comparison of fine-grid simulation with proposed pseudopressure method (and with approximate CVD MB method).

The deliverability loss is greatly over predicted using the CVD MB Method. This is because the condensate saturation needed to mobilize oil throughout the reservoir is relatively high, yielding a low gas relative permeability ("blockage") throughout the reservoir. The actual condensate saturation in Region 2 is close to the CVD liquid dropout corrected for initial water saturation. Thus, Region 2 has a much higher gas relative than predicted using the CVD MB Method, and particularly for lean gas condensates.

The pseudopressure function for the three cases "Proposed Method", "CVD MB Method", and the "Only Region 2" are shown in **Fig. l.12**. The pseudopressure

function for "Only Region 2" is evaluated assuming that only Region 2 exists throughout the reservoir. The difference between the area under the Proposed Method and "Only Region 2" curves, multiplied with the constant C in the rate equation, gives the deliverability loss due to the existence of Region 1. This deliverability loss is customarily referred to as condensate blockage.

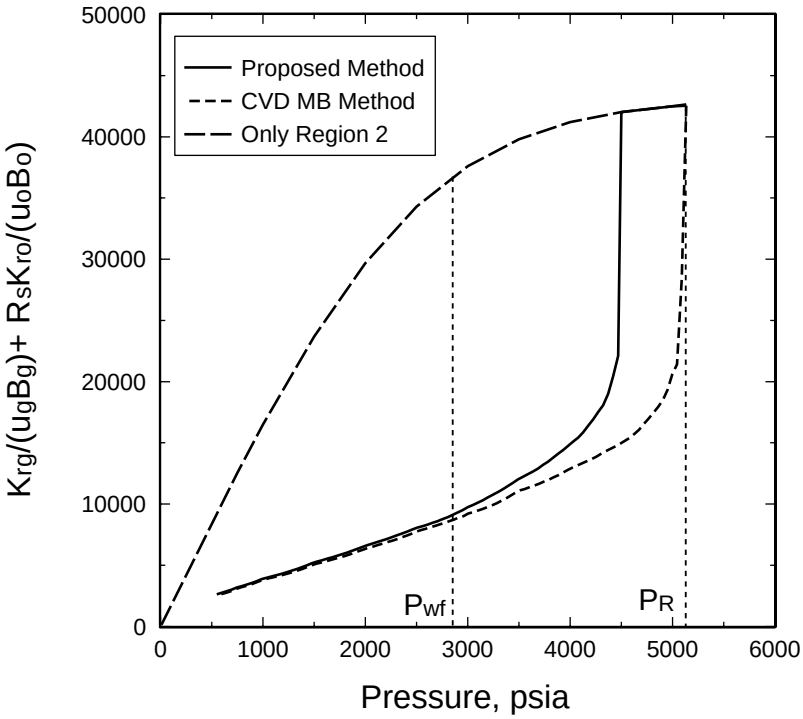

Fig. l.12 The integrand in the pseudo pressure function, for Lean Gas B after 1 year of production. The pseudo pressure is the area under the curve between p_{wf} and p_R

Radial Well - Rich Gas A

The same radial well simulation is run with Rich Gas A. Results are given in **Fig. l.13**. The Proposed Method for evaluating pseudopressure overlays the simulated results almost exactly. The simplified CVD MB method gives accurate results only while Region 2 is small or non existent. A situation of a small (and unimportant) Region 2 exists while the reservoir is sufficiently undersaturated such that $R_p \approx 1/r_{si}$ (or late in depletion when Region 1 is large).

The deliverability loss due to Region 1 with Rich Gas A is much larger than with Lean Gas B. This is because both the size of Region 1, and the condensate saturation in Region 1 increases (see **Figs. l.4 and l.5**). The condensate saturation in Region 1 is higher because the reservoir gas entering Region 1 is richer and looses more dissolved condensate in Region 1 than Lean Gas B (see r_s vs. p, in **Fig. l.7**). The deliverability loss in Region 2 is also significant in this case because the condensate saturation in Region 2 is about 20% ($k_{rg} \approx 0.4$).

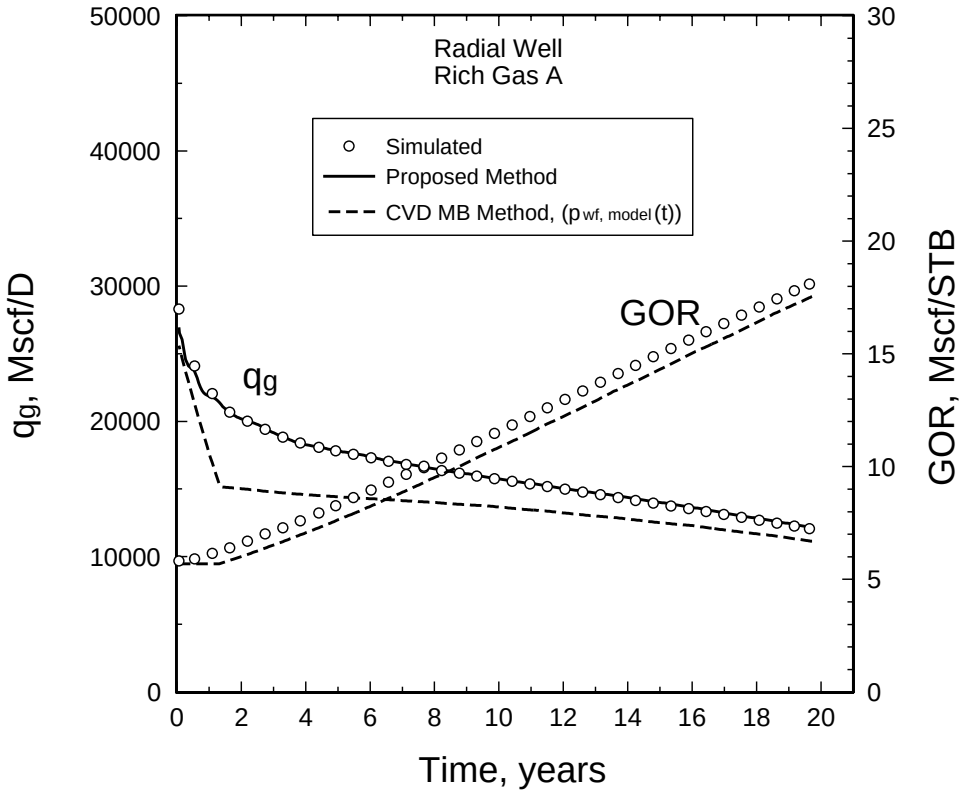

Fig. l.13 Well performance for a radial well with Rich Gas A. Comparison of fine-grid simulation with proposed pseudopressure method (and with approximate CVD MB method).

Vertically Fractured Well - Rich Gas A

A well with a vertical fracture was simulated using the 2D cartesian grid given in **Table 4** (420 grid cells). The results are plotted as circles in **Fig. l.14** .

Before making calculations with **Eq. (l.24)**, the productivity index C had to be determined. The well was simulated producing at a constant gas rate at high pressure (10,000 psia) where only single-phase gas flows. The productivity index C was then calculated by solving the single-phase rate equation for the productivity index C with the reservoir average reservoir pressure and BHFP taken from the simulated pseudosteady state pressure performance.

Using the Proposed Method for calculating pseudopressure, we obtained the rates given by a solid line in **Fig. l.14**. The results are very accurate, overlaying the simulation results with only slight deviation at late times.

The results from **Fig. l.14** show the calculations based on the CVD MB Method with $R_p=1/r_s(p_R)$. Well deliverability is severely underpredicted, except for very late in the depletion. Again, the largest deviations occur when Region 2 is largest (1-3 years).

Another observation from **Fig. l.14** is that the producing GOR after 17 years of production is actually somewhat lower than $1/r_s(p)$. The main reason is that the "steady-state" condensate saturation in Region 1 decreases with time because the reservoir gas entering Region 1 gets leaner with depletion. This observation is in contrast to the common misinterpretation that condensate has a meaningful mobility throughout the reservoir.

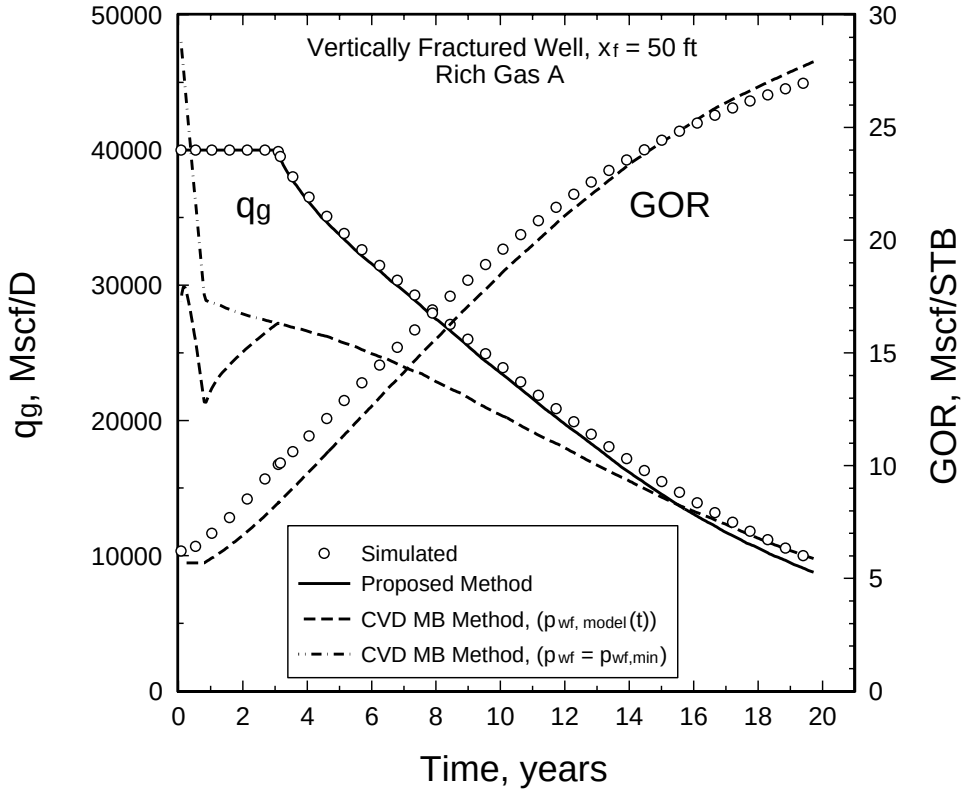

Fig. l.14 Well performance for a vertically fractured well with Rich Gas A. Comparison of fine-grid simulation with proposed pseudopressure method (and with approximate CVD MB method).

Horizontal Well - Rich Gas A

A horizontal well was simulated using the 3D cartesian grid given in **Table 4** (2223 grid cells). Simulation results are given as circles in **Fig. l.15**.

Again, the productivity index C in **Eq. (l.24)** was back-calculated from the well's simulated pseudosteady state pressure performance with single-phase gas at high pressures (10,000 psia).

Gas rates calculated using the Proposed Method are shown with a solid line in **Fig. l.15**. The results match accurately the simulation throughout the 20 years of production (solid line in **Fig. l.15**).

Calculations based on the CVD MB Method with $R_p=1/r_s(p_R)$ underpredicts well

deliverability at all times. The largest deviation occurs when the effect of Region 2 is most significant (1-3 years).

An important observation is that the deliverability of a well with a 50-foot fracture half-length is the same as the deliverability of a 1000-foot long horizontal well!. This result is for a common vertical-to-horizontal permeability ratio k_v/k_h=0.1. Using permeability ratio k_v/k_h=1, the plateau period increases from 3.0 to 9.5 years. This extreme sensitivity to k_v/k_h ratio does not exist for vertically fractured wells. Thus, if horizontal wells are being considered for the development of a gas condensate reservoir, the k_v/k_h ratio should be determined with certainty to avoid overly optimistic production forecasts.

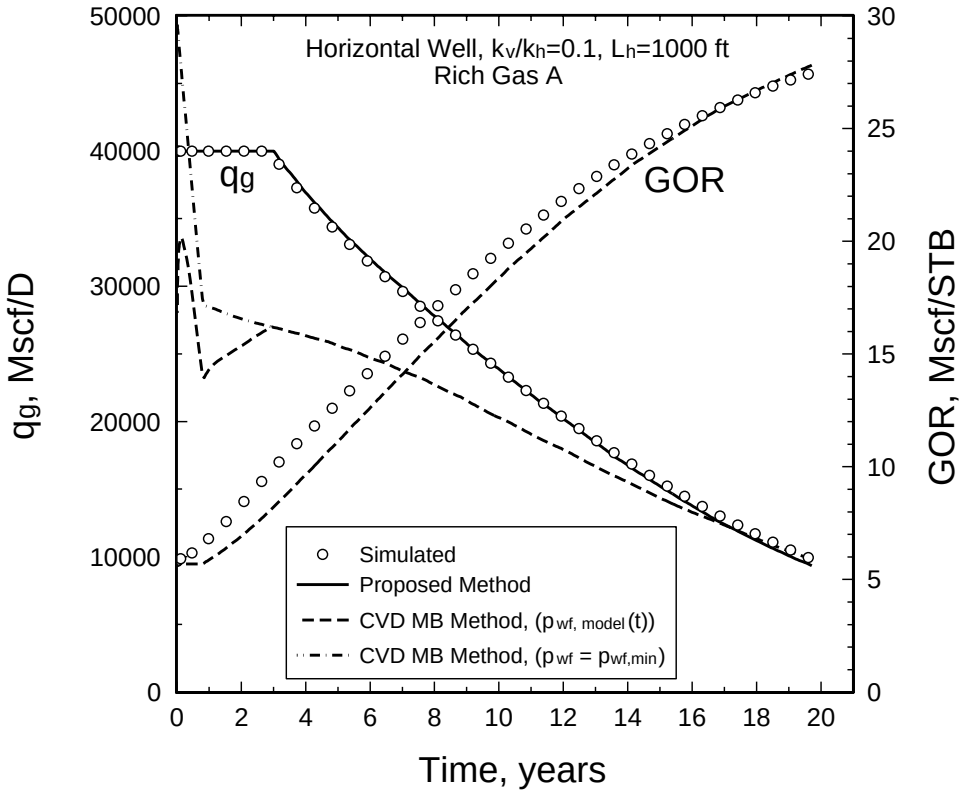

Fig l.15 Well performance for a horizontal well (k_v/k_h=0.1) with Rich Gas A. Comparison of fine-grid simulation with proposed pseudopressure method (and with approximate CVD MB method).

1.6. Multiphase Treatment of Wells In Coarse Grid Simulation

1.6.1. Description of The Proposed Multiphase Pseudopressure Method

The main conclusion from the previous section is that the Proposed Method for calculating the pseudopressure function is accurate for a gas condensate well independently of production mode or well geometry, as long as the producing GOR is known accurately. This has important implications to numerical simulation of gas

condensate fields using coarse-grid models.

In full-field studies, grid refinement has traditionally been used (and needed) to compute well deliverability loss due to Region 1 (condensate blockage). Coarse-grid simulations without grid refinement results in far too optimistic well deliverability, particularly for lean gas fluids.

Based on numerous coarse-grid simulations it was observed that the producing GOR is accurately predicted. Because the producing GOR in coarse-grid simulations are generally accurate, it was apparent that the proposed pseudopressure method should be considered for calculating BHFP from well grid-cell pressure.

Conversion from grid-cell pressure to BHFP for a gas well is usually made using the radial flow equation with a well index J, where $p_{wf} = p_{grid} - q_g/J$. The productivity index, J, is a productivity index consisting of a productivity constant C_{grid}, fluid properties, and k_{rg},

$$J = C_{grid} \frac{k_{rg}}{\mu_g B_{gd}} \qquad \textbf{(I.37)}$$

k_{rg}, μ_g, and B_{gd} are evaluated at average conditions in the well grid-cell. The production rate calculated using conventional approach is then given by

$$q_g = C_{grid} \frac{k_{rg}}{\mu_g B_{gd}} (p_{grid} - p_{wf}) \qquad \textbf{(I.38)}$$

Alternatively the production rate can be calculated using pseudopressure approach,

$$q_g = C_{grid} \Delta p_p \qquad \textbf{(I.39)}$$

where Δp_p is evaluated between p_{grid} and p_{wf}.

Peaceman's equation(s)[38] are usually used in reservoir simulators to calculate the productivity constant C_{grid}. However it was found in this study that more accurate productivity constants were obtained using results from single-phase simulations with a fine grid. The productivity constant C_{grid} for the coarse-grid model were calculated using **Eq. (I.39)** and well grid-cell pressures from a single phase coarse-grid simulation and BHFPs from a single phase fine-grid simulation (with the same production rate for the two models).

In a simulator, all PVT and relative permeability properties are available in each grid-cell. For the sake of efficiency, the pseudopressure function Δp_p can be calculated during initialization for several producing GORs, and then stored as a three-dimensional pseudopressure table $\Delta p_p(p_{wf},p_{grid},R_p)$. Conceivably a different Δp_p function needs to be generated for each PVT/relative permeability region. In the most general case, Δp_p can be stored as a four-dimensional table to handle changing water saturations, $\Delta p_p(p_{wf},p_{grid},R_p,S_w)$.

The accuracy of coarse grid simulation models using the proposed pseudopressure approach for well calculations has been tested using Intera's ECL100 simulator. The pseudopressure table was incorporated in the simulator using a "pseudo" tubing table (as the source code was unavailable). To obtain the grid-cell pressure, an "infinite" well index was used such that the model calculated BHFP equals the grid-cell pressure. The pseudo-tubing table then converts the model calculated "BHFP" to the actual BHFP, based on gas rate and producing GOR.

The pseudo-tubing table approach can be used as a general solution to problems where the well produces from several layers that are in vertical communication (i.e. experiencing reservoir crossflow). However, the approach is not recommended for wells producing from layered no-crossflow systems. The best general solution is to have the well pseudopressure tables generated for each PVT/relative permeability region at initialization, so that any grid-cell that becomes a well grid will automatically have the multiphase pseudopressure method available.

1.6.2. Verification of Coarse Grid Simulation Using Pseudopressure

Coarse Radial Grid

The size of the first near-wellbore grid cells in a radial simulation can be important in accurate prediction of well deliverability in gas condensates. This is shown in **Fig. l.16** where Lean Gas B is used with a first-grid-cell radius of 100 ft (versus 0.7 ft in the fine-grid simulation); the remaining grids are spaced logarithmically. The circles represent the fine-grid simulation results and the dashed line represents the coarse-grid simulation results using the standard well treatment [**Eq. (l.37)**]. The plateau period is more than doubled, from 2.5 years for the fine-grid simulation to 6.25 years for the coarse-grid simulation. Even for an 18 ft inner radius, the plateau period is overpredicted by more than one year. Note that the computed producing GOR is very good for the coarse model as long as the production rates are equal.

The importance of the first-grid-cell size is easiest to understand by looking at condensate saturation distribution as a function of time for the fine-grid results shown in **Fig. l.4**. As seen from the figure, the size of Region 1 reaches about 100 ft first after 10 years of production. Since the conversion from grid-cell pressure to BHFP is done using J [**Eq. (l.37)**] evaluated at average grid properties (pressure, saturation), a much too high k_{rg} is used in the conversion.

Using the multiphase pseudopressure method (based on a pseudo-tubing curve), the correct plateau period of 2.5 years is predicted and the rate-time performance overlays the fine-grid simulation results (solid line). Using the same coarse-radial grid (r_1=100 ft) but with Rich Gas A, the proposed pseudopressure method again predicts the rate-time performance accurately (**Fig. l.17**). Again, the coarse-grid model overpredicts the production rates, but not as much as in the case of the Lean Gas B because Region 1 is much larger for Rich Gas A (**Fig. l.5**).

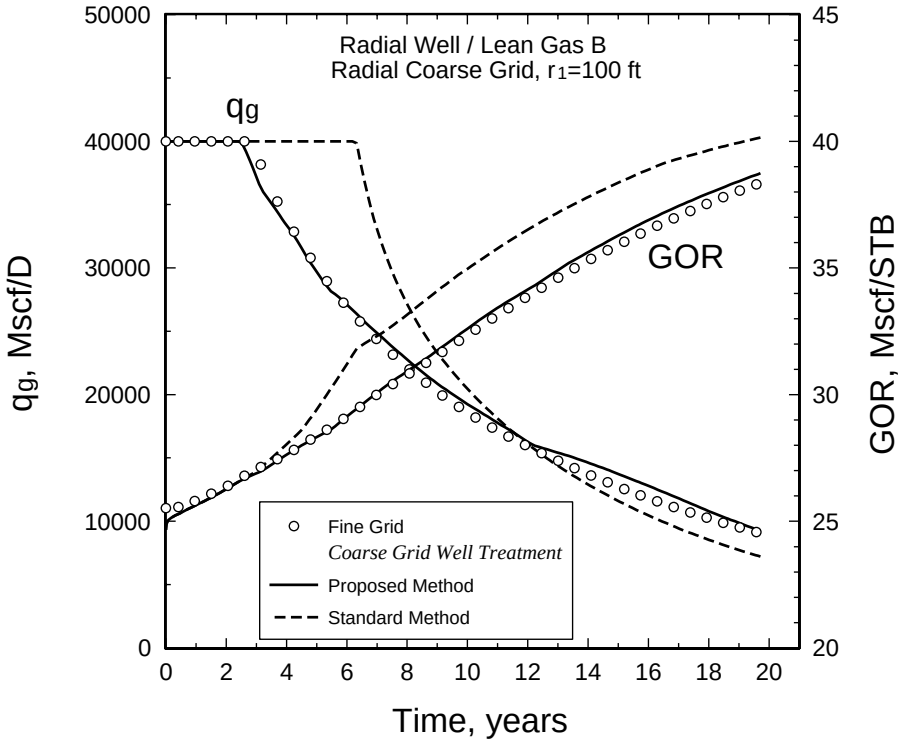

Fig. l.16 Well performance for a radial well with Lean Gas B. Comparison of fine-grid simulation with radial coarse-grid simulation using proposed pseudopressure method for calculating well BHFP.

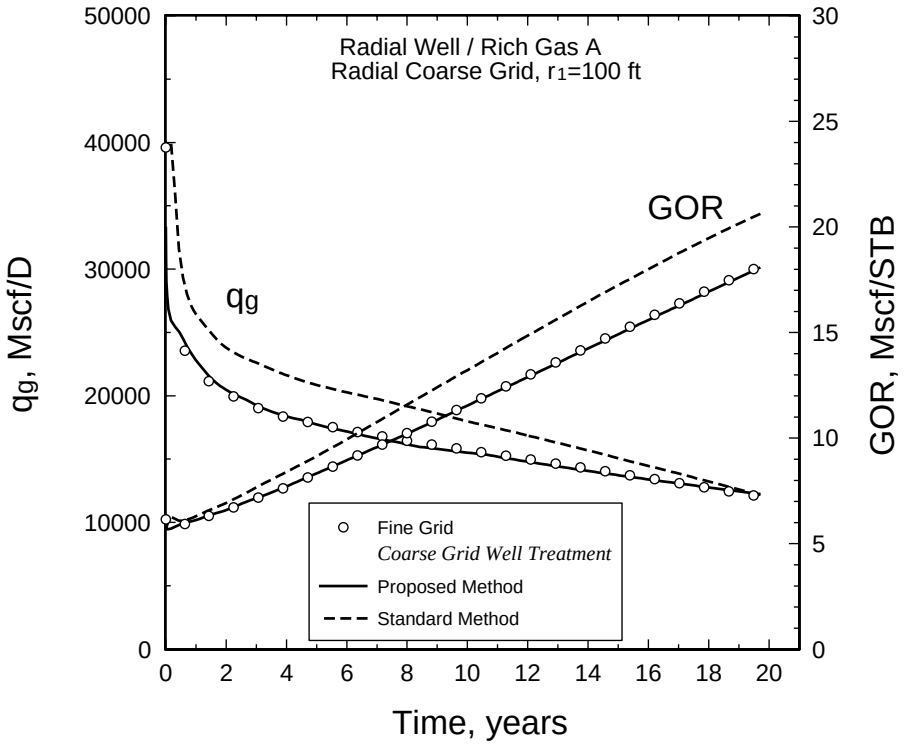

Fig. l.17 Well performance for a radial well with Rich Gas A. Comparison of fine-grid simulation with radial coarse-grid simulation using proposed pseudopressure method for calculating well BHFP.

Coarse Cartesian Grid

The proposed multiphase pseudopressure method using a coarse cartesian grid with a 200x200 ft well grid-cell was also compared with the fine radial grid simulation for Lean Gas B. The computed rate-time performance is shown in **Fig. l.18**. The results are very good when the pseudo-tubing table are used (coarse grid pseudopressure method). Note that the standard well treatment approach [**Eq. (l.37)**] results in a plateau of 6 years compared with the fine-grid plateau of 2.5 years.

The proposed multiphase pseudopressure method was compared with 2D fine-grid simulation results for a vertically fractured well using Rich Gas A. The simulation used a coarse cartesian grid with a 500x500 ft well grid-cell. The rate-time performance is accurately calculated using the proposed pseudopressure method (**Fig. l.19**). The standard well treatment results in a plateau of 6 years compared with the fine grid plateau of 3 years.

The proposed multiphase pseudopressure method was compared with a fine-grid 3D horizontal well simulation for Rich Gas A. The simulation used a coarse cartesian grid with 333x333x25 ft well-grid cells. The rate-time performance is accurately calculated using the coarse-grid pseudopressure method (**Fig. l.20**). The standard well treatment results in a plateau of almost 6 years, compared with the fine-grid plateau of 3 years.

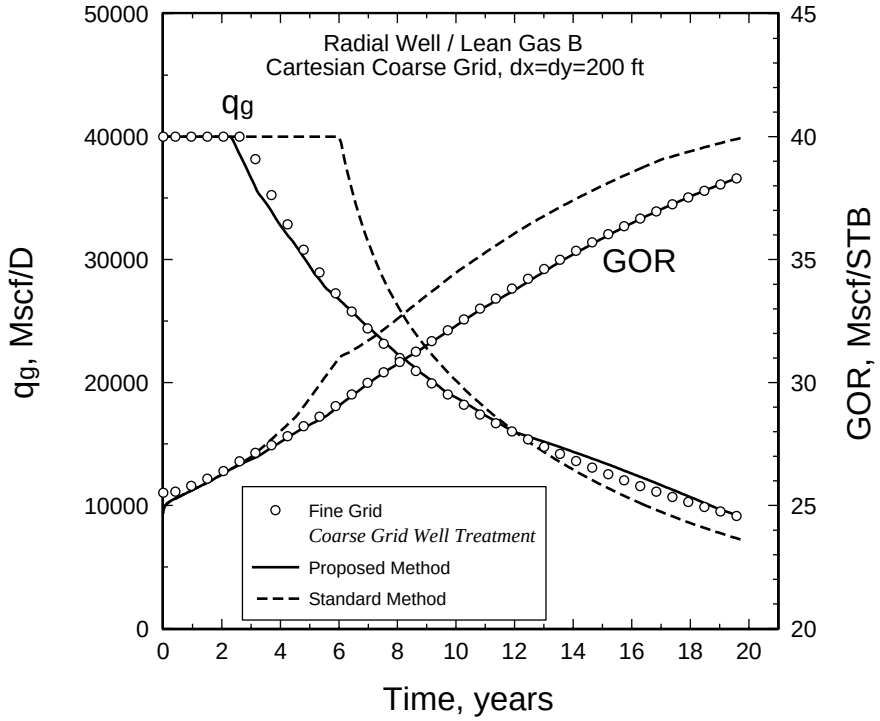

Fig. l.18 Well performance for a radial well with Lean Gas B. Comparison of fine-grid simulation with cartesian coarse-grid simulation using proposed pseudopressure method for calculating well BHFP.

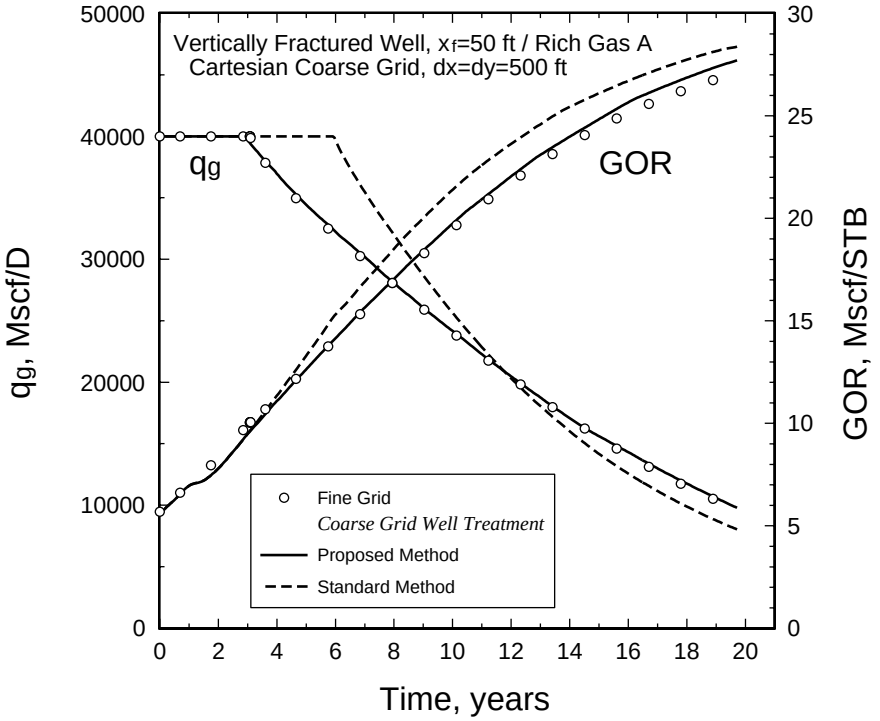

Fig. l.19 Well performance for a vertically fractured well with Rich Gas A. Comparison of fine-grid simulation with cartesian coarse-grid simulation using proposed pseudopressure method for calculating well BHFP.

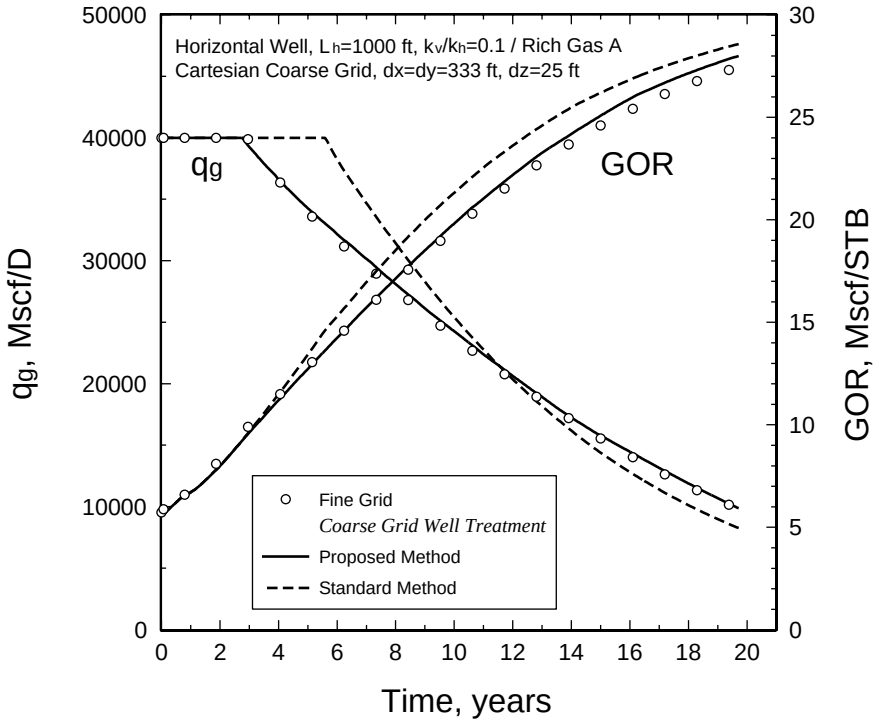

Fig. l.20 Well performance for a horizontal well with Rich Gas A. Comparison of fine-grid simulation with coarse-grid simulation using proposed pseudopressure method for calculating well BHFP.

1.6.3. Discussion of Coarse Grid Simulation Using Pseudopressure

It is shown that local grid refinement around gas condensate wells is not necessary if the proposed multiphase pseudopressure method is used to convert well grid pressure to BHFP. The only requirement is that the producing GOR from the coarse-grid model is reasonably accurate when compared with a fine-grid model.

The proposed multiphase pseudopressure method eliminates Region 2 *in the well grid-cell*. However, the more important Region 1 behavior is treated accurately in the well grid-cell. Surrounding grid-cells automatically treat most of the Region 2 pressure losses. Obviously, if the size of the well grid-cell becomes too large, Region 1 pressure losses will be overestimated because the producing GOR will be too low. In the extreme case, when using a single simulation grid-cell, results with the pseudopressure method will be equivalent to the CVD MB Method (which always underestimates well deliverability).

The maximum size of the well grid-cell depends on (1) the leanness of the gas condensate, (2) the minimum well plateau length, and (3) the degree of gas undersaturation. Smaller well grids are needed for lean gas condensates, short plateau periods, and initially-saturated fluids. In other words, the smallest well grid size is required for a saturated lean gas condensate where production rate decline starts immediately.

In practical applications of the proposed pseudopressure method in coarse-grid simulation, a few sensitivity cases can be run to determine the required well grid size for a given gas condensate reservoir. These cases should evaluate wells producing at the maximum expected rate (dictated by equipment constraints such as tubing diameter and erosional velocity). A simulation case with initial pressure equal to the dewpoint should be used, even for highly undersaturated reservoirs (to evaluate a "late" well being drilled after reservoir depletion reached the dewpoint).

1.7. Compositional vs. Black-Oil PVT Formulation

Radial well simulations presented by Coats[39] show that a modified black-oil PVT formulation gives the same results as a fully compositional Equation of State (EOS) PVT formulation. Results are given for a rich gas condensate producing on rate decline for 8 years. The EOS fluid characterization uses seven components with *one* C_{7+} fraction.

Results from Coats' example should probably be used with caution. A serious limitation is that only one C_{7+} fraction is used in the EOS fluid characterization. With a more detailed C_{7+} split, the difference in oil viscosity between black-oil and compositional formulations may yield noticeable differences in well deliverability.

The problem is illustrated through computations performed here and presented in **Fig. l.21** where oil viscosity is plotted versus pressure for several depletion stages. The solid line represents black-oil data, and the symbols represent results taken from compositional simulation of Rich Gas A. The figure shows that differences in oil viscosities between a compositional and a black-oil approach increases significantly during depletion. The oil viscosity in the black-oil model is calculated based on the oil composition in a CVD cell as a function of pressure. This oil is the condensate in Region 2 that never actually flows. The condensate flowing in Region 1 is part of the condensate dissolved in the single phase gas entering Region 1. This condensate is leaner then in Region 2 and contains more of the lighter C_{7+} fractions, particularly late in depletion. Consequently, the viscosity of the mobile condensate is much lower.

The oil mobility required to flow condensate in Region 1 is basically fixed. Thus a lower oil viscosity in the compositional simulation results in a lower oil relative permeability and lower oil saturation than in the black-oil simulations. Lower oil saturation results in higher gas relative permeability and better well deliverability for the compositional simulations (**Fig. l.22**), in comparison with the black-oil method.

It is proposed that this problem can be improved using a modified $\mu_o(p)$ relationship in the black-oil simulator. The dashed line in **Fig. l.21** passes through the "important" compositional results (data at pressures lower than the point where μ_o reaches a minimum). This same trend can be determined using a PVT simulator. It is shown here that when the modified $\mu_o(p)$ relation is used in a black-oil reservoir simulation, rate-time behavior is closer to compositional results (dashed line in **Fig. l.22**).

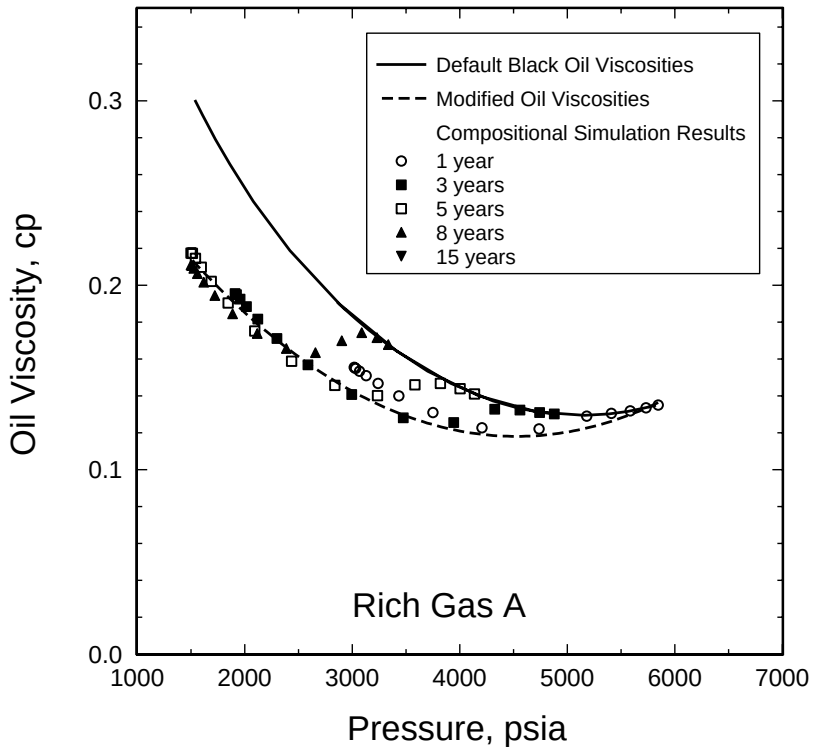

Fig. l.21 Changing oil viscosities as a function of pressure for black-oil and compositional PVT models.

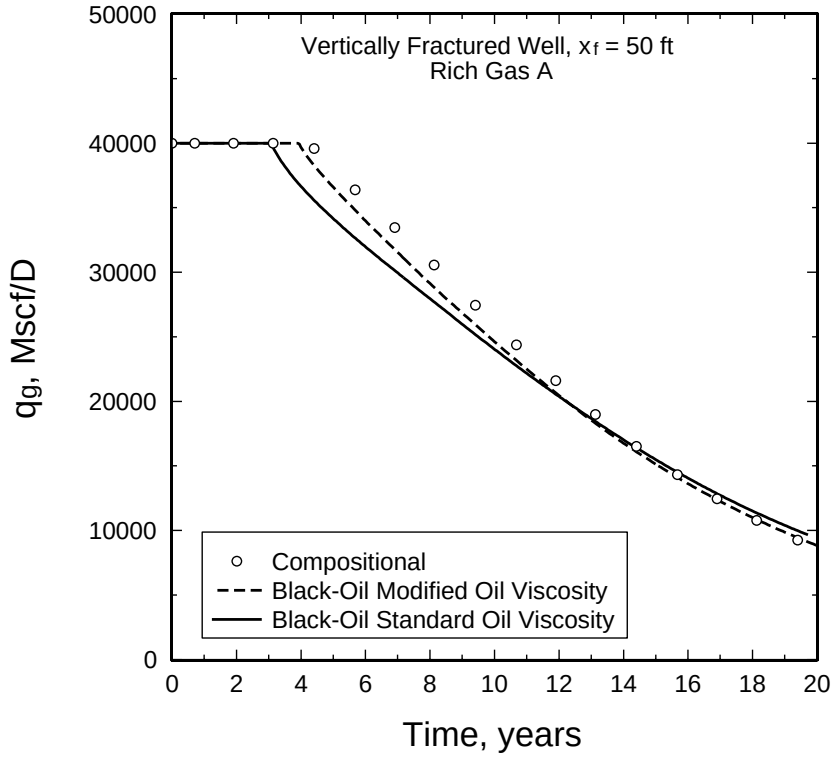

Fig. l.22 Effect of oil viscosity on well deliverability for black-oil and compositional simulations of a vertically fractured well with Rich Gas A.

1.8. Relative Permeability Effects

1.8.1. Primary Functional Relationship $k_{rg} = f(k_{rg}/k_{ro})$

Deliverability loss of a well due to condensate blockage is attributed mainly to Region 1 contribution to the pseudopressure integral (see **Fig. l.12**). This contribution is calculated through a relationship between k_{rg} and the ratio k_{rg}/k_{ro}. (It is readily shown that the oil contribution to the pseudopressure integral is negligible.) **Fig. l.23** shows a plot of k_{rg} vs. (k_{rg}/k_{ro}) based on the widely used Corey equation[37], using different pore size distribution parameters λ. Note that in **Fig. l.23** gas relative permeability is normalized with respect to $k_{rg}(S_{wi})$ $[k_{rg}(S_{wi}) = 1]$.

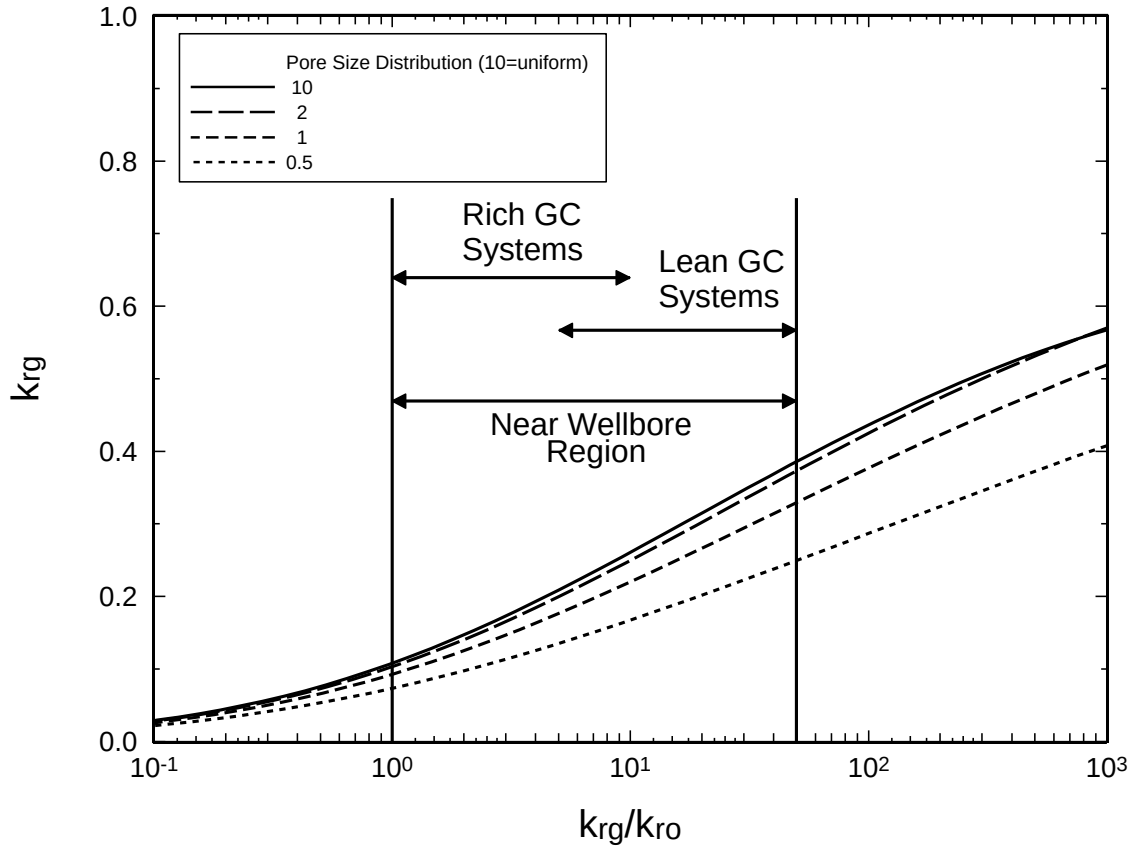

Fig. l.23 Generalized k_{rg} vs. k_{rg}/k_{ro} plot based on the Corey relative permeability model. Important range of k_{rg}/k_{ro} in near-wellbore Region 1 is defined.

For any *flowing mixture* in Region 1 the relevant range of (k_{rg}/k_{ro}) that extends from the dewpoint to the minimum BHFP can be found directly from PVT properties and **Eq. (l.29)**. The flowing mixtures in Region 1 are readily obtained from the gas composition in a CVD experiment at different stages of depletion. The richest gas that will enter Region 1 is the original reservoir gas.

Calculation of $k_{rg}/k_{ro}(p)$ from **Eq. (l.30)** can be done with a PVT simulator. Calculated results for the Rich Gas A and the Lean Gas B are shown in **Figs. l.24-l.25**, together with plots of $V_{roCCE}(p)$. The lowest k_{rg}/k_{ro} ratio of interest can be read straight from the $k_{rg}/k_{ro}(p)$ curve for the initial fluid. The upper limit for k_{rg}/k_{ro} of interest is about 10 for richer gas condensates and about 50 for leaner gas condensates. An upper limit ratio of 50 will apply practically for all gas condensates because: (1) k_{rg} is relatively high for k_{rg}/k_{ro} ratios higher than 50 (**Fig. l.23**); (2) k_{rg}/k_{ro} ratios higher than 50 only exists in the outer part of Region 1; and (3) k_{rg} can be extrapolated to higher (k_{rg}/k_{ro}) ratios with a best-fit parametric relative permeability equation if $krg = f(k_{rg}/k_{ro})$ is well established for lower k_{rg}/k_{ro} ratios. The importance and implications of these observations is discussed below and in the following section.

To illustrate the importance of the k_{rg} vs. k_{rg}/k_{ro} relationship for well deliverability, a reservoir with Rich Gas A produced from a vertical (radial) well was simulated using relative permeability Set B (shown as solid lines in **Figs. l.26 and l.27**).

Another simulation case was set up with a set of relative permeability curves completely different for $k_{rg}/k_{ro} > 10$ (Set B'). Set B' is shown as the short dashed line in **Figs. l.26 and l.27**. The limiting ratio $k_{rg}/k_{ro} = 10$ was used in this case since the fluid is relatively rich. The key is that Set B and Set B' have the same k_{rg} vs. k_{rg}/k_{ro} relationship for all saturations as shown in **Fig. l.28**

The simulated rate-time performance using Set B and Set B' relative permeability curves are shown in **Fig. l.29**. The rate-time performance for these two cases are practically identical. These results are not a special case, but for all gas condensates k_{rg} vs. k_{rg}/k_{ro} is the governing relationship in Region 1, and not $k_{rg}(S_o)$ and $k_{ro}(S_o)$. In other words, the function k_{rg} vs. k_{rg}/k_{ro} dictates the well deliverability loss due to condensate blockage.

The consequence of this observation is particularly important for designing relative permeability measurements (the topic of Chap. 2). These findings simplify relative permeabilities measurements, and secure the relevant relative permeability data needed for modeling well deliverability in gas condensate reservoirs.

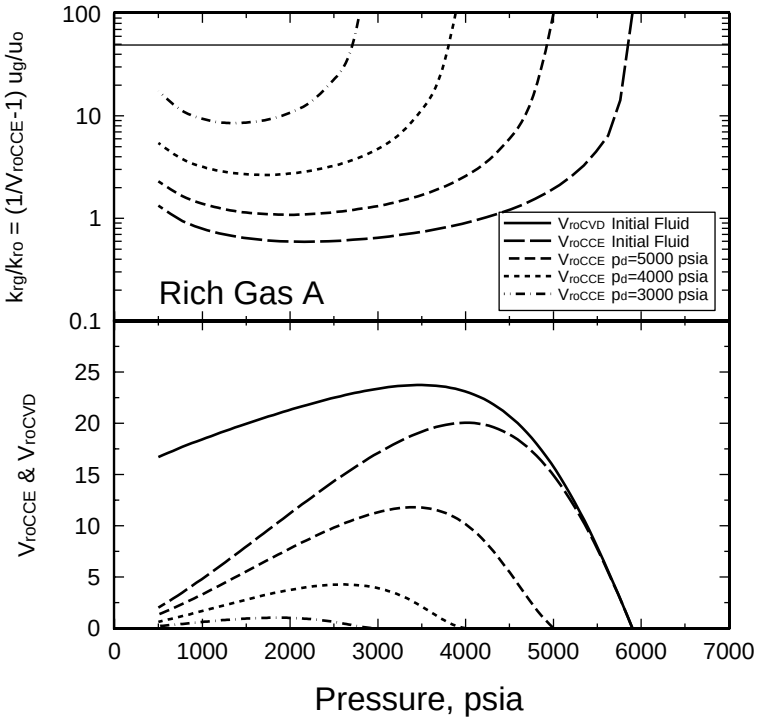

Fig. l.24 Diagnostic plots for Rich Gas A showing the variation of k_{rg}/k_{ro} (in Region 1) and CCE oil relative volume as a function of pressure during depletion.

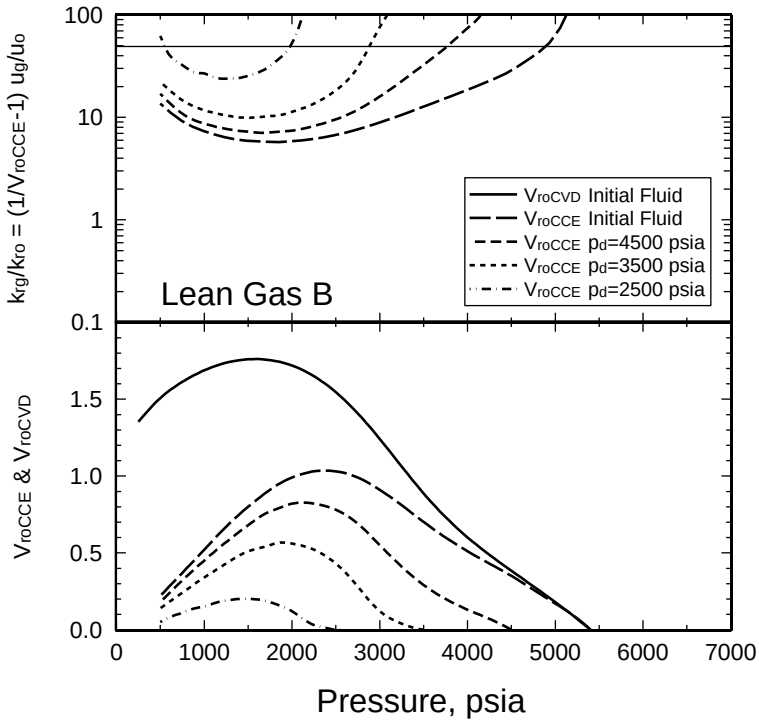

Fig. l.25 Diagnostic plots for Lean Gas B showing the variation of k_{rg}/k_{ro} (in Region 1) and CCE oil relative volume as a function of pressure during depletion.

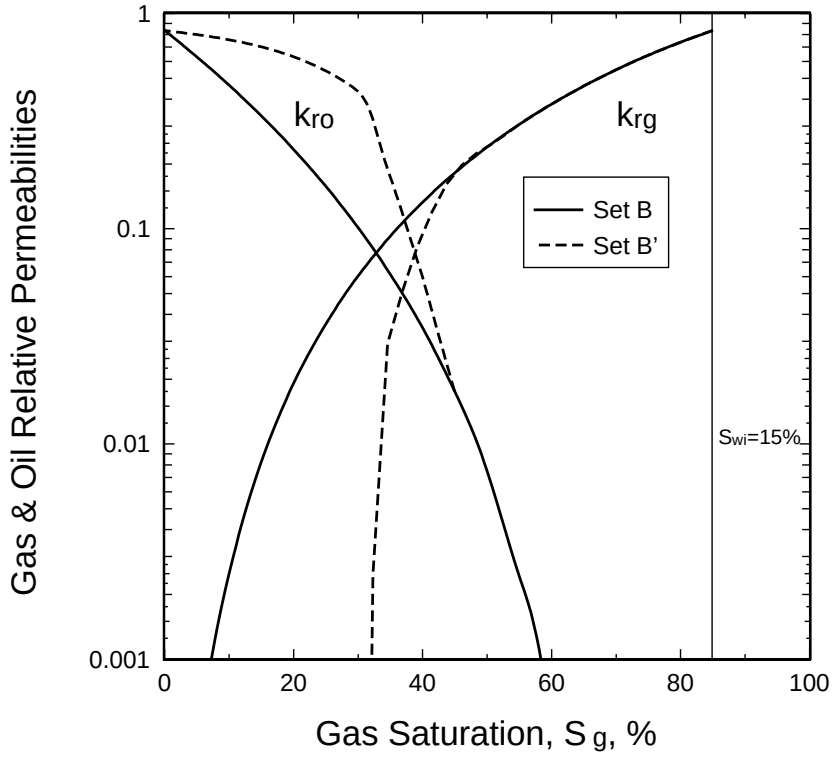

Fig. l.26 Two sets of gas/oil relative permeability curves that have identical $k_{rg} = f(k_{rg}/k_{ro})$ relationships.

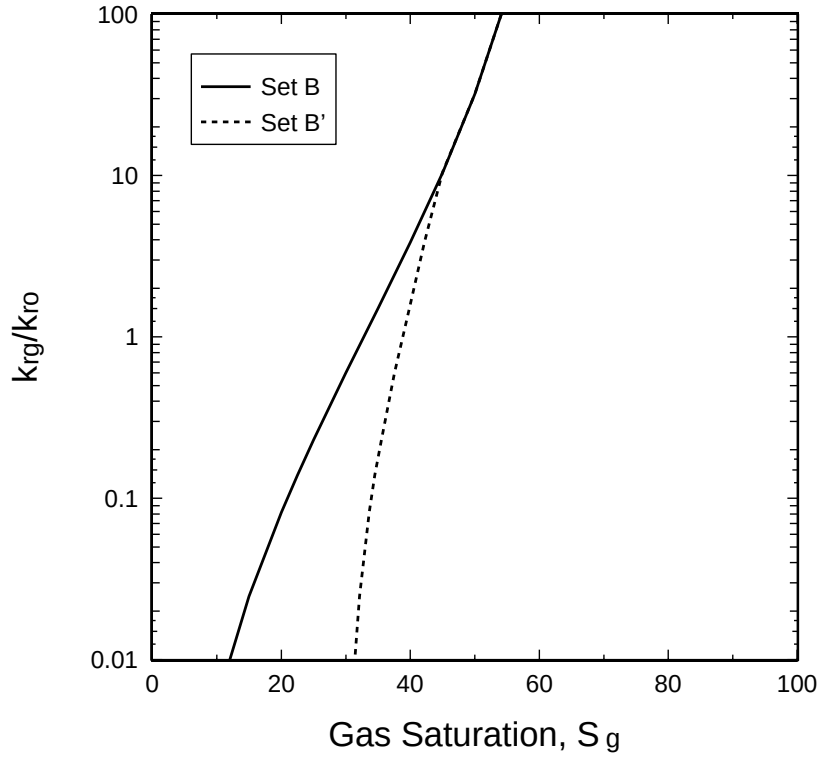

Fig. l.27 k_{rg}/k_{ro} vs. S_g for two sets of gas/oil relative permeability curves that have identical $k_{rg} = f(k_{rg}/k_{ro})$ relationships.

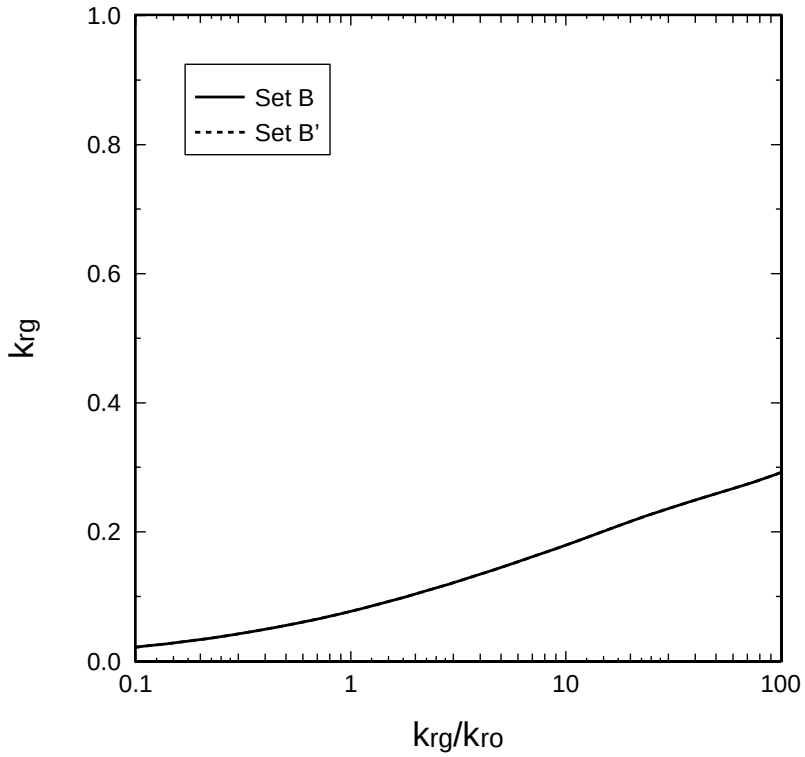

Fig. l.28 Identical $k_{rg} = f(k_{rg}/k_{ro})$ relationship for two completely different sets of $k_{rg}(S_g)$ and $k_{ro}(S_g)$ curves.

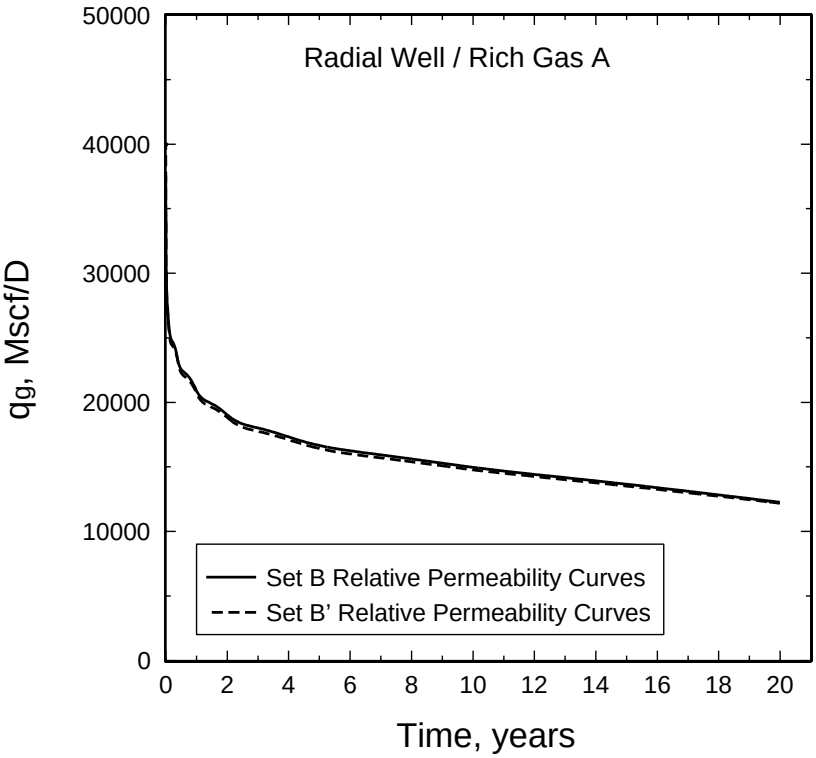

Fig. l.29 Rate-time performance of a radial well with Rich Gas A, based on fine-grid simulations using two dramatically different sets of gas/oil relative permeabilities (see **Fig. l.26**).

1.8.2. Critical Oil Saturation

It has been suggested that critical oil saturation (S_{oc}) is an important parameter in defining relative permeabilities for modelling well deliverability of gas condensates. Because the well deliverability loss due to condensate blockage occurs mostly in Region 1, the oil saturation in Region 1 must be close to S_{oc} for S_{oc} to have any effect on well deliverability. However, the k_{rg}/k_{ro} values in Region 1 even late in depletion are far from the near-infinite values expected close to the critical oil saturation (**Figs. l.24-l.25**). S_{oc} *may* have an effect on well deliverability if it is used in a parametric equations, where effective oil saturation S_o^* is normalized with S_{oc}, e.g.

$$k_{ro} = (S_o*)^2 \left(\frac{S_o}{1-S_{wi}}\right)^{(2+\lambda)/\lambda} \quad \textbf{(l.40)}$$

where

$$S_o* = \frac{S_o - S_{oc}}{1 - S_{wi} - S_{oc}}$$

When this is done, a change in S_{oc} affects k_{ro}, and consequently (k_{rg}/k_{ro}), at *all* saturations. The result is a totally different $k_{rg} = f(k_{rg}/k_{ro})$ relationship, even though $k_{rg}(S_g)$ is unchanged (**Fig. l.30)**.

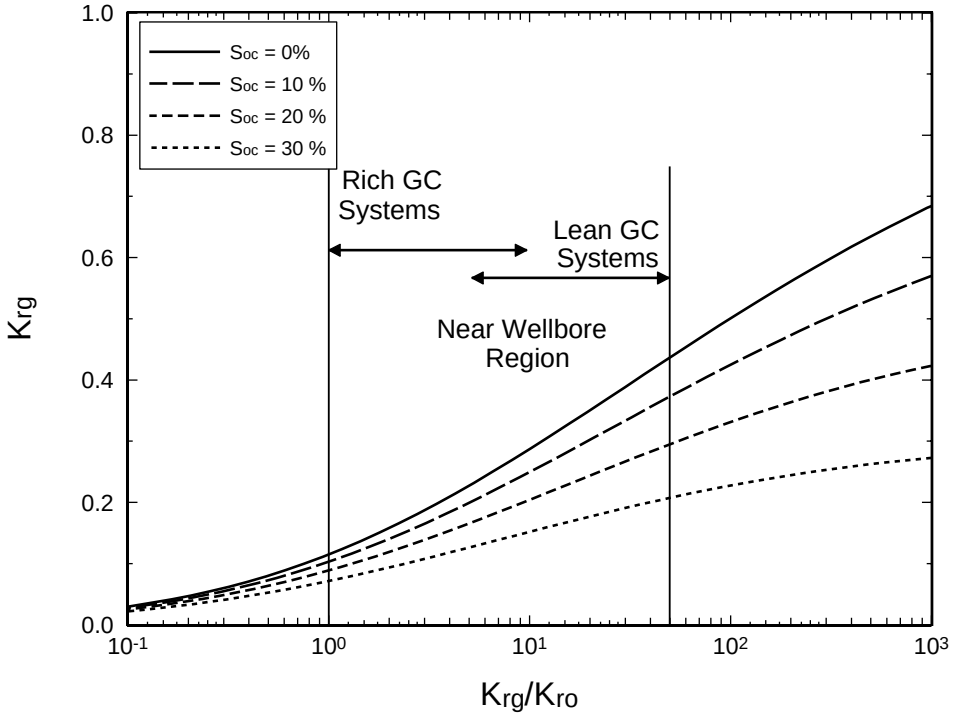

Fig. l.30 k_{rg} vs. k_{rg}/k_{ro} for different S_{oc} using **Eq.(l.40)**.

For richer gas condensate S_{oc} has an effect on well deliverability only if it changes the producing GOR. However, the gas-oil mobility ratio close to S_{oc} is so high that effectively no condensate is transported from Region 2 into Region 1. Furthermore, gas relative permeability at low oil saturations is not affected directly by S_{oc}.

To verify the insignificance of S_{oc}, Rich Gas A was simulated with radial and vertically fractured well geometries using Set A relative permeabilities (S_{oc}=10%). In addition, two other oil relative permeability curves were generated with different extrapolations of the oil relative permeability curves for k_{rg}/k_{ro} ratios higher than three. Extrapolations of k_{ro} were made with S_{oc}=0% and S_{oc}=20%. The resulting oil relative permeability curves are shown in **Figs. l.31 and l.32**. The same (Set A) gas relative permeability curve were used in all three cases.

For this fluid, the important region of k_{rg}/k_{ro} is less than 10 for most of depletion. However, for the extrapolations to be clearly different for high k_{rg}/k_{ro} ratios the extrapolations were done from k_{rg}/k_{ro} ratios higher than three. As seen in **Fig. l.33**, the simulated rate-time performance is practically identical for S_{oc}=0% and 20%, compared with the base case using S_{oc}=10%. The producing GOR is also practically equal for the three cases (not shown).

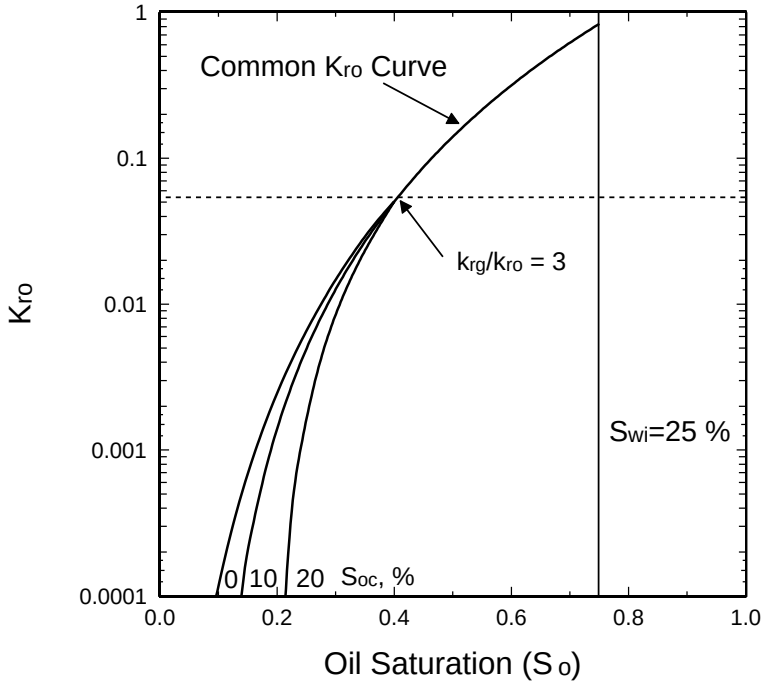

Fig l.31 Variation of k_{ro} curve as a function of oil saturation used in simulations. $k_{ro}(S_o)$ is *unaltered* for k_{rg}/k_{ro} < 3 (k_{ro}>0.05).

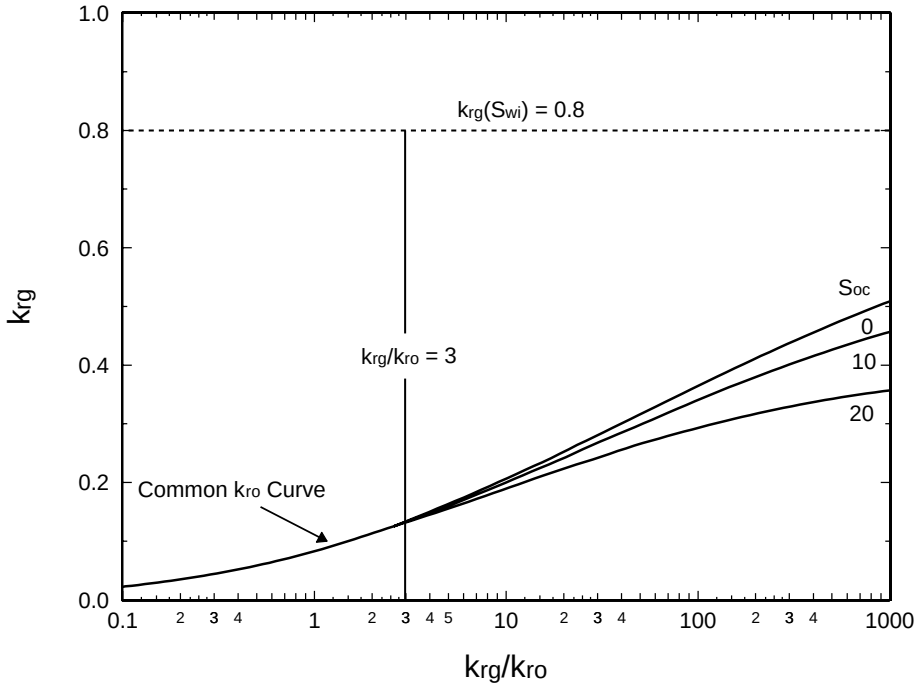

Fig. l.32 Variation of k_{ro} for $k_{rg}/k_{ro} < 3$ as a function of k_{rg}/k_{ro} used in simulations. $k_{ro}(S_o)$ is *unaltered* for $k_{rg}/k_{ro} < 3$ ($k_{ro}>0.05$).

Simulations at lower BHFP (250 psia) were also run to see if low oil saturations in Region 1 (due to vaporization) would result in significant differences in well deliverability for the three oil relative permeability curves with different S_{oc} values. As seen in **Fig. l.34**, the effect is very small.

In the absence of relative permeability data, or if available data are questionable, any "sensitivity" studies should be run by systematically varying the $k_{rg}=f(k_{rg}/k_{ro})$ relationship (in the range $1<k_{rg}/k_{ro}<50$), for example using pore size distribution λ in the Corey equation. It is a bad idea to make "sensitivity" studies of relative permeability using S_{oc} as a parameter in a general correlation. *If* S_{oc} is used as a parameter in sensitivity studies, the effect it has on well deliverability should be recognized as the effect S_{oc} has on the $k_{rg} = f(k_{rg}/k_{ro})$ relationship, and not on k_{ro} or k_{rg} values near S_{oc}.

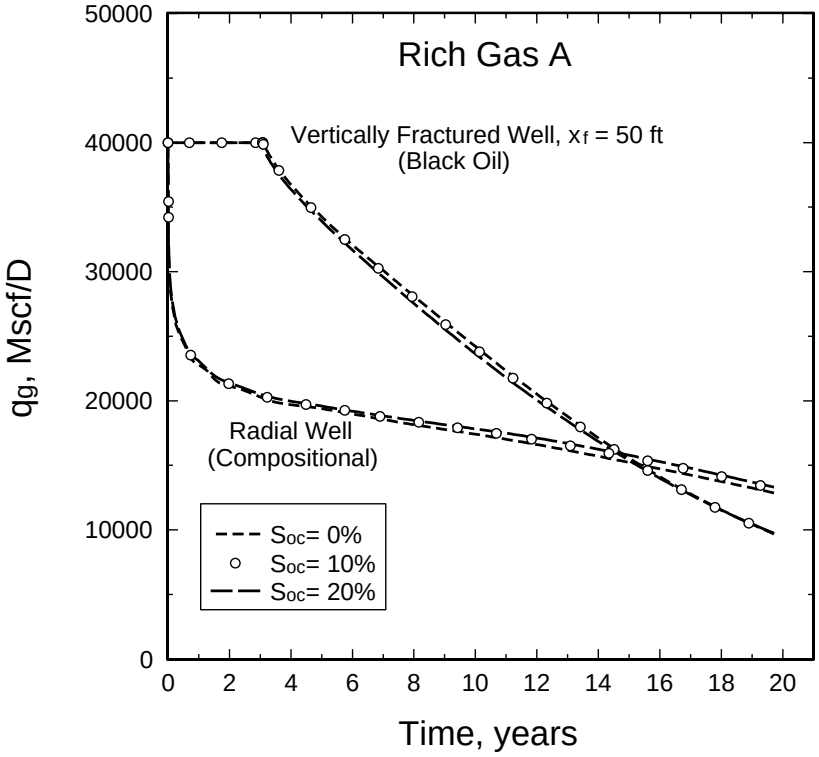

Fig. l.33 Rate-time performance of radial and vertically-fractured wells with Rich Gas A, showing the insensitivity on well performance to S_{oc} (**Figs. l.31 and l.32**).

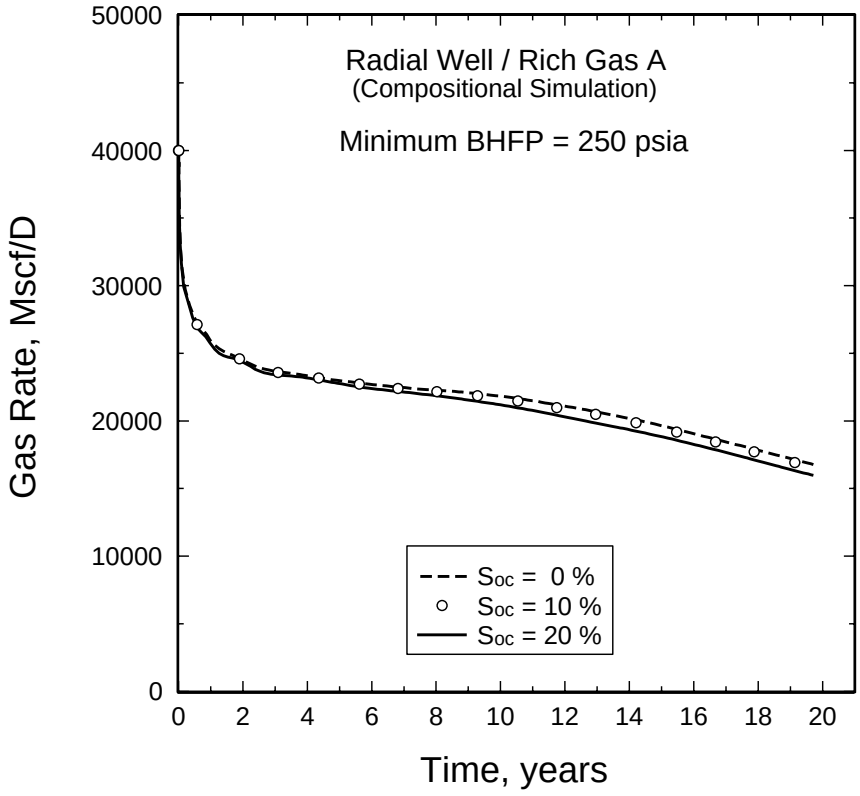

Fig. l.34 Rate-time performance of radial well with Rich Gas A, showing the insensitivity of well performance to S_{oc} (**Figs. l.31 and l.32**).

1.8.3. Gas-Oil Interfacial Tension Effect's on Well Deliverability

Probably the most misleading and deceptive concept put forth by earlier publications on gas condensates is the importance of gas-oil IFT on relative permeabilities. Many workers have discussed the potential effect, functional dependence, and methods for measuring the IFT effect on relative permeabilities. No one has yet shown that reservoir performance is significantly altered by "straightened" relative permeabilities due to low IFTs.

The two reservoir mechanisms that are *potentially* affected by relative permeabilities in gas condensate reservoirs are: (1) well deliverability and (2) gravity segregation of condensate that can theoretically occur in high-permeability or fractured reservoirs.

The physics of IFT effect on relative permeabilities is not well understood. Measurements quantifying the effect in a systematic way are lacking, and the data available are not reliable enough to build a theoretical (or empirical) model for predicting the effect. The existing conceptual model states that IFTs must be lower than a "threshold" IFT σ^* before relative permeabilities are affected. Furthermore, as IFT approaches zero the relative permeabilities approach straight lines with zero residual saturations. The model is given by

$$
\begin{aligned}
k_r &= F\,k_{r,\text{Immiscible}} + (1-F)\,k_{r,\text{Miscible}} \\
S_r &= F\,S_{r,\text{Immiscible}} \\
k_{r,\text{Miscible}} &= (S-S_r)/(1-S_{wi}-S_r) \\
F &= \left(\frac{\sigma}{\sigma^*}\right)^a \quad , \sigma<\sigma^* \quad ; \quad F = 1 \quad , \sigma\geq\sigma^*
\end{aligned}
\qquad \textbf{(l.41)}
$$

Recent measurements indicate that σ^* ranges from 0.1 to 0.3 mN/m (see Chap. 2). Exponent a=0.1 is recommended, though this is based more on physical intuition than experimental evidence.

The effect IFT has on gas-oil relative permeabilities using the model presented in **Eq. (l.41)** for different a's are shown in **Fig. l.35 and l.36**.

This section deals mostly with the potential effect of IFT on well deliverability. Some general comments regarding gravity segregation, based on earlier studies (not presented here), are: (1) segregation is negligible unless permeability is high (> 1000 md) and near-straight-line relative permeability curves exist throughout depletion, (2) the low-IFT period just below the dewpoint (with near-straight-line curves) is short-lived, (3) IFTs exceeding the "threshold" IFT (ranging from 0.1 to 0.3 mN/m) exist during the major part of depletion even for near-critical systems (see **Fig. l.37**); IFT effect on relative permeability is nonexistent for IFTs exceeding the threshold IFT.

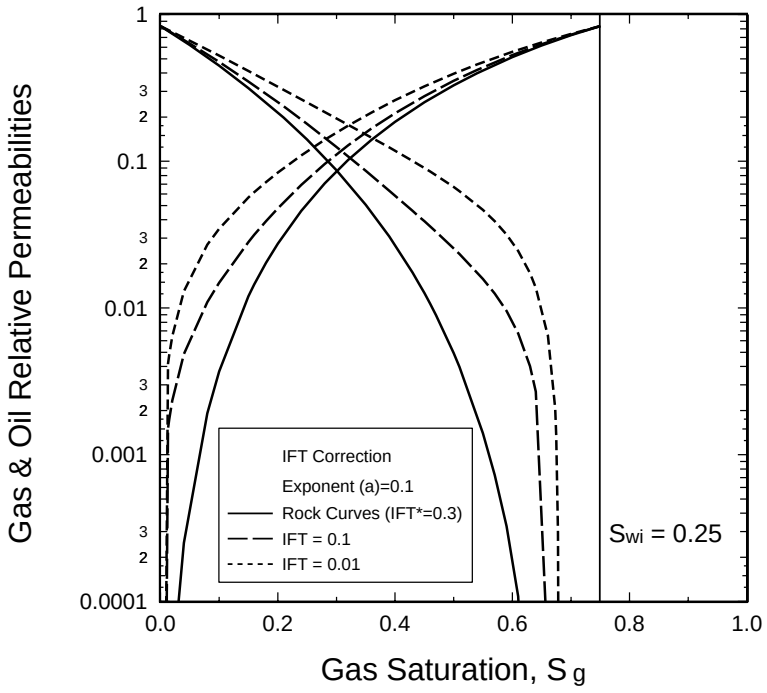

Fig. l.35 Shows the effect of IFT on Set A relative permeability curves using the IFT model presented in **Eq.(l.41)** with $\sigma_* = 0.3$ and n = 0.1.

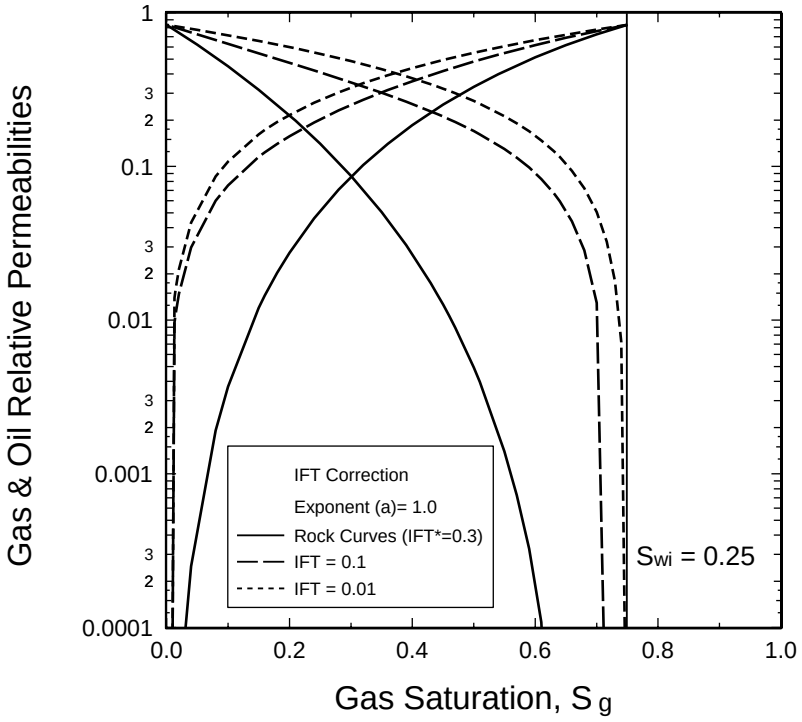

Fig. l.36 Shows the effect of IFT on Set A relative permeability curves using the IFT model presented in **Eq.(l.41)** with $\sigma_* = 0.3$ and n = 1.0.

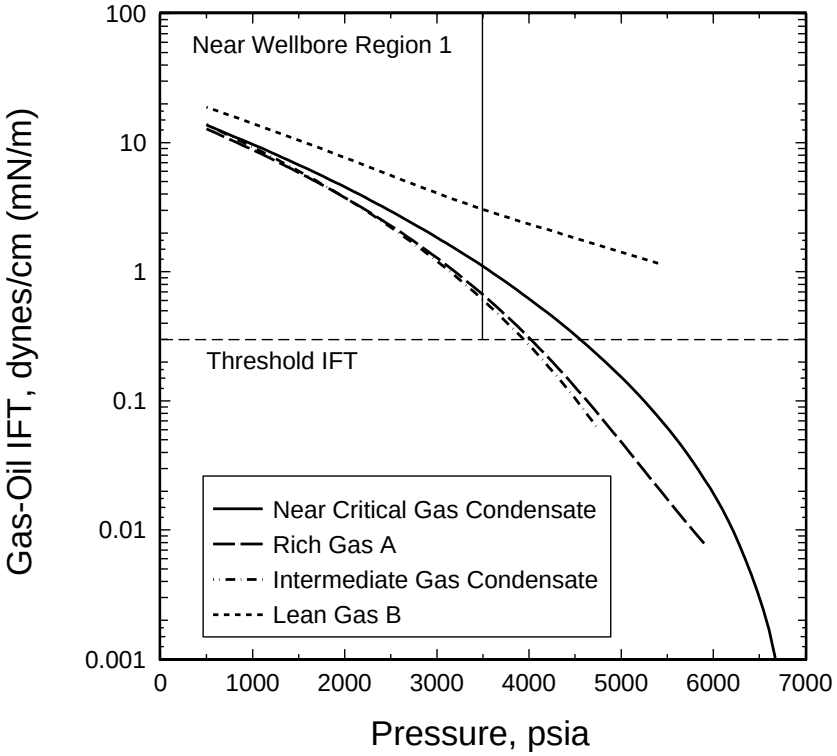

Fig. l.37 General pressure dependence of gas-oil IFT for different gas condensate systems.

Concerning the effect of IFT on well deliverability, the following observations are made (supported by simulations presented below): (1) gas condensate reservoirs will generally never experience IFTs lower than threshold IFTs of 0.1 to 0.3 mN/m in near-wellbore Region 1 (*when BHFP reaches a minimum and the well goes on decline*); and (2) low IFT in Region 2 and the resulting improvement in gas relative permeability has only a minor effect (if any) on deliverability.

Simulation of a "worst" case using Rich Gas A is given for radial and vertically fractured wells. The IFT model given by **Eq. (l.41)** uses Set A "Immiscible" relative permeability curves, σ^*=0.3 mN/m, and a=0.1. Simulated rate-time performance is shown in **Figs. l.38 and l.39**, indicating relatively little effect of IFT-corrected relative permeabilities on well deliverability. Absolutely no effect of IFT on well deliverability is found for Lean Gas B, because $\sigma>\sigma^*$ at all $p<p_d$ (**Fig. l.37**).

The potential effect of IFT on well deliverability will be greatest for rich, near-critical fluids producing on decline initially (no plateau). However, for this type of low-permeability well the IFT effect on relative permeabilities will be only one of several major uncertainties (absolute permeability, fracture length, rock relative permeabilities, and oil viscosity). Practically, it will be impossible to separate IFT effects from these other effects, and it also will be difficult to "sell" the optimistic effect of low IFTs to project economics when the IFT/relative permeability phenomena is so poorly understood.

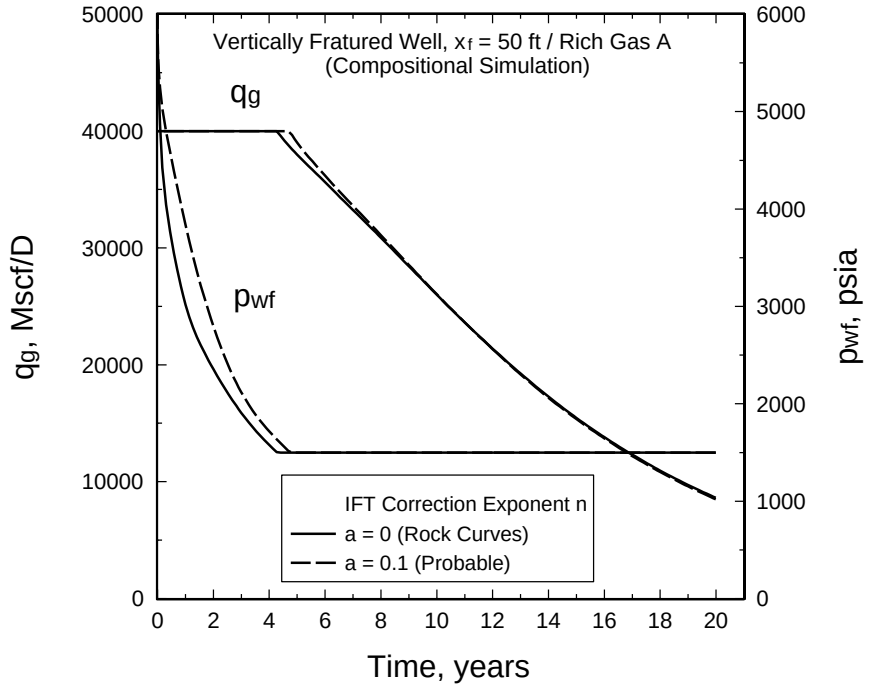

Fig. l.38 Well performance of a vertically fractured well with Rich Gas A, based on fine-grid compositional simulations with and without IFT corrections to relative permeability.

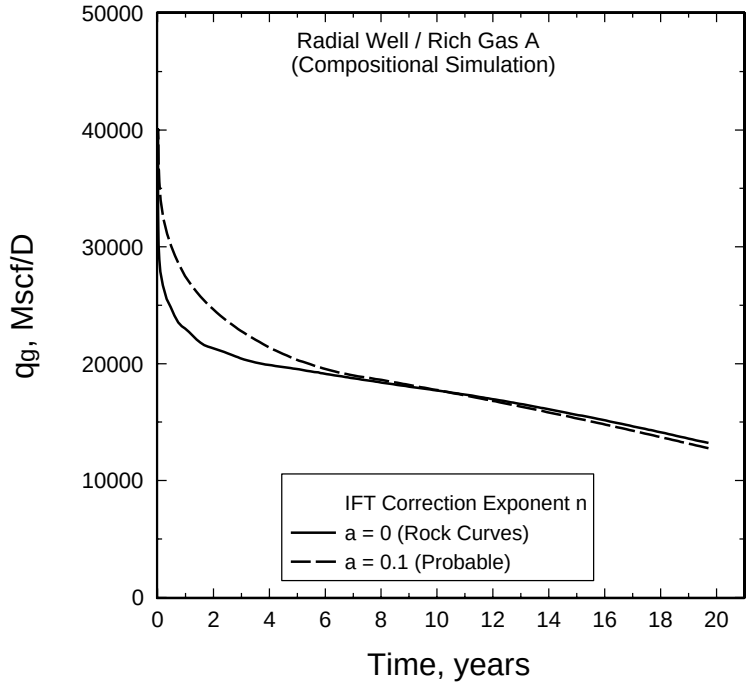

Fig. l.39 Well performance of a radial well with Rich Gas A, based on fine-grid compositional simulations with and without IFT corrections to relative permeability.

1.9. Conclusions

1. Gas condensate wells producing with BHFP below the dewpoint have up to three flow regions. *Region 1* has a constant flowing composition (GOR) where both gas and oil flow simultaneously. Most of the deliverability loss is caused by reduced gas permeability in Region 1. *Region 2* is where condensate accumulates but has no mobility. *Region 3* is the outer region where reservoir pressure is greater than the dewpoint and only gas flows.

2. Gas well deliverability can be accurately determined using a simple rate equation, **Eq. (l.23) or Eq. (l.24)**. The multiphase pseudopressure function is calculated from producing GOR (composition), relative permeabilities, and PVT properties. The effect of reduced gas permeability (condensate blockage) is incorporated in the pseudopressure function. All other well terms (well geometry, damage skin, etc.) are accounted for in the "productivity" constant C. The method is shown to work for radial, vertically fractured, and horizontal wells.

3. The multiphase pseudopressure function is calculated in three parts, based on the three flow regions. Region 1 pseudopressure is calculated using the Evinger-Muskat approach, modified for gas condensate systems. Region 2 uses the $k_{rg}(S_o)$ relationship, and $S_o(p)$ estimated from the liquid dropout curve from a CVD experiment. Region 3 pseudopressure is the same as for single phase gas.

4. Local grid refinement is not needed for gas condensate wells in full-field models. The proposed pseudopressure method calculates well deliverability accurately in coarse-grid models, without any near-well grid refinement. Examples are given for radial, vertically fractured, and horizontal wells.

5. The primary relative permeability relationship affecting condensate blockage (in Region 1), and thus the primary cause of reduced well deliverability, is k_{rg} as a function of k_{rg}/k_{ro}. Saturation does not enter the calculation directly.

6. Critical oil saturation S_{oc} has no effect on gas condensate well deliverability.

7. Gas-oil interfacial tension has little effect on gas condensate well deliverability (unless a physically questionable model is used for the dependence of relative permeability on IFT).

9. Deliverability of horizontal gas condensate wells is strongly affected by the k_v/k_h ratio. Severe deliverability loss is shown even for a normal k_v/k_h ratio of 0.1, compared with the performance of the same horizontal well with k_v/k_h=1.

1.10. References

1. Muskat, M.: *Physical Principles of Oil Production*, McGraw-Hill Book Company, Inc. (1949).

2. Fetkovich, M.J.: "The Isochronal Testing of Oil Wells," paper SPE 4529 presented at the 1973 SPE Annual Technical Conference and Exhibition, Las Vegas, Sept. 30-Oct. 3.

3. Kniazeff, V.J. and Naville, S.A.: "Two-Phase Flow of Volatile Hydrocarbons," *SPEJ* (1965) 37-44; *Trans.*, AIME, **234**.

4. Eilerts, C.K., Sumner, E.F., and Potts, N.L.: "Integration of Partial Differential Equation for Transient Radial Flow of Gas-Condensate Fluids in Porous Structures," *SPEJ* (1965) 141-152

5. Eilerts, C.K. and Sumner, E.R.: "Integration of Partial Differential Equations for Multicomponent, Two-Phase Transient Radial Flow," *SPEJ* (1967) 125-135

6. Gondouin, M., Iffly, R., and Husson, J.: "An Attempt to Predict the Time Dependence of Well Deliverability in Gas Condensate Fields," *SPEJ* (1967) 112-124; *Trans.*, AIME, **240**.

7. O'Dell, H.G. and Miller, R.N.: "Successfully Cycling a Low Permeability, High-Yield Gas Condensate Reservoir," *JPT* (1967) 41-47; *Trans.*, AIME, **240**.

8. Fussell, D.D.: "Single-Well Performance Predictions for Gas Condensate Reservoirs," *JPT* (1973) 258-268, 860-870; *Trans.*, AIME, **255**.

9. Jones, J.R. and Raghavan, R.: "Interpretation of Flowing Well Response in Gas Condensate Wells," paper SPE 14204 presented at the 1985 SPE Annual Technical Conference and Exhibition, Las Vegas, Sept. 22-25.

10. Jones, J.R., Vo, D.T., and Raghavan, R.: "Interpretation of Pressure Buildup Responses in Gas Condensate Wells," paper SPE 15535 presented at the 1986 SPE Annual Technical Conference and Exhibition, New Orleans, Oct. 5-8.

11. Craft, B.C. and Hawkins, M.: *Applied Petroleum Reservoir Engineering*, 1st ed., Prentice Hall, Inc., Englewood Cliffs, NJ (1959).

12. Bruns, J.R., Fetkovich, M.J., and Meitzen, V.C.: "The Effect of Water Influx on p/z-Cumulative Gas Production Curves," paper SPE presented at the 1964 SPE Annual Technical Conference and Exhibition, Houston, Oct. 11-14.

13. Van Everdingen, A.F. and Hurst, W.: "The Application of the Laplace Transformation to Flow Problems in Reservoirs,", *Trans.*, AIME, **186**, 305-324

14. Fetkovich, M.J.: "A Simplified Approach to Water Influx Calculations-Finite Aquifer Systems," *JPT* (1971) 814-828

15. Land, C.S.: "Calculation of Imbibition Relative Permeability for Two- and Three-Phase Flow from Rock Properties," *SPEJ* (1968) 149-156; *Trans.*, AIME, **243**.

16. Fetkovich, M.J., Reese, D.E., and Whitson, C.H.: "Application of a General Material Balance for High-Pressure Gas Reservoirs," paper SPE 22921 presented at the 1991 Annual Technical Conference and Exhibition, Dallas, Oct. 6-9.

17. Matthews, C.S., Brons, F., and Hazebroek, P.: "A Method for Determination of Average Pressure in a Bounded Reservoir," *Trans.*, AIME **201**, 182-191.

18. Fetkovich, M.J., Bradley, M.D., Works, A.M., and Thrasher, T.S.: "Depletion Performance of Layered Reservoirs Without Crossflow," *SPEFE* (1990) 310-317

19. Fetkovich, M.J., Bradley, M.D., Works, A.M., and Thrasher, T.S.: "Depletion Performance of Layered Reservoirs Without Crossflow," paper SPE 18266 presented at the 1988 SPE Annual Technical Conference and Exhibition, Houston, Oct. 2-5.

20. Arps, J.J. and Roberts, T.G.: "The Effect of the Relative Permeability Ratio, the Oil Gravity, and the Solution Gas-Oil Ratio on the Primary Recovery from a Depletion Type Reservoir," *Trans.*, AIME **204**, 120-127.

21. Fetkovich, M.J., Vienot, M.E., Bradley, M.D., and Kiesow, U.G.: "Decline Curve Analysis Using Type Curves - Case Histories," paper SPE 13169 presented at the 1984 SPE Annual Technical Conference and Exhibition, Houston, Sept. 16-19.

22. Whitson, C.H. and Brule, M.R.: *Phase Behavior*, Monograph, SPE of AIME, Dallas (1994) **(in print)**.

23. Golan, M. and Whitson, C.H.: *Well Performance*, 2nd ed., Prentice-Hall (1986).

24. Earlougher, R.C., Jr.: *Advances in Well Test Analysis*, Monograph, SPE, Dallas (1977).

25. Forchheimer, P.: "Wasserbewegung durch Boden," *Zeitz. Ver. Deutsch Ing.* (1901) 1781-1788

26. Al-Hussainy, R., Ramey, H.J., Jr., and Crawford, P.B.: "The Flow of Real Gases Through Porous Media," *JPT* (1966) 624

27. Rawlins, E.L. and Schellhardt, M.A.: "Back-Pressure Data on Natural Gas Wells and Their Application to Production Practices," U.S. Bureau of Mines Monograph 7 (1936).

28. Fetkovich, M.J.: "Multipoint Testing of Gas Wells," paper SPE presented at the 1975 SPE Annual Technical Conference and Exhibition, March 17.

29. Whitson, C.H.: "Reservoir Well Performance and Predicting Well Deliverability," *paper SPE 12518* (1983)

30. Whitson, C.H.: "Topics on Phase Behavior and Flow of Petroleum Reservoir Fluids," Dr. Techn. thesis, University of Trondheim, Norwegian Institute of Technology (1983).

31. Fetkovich, M.J.: "Decline Curve Analysis Using Type Curves," *JPT* (1980) 1065-1077

32. Edwardson, M.J., *et al.*: "Calculation of Formation Temperature Disturbances Caused by Mud Circulation," *JPT* (1962) 416-426; *Trans.*, AIME, **225**.

33. Whitson, C.H. and Torp, S.B.: "Evaluating Constant Volume Depletion Data," *JPT* (1983) 610-620; *Trans.*, AIME,

34. Evinger, H.H. and Muskat, M.: "Calculation of Theoretical Productivity Factor," *Trans.*, AIME (1942) **146**, 126-139.

35. Fetkovich, M.D., Guerrero, E.T., Fetkovich, M.J., and Thomas, L.K.: "Oil and Gas Relative Permeabilities Determined From Rate-Time Performance Data," paper SPE 15431 presented at the 1986 SPE Annual Technical Conference and Exhibition, New Orleans, Oct. 5-8.

36. Chopra, A.K. and Carter, R.D.: "Proof of the Two-Phase Steady-State Theory for Flow Through Porous Media," *SPEFE* (1986) 603-608

37. Standing, M.B.: "Notes on Relative Permeability Relationshops," *Proc.*, University of Trondheim, NTH, Norway (1975) .

38. Peaceman, D.W.: "Interpretation of Well Block Pressures in Numerical Reservoir Simulation," *SPEJ* (1978) 183-194; *Trans.*, AIME 253,

39. Coats, K.H.: "Simulation of Gas Condensate Reservoir Performance," *JPT* (1985) 1870-1886

Chapter 2.

Gas-Condensate Relative Permeability

2.1. Introduction

Chapter 1 gives a description of reservoir fluid flow for gas condensates, and verifies that three fundamentally different flow regions may exist. This chapter makes use of the three-region flow model to develop laboratory procedures for measuring gas-oil relative permeabilities. The experimental procedures are based on the two-phase flow characteristics of Regions 1 and 2, and with the intention of measuring relative permeabilities needed specifically for well deliverability calculations.

The (theoretical) potential for gravity segregation is yet another reason for measuring relative permeabilities in gas condensate reservoirs. The argument[1] is supposedly that gravity segregation and development of an oil rim may occur for rich gas condensates with the following characteristics: (1) low gas-oil interfacial tensions, (2) nearly straight relative permeability curves, (3) rapidly-developed high condensate saturations, and (4) low critical oil saturations.

It is traditionally been assumed that relative permeability of a fluid phase is mainly a function of (1) pore size distribution, (2) rock wettability, (3) saturation, (4) saturation history, and (5) IFT. More uncertain is the effect of capillary number[2] ($N_c=\Delta p_{visc}/p_c$) on relative permeability. Recent publications indicate that relative permeabilities are improved at high capillary numbers. Furthermore, water

[1]Arguments have mostly been "implied" in papers on relative permeability measurements, or suggested in oral discussions during meetings and forums. Apparently missing is any documentation of a specific case study, actual field data or rigorously simulated example, showing that gravity drainage does actually develop a significant oil rim which can be produced in a way that increases overall condensate recovery.

[2] Capillary number is a dimensionless number describing the ratio of viscous to capillary forces. Capillary number was originally introduced in connection with surfactant flooding and used for correlating residual oil saturation.

vaporization near the wellbore may have a pronounced effect on gas/oil relative permeability; to date no one has published measurements or simulations addressing the water vaporization issue.

Historically the main issues in connection with measurements of relative permeability for gas-condensate systems have been:

- Establish laboratory procedures for measuring relative permeability
- Verify whether measured relative permeability curves represent an imbibition or a drainage process
- Account for gas-oil interfacial tension
- Determine critical and/or residual oil saturations
- Predict gravity segregation

Relative permeability data are obtained in the laboratory by two methods: (1) directly measurements by a steady-state flow process[1,2] or (2) back-calculated using fractional-flow theory[3,4] from an unsteady state experiment where gas displaces oil[5]. Both methods have been and currently are being used.

Another aspect of relative permeability is that gas-oil relative permeabilities appear to be affected by interfacial tension (IFT), but only at low IFTs. Many investigators have studied the IFT effect[5-11], but systematic measurements quantifying the effect are still lacking. Most publications agree that IFT must be lower than a "threshold" value before relative permeabilities are affected. Reported threshold IFTs vary in the literature, mostly ranging from 0.3-0.4 mN/m, but some have reported considerably higher values, as high as 12 mN/m. Earlier publications have discussed the potential IFT effect on gas-oil relative permeabilities, but no one has apparently considered the consequence of *IFT effects on well deliverability*.

The saturation process in the condensate buildup Region 2 is *clearly* an imbibition process, with condensate saturation increasing monotonically. Thus, gas-oil relative permeabilities used to simulate the flow behavior in Region 2 should be determined from an imbibition experiment where k_{rg} is quantified in terms of condensate saturation and k_{ro} values are assumed to be practically zero (i.e. $S_o<S_{oc}$).

A fundamental concept in reservoir engineering states that the minimum phase saturation where a fluid phase is mobile depends on the nature of the saturation process. The minimum mobile oil saturation is called residual oil saturation (S_{or}) if measured during a drainage-type experiment (end of oil flow). The minimum oil saturation is called critical oil saturation (S_{oc}) if it is measured during an imbibition type experiment (onset of oil flow).

Practically, the only reason for measuring oil relative permeability at very low oil saturations in gas condensate systems is to evaluate the possibility for gravity segregation. Oil flow in Region 2 where oil mobility is either zero or much less than

gas mobility, and consequently k_{ro} at saturations close to S_{oc} are unimportant. Residual oil saturation itself and measurements of k_{ro} near S_{or} have no relevance to any gas condensate reservoir process.

The flow process in the near wellbore Region 1 is eventually a steady-state flow process, without accumulation of liquid, as discussed in Chapter 1. During the development of Region 1, a short-lived imbibition process occurs (Region 2 behavior). Once Region 1 is established, however, two-phase flow is clearly steady state and relative permeability data needed for Region 1 should be measured with a steady-state method.

To date, no standardized laboratory procedure for measuring gas-oil relative permeabilities for gas condensate systems exists. This has caused a lot of problems for the industry. Procedures used to measure relative permeability have varied greatly, and much time and effort has been spent measuring relative permeability data which have no relevance to well deliverability -- e.g. critical oil saturations, gas-oil relative permeabilities at low IFTs (< 0.05 mN/m).

A new experimental procedure for measuring the key relative permeability data needed for modeling well deliverability in gas condensate wells is proposed here. The proposed procedure is based on the analysis of the three flow Regions presented in Chapter 1, and designed specifically to establish the $k_{rg} = f(k_{rg}/k_{ro})$ relationship needed for Region 1 calculations. The procedure also includes a method for measuring gas relative permeability needed for Region 2 calculations. The main advantages with the proposed procedures are:

- Real reservoir fluid can be used (and are recommended).
- The procedure mimics the real flow in the reservoir.
- Design of key relative permeability data using only PVT data.
- IFT/velocity and/or IFT effects are easily measured.
- Saturation measurements are accurate and readily measured.
- The number of saturation measurements is reduced.
- The laboratory equipment is relatively simple.

The first section in this chapter examines the possibility for gravity segregation of condensate in gas condensate reservoirs, first by evaluating the important reservoir and fluid properties controlling gravity segregation, and secondly by evaluating published experimental results.

Section 2 summarizes the characteristics of the two flow Regions 1 and 2, analyzing how relative permeabilities should be measured in the different regions. A PVT-derived design plot is proposed for determining the relevant range of k_{rg}/k_{ro} for treating Region 1 flow behavior. Considerable published data concerning the effect of IFT on relative permeability is reviewed, to find an explanation for the large variation in threshold IFT. The last part of Section 2 discusses the potential effect

of high capillary number on relative permeability (and well deliverability).

Section 3 presents a new laboratory procedure for measuring gas-oil relative permeabilities for gas condensate systems. The new procedure is designed to obtain relative permeability data needed for well deliverability calculations. It also shows how the PVT design plot can be used to determine the laboratory conditions that secure measurements of k_{rg} in the relevant k_{rg}/k_{ro} range. A discussion is given of the advantages and drawbacks of using different fluids in flow test (reservoir fluid, synthetic mixtures, and simple fluids). Finally, Section 3 discusses end effect, and a design criteria[1] for minimizing boundary effects on relative permeability measurements.

2.2. Gravity Segregation

This section evaluates the possibility for gravity segregation of condensate in gas condensate reservoirs. The main controlling factors are: (1) density difference between gas and condensate, (2) condensate relative permeability at low oil saturations, and (3) vertical flow barriers and effective permeability to flow in the vertical or down-dip direction.

Significant condensate mobilities in a non-fractured reservoir at low oil saturations will only exist if gas-oil relative permeabilities are "straightened" by interfacial tension effects. The physics of IFT effects on relative permeability are not well understood, but recent published measurements suggest that IFT must be below a "threshold" IFT before relative permeabilities are affected. These measurements indicate that the threshold IFT ranges from 0.1 to 0.3 mN/m. Even for a rich gas condensate the pressure region where IFT is less than such threshold values will be short-lived (see **Fig. 2.13**). The driving potential for gravity segregation, $\Delta\rho_{og}$, is smallest when IFT is lowest.

In reality, all reservoirs are heterogenous. It is rather common that permeability, and particularly perpendicular to the bedding plane, exhibits a vertical to horizontal permeability ratio $k_v/k_h < 0.1$. Furthermore, reservoirs often have thin layers with large lateral extension which are sealing or partially sealing. Thus gravity segregation will be strongly inhibited in most gas condensate reservoirs simply due to geological factors.

Heriot-Watt Measurements

Danesh et. al.[12] study the possibility for gravity drainage by measuring critical oil saturation. S_{oc} was measured for different initial water saturations using a Clashach and a Berea rock core. A five-component synthetic gas condensate at elevated pressure and at 100 ^{o}F were used. The synthetic gas condensate had a maximum CVD liquid dropout of about 17%. The Berea and the Clashach cores had permeabilities of 350 md and 890 md, respectively. The length of each core was 2.6 ft. The cores were initially saturated with water and gas condensate above the dewpoint. Four experiments were conducted using the Clashach core with water saturations of 0%, 28.5%, 30.4% and 38.5%, and one using the Berea core with a water saturation of 45%. The cores were mounted vertically.

The cores were depleted by producing from the bottom of the core. The production rate corresponded to a depletion rate of about 50 psi/day. The production was stopped for a period of 24 hours at some preset pressures. After the 24 hour resting period, a small amount of equilibrium gas was injected to produce any condensate that had accumulated at the bottom. Critical oil saturation was taken as percentage of the core pore volume occupied by condensate, when sustained condensate flow was observed during injection of equilibrium gas into the core.

Danesh et. al. found that the critical condensate saturation was about 20% with no water in core, and about ten percent when the initial water saturation was about 30%. The critical oil saturation of 20 % with no water was obtained by injecting original gas into the core through a pressure regulator.

Some shortcomings with this experimental procedure include:

1. Only the onset of gravity segregation is measured, not the rate of drainage or change in rate of drainage as depletion continues. Drainage rates will depend primarily on k_{ro} at low S_o, $\Delta\rho_{og}=\rho_o-\rho_g$, and absolute permeability in the direction of segregation flow.

2. Capillary pressures are not measured, and neither is oil relative permeability. Both data are needed to model the experimental results and to upscale the gravity drainage process to a reservoir scale. Furthermore, capillary pressure and relative permeability dependence on low IFTs must also be determined experimentally.

Elf Measurements

Alonso and Nectoux [13] performed experiments to investigate the possibility for gravity drainage in a fractured tight dolomite reservoir with a near critical fluid. The experiments were conducted with a real reservoir fluid. The reservoir fluid had a dewpoint pressure of 5150 psia at reservoir temperature of 270 ^oF and a maximum CVD liquid dropout of 45%. The experiments were performed without water in the cores. Two composite cores were made: (1) a matrix core consisting only of reservoir rock covered with metal alloy, and (2) a "fractured" composite core, where the "fractures" were made by having a metallic shell with four vertical grooves and several radial grooves around the core. Each composite core had a length of 6 ft, and were made from 30 reservoir core samples (15 core samples were used for each composite core). The matrix composite core had a porosity of about 10% and a vertical permeability of 5 md, consisting only of reservoir rock. The fractured core had a vertical permeability of 5000-6000 md, but with about the same porosity.

All fluids were produced from the bottom of the cell. The initial gas production rate was 0.54 cm^3/d corresponding to depletion rate of 12 psi/d. After 50 days the production rate was increased to 3.2 cm^3/d corresponding to an average depletion rate of 20 psi/d. The experiment was stopped after about 220 days. The pressure in the core at the end of the experiment was 1600 psia.

The producing GOR from the *matrix* core decreased steadily during the first 100 days of production, from 4550 scf/STB to about 2200 scf/STB after 100 days of production. Then the producing GOR increased rapidly and was 27,000 scf/STB after 150 days. Because the producing GOR decreases as the core depletes, gravity segregation must have occurred. However, it is difficult to evaluate how much effect gravity segregation has because no CVD data are presented. According to the

authors, 50% of the condensate is recovered at the end of the experiment. It is not clear if the produced condensate includes condensate produced from the reservoir gas. The reported oil saturation at the end of the experiment was 19.5%

The producing GOR from the *fractured* core decreases from 3370 scf/STB to about 1123 scf/STB after 120 days of production. The producing GOR then increases the first 50 days and then decreases again for 20 days, before it increases again. The second decrease in producing GOR is contributed to gravity drainage from the core into the fracture. Note that the producing GOR in this case is initially about 25% lower. The dewpoint pressure seems to be different for the two experiments, also, because in this case the producing GOR is constant the first 40 days of production compared to only 20 days in the case of the matrix core. No explanation is given for the difference in the initial producing GOR. Both experiments were history matched using a fluid similar to the one used in the matrix core. According to the authors 71% of the condensate is recovered at the end of the experiment, but it is uncertain if this includes condensate produced form the reservoir core. The reported oil saturation at the end of the experiment was 17.9%

Morel et. al.[8] study the effect of gravity drainage with a pressure depletion experiment. The experiment was performed to evaluate the possibility for gravity segregation in a specific field. Thus it was conducted at reservoir conditions (p_i=6000 psia and T_R=286 ^oF) using a recombined reservoir fluid. The reservoir fluid had a dewpoint pressure of 5568 psia and a maximum CVD liquid dropout of 22%. A stack of ten cores taken from the actual reservoir with a total length of 6 ft was used. The permeability of the individual cores range from 4.2-46.8 md. The arithmetic averaged permeability of the whole core-stack was 5 md, with an average initial water saturation of about 20%. The core was mounted vertically.

The pressure depletion process was done in two steps. First from 6000 psia down to 4750 psia by producing fluid from the bottom, with an initial rate of 2 cc/day corresponding to a pressure drop of 15 psi/day at the beginning and 8 psi/day at the end (4750 psia). Then the withdrawal was stopped for 23 days. The CVD liquid dropout at 4750 psia was about 13%. Then the core pressure was lowered from 4750 psia to 2900 psia in one day, and held at 2900 psia for 18 days. A windowed sampling cell at the bottom was used to collect any condensate produced out of the cell during the test.

Some condensate was produced from the bottom of the core almost immediately after the dewpoint was reached. However, as the pressure declined the condensate production slowed down and became very low. At the end of the experiment only 1.5% of the free condensate was produced from the bottom of the core. Very small amounts of condensate were produced when the core was blown down from 4750 to 2900 psia, indicating that little gravity segregation had occurred.

Morel et. al. used a threshold IFT of 0.15 mN/m to history match this gravity drainage experiment. Wang et al.[14] simulated the same data using a critical IFT value of 0.05 mN/m. This indicates that the period of improved oil relative permeabilities due to IFT effects is short lived.

To summarize the results of the three experiments, it may be concluded that gravity drainage only occurred in the case with a near-critical fluid, and only during a limited pressure interval (from the dewpoint to 2200 psia below it). Neither of the two other experiments indicated significant gravity drainage rates or cumulative condensate production. Heriot-Watt experiments were conducted on a high permeable core, using only a slightly rich condensate. The Elf experiment used a reservoir fluid and reservoir rock. The reservoir fluid was rich but the reservoir permeability was low.

2.3. Effect on Well Deliverability

2.3.1. Flow Regimes and Primary Flow Behavior

Fluid flow towards a gas condensate well can be divided into three main flow regions, as discussed in Chapter 1.

Region 1 A near wellbore region (condensate blockage zone) where both gas and condensate flow towards the well. The flowing composition (GOR) is constant in Region 1.

Region 2 A condensate build up region where only gas is mobile. The oil saturation in this region is approximately equal to $V_{ro,CVD}$ corrected for initial water saturation. The oil and gas composition is approximately equal to the compositions in a CVD experiment.

Region 3 A single-phase gas region where the pressure is greater than the dewpoint pressure.

The three regions are illustrated in **Fig. 2.1** using the lean gas B.

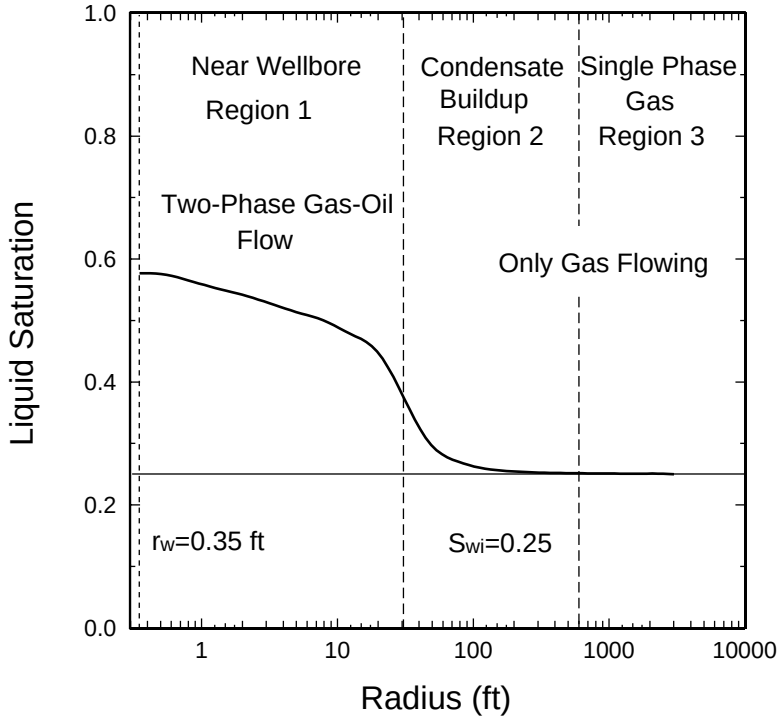

Fig. 2.1 Flow regions for a radial well producing from a gas condensate reservoir.

Near Wellbore Region (Region 1)
The main deliverability loss occurs in the near wellbore Region 11. The deliverability loss is due to the gas relative permeability in Region 1, and the size of the near wellbore region.

The size of Region 1 is mainly dependent on the production rate, the type of well (e.g. radial, vertically fractured, or horizontal), and PVT properties of the gas. The main PVT properties affecting the extent of Region 1 are: gas richness and solution OGR as a function of pressure. The size of Region 1 is somewhat dependent on gas-oil relative permeabilities for k_{rg}/k_{ro} ratios greater than 10. The size of Region 1 can vary from a few feet up to several hundred feet.

Fig. 2.2 shows the saturation distribution as a function of time for a radial well producing Lean Gas B. Region 1 is the part of the reservoir with a liquid saturation higher than about 35%. As explained in Chapter 1 the size of Region 1 increases monotonically as a function of time. The liquid saturation close to the wellbore first increases then decreases later in depletion. The increase early in depletion is due to a decrease in BHFP. The condensate saturation close to the well always decreases when the well goes on decline, because gas entering Region 1 gets leaner as the reservoir depletes.

Pseudosteady state flow conditions exist in Region 1, meaning that the flow can be

represented with steady-state conditions, but that the steady-state conditions change with time. Since the flow is steady-state, there is no accumulation of mass at a specific time and the flowing composition (GOR) is therefore constant. Thus, the single phase gas entering Region 1 has the same composition as the produced wellstream. The condensate saturation is determined as a function of radius *specifically* to ensure that all liquid that condenses from the single-phase gas entering Region 1 has sufficient mobility to flow through, and out of Region 1.

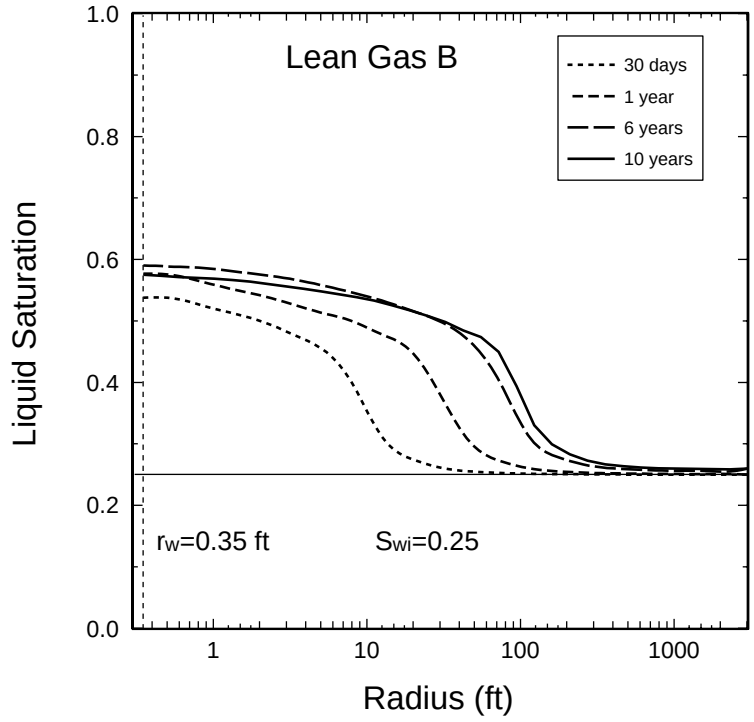

Fig. 2.2 Saturation distribution as a function of time for a vertical well producing from a gas condensate reservoir.

Using Darcy's law for gas and oil, and neglecting capillary forces it can be shown[15,16] that for steady-state flow conditions k_{rg}/k_{ro} is given by

$$\frac{k_{rg}}{k_{ro}}(p) = \frac{q_g}{q_o}\frac{\mu_g}{\mu_o} = \frac{V_g}{V_o}\frac{\mu_g}{\mu_o} = \left(\frac{1}{V_{roCCE}} - 1\right)\frac{\mu_g}{\mu_o} \qquad \textbf{(2.1)}$$

where k_{rg} is gas relative permeability, k_{ro} is oil relative permeability, p is pressure, μ_g is gas viscosity, and μ_o is condensate viscosity, $V_{ro}=V_o/(V_o+V_g)$, V_g and V_o are gas and oil volumes obtained from a CCE flash of the flowing composition at p. The k_{rg}/k_{ro} ratio in Region 1 is only a function of pressure as given by the PVT properties of the gas entering Region 1 [**Eq.(2.1)**]. The gas entering Region 1 changes as a function of depletion. Accordingly, a family of $k_{rg}/k_{ro}(p)$ curves needs to be generated to cover the range of k_{rg}/k_{ro} that existing in Region 1 through out depletion.

To correctly model the deliverability loss for a gas condensate well, it is essential to measure k_{rg} at relevant k_{rg}/k_{ro} ratios in Region 1. Individual phase relative permeabilities (k_{rg} and k_{ro}) can be expressed directly as a function of the ratio k_{rg}/k_{ro} (instead of saturation) since both phases are mobile in Region 1. For a reservoir gas entering Region 1, the range of $k_{rg}/k_{ro}(p)$ existing in Region 1 is easily calculated using a PVT model and **Eq.(2.1)**. To cover the relevant range of $k_{rg}/k_{ro}(p)$ ratios, calculate k_{rg}/k_{ro} vs. pressure from the dewpoint to a pressure lower than the minimum BHFP, for different reservoir gases. The composition of the different reservoir gases entering Region 1 as a function of depletion can be taken from a CVD experiment. The richest gas entering Region 1 is the initial reservoir gas.

It is recommended to make $k_{rg}/k_{ro}(p)$ curves for different stages in depletion, prior to measuring relative permeabilities. This plot should be used to design relative permeability experiments, to insure that relative permeabilities are measured in the relevant k_{rg}/k_{ro} range for the reservoir fluid.

The $k_{rg}/k_{ro}(p)$ ratio for four different gas condensates are shown in **Figs. 2.4, 2.6, 2.8**. The corresponding liquid dropout curves are shown in **Figs. 2.3, 2.5, 2.7**. The k_{rg}/k_{ro} ratio in the main part of the near wellbore region is relatively constant. The ratio depends on gas richness and condensate solubility in the reservoir gas. For normal to rich gas condensates k_{rg}/k_{ro} is approximately constant in the main part of Region 1 early in depletion. The level of k_{rg}/k_{ro} in Region 1 ranges from 0.5 to 2 depending on the richness of the gas. As the reservoir depletes, k_{rg}/k_{ro} increases, and towards the end of depletion $k_{rg}/k_{ro}\approx$10-20 in the main part of Region 1. k_{rg}/k_{ro} may be as high as 50 at the outer part of Region 1, depending on the average reservoir pressure at abandonment.

Condensate Buildup Region (Region 2)

The condensate buildup zone starts where the near wellbore Region 1 ends. In Region 2 the condensate saturation is approximately equal to the liquid drop out saturation measured in a constant volume depletion experiment (CVD), corrected for initial water saturation. The gas leaving Region 2 is leaner than the gas entering Region 2, due to the loss of condensed liquid in this region of accumulation.

The gas relative permeability is relatively high in Region 2. The deliverability loss in Region 2 is only significant for richer gas condensates. For gas condensates with a maximum CVD liquid dropout less than about 10%, there is no reason to measure gas relative permeabilities. The reduction of gas permeability in Region 2 is therefore small (less than 10-20%).

Single Phase Gas Region (Region 3)

The single phase gas region exists in the part of the reservoir where the reservoir pressure is greater than the initial dewpoint pressure. The gas relative permeability is unaltered, and pressure losses can be calculated based on PVT properties B_{gd} and μ_g using the traditional gas pseudopressure function.

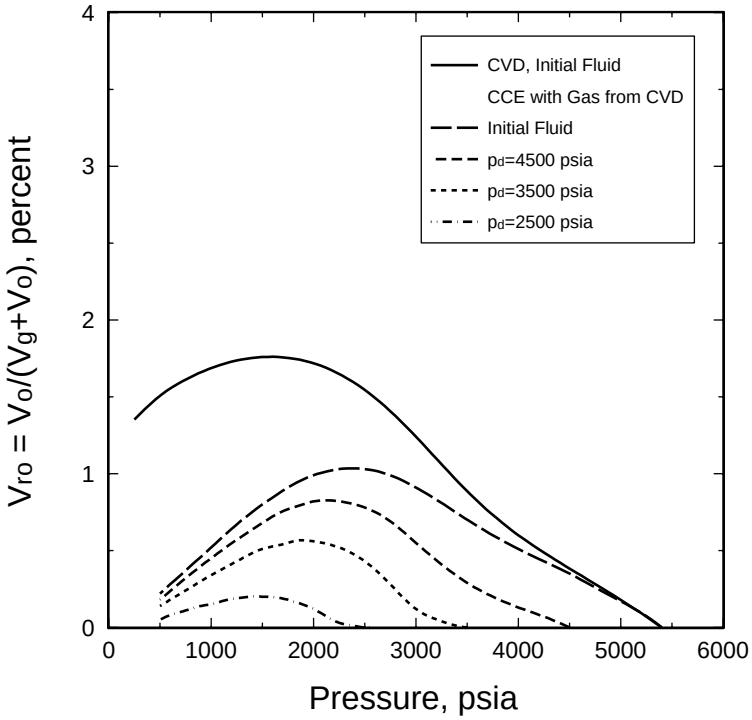

Fig. 2.3 Liquid dropout as a function of pressure, for lean Gas B.

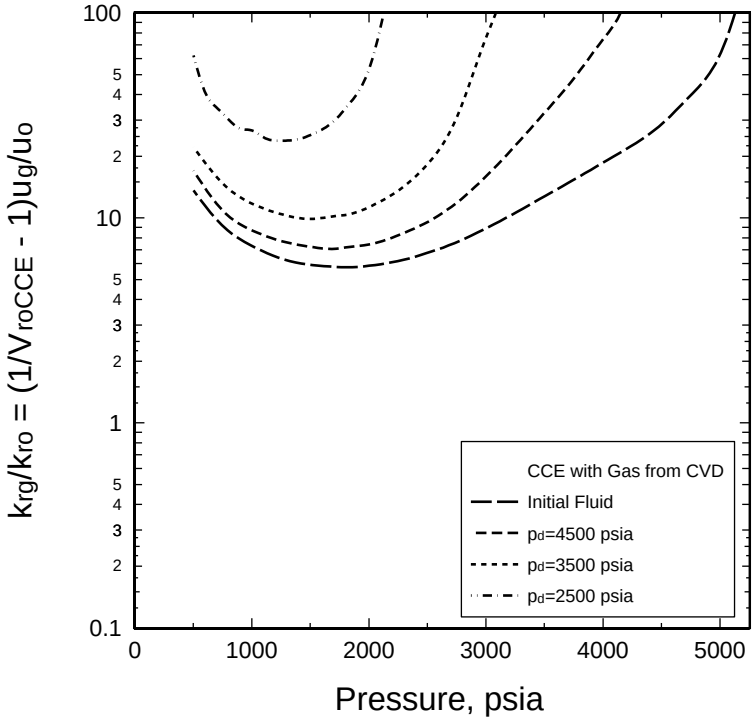

Fig. 2.4 k_{rg}/k_{ro} as a function of pressure for a Lean Gas B.

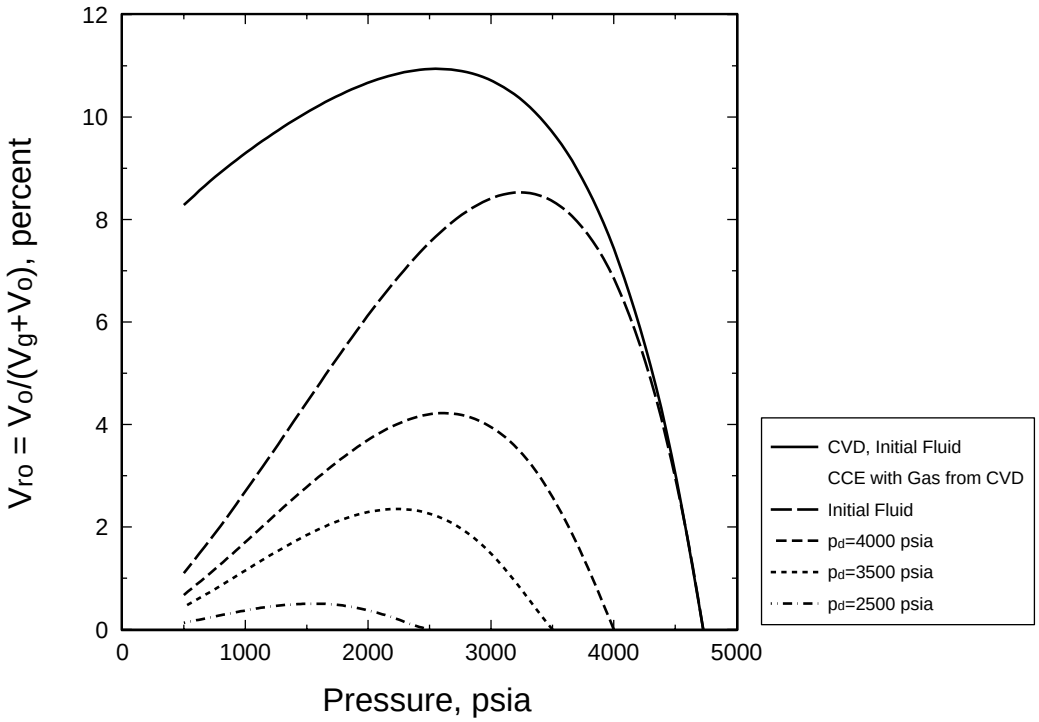

Fig. 2.5 Liquid dropout as a function of pressure, for an intermediate gas condensate.

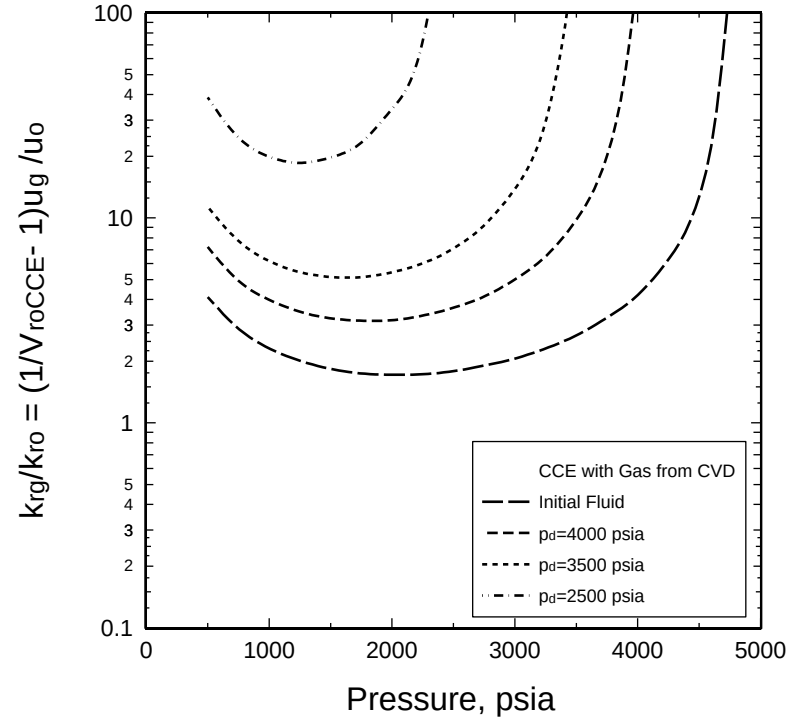

Fig. 2.6 k_{rg}/k_{ro} as a function of pressure for an intermediate gas condensate.

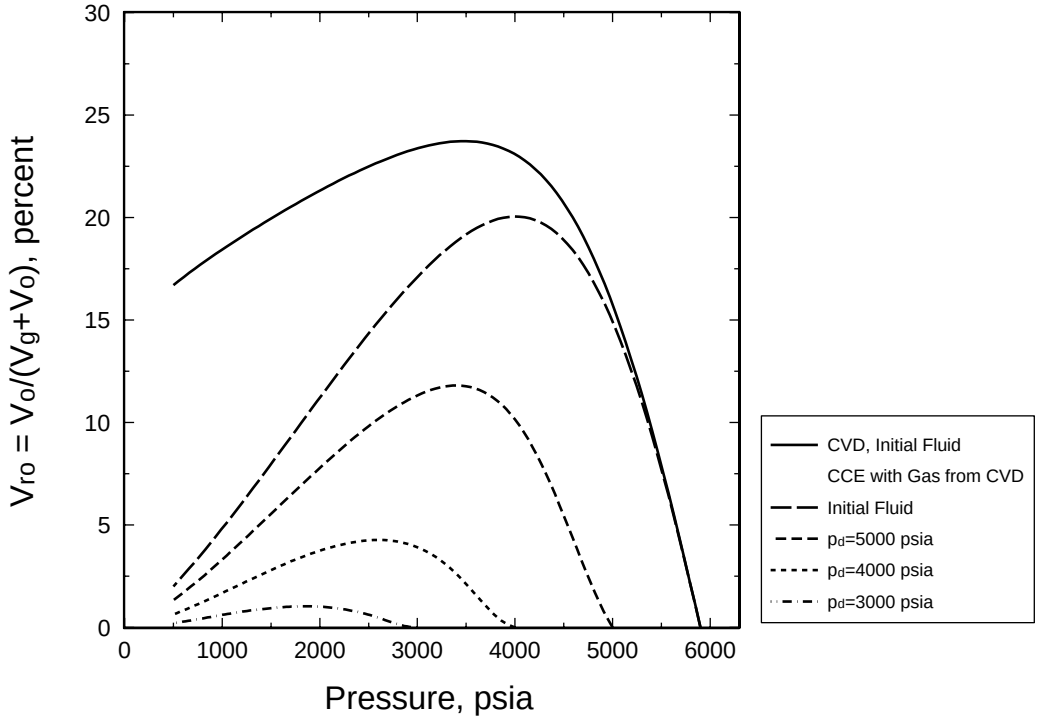

Fig. 2.7 Liquid dropout as a function of pressure, for Rich Gas A.

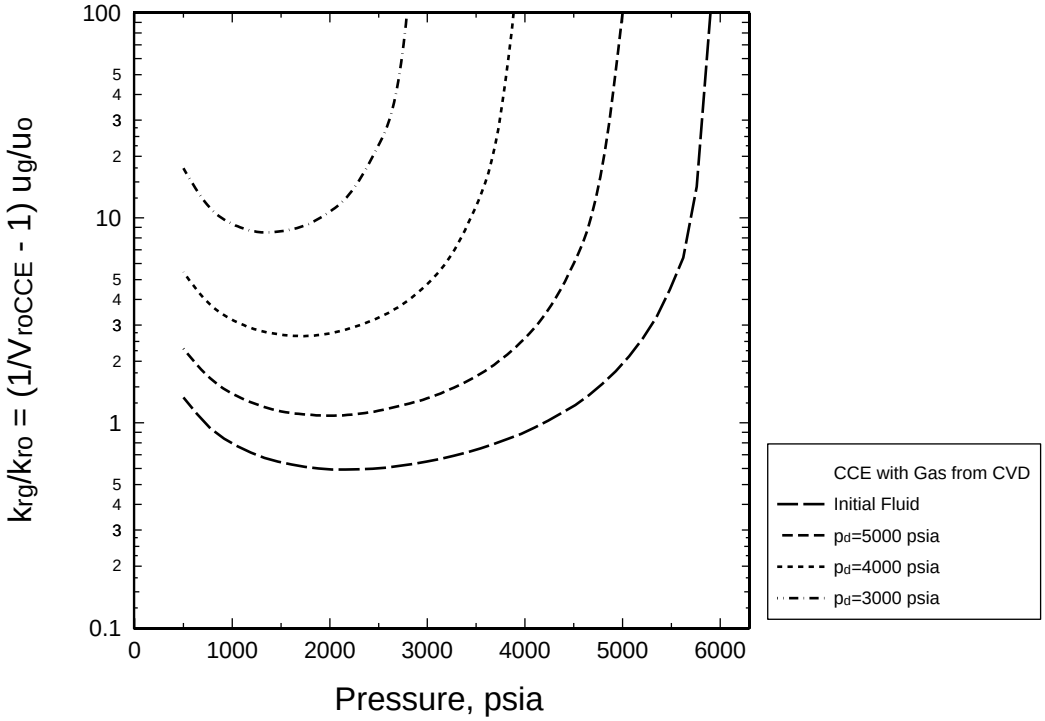

Fig. 2.8 k_{rg}/k_{ro} as a function of pressure for Rich Gas A.

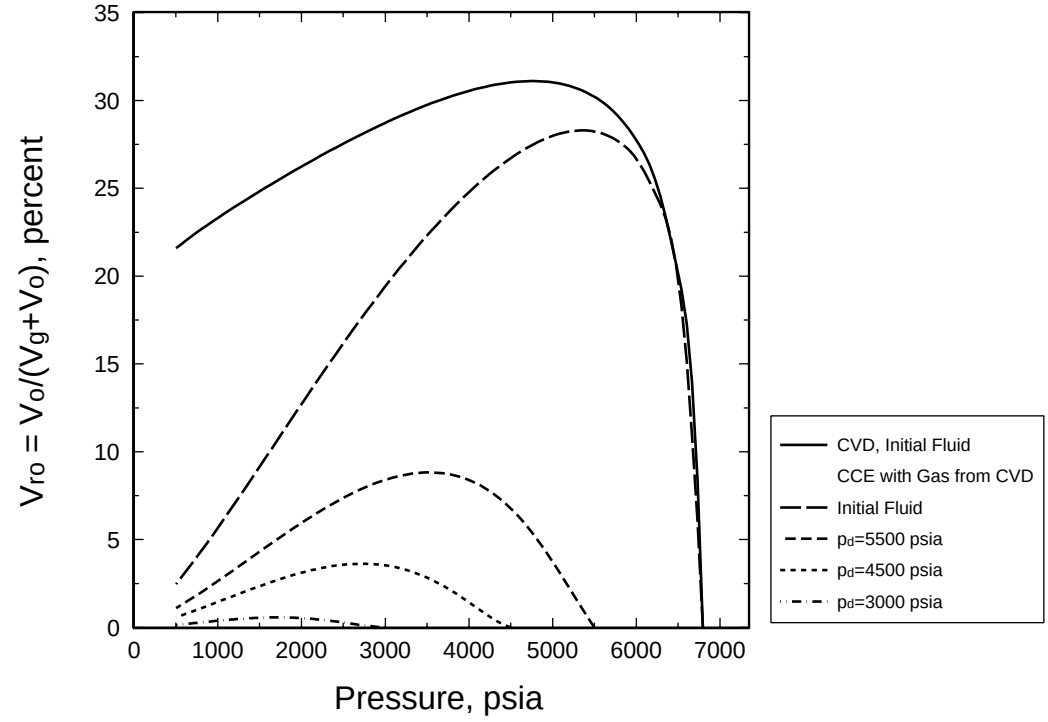

Fig. 2.9 Liquid dropout as a function of pressure for a near critical gas condensate.

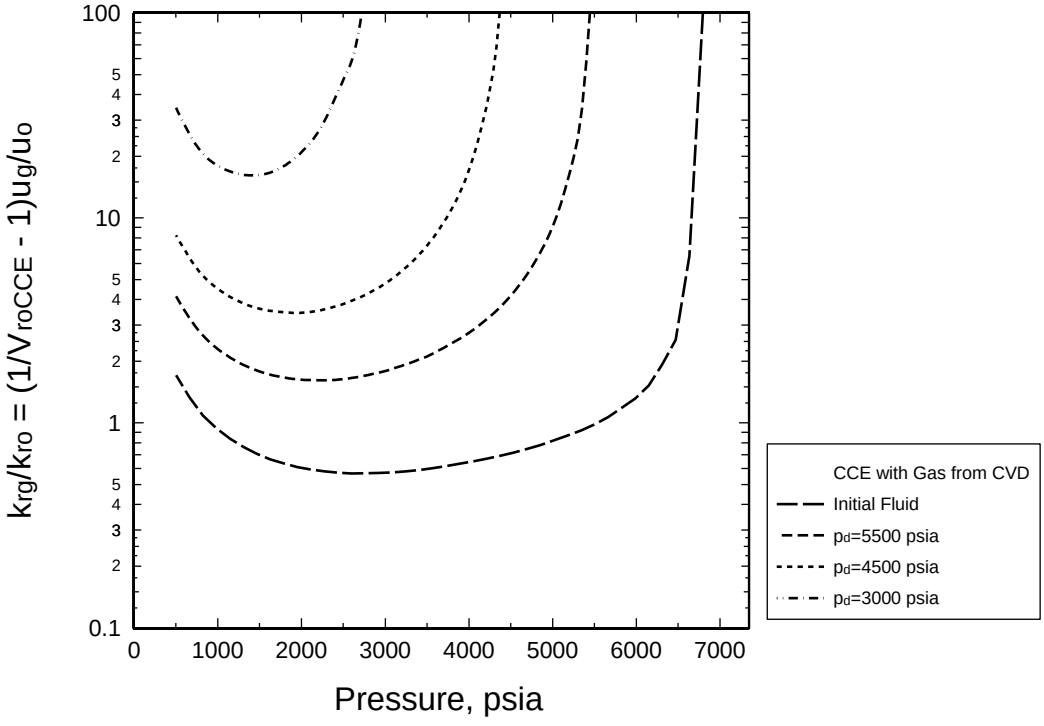

Fig. 2.10 k_{rg}/k_{ro} as a function of pressure for a near critical gas condensate.

2.3.2. Critical Oil Saturation (S_{oc})

Critical oil saturation is the minimum oil saturation where oil is mobile in Region 2. In Region 2 oil drops out of the gas when the pressure drops below dewpoint pressure. In the absence of gravity segregation the oil saturation in Region 2 increases as the reservoir depletes, until it reaches a maximum where the gas starts to vaporize some of the oil. The maximum oil saturation in the reservoir depends on the richness of the gas condensate. It can be from 1-2% for a lean gas condensate to over 40% for a near-critical fluid.

Three different experimental procedures have been reported in the literature for measuring critical oil saturation[11,12,17].

Based on reported measurements, S_{oc} appears to be a function of: (1) initial water saturation (S_{wi})[11,18,19], (2) capillary number N_c[20], (3) flow process[2,19], and (4) IFT below the threshold IFT[2,5,7,8,10,11].

Critical condensate saturation has no direct effect on well deliverability calculations even when the critical saturation is lower than $S_{o,max}$. The gas-oil mobility ratio in Region 2 is infinite or so high that practically no condensate flows from Region 2 to Region 1 (and into the well), as discussed in Chapter 1. For near-critical systems ($S_{oCVD,max}$>40%), Region 1 may actually exist throughout the reservoir. Even when Region 1 exists throughout the reservoir, R_p will only be somewhat lower than $1/r_s(p_R)$, because the gas-oil mobility ratio at the outer part of Region 1 is high.

Traditionally, parametric relative permeability equations are fitted to the measured data. This is done both as a quality check of the measured data, and to obtain relative permeabilities which cover all saturations. Parametric oil relative permeability equations often use S_{oc} as a model parameter. In the Corey relative permeability model S_{oc} is used to normalize S_o,

$$k_{ro} = (S_o*)^2 \left(\frac{S_o}{1-S_{wi}}\right)^{(2+\lambda)/\lambda}$$
$$S_o* = \frac{S_o - S_{oc}}{1 - S_{wi} - S_{oc}} \qquad \textbf{(2.2)}$$

When this is done, a change in S_{oc} affects k_{ro}, and consequently k_{rg}/k_{ro}, at *all* saturations. This result in a totally different $k_{rg} = f(k_{rg}/k_{ro})$ relationship, even though $k_{rg}(S_g)$ is unchanged (see **Fig. 2.11**). Sensitivity studies should probably not use S_{oc} as a sensitivity parameter in a general correlation. If used, then any change in well deliverability due to a parametric change in S_{oc} should be recognized as an effect of an altered $k_{rg} = f(k_{rg}/k_{ro})$ relationship, and *not* because of an altered "physical" S_{oc} (oil relative permeability at low oil saturations).

As shown in Chapter 1, critical oil saturation has effectively no effect on well deliverability. Critical oil saturation used as a parameter in a general relative permeability correlation may have an effect on well deliverability, but *only* because it affects the $k_{rg} = f(k_{rg}/k_{ro})$ relationship. If critical oil saturation is measured in the laboratory, it should *only* be used in a relative permeability correlation if it doesn't alter the measured $k_{rg} = f(k_{rg}/k_{ro})$ relationship.

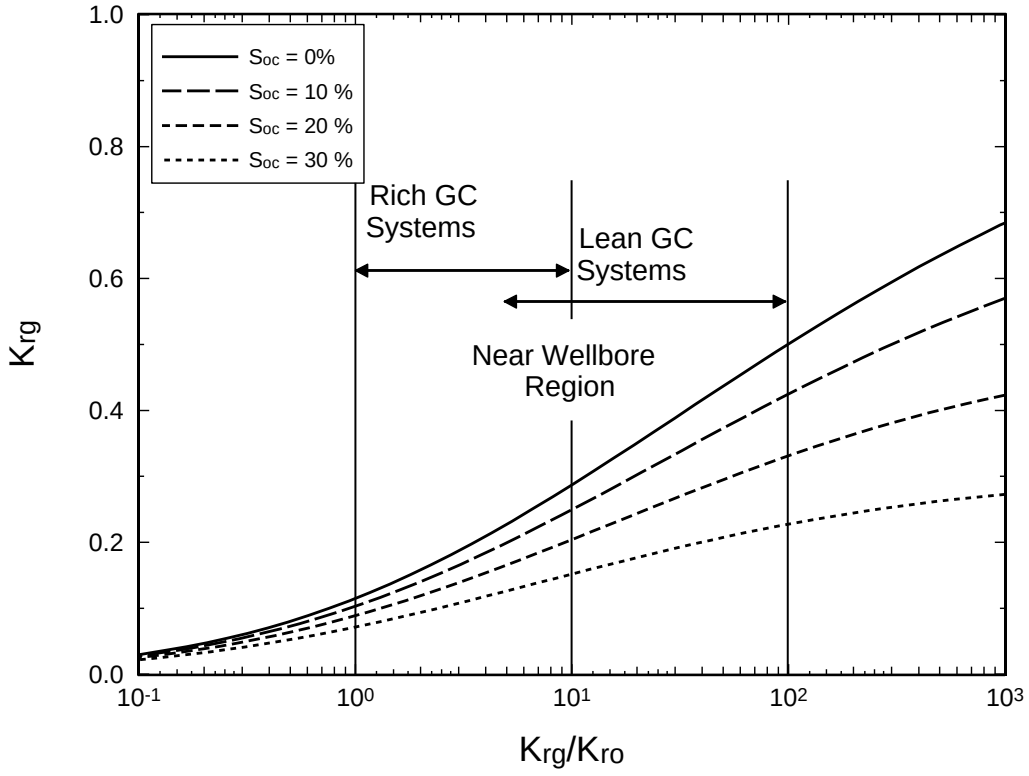

Fig. 2.11 k_{rg} vs. k_{rg}/k_{ro} plot for various S_{oc} based on a Corey relative permeability model.

2.3.3. Interfacial Tension (IFT)

Based on a bundle-of-capillaries model, relative permeability should not be a function of interfacial tension. Some experimental evidence supports this observation.[9]. Theoretically, however, two fluids with zero interfacial tension should have straight line relative permeability curves. Some experimental evidence suggests that the transition from a relative permeability model with no IFT effect to one with some IFT effect occurs at some threshold IFT, with a gradually increasing effect of IFT on relative permeability at decreasing IFTs.

The current empirical IFT/relative permeability model states that relative permeability is only a function of interfacial tension below a threshold IFT. Measurements quantifying the effect in a systematic way are lacking, and the

reported threshold IFT's vary in the literature from 0.05 to 15 mN/m. A review of papers dealing with IFT effects on gas-oil relative permeability is presented below, to seek an explanation for the large variation in reported threshold IFTs.

Relative permeability at low IFTs has been measured using displacement[5,6,9] and steady-state [7,10] flow tests.

Wagner and Leach[6] performed displacement tests on a 2" diameter and 21" long Torpedo core with a porosity of 23% and a permeability of 500 md. A methane-pentane fluid system was used. The experiments were conducted at 100 ^{o}F. Pressure was used to vary IFT, with pressure ranging from 2415 to 1190 psia, corresponding to an IFT range of 0.001-5 mN/m. The production rate was constant throughout each experiment. Only production data before breakthrough was used to interpret the results, using frontal drive calculations. Capillary effects were neglected. Experiments were conducted with the core initially saturated with 100% gas, and with 100% liquid. Wagner and Leach[6] found that oil and gas relative permeabilities were only affected by IFT at IFTs less than 0.07 mN/m.

Bardon and Longron[5] used displacements experiments to determine the effect of low IFT on relative permeability. A wide range of IFTs, from 0.001 to 12.6 mN/m were investigated. A Fontainebleau sandstone with a porosity of 9.9% and a permeability of 82 md was used. The core was about 1 ft long with a diameter of 2 inches. A binary fluid system consisting of methane and normal heptane was used in most of the experiments. They reported oil relative permeability changes for IFTs as high as 12.6 mN/m, but relative permeability to gas remained unchanged until IFT was 0.065 mN/m. The major change in both gas and oil relative permeability occurred at around 0.04 mN/m. Furthermore, Bardon and Longron's measurements indicate that gas relative permeability is reduced for gas saturations higher than 75%, when IFT is lower than 0.065 mN/m. Bardon and Longron used only production after breakthrough to calculate relative permeability. Capillary end effects were not accounted for when relative permeabilities were calculated from the production data.

Asar and Handy[7] measured the influence of IFT on relative permeability using steady-state experiments. A methane-propane fluid system was used. The core was one foot long with a diameter of two inches, and had a permeability of 193 md, and a porosity of 20%. All experiments were performed at 70^{o}F without water in the core. IFT was changed by changing pressure. They found that oil relative permeability decreased faster than gas relative permeability for higher IFTs. However, oil relative permeability at an IFT of 0.82 mN/m was almost equal to oil relative permeability at an IFT of 34 mN/m. The major change in gas-oil relative permeability occurred at 0.2-0.3 mN/m. Capillary end effects were not taken into account in the interpretation of measured data.

Delclaud et al.[9] investigated what influence fluid properties have on gas-oil relative

permeabilities. The effect IFT has on relative permeability was studied using displacement experiments with a binary methane-pentane fluid system. All IFT experiments were performed using a Fontainebleau sandstone with a permeability of 33 md, and a porosity 7.1%. The core was 8 inches long and had a diameter of 3 inches. The experiments covered IFT's from 30 to 0.6 mN/m. The pressure drop over the core was kept constant throughout each of the experiments. The interpretation was performed with a numerical model designed for laboratory experiments. Production data were matched to define gas-oil relative permeabilities. Capillary pressures were scaled according to the Young-Laplace equation[21], assuming that the contact angle was not affected by IFT. No effect of IFT on gas-oil relative permeability was found when IFT correction to the capillary pressure was taken into account.

Haniff and Ali[10] studied the effect of IFT on relative permeability using the steady-state method with a binary methane-propane fluid system. They used a Spynie sandstone with a permeability of 23 md and a porosity of 22%. The core was 0.5 ft long with a diameter of 2 inches. The experiments covered IFTs from 0.2 to 0.001 mN/m. Their results indicate relatively small changes in relative permeability for IFT from 0.2 to 0.05 mN/m. However, below 0.05 mN/m gas-oil relative permeabilities were strongly affected by IFT. They observed a jump in residual and critical oil saturation at 0.05 mN/m. Furthermore, no hysteresis effects were found for IFTs lower than 0.05 mN/m. This supports complete wetting of the solid phase by the liquid, below 0.05 mN/m.

Ronde[22] analyzed the measurements presented by Asar and Handy[7]. He found that the Chan wetting transition takes place at IFT = 0.3 mN/m for a methane-propane system. The Chan wetting transition causes a transition from "separated" channel flow regime to core annular flow regime for pores with an equivalent channel radius larger than 0.1 μm.

Morel et. al. [8] used a threshold IFT of 0.15 mN/m to history match a gravity drainage experiment. Wang et al.[14] simulated the same data presented by Morel et. al. [8] and specified a threshold IFT of 0.05 mN/m.

Published measurements appear to support that gas-oil relative permeabilities only are a function of IFT below some threshold IFT. The threshold IFT seems to be between 0.3 and 0.05 mN/m. Furthermore, it is first when IFT drops below 0.05 mN/m that large changes in gas-oil relative permeabilities are observed. The publications where a threshold IFT higher than 0.3 mN/m was found did not include capillary end effects in their analysis of measured data.

Based on this review and analysis of literature data, it was decided to use a threshold IFT=0.3 mN/m in the simulation cases presented in Chapter 1.

Fig. 2.12 shows IFT as a function of pressure for the original Rich Gas A, and for four reservoir gases entering Region 1 at different stages in depletion. IFT in Region 1 is almost independent on the stage of depletion, as can be seen from the figure.

Fig. 2.13 shows IFT as a function of pressure for four different gas condensates. IFT in Region 1 ranges from about 0.5-20 mN/m with most of Region 1 having IFTs greater than about 1 mN/m. Note that lean gas condensates will probably never experience IFT effects because the IFT at the dewpoint pressure is higher than any probable threshold IFT.

Well deliverability is only important at the end of plateau production, because well deliverability has no effect before rate starts to decline. What a well can make initially is only of theoretical interest. The flowing bottomhole pressure (p_{wf}) at the end of plateau is usually between 1000-2000 psia with an average reservoir pressure p_R > 4000 psia. As can be seen form **Fig. 2.13** interfacial tension between oil and gas is higher than or close to the threshold IFT at the end of plateau. Therefore, the effect interfacial tension has on well deliverability when a well goes on decline is little, if any, even for a near critical gas condensate.

IFT may have a small effect on well deliverability for rich gas condensate systems if the well goes straight on depletion. However, for this type of low-permeability well the IFT effect on relative permeabilities will be one of several major uncertainties. The effect IFT has on well deliverability is discussed in more detail, with examples, in Chapter 1. To conclude, the potential effect IFT has on well deliverability is expected to be either small or non-existent.

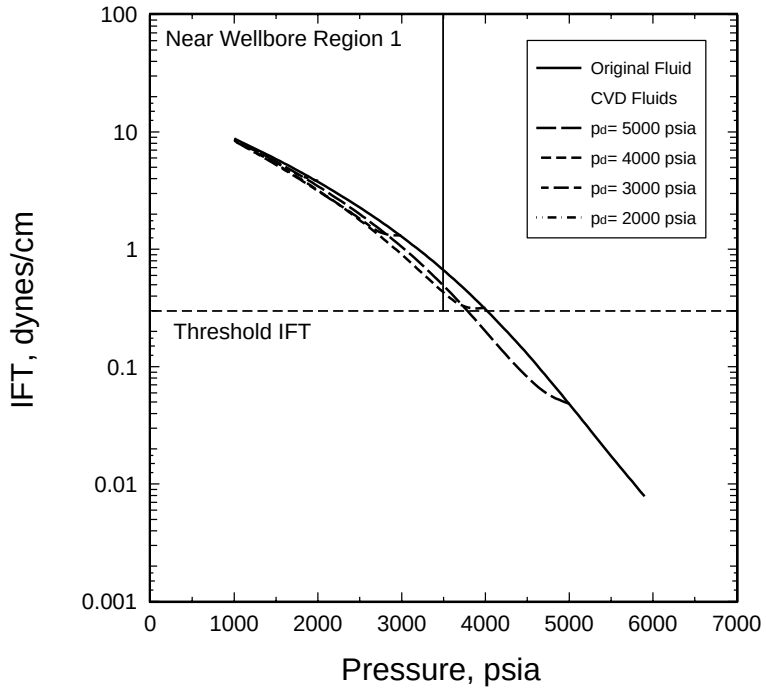

Fig. 2.12 Interfacial tension as a function of pressure for Rich Gas A condensates. IFT's for different CVD gases is calculated from a simulated CCE experiment.

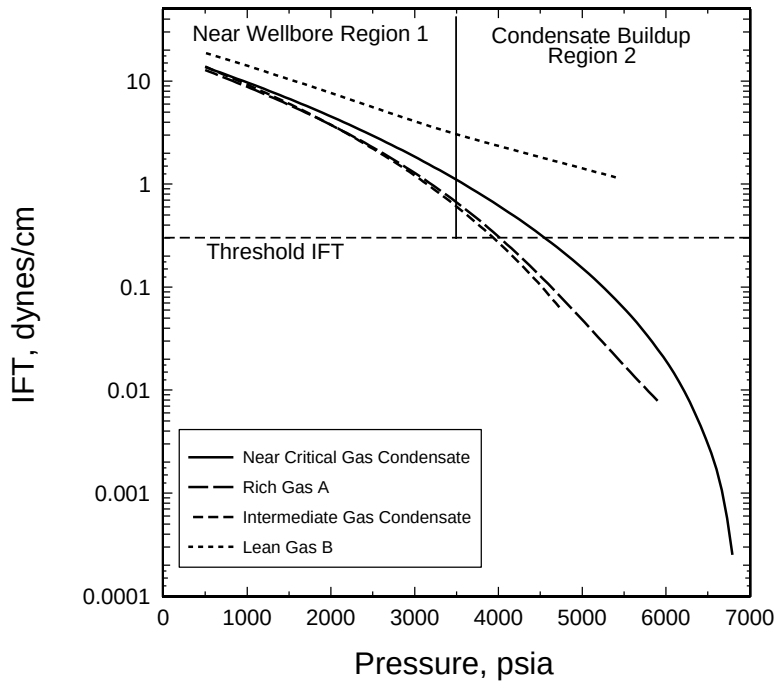

Fig. 2.13 Interfacial tension as a function of pressure for different gas condensates. IFT is calculated from a constant composition expansion experiment of the initial fluid.

2.3.4. Velocity/IFT Effect (Capillary Number N_c)

Ham and Eilerts[23] published one of the first papers studying relative permeabilities for gas condensate reservoirs. They used steady-state experiments to determine gas and condensate relative permeabilities. The experiments were conducted at room temperature and at two pressures (500 and 1500 psia). Most of their experiments were performed using a Berea core with a permeability of 100 md and a porosity of 18%, and without water in the core. Some experiments were conducted using a limestone core from the Hall-Gurney field; the limestone core had a permeability of 16 md. The oil saturation in the core was determined by weighing the core.

Two different condensates were used to determine the effect of liquid viscosity. Nitrogen gas was used. Gas and oil relative permeabilities were measured for several flowing GORs (liquid-vapor ratios), and for three different velocities. Residual oil saturation was also measured for different gas rates. Residual oil saturation was found by injection of only gas after a steady-state measurement.

Ham and Eilerts observed that residual oil saturation and to some extent relative permeability to gas (when $S_o<S_{or}$) was a function of gas rate. Residual oil saturation was 50% for a gas velocity of 200 ft/day and 30% for a gas velocity of 850 ft/day. However, gas and oil relative permeabilities are neither influenced by gas velocity or liquid viscosity when both phases are mobile (see **Fig.(2.14)**).

The length of the core influenced by end effect decreases when the pressure drop over the core increases, which again decreases the average oil saturation in the core. The observed effect of velocity on S_{or} may be an artifact caused by end effects. The fact that $k_{rg}=f(k_{rg}/k_{ro})$ is not influenced by the gas rate supports this interpretation of their data (**Fig. 2.14**).

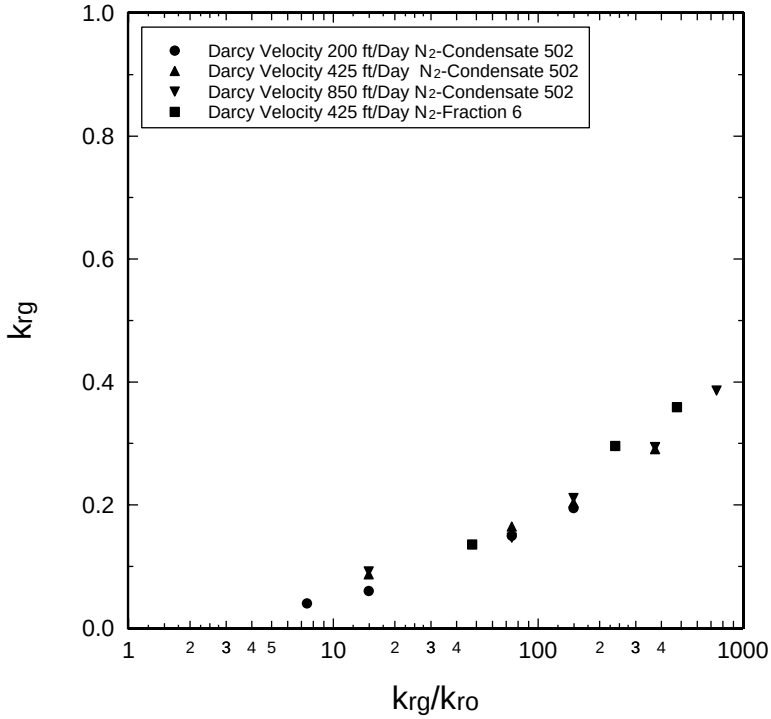

Fig. 2.14 Measured relative permeability data for Berea at 515 psia from Ham and Eilerts{Ham, 1967}. Reference permeability is absolute gas permeability measured at Darcy velocity of 200 ft/d.

Schulte[24] and coworkers at Shell have questioned the validity of using only IFT effect on relative permeabilities for gas condensate systems. They present arguments that indicate an additional improvement in gas-oil relative permeabilities due to high velocities experienced near the wellbore. They claim that capillary number should be used as a correlating parameter instead of IFT alone. Capillary number ($N_c=\mu_g v_s/\sigma$, where v_s is pore velocity) is the ratio of viscous to capillary forces. Some of their results are to be presented at the 1995 Annual SPE Technical Conference & Exhibition[25]. Relative permeability is generally not a function of fluid velocity, but there may exist a threshold velocity or capillary number where relative permeability starts to be a function of velocity.

Henderson et. al[20] studied the effect of velocity on relative permeability for low interfacial tensions (IFT < 0.4 mN/m) on a Berea core. The core was two feet long with a diameter of two inches. The porosity was 18.2 percent with an interstitial water saturation (S_{wi}) of 26.4%. The permeability of the core was 92 md at S_{wi}. A synthetic 5-component gas condensate was used. The relative permeabilities were measured using a combination of a steady-state and an unsteady-state displacement method. Initially the core was saturated with gas condensate above dewpoint pressure. The core was then depleted to a pre-determined pressure (no oil was produced out of the core). Equilibrium oil and gas at a fixed rate was then injected

into the core. When steady-state conditions were achieved, relative permeabilities and saturations were calculated based on a material balance of the production data. Subsequently a displacement experiment was performed to get relative permeabilities at lower oil saturations by injection of only gas at the same rate as used during the steady state experiment. The two systems they used had IFTs of 0.05 and 0.4 mN/m, with flowing velocities ranging from 3 to 120 ft/d. However, only the steady-state value is presented for the highest velocity and highest IFT (120 ft/d and 0.4 mN/m.)

Fig. 2.15 shows a plot of the IFT=0.4 mN/m data plotted as k_{rg} vs. (k_{rg}/k_{ro}). The data for IFT=0.05 mN/m (which is totally irrelevant for well deliverability) is shown in **Fig. 2.16**. The velocity v_s is gas velocity divided by hydrocarbon flow area ($v_s=q_g/[A\phi(1-S_{wi})]$). The interfacial tension seems to change the shape of the curve, while velocity shifts the curve to higher k_{rg}. The relative increase in relative permeability as a function of velocity is about the same for the two IFT's.

Table 2.1 Gas pore velocity v_s, and Capillary number N_c as a function of radial distance from a radial well. The reservoir is the same as in Chapter 1.

Gas Rate (MMscf/D)	Distance From Wellbore Center					
	1 ft		5 ft		100 ft	
	v_s (ft/d)	N_c	v_s	N_c	v_s	N_c
1*	27	$9.7\cdot10^{-7}$	5.4	$1.9\cdot10^{-7}$	0.27	$9.7\cdot10^{-9}$
10*	268	$9.7\cdot10^{-6}$	54	$1.9\cdot10^{-6}$	2.7	$9.6\cdot10^{-8}$
40*	1073	$3.9\cdot10^{-5}$	215	$7.7\cdot10^{-6}$	10.7	$3.9\cdot10^{-7}$
1**	44.9	$3.6\cdot10^{-7}$	9.0	$7.3\cdot10^{-8}$	0.45	$3.6\cdot10^{-9}$
10**	449	$9.6\cdot10^{-6}$	90	$7.3\cdot10^{-7}$	4.5	$3.6\cdot10^{-8}$
40**	1797	$1.5\cdot10^{-5}$	360	$2.9\cdot10^{-6}$	18	$1.5\cdot10^{-7}$

* Fluid properties from Rich Gas A at 2500 psia
** Fluid properties from Rich Gas A at 1500 psia

Fig. 2.17 plots krg at (k_{rg}/k_{ro})=10 vs. capillary number N_c for the six velocity/IFT conditions reported. A clear increasing k_{rg} with N_c is seen. However, the practical range of N_c expected in the near wellbore Region 1 (when a well is approaching the minimum BHFP) is less than $5.0\cdot10^{-3}$ (**Table 2.1**).

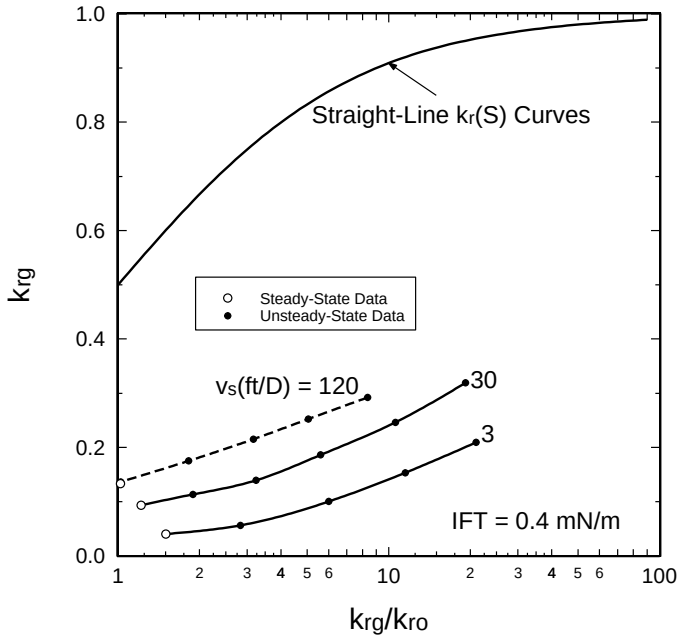

Fig. 2.15 Velocity effect on $k_{rg} = f(k_{rg}/k_{ro})$ relationship for a Berea sandstone and a synthetic gas condensate mixture at IFT of 0.4 dens/cm. Data taken from Henderson et al.

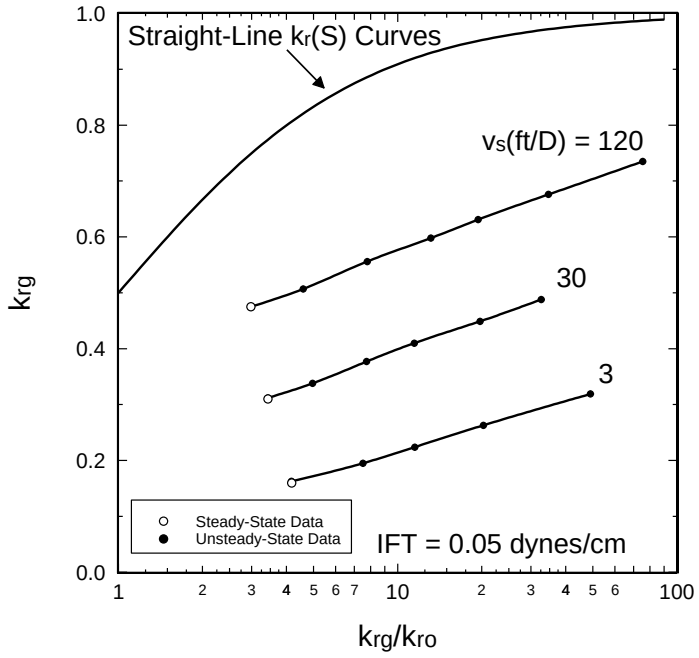

Fig. 2.16 Velocity effect on $k_{rg} = f(k_{rg}/k_{ro})$ relationship for a Berea sandstone and a synthetic gas condensate mixture at IFT of 0.05 dens/cm. Data taken from Henderson et al.

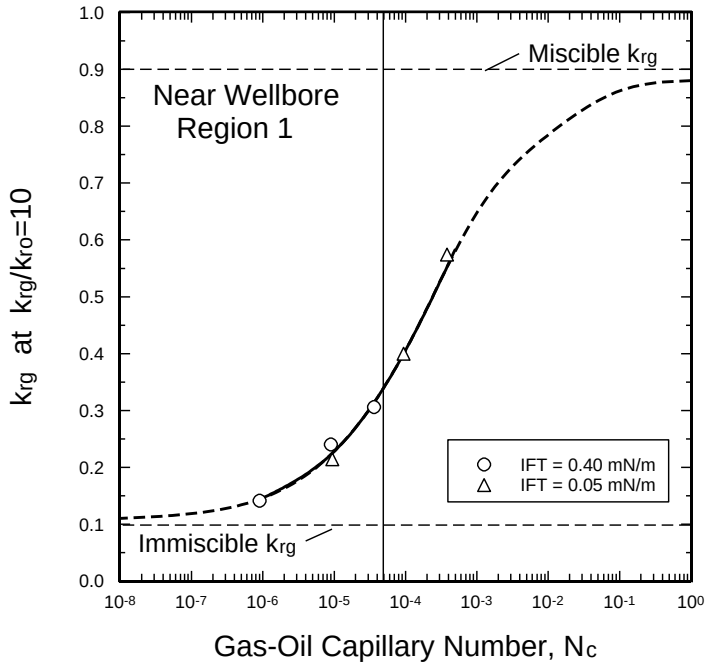

Fig. 2.17 Combined velocity effect on k_{rg} as a function of gas/oil capillary number for data presented by Hendersen et al.

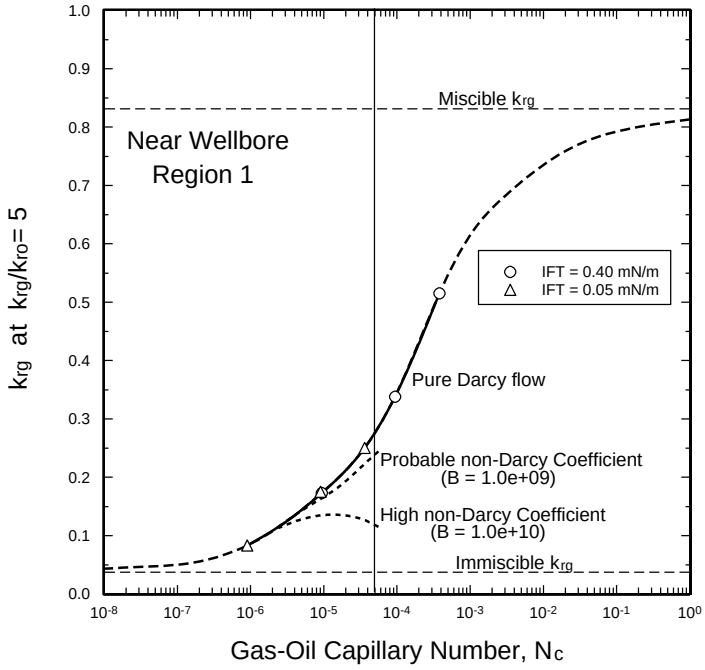

Fig. 2.18 Combined velocity/IFT and non-Darcy effect on k_{rg} as a function of gas/oil capillary number for data presented by Hendersen et al.

Near the wellbore where the velocity is highest, any positive effect that high N_c has on "Darcy" relative permeability may be reduced by non-Darcy flow effects. To estimate how much the non-Darcy flow effects reduces the positive effect caused by high N_c, some calculations were made using Rich Gas A and the same reservoir used in Chapter 1.

The Forchheimer equation[26,27] was used to model high-velocity flow,

$$-dp/dl = \frac{\mu_g}{k} v + \beta \rho v^2 \qquad \textbf{(2.3)}$$

where v is Darcy velocity and k is rock permeability. ρ is fluid density, and β is the non-Darcy flow coefficient.

Evans and Civan[28] suggest the following correlation for the non-Darcy flow β coefficient for single phase systems:

$$\beta = \frac{1.485 \cdot 10^9}{\phi k^{1.021}} \qquad \textbf{(2.4)}$$

For multiphase systems Evans and Civan[28] found that the β-coefficient can be estimated using the single phase correlation by replacing the rock permeability with the effective permeability. The β-coefficient for multiphase systems is:

$$\beta = \frac{1.485 \cdot 10^9}{\phi (k k_r)^{1.021}} \qquad \textbf{(2.5)}$$

To quantify the effect of non-Darcy pressure loss, an effective gas relative permeability $k_{rg,eff}$ is defined. $k_{rg,eff}$ is defined such that the pressure drop using only Darcy's law with $k_{rg,eff}$ is equal to the pressure drop using **Eq.(2.3)**. $k_{rg,eff}/k_{rg}$ is then:

$$\frac{k_{rg,eff}}{k_{rg}} (v_g) = \left[1 + \frac{k k_{rg}}{\mu_g} \beta \rho_g v_g \right]^{-1} \qquad \textbf{(2.6)}$$

Fig. 2.18 plots k_{rg} at $(k_{rg}/k_{ro})=5$ vs. capillary number N_c. The solid line represents the data given by Henderson et al. (pure Darcy flow). The short dashed lines represents the effective $k_{rg,eff}$ (for two different β-coefficients) when Forchheimer's equation (**Eq.(2.3)**) is used to model flow. IFT (σ=2 mN/m) and other fluid properties are taken at 2500 psia. The data used to make **Fig. 2.18** are given in the **Table 2.2.** The Darcy velocity one foot from the wellbore center is 240 ft/D, for a production rate of 40 MMscf/D using the reservoir presented in Chapter 1.

Table 2.2 Effective gas relative permeability $k_{rg,eff}$ as a function of gas velocity, for Rich Gas A.

Gas Velocity v(ft/D)	Capillary Number $N_c=\mu_g v_s/\sigma$	k_{rg} (N_c Effect only)	β from Eq.(2.5) (single phase $\beta=1.0\cdot10^{9}$ ft^{-1})		Single phase $\beta=1.0\cdot10^{10}$ ft^{-1} (High value)	
			$k_{rg,eff}/k_{rg}$	$k_{rg,eff}$	$k_{rg,eff}/k_{rg}$	$k_{rg,eff}$
6	$9.6\cdot10^{-7}$	0.084	1.000	0.084	0.975	0.081
15	$2.4\cdot10^{-6}$	0.120	0.994	0.119	0.941	0.113
30	$4.8\cdot10^{-6}$	0.143	0.988	0.141	0.890	0.127
120	$1.92\cdot10^{-5}$	0.201	0.953	0.192	0.670	0.135
240	$3.84\cdot10^{-5}$	0.248	0.911	0.226	0.505	0.125
350	$5.6\cdot10^{-5}$	0.279	0.875	0.244	0.412	0.115
All fluid properties are taken at 2500 psia						

Henderson et. al[20] also conducted some conventional gas-oil displacement tests with the same core. In these tests the core was saturated with equilibrium oil prior to the unsteady-state drainage tests. Displacement experiments were performed for three different gas rates (30 ft/D, 120 ft/D and 230 ft/D) at an IFT=0.14 mN/m. Almost no rate effect on relative permeability was observed.

The actual profile of N_c in Region 1 needs to be studied in more detail. It is suspected that this profile will be very different in radial and vertically fractured wells. Although, the results in the paper by Henderson et. al[20] are interesting, they need to be confirmed with measurements at higher IFTs which are more representative for Region 1. According to **Fig. 2.13** the IFT in Region 1 ranges from 1 to 20 mN/m.

2.4. Proposed Experimental Procedure

2.4.1. General Description

The main use of relative permeabilities in gas condensate reservoirs is for well deliverability calculations. The deliverability loss is largest near the wellbore (Region 1). The most important relative permeability data for well deliverability calculations is therefore $k_{rg}=f(k_{rg}/k_{ro})$, as shown in Chapter 1. It is recommended that this relation always be determined accurately for k_{rg}/k_{ro} values ranging from a maximum of $(k_{rg}/k_{ro})=50$ to a minimum determined by PVT calculations, based on **Eq.(2.1)** with the original reservoir fluid ($R_p=1/r_{si}$).

Gas relative permeability as a function of oil saturation at lower oil saturations may be useful for calculations in the condensate buildup region (Region 2). The range of oil saturations needed for Region 2 is defined by the CVD liquid dropout curve. This data is usually only needed for gas condensates where the maximum liquid dropout is greater than 10%. For leaner gas condensates the, the maximum reduction in k_{rg} in Region 2 is less than 10-20%.

Region 1: Steady-State Flow Measurements [$k_{rg}=f(k_{rg}/k_{ro})$]
Flow in the near wellbore region is a steady-state process. In Region 1, the mixture entering a volume element ΔV at radius r is the same mixture leaving the volume element. Practically, a core plug can be considered as such a volume element. The proposed procedure is based on conducting steady-state flow tests on core plugs. Core plug flow tests should be conducted such that they are representative of conditions in Region 1 throughout depletion. It is recommend to use gas from different CVD pressure stages in the steady-state flow tests. The gas is flashed through a choke or a back pressure regulator to the core pressure. The resulting gas-oil mixture flows through the core.

At least five or six steady state points should be measured to define the $k_{rg} = f(k_{rg}/k_{ro})$ relation. Flowing conditions for these points are determined using the PVT-derived plot of $k_{rg}/k_{ro}(p)$ from **Eq.(2.1)** [using equally spaced $\log(k_{rg}/k_{ro})$ values] evaluated, at or close to minimum BHFP. An example is shown in **Fig. 2.19** for Lean Gas B.

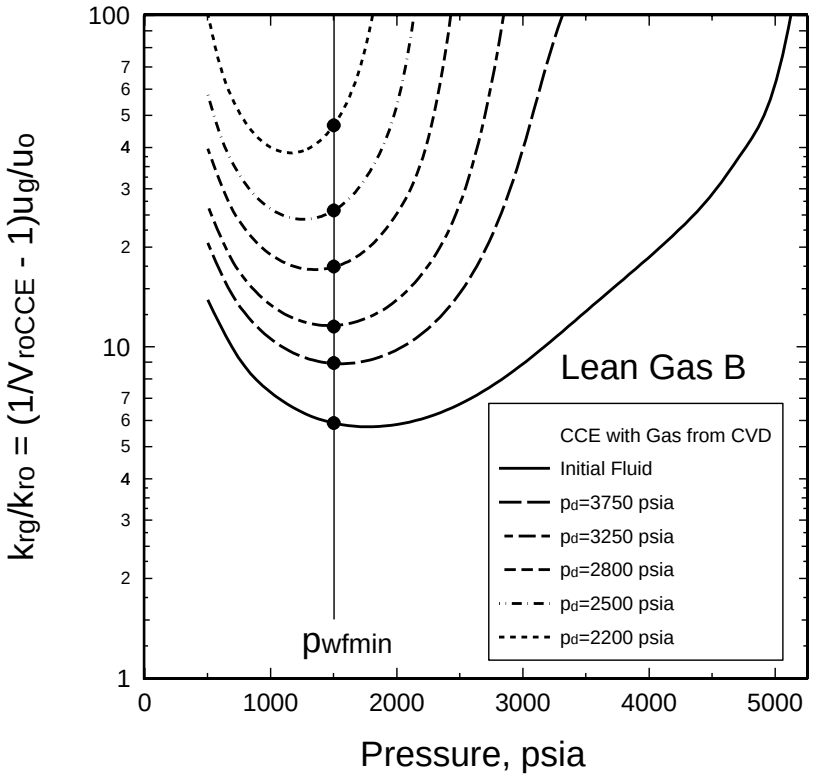

Fig. 2.19 Design plot for Lean Gas B showing the range of k_{rg}/k_{ro} values that should be measured experimentally for accurate modelling of Region 1 flow behavior.

Equipment

A diagram of the apparatus is shown in **Fig. 2.20**. The apparatus consists of the following components:

1. Two high-pressure containers. At the beginning of each steady-state experiment Container 1 is full and Container 2 is empty. During the flow period all of the produced fluid is collected in Container 2. After steady-state conditions are achieved and relative permeability is measured, Container 2 and the core is brought to a pressure significantly above the pressure in Container 1. The pressure in Container 1 is the dewpoint pressure of the total fluid mixture in Container 2 and in the core. All fluid is then pumped back into Container 1.

2. Two Back pressure regulators (BPR): BPR 1 is needed to keep the pressure in Container 1 constant. BPR 2 is needed to keep the pressure in the core constant. (The pump connected to Container 2 can also be used to keep the pressure in the core constant.)

3. Coreholder with an absolute pressure transducer, and a differential pressure

transducer to measure pressure drop during flow experiments. To avoid problems with gas overrun, it is recommended to mount the core vertically.

4. View glass (sapphire glass): The view glass is mainly needed to check if condensate is produced out of the core during measurements of $k_{rg}(S_o)$ at low oil saturations (Region 2 calculations), but it may also be useful during the steady-state experiments.

5. A valve to deplete the system pressure.

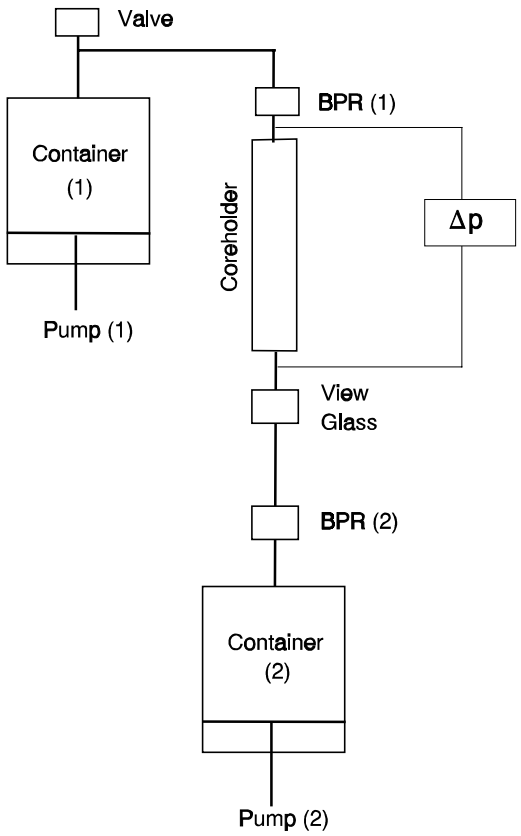

Fig. 2.20 Sketch of the apparatus for relative permeability measurements.

Procedure

The first data is measured using the original reservoir fluid. This mixture is flowed through the core at a pressure equal to the minimum BHFP until steady-state conditions are reached. The pressure drop across the core is used to calculate phase mobilities using

$$k_{rg} = q_{g,core} \frac{L}{kA\Delta p} \mu_g$$
$$k_{rg} = q_{o,core} \frac{L}{kA\Delta p} \mu_o \qquad \textbf{(2.7)}$$

$$q_{g,core} = q_{inj}(1 - V_{ro,core})\frac{V_{rt,core}}{V_{rt,inj}}$$
$$q_{o,core} = q_{inj} V_{ro,core} \frac{V_{rt,core}}{V_{rt,inj}} \quad \textbf{(2.8)}$$

where $V_{ro}=V_o/(V_g+V_o)$ and $V_{rt}=(V_g+V_o)/V_d$ are relative volumes from a CCE test of the flowing reservoir mixture. Subscript "core" indicates that the quantity is evaluated at the pressure in the core, and "inj" indicates the quantity is evaluated at the pressure of Container 1. Core and Container 1 temperatures are assumed equal in **Eqs. (2.8)**. If the steady-state experiment is influenced by capillary end effects, it is more complicated to calculate gas and oil relative permeabilities. The end effect is discussed in a subsequent section.

Before the next depletion stage can be performed, the condensate in the core and in Container 2 must be removed and returned to Container 1 and the coreholder. The easiest way to remove the condensate is by vaporization. This is done using the following procedure:

> Raise the pressure in Container 2 and in the core significantly above the pressure in Container 1. Pump the fluid in Container 2 through the core into Container 1. Check if original permeability is obtained in the core by flowing equilibrium gas through the core. If original permeability is not obtained, pump all equilibrium gas from Container 1 into Container 2. Raise the pressure in Container 2 significantly and pump the gas through the core into Container 1. Keep on with this "circulation" until original permeability is obtained in the core. Before the next depletion step, pump all fluid in Container 2 back into Container 1.

The entire system pressure [Container 1 and the coreholder] is lowered by producing gas out of the system. The depletion pressures are determined from a design plot similar to **Fig. 2.19**. The rate of depletion should not be higher than 18 psi/min to keep equilibrium between the gas and the condensate during pressure depletion (Saeidi and Handy[18]). This results in a depleted reservoir gas (similar to that obtained from a CVD process). This gas mixture is flowed through the core at minimum BHFP until steady state conditions are reached. The pressure in Container 1 should be held constant during each steady-state experiment to keep the mixture entering the core constant.

This process is continued until a reservoir gas with $(k_{rg}/k_{ro})=50$ is reached in the core (at minimum BHFP). The Container 1 "depletion" pressure of this last data is known from calculations made earlier using **Eq. (2.1)**.

A plot is made of k_{rg} vs. (k_{rg}/k_{ro}) using a semilog scale. The relation describing these data are the key to accurate description of well deliverability.

Several steady-state points can be measured for a given reservoir gas mixture (if sufficient fluid sample is available). For example, injection rate can be varied to study velocity effects, and/or to minimize end effects. Flow tests at core pressures greater than minimum BHFP can also be made, e.g. to study the potential effect of IFT on relative permeability (i.e. on the k_{rg} vs. k_{rg}/k_{ro} relationship). For practical purposes, IFT is only dependent on pressure, so a suite of steady-state measurements can be made at three or four pressures to establish any IFT effect on the krg=f(k_{rg}/k_{ro}) relationship.

Saturation Measurement for Steady State Test.
Although saturations do not need to be measured for each steady-state test, it is recommended to measure oil saturation for one test, and preferably the final test. This additional data will help to convert the $k_{rg} = f(k_{rg}/k_{ro})$ function to a saturation-dependent relation that can be input to a simulator. It is recommended to measure saturations for the highest k_{rg}/k_{ro}, mainly because this data point together with k_{rg} measurements at immobile oil saturations secure good $k_{rg}(S_o)$ data for Region 2 calculations. Oil saturation at high k_{rg}/k_{ro} values also have some influence on the size of Region 1.

After reaching steady state conditions with the final reservoir gas mixture, flow is stopped. Container 2 is brought to the pressure conditions that existed in the coreholder during the last steady-state experiment and the condensed oil is removed temporarily from the system. The remaining gas in Container 2 is compressed to a high pressure, and connected with the core. The compressed gas is used to displace the fluids in the core at elevated pressure into a receiving container.

After sufficient displacement at high pressure, flow is stopped, the receiving container is disconnected from the core and brought to the pressure conditions that existed in the coreholder during the last steady-state experiment. Oil volume is measured, where this volume is easily shown to equal the average core oil saturation times pore volume.

Equilibrium Gas Flow (Region 2): $k_{rg} = f(S_o)$.
For richer gas condensates, the deliverability loss due to condensate accumulation in Region 2 can also be significant. Here k_{rg} as a function of saturation is needed directly. The procedure recommended for measuring $k_{rg}(S_o)$ uses a CVD type process. At each depletion stage, the *entire* system (core and Container 1) is brought to equilibrium by removing gas from the system. If limited amount of fluid is available it is recommend that the removed gas is stored in Container 2. The rate of depletion should not be higher than 18 psi/min to keep equilibrium between the gas and the condensate during pressure depletion(Saeidi and Handy[18]). This procedure were also used by Graver et al.[17] to obtain gas relative permeability at low condensate saturation.

At each depletion pressure, equilibrium gas is flowed through the core and the pressure drop is measured. k_{rg} is calculated from **Eq. (2.7)**, and saturation is taken from the CVD liquid dropout curve, $S_o=V_{roCVD}(1-S_{wi})$. Measurements are made at decreasing pressures until the maximum liquid dropout occurs, or until oil flow is observed. A sight glass downstream to the core holder is used to detect oil flowing from the core (**Fig. 2.20**).

Any IFT effect on k_{rg} at these high pressures will automatically be included in the $k_{rg}(S_o)$ measurements. For rich gas condensates this may lead to overpredictions of gas relative permeability in Region 2 late in depletion, since the liquid dropout curve has a maximum. To quantify any IFT effects, gas relative permeability can be measured on "both sides" of the maximum liquid dropout. However, as shown in Chapter 1, Region 2 is very small (if existent) for rich gas condensates late in depletion.

2.4.2. Choosing the Fluid System

Reservoir Fluids
One of the main reasons for using reservoir fluid in gas condensate relative permeability measurements is the large uncertainty in oil viscosity. Oil viscosity is (almost) never measured, and viscosity correlations seldom predict oil viscosity accurately. The consequence of an erroneous calculated oil viscosity is that oil saturation in Region 1 will be in error, because the oil mobility in Region 1 is basically fixed. An erroneous oil saturation will lead to an erroneous gas relative permeability. The effect of an erroneous calculated oil viscosity is reduced when reservoir fluid is used in the experiment. However this requires that the same fluid characterization (EOS and viscosity correlation) be used *both* in simulation and to interpret the relative permeability measurements. The effect of an erroneous oil viscosity is reduced because any error in the EOS calculated oil viscosity will be canceled by an "opposite" error in the oil relative permeability when oil relative permeabilities are calculated from the laboratory results.

Using real reservoir fluid in relative permeability measurements also ensures that the relevant range of k_{rg}/k_{ro} is covered. Another advantage is that relative permeabilities are measured under conditions similar to the actual conditions existing near the wellbore throughout depletion.

Synthetic Fluids
The advantage with synthetic fluids is that phase behavior and physical properties as a function of pressure and temperature may already be known, or readily measured. Furthermore, for a synthetic fluid the pressure and conditions where retrograde condensation exist are closer to ambient temperature conditions. Properly selected synthetic fluids can have the desired phase behavior close to ambient temperature but at elevated pressure.

To secure that a relevant range of k_{rg}/k_{ro} is covered when a synthetic gas condensate is used to measure relative permeabilities, a design plot both for the reservoir gas and for the synthetic gas condensate must be made. The synthetic CVD gases to be injected are defined such that they cover the relevant k_{rg}/k_{ro} range existing in Region 1 throughout depletion (for the actual reservoir fluid). The relevant range of k_{rg}/k_{ro} in Region 1 is taken from the design plot of the reservoir fluid. Comparison of calculated IFTs for the synthetic and actual reservoir fluids will ensure that unintentional IFT effects on measured relative permeability data are avoided.

Traditionally binary systems have been used to measure relative permeabilities in gas condensates, mainly because binary systems have properties and compositions that are only a function of pressure and temperature (independent of overall composition).

Simple Fluids (N_2-Condensate)
Simple fluid systems are often used when experiments are conducted at ambient pressure and temperature conditions. The disadvantage with this approach is that the phase behavior does not mimic what happens in a gas condensate reservoir. Furthermore, IFT and especially the viscosity ratio is far from the actual gas condensate system. The advantage with a simple fluid system is that much simpler laboratory equipment can be used. More experimental work is needed both with reservoir fluids and simple fluids to verify that relative permeability measurements can be performed using simple fluid systems. Measuring gas relative permeabilities for Region 2 calculations is particularly difficult with simple fluids.

2.4.3. Interpreting Laboratory Results

Region 1 effect on well deliverability is controlled by the fundamental relationship k_{rg} vs. k_{rg}/k_{ro}. Saturations are of secondary importance, and they are often expensive to measure. Thus, it is suggested to measure saturation for only one or two steady-state flow experiments.

The measured data must be expressed, finally, in a form that can be used in reservoir simulation, namely k_{rg} and k_{ro} as functions of saturation(s). This conversion process is readily automated by fitting the parameters in a relative permeability model (Corey[29], Honarpour et al.[30], Chierici,[31] etc.) to the steady-state k_{rg} vs. k_{rg}/k_{ro} data, and the available saturation data from one or more of the steady-state tests.

The proposed interpretation procedure ensures that $k_{rg}=f(k_{rg}/k_{ro})$ is measured for the relevant range of k_{rg}/k_{ro} in Region 1, and that $k_{rg}(S_o)$ is measured at low oil saturations. $k_{rg}(S_o)$ and $k_{ro}(S_o)$ may not be correct at higher oil saturations, but this will not influence well deliverability.

To verify that laboratory experiments conducted using the proposed procedures result in a "unique" description of well deliverability, the following test was made.

Measured relative permeability data described by two different parametric relative permeability equations, shown as Set B and Set B' in **Figs. 2.21-2.23**. Saturations are only measured after the last two-phase flow experiment (k_{rg}/k_{ro} = 10). The two parametric equations fit the same "measured" data equally well, but have completely different relative permeability curves at higher oil saturations (**Figs. 2.21 and 2.22**). As shown in **Fig. 2.24**, the two parametric equations give the same rate-time behavior. We have found that this is not a special case, but general for all gas condensates.

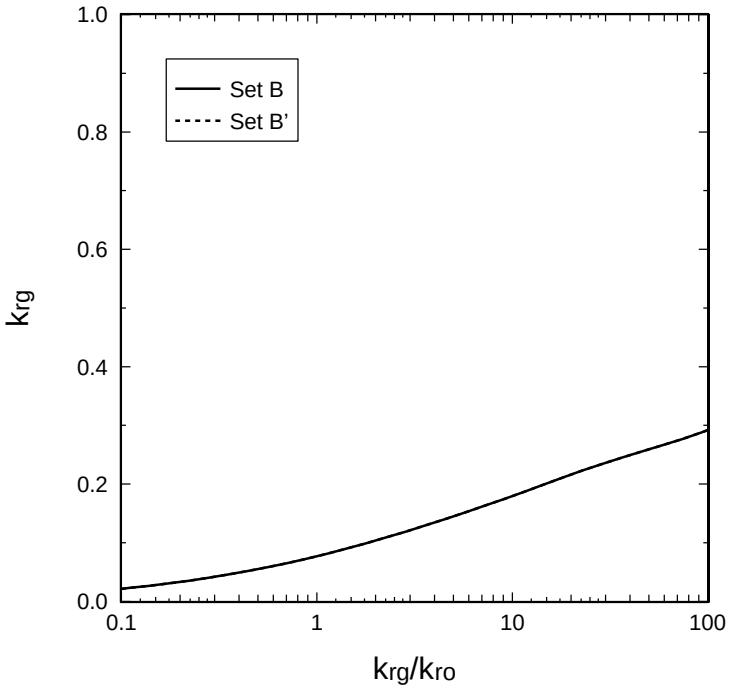

Fig. 2.21 Identical k_{rg} vs. k_{rg}/k_{ro} for the two completely different sets of $k_{rg}(S_g)$ and $k_{ro}(S_g)$ curves.

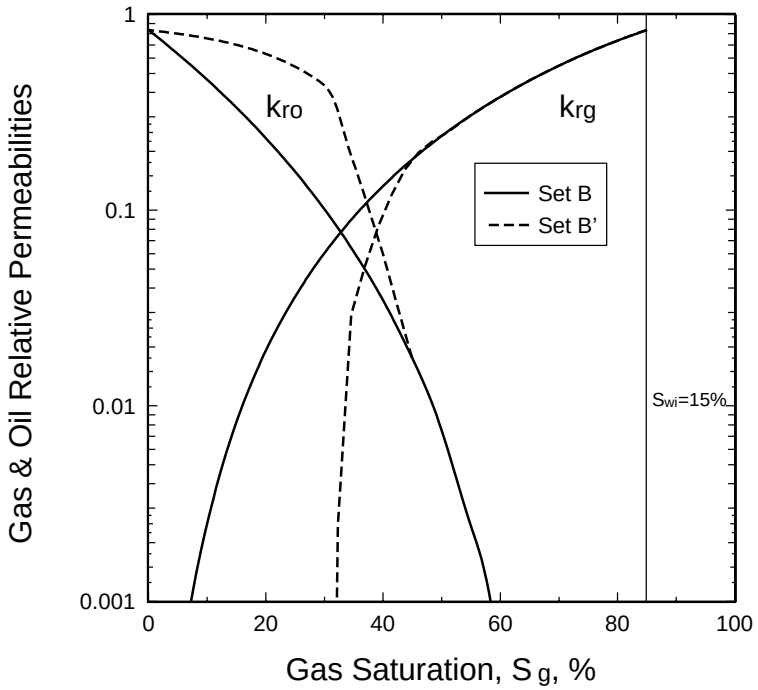

Fig. 2.22 Two sets of gas-oil relative permeability curves that have identical $k_{rg}=f(k_{rg}/k_{ro})$ relationships.

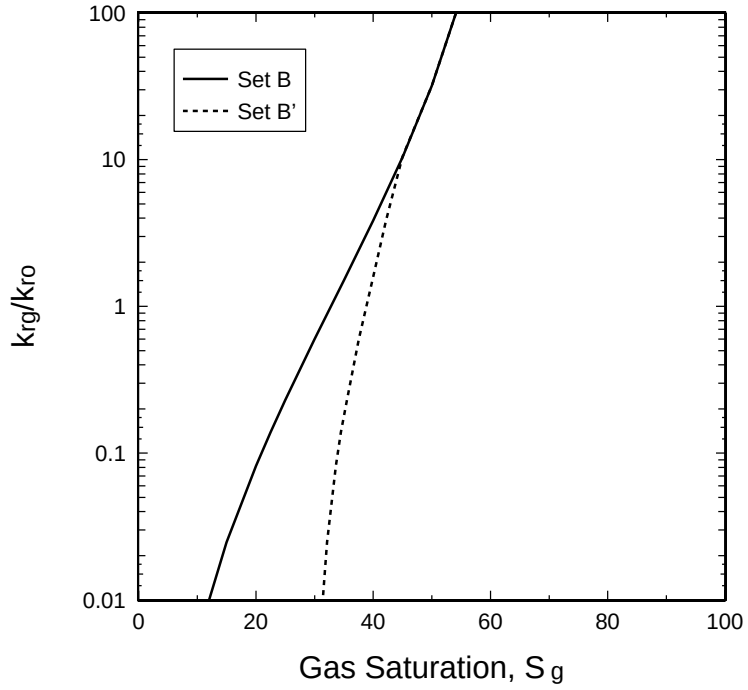

Fig. 2.23 k_{rg}/k_{ro} vs. S_o for two sets of gas-oil relative permeability curves that have identical $k_{rg}=f(k_{rg}/k_{ro})$ relationships.

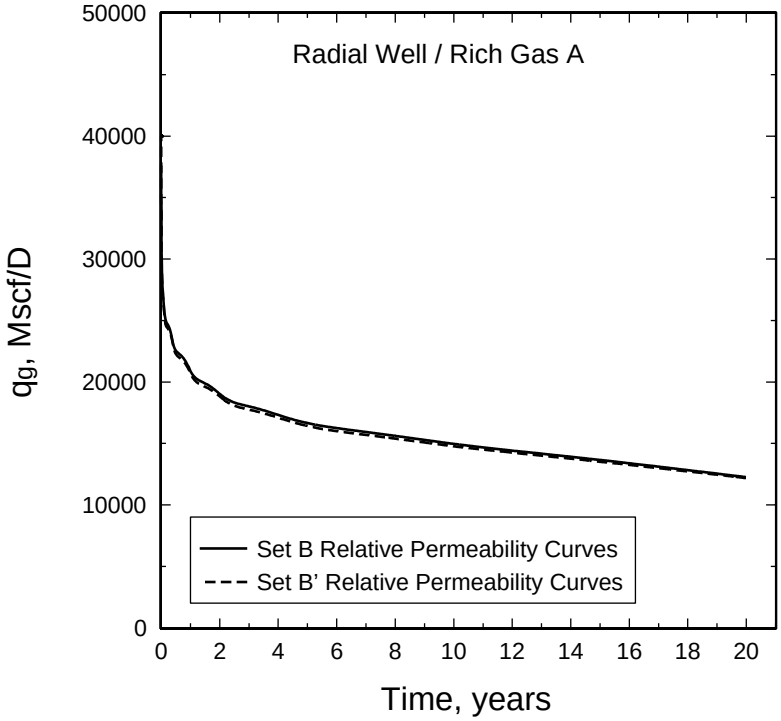

Fig. 2.24 Rate-time performance of a radial well with Rich Gas A, using two dramatically different sets of gas-oil relative permeabilities (**Fig.** 2.22)

2.4.4. Boundary Effects

When relative permeability is calculated from experimental data obtained by the steady-state method, capillary end effects are usually neglected. It is often assumed that: (1) the saturation is constant along the core, (2) the pressure gradient along the core is constant, and equal to the difference in terminal pressures over the core divided by the core length, and (3) gas and oil pressures are either equal along the entire core length, or uniformly different by a constant capillary pressure. Gas and oil relative permeabilities are then obtained using **Eq. (2.7)**.

The capillary forces existing in a porous medium tend to retain the wetting fluid, resulting in a higher wetting fluid saturation near the outflow end. This is usually called "end effect". The end effect causes a capillary transition zone near the outlet end which again induces a saturation gradient in the core. Inaccuracies in calculated relative permeabilities using **Eq. (2.7)** depend on the relative size of the capillary transition zone compared with the total length of the core. Richardson et al.[1] found that if the capillary transition zone covers less than 5% of the core length then the capillary transition zone can be neglected, and **Eq. (2.7)** can then be used to calculate relative permeabilities.

The size of the region influenced by an outflow end effect depends on capillary pressures and fluid velocity. If fluid velocity is increased, the extent of the core portion influenced by end effect decreases, and consequently the fraction of the total pressure drop influenced by end effect decreases.

The initial fluid in the core at the start of a steady-state flow test can be either the wetting phase or the non-wetting phase. The saturation and capillary pressure conditions at the outlet end, once steady state is reached, depends on the fluids in the core before the steady-state experiment starts. If the core is initially saturated with the *wetting phase* it is a *drainage* steady-state experiment. If the core is initially saturated with the *non-wetting phase* it is an *imbibition* steady-state experiment. Let us consider first a drainage steady-state experiment.

Drainage Steady-State Experiment

Richardson et al.[1] studied the boundary effect by measuring the oil and gas saturation along the core during steady-state *drainage* experiments. Based on the experimental results they developed a theoretical procedure to calculate saturations along the core for steady-state experiments.

Richardson et al. observed that the gas saturation (non-wetting fluid) at the outflow face was always equal to the critical gas saturation. Furthermore, they found that the oil (wetting fluid) pressure was continuous across the outflow boundary whereas the gas pressure was discontinuous at the outflow boundary. On the other hand the gas pressure was continuous across the inflow boundary, whereas the oil was discontinuous at the inflow boundary. The pressure drop of the oil caused by flow in the core was equal to the pressure drop measured over the core minus the capillary pressure at the entrance.

Richardson et al. observed that relative permeability of the gas (non-wetting) phase was the only one appreciably affected by saturation gradients associated with the end effect. At low flow rates the error in the measurements of relative permeability was primarily due to the inability to determine the correct pressure gradients simply by measuring terminal pressures and core length.

When equilibrium gas and oil flow through a horizontal core (at velocities where Darcy law is valid) the following three equations can be used to describe the flow when oil is the wetting phase:

$$dp_o = \frac{q_o \mu_o dl}{k k_{ro} A}$$

$$dp_g = \frac{q_g \mu_g dl}{k k_{rg} A} \qquad \textbf{(2.9)}$$

$$dp_c = dp_o - dp_g$$

where the first equation is Darcy's law applied to the oil phase, the second is Darcy's law applied to the gas phase, and the third equation relates the fluid pressures through capillary pressure. By substituting the fluid pressures in the Darcy equations with capillary pressure the following equation can be obtained (Richardson et al.[1]):

$$\frac{dS_o}{q_g dL} = \left(\frac{F_{og}\mu_o}{kk_{ro}} - \frac{\mu_g}{kk_{rg})} \right) \frac{1}{A} \frac{1}{dp_c/dS_o} \qquad \textbf{(2.10)}$$

where q_g is gas rate, k is absolute permeability, S_o and S_g are oil and gas saturation respectively, p_c is gas-oil capillary pressure, F_{og} is the flowing in-situ OGR.

The oil saturation along the core for different fluid velocities in a drainage experiment can be calculated using **Eq. (2.10)** in the following procedure[1]:

1. Calculate dp_c/dS_o for 10 to 20 different oil saturations. The oil saturations should range from $S_o=1-S_{gc}-S_{wi}$ (maximum oil saturation) to the lowest oil saturation in the core during all the steady-state flow tests. The lowest oil saturation (S_{omin}) in the core can be obtained by finding the oil saturation that satisfies the equation, $[k_{ro}/k_{rg}(S_{omin})=F_{ogmin}\ \mu_o/\mu_g]$, where $F_{og,min}$ is the lowest oil-gas ratio used in steady-state experiments.

2. Find k_{ro} and k_{rg} for the oil saturations chosen in step 1. If the relative permeability is already measured (potentially with errors due to end effect), use the measured data curves. Alternatively if designing an experiment, use a relative permeability model to obtain k_{ro} and k_{rg}. A model that uses information from the capillary pressure curve is recommended (e.g. a Corey model[29]).

3. Calculate ratio $dS_o/q_g dL$ from **Eq.(2.10)** for the oil saturations chosen in step 1 using a constant F_{og}. A constant $F_{og,min}$ should be used If this plot is made for design purposes because the end effect is largest for $F_{og,min}$.

4. Establish $q_g L$ vs. S_o by numerical integration using the reciprocal of $dS_o/q_g dL$ ($[dS_o/q_g dL]^{-1}$). Start at the outflow face with critical gas saturation and continue until oil saturation reaches a constant value.

4. Plot the relationship S_o vs. $q_g L$.

5. Choose a core length and a gas velocity such that the saturation gradient caused by the boundary effect does not extend more than 5% into the core (if the end effect is to be neglected when interpreting the measured data).

The saturation at the outlet end is always very close to the critical oil saturation. This corresponds to the lowest capillary pressure where the gas still has mobility to flow out of the core. The oil saturation along the core always decreases from the

outlet until it reaches a nearly constant value. The oil and gas saturation in the part of the core unaffected by the end effects is determined by the following relationship [$k_{ro}/k_{rg}(S_o)=F_{og}\ \mu_o/\mu_g$]. This relationship is readily obtained by setting the differential capillary pressure equal to zero in **Eq. (2.10)**.

Outlet End Imbibition Steady-State Experiment

For an imbibition process the capillary pressure is zero for a wetting phase saturation less then 100%. The capillary pressure at the outlet in an imbibition steady-state experiment is zero because this will result in a continues phase pressure for both the oil and the gas phase. Thus, the wetting and non-wetting saturations at the outlet end are, in this case, always equal to the saturation in the core after a spontaneous imbibition experiment. Consequently, the wetting phase saturation upstream the outlet face may increase or decrease depending on the injection ratio of the wetting to the non-wetting phase. The capillary pressure in the core can accordingly ether increase or decrease along the core.

The procedure by Richardson can also be used to design an imbibition steady-state experiment. The only difference is that an imbibition capillary pressure curve should be used instead of a drainage capillary pressure curve. Furthermore, the capillary pressure at the outlet end is zero, as mentioned already.

The proposed steady-state experimental procedure for obtaining relative permeabilities for gas condensate systems is an *imbibition* steady-state experiment. This is because the core is initially saturated with gas and some condensate prior to each depletion experiment. The initial condensate saturation comes from bleeding core pressure core from the current pressure stage to the core pressure where the steady-state experiment is performed.

2.5. Conclusions

1. A new laboratory method for measurement of gas condensate relative permeabilities is proposed. The method is specifically designed to obtain relative permeability data needed for well deliverability calculations.

2. Relative permeabilities are measured under conditions that mimic the flow in the reservoir during depletion. The fundamental relationship $k_{rg}=f(k_{rg}/k_{ro})$ that exists in Region 1 is established by injecting different gas-oil mixtures through the core at pressures expected near the wellbore when the well goes on decline. The different injection reservoir gas mixtures are obtained from a simple constant volume depletion of the original reservoir mixture.

3. Reservoir fluids can readily be used to perform the relative permeability measurements. Using reservoir fluids is recommended, in fact, to minimize potential errors in relative permeability data due to inaccuracies in oil (and gas) viscosity.

   Alternatively, synthetic mixtures with phase and volumetric behavior similar to the reservoir fluid can be used. Synthetic mixtures will most often be required for lean gas condensates where sufficient sample volumes of reservoir fluid are not available.

4. Velocity effects on the $k_{rg} = f(k_{rg}/k_{ro})$ relationship can easily be measured by varying the velocity for each steady-state point. IFT effects on the $k_{rg} = f(k_{rg}/k_{ro})$ relationship can also be measured by varying the core pressure.

5. A design plot based only on PVT properties can be used to determine the range of conditions for steady-state flow tests. The design plot ensures that k_{rg} is measured at relevant conditions of pressure, IFT, velocity, and (most importantly) k_{rg}/k_{ro} existing in the near-wellbore Region 1 when wells are on decline, and throughout depletion of the reservoir.

6. Only one direct saturation measurement is necessary. The proposed method for measuring saturation in the core (after a steady-state experiment) is accurate and simple.

7. The proposed laboratory procedure and required equipment greatly simplify relative permeability measurements for gas condensates, while still ensuring that the most important data required for well deliverability calculations are obtained.

2.6. References

1. Richardson, J.G., Kerver, J.K., Hafford, J.A., and Osoba, J.S.: "Laboratory Determination of Relative Permeability," *Trans.*, AIME **195**, 187-196.

2. Henderson, G.D., Danesh, D.H., and Peden, J.M.: "An Investigation Into Processes Governing Flow and Recovery in Different Flow Regimes Present in Gas Condensate Reservoirs," Paper SPE 2661 pressented at the 1993 Annual Technical Conferance and Exhibition (Oct. 3-6), Houston.

3. Buckley, S.E. and Leverett, M.C.: "Mechanism of Fluid Displacement in Sands," *Trans.*, AIME, **146**, 107-116.

4. Craft, B.C. and Hawkins, M.: *Applied Petroleum Reservoir Engineering*, 1st ed., Prentice Hall, Inc., Englewood Cliffs, NJ (1959).

5. Bardon, C. and Longeron, D.G.: "Influence of Very Low Interfacial Tensions on Relative Permeability," *SPEJ* (1980) 391-401

6. Wagner, O.R. and Leach, R.O.: "Effect of Interfacial Tension on Displacement Efficiency," *Soc. Pet. Eng. J.* (1966) 335-344; *Trans.*, AIME, **166**.

7. Asar, H. and Handy, L.L.: "Influence of Interfacial Tension on Gas-Oil Relative Permeability in a Gas-Condensate System," paper SPE 11740, presented at the 1983 SPE Annual Technical Conference and Exhibition,.

8. Morel, D.C., Lomer, J.-F., Morineau, Y.M., and Putz, A.G.: "Mobility of Hydrocarbon Liquids in Gas Condensate Reservoirs: Interpretation of Depletion Laboratory Experiments," Paper SPE 24939 presented at the 1992 Annual Technical Conferance and Exhibition (Oct. 4-7), Washington.

9. Delclaud, J., Rochon, J., and Nectoux, A.: "Investigation of Gas/Oil Relative Permeabilities: High-Permeability Oil Reservoir Application," paper SPE 16966 presented at the 1987 Annual Technical Conference and Exhibition, Dallas, Sept. 27-30.

10. Haniff, M.S. and Ali, J.K.: "Relative Permeability and Low Tension Fluid Flow in Gas Condensate Systems," Paper SPE 20917 presented at the 1990 EUROPEC meeting (Oct. 22-24) (1990)

11. Bourbiaux, B.J. and Limborg, S.G.: "An Integrated Experimental Methodology for a Better Prediction of Gas-Condensate Flow Behavior," Paper SPE 28931 Presented at the 1994 Annual Technical Conferance (Sept. 25-28), New Orleans.

12. Danesh, A., Henderson, G.D., and Peden, J.M.: "Experimental Investigation of Critical Condensate Saturation and Its Dependence on Interstitial Water Saturation in Water-Wet Rocks," *SPERE* (1991) 336-342

13. Alonso, M.E. and Nectoux, A.C.: "Experimental and Numerical Investigations of the Primary Depletion of a Critical Fluid.," SPE paper 13266 presented at the 1984 Annual Technical Conference and Exhibition, Sept.16-19 (1984)

14. Wang, P., Stenby, E.H., and Pope, G.A.: "Compositional Modeling of Low Interfacial Tension Effects on Flow Behavior of Gas Condensate," Paper presented at the 1993 European IOR Symposium, Moscow, Oct. 27-29 (1993)

15. Jones, J.R. and Raghavan, R.: "Interpretation of Flowing Well Response in Gas Condensate Wells," paper SPE 14204 presented at the 1985 SPE Annual Technical Conference and Exhibition, Las Vegas, Sept. 22-25.

16. Chopra, A.K. and Carter, R.D.: "Proof of the Two-Phase Steady-State Theory for Flow Through Porous Media," *SPEFE* (1986) 603-608

17. Gravier, J.F., Lemouzy, P., Barroux, C., and Abed, A.F.: "Determination of Gas-Condensate Relative Permeability on Whole Cores under Reservoir Conditions," *SPEFE* (1986) 9-15

18. Saeidi, A. and Handy, L.L.: "Flow and Phase Behavior of Gas Condensate and Volatile Oils in Porous Media," paper SPE 4891 presented at the 1974 SPE Annual Technical Conference and Exhibition, San Francisco, April 4-5.

19. Danesh, A., Henderson, G.D., Krinis, D., and Peden, J.M.: "Experimental Investigation of Retrograde Condensation in Porus Media at Reservoir Conditions," Paper SPE 18316 presented at the 1988 Annual Technical Conferance and Exhibition (Oct. 2-5), Houston.

20. Henderson, G.D., Danesh, A., Tehrani, D., and Peden, J.M.: "The Effect of Velocity and Interfacial Tension on the Relative Permeability of Gas Condensate Fluids in the Wellbore Region," Paper Presented at the 8th European IOR Symposium (May 15-17, 1995), Vienna.

21. Amyx, J.W., Bass, D.M., Jr., and Whiting, R.L.: *Petroleum Reservoir Engineering*, McGraw-Hill Book Co., New York (1960).

22. Ronde, H.: "Effect of Low Interfacial Tensions on Relative Permeabilities in Some Gas Condensate Systems," Paper SPE 25072 Presented at the 1992 EUROPEC (Nov. 16-18), Cannes.

23. Ham, J.D. and Eilerts, C.K.: "Effect of Saturation on Mobility of Low Liquid-Vapor Ratio Fluids," *SPEJ* (1967) 11-19

24. Schulte, A.: "Simulation Mechanisms of Well Impairment Due to Condensate Dropout," SPE Forum Series in Europe, Gas Condensate Reservoirs, Seefeld, Austria (1994).

25. Boom, W., *et al.*: "Experimental Evidence for Improved Condensate Mobility at Near Wellbore Flow Conditions," paper SPE 30766, presented at the 1995 SPE Annual Technical Conference & Exhibition, Oct. 22-25, Dallas.

26. Golan, M. and Whitson, C.H.: *Well Performance*, 2nd ed., Prentice-Hall (1986).

27. Forchheimer, P.: "Wasserbewegung durch Boden," *Zeitz. Ver. Deutsch Ing.* (1901) 1781-1788

28. Evans, R.D. and Civan, F.: "Characterization of Non-Darcy Multiphase Flow in Petroleum Bearing Formation," DOE Report No. DOE/BC/14659-7 (1994).

29. Standing, M.B.: "Notes on Relative Permeability Relationshops," *Proc.*, University of Trondheim, NTH, Norway (1975) .

30. Honarpour, M., Koederitz, L.F., and Harvey, A.H.: "Empirical Equations for Estimating Two-Phase Relative Permeability in Consolidated Rock," *JPT* (1982) No. 12, 2905-2908

31. Chierici, G.L.: "Novel Relation for Drainage and Imbibition Relative Permeabilities," *Soc. Pet. Eng. J.* (1984) 275-276

Nomenclature

a	=	exponent in IFT correction
B_{gd}	=	dry gas FVF, RB/scf or m^3/m^3
B_o	=	oil FVF, RB/STB or m^3/m^3
C	=	gas rate constant
C_{bp}	=	gas rate constant in backpressure equation
C_t	=	trapping constant
c	=	compressibility, psi^{-1} or pa^{-1}
$\overline{c}$	=	cumulative compressibility, psi^{-1} or pa^{-1}
c_{aq}	=	aquifer compressibility, psi^{-1} or pa^{-1}
$\overline{c}_e$	=	cumulative effective compressibility, psi^{-1} or pa^{-1}
$\overline{c}_f$	=	cumulative formation compressibility, psi^{-1} or pa^{-1}
$\overline{c}_{tw}$	=	cumulative water compressibility, psi^{-1} or pa^{-1}
F	=	IFT correlating parameter
G_{CVD}	=	current surface gas in place in CVD cell, scf or m^3
G	=	initial surface gas in place, scf or m^3
G_p	=	produced surface gas, scf or m^3
G_{pw}	=	produced wet surface gas, scf or m^3
G_w	=	initial wet surface gas in place, scf or m^3
h	=	reservoir thickness, ft or m
J	=	productivity index, scf/D/psi or $m^3/s/Pa$
k	=	absolute permeability, md (μm^2)
k_r	=	relative permeability (generic)
k_{rg}	=	gas relative permeability
k_{ro}	=	oil relative permeability
k_v/k_h	=	vertical-to-horizontal permeability ratio
L	=	core length, ft or m
M_g	=	gas molecular weight
M_o	=	oil molecular weight
n	=	exponent in gas backpressure equation
N_{CVD}	=	Current STO in place in CVD cell, STB or m^3
N_p	=	cumulative produced STO, STB or m^3
N_c	=	Dimensionless viscous-to-capillary number
p	=	pressure, psia or Pa
p	=	initial reservoir pressure, psia or Pa
p^*	=	pressure at outer boundary of Region 1, psia or Pa
p_d	=	dewpoint pressure, psia or Pa
Δp	=	total pressure drop (across core), psi or Pa
Δp_p	=	total pseudopressure, psi/cp or 1/s
p_R	=	average reservoir pressure, psia or Pa
p_{sc}	=	standard condition pressure, psia or Pa

p_{wf} = wellbore bottomhole flowing pressure (BHFP), psia or Pa
q_g = surface gas rate, scf/D or m^3/s
$q_{g,core}$ = gas flow rate at core conditions, ft^3/D or m^3/s
$q_{o,core}$ = oil flow rate at core conditions, ft^3/D or m^3/s
q_{inj} = pump injection rate, ft^3/D or m^3/s
r = radius, ft or m
r_e = external drainage radius, ft or m
r_s = solution OGR, STB/scf or m^3/m^3
r_w = wellbore radius, ft
R = gas constant
R_p = producing GOR, scf/STB or m^3/m^3
R_s = solution GOR, scf/STB or m^3/m^3
s = skin factor
S* = normalized saturation
S_g = gas saturation
S_o = oil saturation
S_{oc} = critical oil saturation
S_r = residual saturation (generic)
S_w = water saturation
S_{wi} = irreducible water saturation
t = time, days or second
T = reservoir temperature, ^oR or K
T_{sc} = standard condition temperature, ^oR or K
V_{aq} = aquifer volume, RB or m^3
V_d = dewpoint volume, ft^3 or m^3
V_{pNNP} = pore volume of non-net pay, RB or m^3
V_{pR} = reservoir pore volume, RB or m^3
V_{ro} = CCE oil relative volume, $V_o/(V_g+V_o)$
V_{ro} = CVD oil relative volume, V_o/V_d
V_{rt} = CCE total relative volume, $(V_g+V_o)/V_d$
v_s = pore velocity = $v/[\phi(1-S_{wi})]$, ft/D or m/s
W_{ei} = initial encroachable water in place, RB or m^3
$W_e(p_R)$ = encroachable water as a function of average reservoir pressure, RB or m^3
z = gas compressibility factor
z_2 = two-phase gas compressibility factor
β_s = surface gas mole fraction in wellstream
λ = Corey pore size distribution factor
μ_g = gas viscosity, cp or Pa·s
μ_o = oil viscosity, cp or Pa·s
ρ_g = gas density, lb/ft^3 or kg/m^3
ρ_o = oil density, lb/ft^3 or kg/m^3
σ = gas-oil IFT, dynes/cm or N/m
σ^* = threshold gas-oil IFT, dynes/cm or N/m
ϕ = porosity

Appendix A

Accurate Insitu Compositions in Petroleum Reservoirs (SPE 28829)

SPE 28829

Accurate Insitu Compositions in Petroleum Reservoirs

by Øivind Fevang* and Curtis H. Whitson,* *U. Trondheim*
*SPE Member

This paper was prepared for presentation at the EUROPEC Petroleum Conference held in London, October 25-27, 1994.

Abstract

This paper describes experimental procedures for determining accurate estimates of original insitu reservoir oil and gas compositions. The proposed *equilibrium contact mixing* (ECM) method can use samples which are clearly *not* representative of insitu fluids (e.g. due to near-wellbore multiphase behavior, reservoir depletion, or separator sampling problems). ECM procedures are recommended for saturated, undersaturated, and depleted reservoirs.

Examples are given for reservoir fluids ranging from very lean-gas/black-oil systems to highly volatile gas/oil systems. Furthermore, it is shown that the proposed ECM method can be used to obtain depth-weighted average insitu compositions in reservoirs with gravity-induced vertical compositional gradients.[1]

The Peng-Robinson (PR) and Soave-Redlich-Kwong (SRK) equations of state (EOS) are used in calculations, with extensive characterization of the C_{7+} fractions. Static PVT experiments and radial 1D/2D compositional simulations of typical fluid-sampling conditions are used to verify the proposed methods.

Partly due to the success of the ECM method, the traditional definition of a "representative" sample is reconsidered, and a more general definition is recommended. The general definition ("*reservoir-representative*") is any sample produced from a reservoir, where the measured composition and PVT properties are of good quality. The traditional definition ("*insitu representative*") is a special case where the sample represents an insitu reservoir composition at a specific depth (or an average composition for a depth interval).

References and illustrations at end of paper

Separator sampling of gas condensate and volatile oil reservoirs is widely used. We present an analysis of traditional separator sampling methods, potential errors in separator sampling, and a critical evaluation of the "isokinetic" sampling method. Isokinetic sampling is currently used to sample separator gas streams when separator liquid "carryover" is suspected. Problems with the isokinetic method are discussed, and we suggest field and laboratory measurements which are needed to confirm the validity of isokinetic sampling.

Introduction

Historically, the only acceptable method for determining initial reservoir compositions has been to *directly* obtain bottomhole or recombined separator samples which truly represent insitu compositions. Sampling procedures have been developed to assist in obtaining insitu-representative samples, but for reservoirs that are initially saturated or only slightly undersaturated, it may be impossible to obtain such samples. When flowing bottomhole pressure drops below the reservoir fluid's saturation pressure, multiphase behavior near the wellbore may result in mixtures flowing into the wellbore which are clearly *not* insitu representative.

When reliable insitu-representative samples can not (or have not) been obtained early in the life of a reservoir, considerable uncertainty in initial hydrocarbons (oil and gas) in place may exist. One consequence is that process facilities may need to be overdesigned to account for these uncertainties. Accurate insitu-representative samples are particularly important for gas condensate reservoirs where significant income may come from processed LPGs, NGLs, and stabilized condensate.

Obtaining accurate insitu *oil* composition early in the life of a reservoir is not usually a problem, even when flowing bottomhole pressure drops below the original bubblepoint. Separator samples can be recombined in a ratio (not necessarily the same as measured during sampling) that yields a

bubblepoint pressure equal to the reservoir pressure at the gas-oil contact (GOC). This approach generally works well, mainly .because separator gas and separator oil compositions are relatively insensitive to multiphase effects near the wellbore.

A problem in many older oil reservoirs is that samples were not collected initially (e.g. many West Texas CO_2 candidate reservoirs). No generally-accepted procedure has been published for determining the initial oil compositions in depleted reservoirs. Usually the only alternative is to recombine currently-producing separator oil and separator gas samples in a ratio that yields the initial reservoir bubblepoint pressure.

Already in the late 1930s, special sampling methods had been designed for obtaining accurate samples from gas condensate wells.[2-4] Based on "isokinetic" sampling of wellstream mixtures at the wellhead, extensive compositional and PVT data were measured onsite during production tests. These methods were still used in the mid-1950s (and probably later).[5]

During the past thirty years, commercial service companies have used standard separator sampling techniques, collecting separator oil and separator gas samples directly from a standard test or production separator. Separator sampling is still the industry standard for gas condensates, but it is also used for sampling oil wells (as a supplement to bottomhole samples, and when larger samples are needed for special PVT analyses).

More recently, several oil companies (and subsequently service companies) have again started using techniques similar to the isokinetic wellstream sampling methods developed in the late 1930s. Unfortunately, information and test results from these newer methods have not yet been published. The lack of open verification of the newer testing methods has caused concern in the industry. There is also a general skepticism about whether the significant additional costs of these methods is commensurate with the results obtained.

Two recent publications address the problem of obtaining accurate insitu-representative samples of saturated gas condensates.[6,7] McCain and Alexander[6] use compositional reservoir simulation to study the problem. They conclude that accurate insitu-representative samples of saturated gas condensates *can be* obtained at an early stage of depletion when sampling at low rates (with minimum drawdown), even when bottomhole flowing pressure is below the original dewpoint. However, they also indicate that production rates must be "stabilized," where stabilization can require from several days (for moderate-permeability reservoirs) to several months (for low-permeability reservoirs).

McCain and Alexander study the effect of producing from several commingled layers with contrasting permeabilities ($k_{max}/k_{min} \simeq 100$, where the layers are communicating). Results indicate that it is more difficult to obtain accurate insitu-representative samples in a layered system. The authors recommend that samples be collected as early as possible in layered systems, and with rates as low as possible.

Several other observations were made by McCain and Alexander: (1) shutting in a well prior to low-rate sampling is not recommended, (2) at high gas rates the producing GOR may appear constant without the wellstream being representative of the original reservoir fluid, and (3) a wellstream dewpoint compared with average reservoir (or bottomhole flowing pressure) is not a reliable means for determining if a sample is insitu representative.

The last observation was also made by Standing[8] in 1951. Standing warned that the dewpoint pressure of a gas condensate sample can be lower, equal to, or higher than the original dewpoint without the sample being representative of the original reservoir fluid. The reason is that dewpoint pressure is not a monotonic function of the recombination GOR (a maximum in the dewpoint-GOR is often observed, see Standing's Fig. 40).

Reffstrup and Olsen[7] study the problem of obtaining insitu-representative samples from low-permeability, saturated gas-condensate reservoirs. Black-oil *radial* well simulations and static PVT calculations based on a detailed EOS characterization are used in this study. The authors show that for an *idealized single-rate testing sequence*, the produced wellstream will always have a lower dewpoint than the original dewpoint. Initially the wellstream dewpoint will be about equal to the flowing bottomhole pressure, but gradually the wellstream dewpoint becomes more representative of the reservoir gas at average reservoir pressure (i.e. outer-boundary pressure).

The procedure recommended by Reffstrup and Olsen for obtaining original reservoir composition is to first characterize the produced wellstream mixture using an EOS. Using the EOS characterization, calculate the incipient oil composition at the wellstream's dewpoint (the sampled mixture is assumed to have a dewpoint lower than the original dewpoint). A new mixture is created by adding incipient oil to the sampled wellstream until the dewpoint equals the initial reservoir pressure (i.e. the original dewpoint). The authors note that several "contacts" may be required in this procedure. The resulting mixture with dewpoint equal to initial reservoir pressure is shown to yield a good approximation of the original reservoir gas.

Representative Samples

The concept of a "representative" sample has traditionally meant a sample that represents the "original" reservoir fluid. This definition may be misleading for the following reasons:

1. Even if a sample is obtained, representative of an original insitu fluid, this sample may only be representative of a specific depth or depth interval of the reservoir. A uniform fluid composition does not always exist throughout a reservoir because of compositional variations; vertical variations due to gravity and thermal effects, and other variations between fault blocks and non-communicating layers.
2. It may be impossible to obtain a truly representative sample of insitu fluids because of near-wellbore multiphase behavior in saturated, slightly undersaturated, and low-permeability reservoirs.

3. Samples which are not representative of insitu fluids can be used to "create" near-exact representations of original insitu fluids (as shown in this paper).
4. Accurate PVT data and compositions of samples that are *not* representative of insitu fluids are still useful in developing an EOS fluid characterization (as useful as samples that are representative of insitu fluids).

Based on these observations, we introduce a more general definition of a representative sample: *a "reservoir-representative" sample is any sample produced from a reservoir*. As a special case, *an "insitu-representative" sample represents the volume-weighted average of original fluid(s) in the depth interval drained by a well during sampling.*

Reservoir-representative samples are readily obtained, and in many cases they can be used to create accurate estimates of insitu-representative fluids. Direct sampling of insitu-representative fluids, on the other hand, may be difficult or impossible.

Two important points should be made about the application of representative samples:

1. Accurate insitu-representative samples are used to determine the initial hydrocarbons (oil and gas) in place. Insitu-representative samples may vary as a function of depth, from one fault block to another, and between non-communicating layers. All insitu-representative samples are needed in the difficult task of defining hydrocarbons in place.
2. All reservoir-representative samples having reliable PVT data and accurately-determined compositions should be used *simultaneously* in developing an EOS fluid characterization. The resulting characterization, with a *single* set of EOS parameters, can be used to consistently describe the phase and volumetric behavior of *all* fluids within the reservoir.

Unfortunately, the "mapping" of original insitu compositions for a reservoir may not be possible until several wells have been drilled and production data become available. On the other hand, an EOS fluid characterization can be developed as soon as one reservoir-representative sample is available. This characterization can be used for preliminary calculations based on simplified assumptions about the original hydrocarbons in place.

As additional representative samples and PVT data become available, the EOS characterization can be modified as necessary to match both the old and the new PVT data. If additional insitu-representative samples become available, new estimates can also be made of the original hydrocarbons in place.

Equilibrium Contact Mixing (ECM)

Laboratory methods have been developed to obtain accurate samples of original insitu fluids in saturated reservoirs. The methods are based on mixing a reservoir oil sample and a reservoir gas sample together at a specified reservoir condition, bringing the system to equilibrium through one or more contacts ("equilibrium contact method"). Neither reservoir sample used in the mixing procedure needs to be representative of an insitu fluid.

Description of the ECM Methods

Collecting and Preparing Reservoir Samples

Samples of the reservoir oil and reservoir gas are first made up in the laboratory. Separator samples should always be used for the reservoir gas, and usually for the reservoir oil. Bottomhole samples *can* be used for the reservoir oil when available (and considered "reliable"), though separator samples are preferred if available.

The reservoir gas is made by recombining separator samples to yield the *actual* test wellstream (i.e. using *measured* separator GORs in the recombination, corrected if necessary for liquid carryover, etc.). The separator samples from the gas zone should *not* be recombined specifically to obtain a dewpoint equal to the initial pressure at the GOC.

When using separator samples to recombine a reservoir oil, the actual test GOR should be used to make the recombination, taking into account any valid corrections to the recombination GOR (oil meter corrections, gas rate corrections, etc.).

An *initial* recombined oil sample should have a bubblepoint close to the original reservoir pressure. A recombined oil bubblepoint much less than the original reservoir pressure might indicate compositional grading with depth. A recombined oil bubblepoint much greater than the original reservoir pressure might indicate gas coning during sampling. In both cases, the proposed ECM procedures require that test GOR be used for recombination of the reservoir oil sample to obtain a true sample of the produced wellstream.

Initially Saturated Gas/Oil Reservoirs (ECM1)

The containers with reservoir gas and reservoir oil samples should be brought to single-phase conditions. The two samples are transferred to a PVT cell in a ratio that results in an oil volume fraction of 50% or greater at equilibrium. Slightly more accurate equilibrium compositions are obtained using higher oil fractions, but with the disadvantage that smaller reservoir gas samples are available for subsequent studies (e.g. constant volume depletion).

The PVT cell is brought to initial reservoir conditions at the gas-oil contact and mixed thoroughly to establish equilibrium. The resulting equilibrium oil and equilibrium gas should provide excellent estimates of the original insitu fluids at the GOC. Each phase is removed to separate containers for further analysis. Compositions and PVT data are measured for each sample separately. This procedure represents the equilibrium contact mixing method ECM1.

The ECM1 method can also be used for an initial oil well test with gas coning. The separator samples are recombined at the producing GOR measured at the time of sampling. The mixture is brought to initial conditions at the GOC and mixed thoroughly to establish equilibrium. The resulting equilibrium

oil and equilibrium gas should provide excellent estimates of the original insitu fluids at the GOC.

For systems with gravity-induced compositional gradients having a saturated GOC, the ECM1 method (applied at initial GOC conditions) does *not* provide estimates of equilibrium composition *at* the GOC. Instead, the method provides a depth-averaged estimate of the insitu oil between the GOC and oil-sampling depth, and a depth-averaged estimate of the insitu gas between the GOC and the gas- sampling depth.

Depleted Solution Gas Drive Oil Reservoirs (ECM2)

A second ECM method (ECM2) can be applied to oil reservoirs currently being depleted by solution gas drive (producing GOR must be greater than the solution GOR at current average reservoir pressure). The method provides an estimate of original insitu oil composition, when this composition was not obtained initially. The method works for initially saturated and undersaturated oil reservoirs.

The produced wellstream sample is prepared by recombining separator samples using the test GOR. The recombined mixture is brought to equilibrium at the current average reservoir pressure and temperature. All of the equilibrium gas is removed at constant pressure to another container. The equilibrium oil remains in the PVT cell.

The equilibrium gas is injected incrementally back into the PVT cell containing equilibrium oil. After each injection, the bubblepoint is measured. When the bubblepoint reaches the original reservoir bubblepoint, this mixture can be considered a very good approximation of the original reservoir oil. As shown in the examples below, the resulting composition is better than simply recombining separator gas and separator oil samples in a ratio that yields the original bubblepoint pressure (particularly for intermediate components C_2-C_6, but also for C_1 and C_{7+}).

Undersaturated Produced Oil Sample

Accurate estimates of original oil composition can usually be obtained if the produced reservoir oil sample is undersaturated relative to the current average reservoir pressure. This might occur during the period of critical gas saturation buildup, or in a partially depleted solution gas drive reservoir that has subsequently undergone water flooding.

During the period when reservoir pressure first drops below the original bubblepoint and a critical gas saturation is building up, the produced wellstream may be undersaturated relative to the current reservoir pressure (ECM1 and ECM2 methods will not work). Recombining separator samples at a GOR that yields the original bubblepoint pressure has been found to give accurate estimates of the original reservoir oil.

Many oil reservoirs have been repressurized by water flooding after previously having undergone depletion by solution gas drive (e.g. many West Texas CO_2-flood reservoirs). The only *practical* laboratory method we have found successful for creating an approximation of the original reservoir oil is recombination of currently producing separator samples to the original bubblepoint pressure.

The recombination method of depleted oil samples works well in the two examples presented below, but we are unsure how accurate the method will work in other reservoirs. For example, a reservoir where separator gas composition has changed significantly during depletion, the separator recombination method may not work well.

Depleted/Saturated Gas Condensate Reservoirs

An estimate of the original gas composition of an initially saturated gas zone (with underlying oil) can be achieved in a depleted reservoir. Separator samples must be collected from both the gas zone and the oil zone. First an ECM2 procedure is performed on the reservoir oil to create an estimate of the original reservoir oil. The resulting ECM2 oil sample is mixed with the reservoir gas sample using the ECM1 procedure. The final mixture is brought to equilibrium at the original GOC conditions, with the equilibrium gas providing an accurate estimate of the original reservoir gas.

Depleted/Undersaturated Gas Condensate Reservoirs

A reliable ECM method has not yet been developed for estimating the original reservoir gas composition in a depleted gas condensate reservoir that was initially undersaturated (i.e. where an original reservoir oil sample is not available). One approach, a modification of the ECM2 method, has been tested. Reasonable results were obtained for a gas condensate with liquid yield of about 45 STB/MMscf, but we are not finished testing the method for other systems.

Verification of Equilibrium Contact Method

The proposed ECM methods have been tested for a wide range of gas/oil reservoir systems:

BO	black oil / very lean condensate
SVO	slightly volatile oil / lean condensate
MGC	medium gas condensate / somewhat volatile oil
VO	volatile oil / rich condensate
NCO	near-critical oil / gas

Each fluid system was described using a cubic equation of state (Peng-Robinson, PR, or Soave-Redlich-Kwong, SRK) and a detailed C_{7+} characterization tuned to match experimental PVT data. All fluid systems except MGC are taken from Whitson and Belery[1].

The ECM laboratory procedures are tested and verified in the results presented below. Static PVT experiments were first simulated to verify the potential of the ECM approach. Thereafter a series of detailed compositional simulations were made to study realistic testing and sampling procedures. A radial grid was used in the simulations, with an innermost block radius of 1.2 ft, and 14 logarithmically-spaced grids out to a total radius of 2000 ft. Most simulations used 10 layers with a total thickness of 200 ft.

Static PVT Cell Simulations

MGC fluids were used in the static PVT cell simulations. The MGC system has a saturation condition of 4808 psia at 259°F. The saturated reservoir gas has a solution OGR of 43.5

STB/MMscf (GOR of 23 Mscf/STB) and the saturated reservoir oil has a solution GOR of 855 scf/STB.

The original reservoir gas and reservoir oil were separately subjected to constant composition expansions (CCE). At each stage in the CCE experiment, equilibrium gas and oil compositions were calculated. These are shown as dash-dot lines in **Fig. 1** for methane and C_{7+}. To test the ECM procedure at a given stage of depletion, the equilibrium gas from the reservoir gas CCE was mixed with equilibrium oil from the reservoir oil CCE at initial saturation conditions of 4808 psia and 259ºF. Equilibrium compositions at these conditions should approximate the original reservoir oil and gas.

The amount of each phase being mixed was chosen so that the final equilibrium volumes were 50% (though results are not really sensitive to this ratio). **Fig. 1** shows results of the ECM1 method as short dashed lines.

If *original reservoir oil* is mixed with equilibrium gas from the reservoir gas CCE experiment, somewhat better estimates of the original reservoir gas are obtained (see **Figs. 1a-1b**), particularly far into depletion. This result is the basis for proposing the combined ECM2/ECM1 approach for depleted (initially saturated) gas condensate reservoirs.

Initial Test Simulations

The MGC system was again used to test the proposed ECM methods, this time based on reservoir simulations of actual testing and sampling conditions. First we give a summary of the simulation tests used to obtain "initial" samples (prior to the start of depletion).

Description of Well Tests and Sampling

Low-Drawdown Gas Test (DST 1). This gas test produces at a relatively low drawdown for 2.5 days. **Fig. 2** show the production characteristics during the test. The producing GOR decreases gradually during the test, only about 1 to 1.5% higher than the insitu GOR. Dewpoint of the produced wellstream is essentially constant about 200 psi below the insitu dewpoint of 4808 psia. Flowing BHP drops to about 4300 psia at 1 day when Sample 1 is taken.

The original reservoir gas composition is shown in **Table 1** (column A). This composition can be compared with Sample 1 (column B), which is too lean. The difference in compositions is not significant except for the heaviest components.

When separator gas and oil representing Sample 1 are recombined at a GOR to obtain the correct dewpoint pressure (4808 psia), a much poorer (too rich) wellstream results (column C). The economic consequences of using this overly-rich wellstream is obvious. In fact, the error in using the dewpoint-corrected composition is much greater than using Sample 1 *with a dewpoint underpredicted by 200 psi*.

High/Low-Rate Gas Test (DST 2). This gas test produces at about 50 MMscf/D for two days, followed by a rate reduction to 1 MMscf/D for two days (see **Fig. 3**). Flowing BHP drops to 2000 psia during the high-rate period, then increases to about 4700 psia during the low-rate period. GOR decreases gradually from about 26 to 24 Mscf/STB during the high-rate period, then drops sharply to about 12 Mscf/STB when rate is reduced, increasing rapidly towards 21 Mscf/STB during the two-day low-rate period (initial solution GOR is 23 Mscf/STB). Produced wellstream dewpoint is slightly increasing during the high-rate period, about 500 psi lower than the insitu dewpoint of 4808 psia. Following the rate reduction the produced wellstream dewpoint increases almost 1200 psi (900 psi above the insitu dewpoint), then decreases sharply towards the insitu dewpoint during the two-day low-rate period.

Sample 1 is taken at 1 day during the high-rate period, Sample 2 is taken at 2.06 days (1.5 hours after the rate reduction), and Sample 3 is taken at 2.5 days. The compositions of Samples 1-3 are given in **Table 3** (columns B, D, and F).

Fig. 6 shows the complicated relationship between produced wellstream dewpoint and GOR during both rates in DST 2. During the high-rate period the wellstream dewpoint-GOR trend appears to extrapolate to the insitu dewpoint/GOR. However, already at 1.5 days the GOR and dewpoint have become essentially constant.

When separator samples representing Sample 1 are recombined at varying ratios, the trend in dewpoint-GOR is given by the lower dashed line. A mixture with GOR of about 15.3 Mscf/STB (column C, **Table 3**) yields the insitu dewpoint of 4808 psia. This mixture obviously does not represent the insitu reservoir gas GOR of 23 Mscf/STB. Clearly the danger of recombining separator samples to match the (assumed) insitu dewpoint is obvious from this example (and DST 1 results).

The upper part of **Fig. 6** shows the wellstream dewpoint-GOR trend during the low-rate period. Even though the dewpoint approaches the insitu dewpoint, the producing GOR is still lower than the insitu value.

When separator samples for Sample 2 are recombined at varying ratios, the trend in dewpoint-GOR is somewhat similar to the produced wellstream trend. The recombination mixture yielding the insitu dewpoint has a GOR of 21.6 Mscf/STB (column E, **Table 3**), somewhat lower than the insitu value of 23 Mscf/STB.

High-Drawdown Oil Well Test (DST 3). This oil test produces with a relatively high drawdown for 2.5 days (see **Fig. 4**). The producing GOR increases gradually from 770 to 815 scf/STB (insitu solution GOR is 855 scf/STB). The wellstream bubblepoint increases accordingly, from about 4530 to 4640 psia, compared with insitu bubblepoint of 4808 psia. (Bubblepoint is a simple *monotonic* function of GOR, in contrast to the complicated relationship between dewpoint and GOR.) Flowing BHP drops more than 2600 psi during the test.

Sample 1 is taken after 12 hours of production. The composition of Sample 1 is given in **Table 4** (column B). When separator samples representing Sample 1 are recombined to the insitu bubblepoint, the resulting mixture (column C) has a composition very close to the original reservoir oil.

Oil Well Test with Gas Coning (DST 4). This test produces from the oil zone 20 ft below the GOC. Gas coning occurs shortly after production begins, as seen in **Fig. 4**. Sample 1 is collected after 1 day with a producing GOR of 950 scf/STB, and Sample 2 is collected at the end of the test (2.5 days) with a producing GOR of 1370 scf/STB. Wellstream bubblepoint increases almost linearly during the test, reaching 6600 psia at the end of the test.

In general, samples collected during an oil test with gas coning are considered "unrepresentative." Therefore, separator samples from such a test would not usually be recombined in the laboratory (e.g. to match an assumed insitu bubblepoint). If done, the resulting oil composition would be too light compared with the original reservoir oil (see column B, **Table 6**).

Standard ECM1 Application (DSTs 1 & 3)

Gas Sample 1 collected during DST 1 (low drawdown) was mixed with oil Sample 1 collected during DST 3 (high drawdown) using the standard ECM1 method. The resulting equilibrium compositions at the original GOC conditions (4808 psia and 259°F) are shown in **Tables 1 and 2** [columns labelled ECM(a)]. Resulting equilibrium gas and oil compositions are practically identical to the original reservoir fluids.

An ECM1 procedure was also conducted using the same gas Sample 1 from DST 1, but mixed with the bubblepoint-adjusted Sample 1 from DST 3. Even though this reservoir oil is closer to the original reservoir oil, ECM1 results are slightly poorer [compare columns ECM(a) and ECM(b) in **Tables 1 and 2**].

Application of ECM1 to High/Low-Rate Gas Test (DSTs 2 & 3)

The ECM1 method was applied (separately) using reservoir oil Sample 1 from DST 3 with the three reservoir gas samples collected during DST 2. The method was also applied using oil Sample 1 from DST 3 and dewpoint-corrected Sample 2 from DST 2.

Results are shown in **Tables 3 and 4**. In *all* cases the resulting equilibrium oil and gas compositions from the ECM1 method are very close to the original reservoir fluids, and they are superior to the sampled compositions.

The real improvement using the ECM1 method is obtaining a *consistently accurate* estimate of original gas composition. For example, dewpoint-adjusted gas compositions can (and usually are) erroneous (as shown in DST 1 Sample 1 and DST 2 Sample 1). By chance, a dewpoint-adjusted gas composition can be reasonably accurate, as is the case for Samples 2 and 3 in DST 2. However, the estimate of original reservoir gas composition based on the ECM1 method is consistently accurate, almost independent of the reservoir samples used in the ECM1 procedure.

This observation is also seen when comparing the solution OGR (r_s) versus pressure for the different reservoir gases (**Fig. 7**). All reservoir gas compositions determined using the ECM1 method overlay the r_s curve of the original reservoir gas. Dewpoint-adjusted samples do not, even though they appear to have a reasonable initial composition (e.g. Sample 2, DST 2).

Interestingly, all reservoir oil samples have essentially the same PVT properties, as seen in **Fig. 8**. The original Sample 1 from DST 3 has a bubblepoint some 500 psi too low, but the PVT properties (R_s and B_o) fall on the same saturated curve as the original oil.

Effect of Mixing Volumes on ECM1 Results

A study has been made of the effect that oil volume ratio has on equilibrium compositions using oil Sample 1 (DST 3) and gas Sample 1 (DST 2). Results are shown in **Fig. 9**. It is clear that an acceptable oil volume ratio is 0.5 or greater. In our examples we use (conservatively) a volume ratio of 0.5 for all ECM calculations. A higher ratio would have given even better results. For ECM applications with coning samples (as shown below), the producing GOR at the time of sampling automatically determines the oil volume ratio.

Application of ECM1 to Gas Coning During an Oil Test (DST 4)

Sample 1 (DST 4) was brought to conditions at the GOC using the ECM1 procedure. Resulting equilibrium compositions are shown in **Tables 5 and 6**. Sample 2 (DST 4) was also brought to conditions at the GOC using the ECM1 procedure, with resulting equilibrium compositions shown in **Tables 5 and 6**. For both samples the resulting ECM1 estimates of initial reservoir compositions are nearly exact.

Based on these results, it is clear that samples collected during an initial oil test with gas coning can provide a unique opportunity to obtain *very* accurate samples of the original saturated oil and gas. The main reason for better accuracy with this method is that the produced reservoir gas has a minimum "loss" of condensed retrograde liquid as it flows to the wellbore. The reservoir gas is flowing through the oil zone to reach the wellbore - i.e. through pores that already have a high oil saturation. This ensures immediate and complete mobility of any liquid condensed from the reservoir gas on its path to the wellbore.

In fact, we *recommend* designing oil well tests *with gas coning*, specifically to obtain the most accurate samples of original reservoir fluids. (As a bonus, coning tests give valuable reservoir information about vertical communication). Another advantage of sampling during a test with coning is that separator liquid carryover will not be a problem, as it might be if the gas zone is tested separately. And finally, the drawdown can practically be as large as desired (or necessary to induce coning). The quality of results using coning samples evaluated with the ECM1 method do not depend on the level of drawdown.

To ensure a reasonable oil ratio ($V_o/V_t>0.5$), the samples should be collected before reaching a maximum GOR_{max} which be estimated from the relation

$$V_o/V_t = V_o/(V_o+V_g) = \frac{B_{ob}(R_{sb}(p_b),T,\gamma_o,\gamma_g)}{B_{tb}(GOR_{max},p_b,T,\gamma_o,\gamma_g)} > 0.5 \qquad (1)$$

p_b is the bubblepoint pressure (i.e. reservoir pressure at the GOC), T is reservoir temperature, γ_o is the STO specific gravity, and γ_g is the surface gas specific gravity. B_{ob} is the oil FVF at p_b, R_{sb} is the solution GOR at p_b, and B_{tb} is the total FVF evaluated at p_b, where all three properties can be estimated from correlations.[9,10]

Depletion Simulations

Application of ECM2 to Depleted MGC Reservoir (Oil Zone)

Fig. 10 shows the production performance from the oil zone in the MGC reservoir during five years of solution gas drive depletion where reservoir pressure drops about 1800 psi to 3000 psia. GOR increases from 855 to 2000 scf/STB, and the wellstream saturation pressure increases to nearly 10,000 psia (becoming a dewpoint between 7000 and 8000 psia).

Sample 1 was taken after 180 days of production when producing GOR had decreased to 750 scf/STB with a wellstream bubblepoint of 4330 psia. Recombining separator samples from Sample 1 at a ratio that results in the original bubblepoint provides a composition that closely resembles the original reservoir oil (column B of **Table 7**).

Sample 2 was collected at 1800 days when reservoir pressure was 3065 psia and producing GOR was 1975 scf/STB. Several approaches were tried for reestablishing an accurate estimate of the original oil using Sample 2. The first method recombined separator samples to obtain the original bubblepoint pressure. Results are reasonably accurate, as shown in column C of **Table 7**.

The second approach was the ECM1 procedure using the produced wellstream directly. Sample 2 was brought to conditions at the original GOC, with the resulting equilibrium oil composition shown in column D of **Table 7**. Results are poor.

The recommended method (ECM2) brings the produced wellstream (Sample 2) to the reservoir pressure at the time of sampling. Equilibrium gas is removed to a second container. This gas is then reinjected incrementally to the equilibrium oil until the original bubblepoint is reached. Results from this method are very accurate, as shown in column E of **Table 7**.

Finally we evaluate the possibility of reconstructing the original oil composition when only a depleted reservoir oil sample is available. For example, if the reservoir is water flooded after five years of depletion, then samples collected later in the water flood would consist only of reservoir oil. This reservoir oil was saturated at the end of depletion, but it would be undersaturated at the time of sampling (relative to the current reservoir pressure).

We have found that the best experimental method for creating an approximate sample of the original reservoir oil is simply to recombine the current separator samples in a ratio that gives the original bubblepoint. In this example, separator samples of the reservoir oil at the end of depletion (1800 days) were recombined to obtain the original bubblepoint. The resulting composition is shown in column F of **Table 7**.

Application of ECM1 to Depleted MGC Reservoir (Gas Zone)

Fig. 11 shows the depletion performance of the gas zone in the MGC reservoir for a five-year period. Two samples are taken at about the same reservoir pressure as Sample 2 in the oil zone depletion study (the gas zone and oil zone depletion simulations were run independently). Sample 1 was taken at the plateau production rate of 50 MMscf/D (column B **Table 8**), and Sample 2 was taken during a short rate reduction to 0.5 MMscf/D (column C **Table 8**). From Sample 1 to Sample 2 the producing GOR dropped from 33.2 to 29.5 Mscf/STB (OGR increased from 30 to 34 STB/MMscf), with dewpoint increasing from 3206 to 3446 psia (average reservoir pressure was 3254 psia at the time of sampling).

The ECM1 method was used to obtain an estimate of the original reservoir gas. The ECM2-created oil from the oil zone was mixed with Sample 1 from the gas zone at original GOC conditions. The resulting equilibrium gas composition is shown in **Table 8** (column D). An additional ECM1 contact was made with the same two reservoir samples using a higher oil volume ratio (90% instead of 50%). A noticeable improvement in the estimated original gas composition is observed, as shown in **Table 8** (column E).

The ECM1 procedure was also done using the ECM2-created oil from the oil zone and Sample 2 from the gas zone. These results are also in **Table 8** (column F). Results from both ECM1 procedures are accurate.

We also tried a procedure similar to the ECM2 method for Sample 2 from the gas zone, as this sample had a dewpoint higher than the current reservoir pressure. Sample 2 was brought to current reservoir pressure. All of the equilibrium oil was removed, and some of the equilibrium gas. The equilibrium oil was reinjected incrementally to the remaining equilibrium gas until the original dewpoint was reached. The resulting composition is shown in **Table 8** (column G).

This modified ECM2 procedure gives only approximate estimates of original reservoir gas, and the method is only recommended for depleted gas condensates when a reservoir oil sample is unavailable. Using a bottomhole sampler, it may be possible to obtain larger quantities of free reservoir oil during rate reduction or shutin in depleted condensate wells. Such BH samples would probably make a modified ECM2 method more accurate, and easier to implement in the laboratory.

Application of ECM2 to Depleted VO Reservoir (Oil Zone)

A second example testing the ECM2 method for depleted reservoir oil is presented for a more volatile system. **Fig. 12** shows the production performance of a volatile oil during five years of depletion from an initial undersaturated pressure of 7000 psia to less than 3000 psia. Producing GOR increases from 2000 scf/STB to almost 20,000 scf/STB. Bubblepoint pressure of the produced wellstream varies from an initial

value of 5850 psia to a maximum of nearly 8000 psia reached after 2.5 years.

Sample 1 was taken at 720 days when reservoir pressure had declined to about 4200 psia with a producing GOR of 5700 scf/STB. Separator samples were recombined in a ratio to give a bubblepoint of the original oil (5850 psia). The resulting composition is very poor (much too light), as shown in **Table 9** (column B).

Sample 1 was brought to original reservoir conditions using the ECM1 method. The resulting equilibrium oil is again very poor (much too heavy), as shown in **Table 9** (column C).

Sample 1 was then brought to current reservoir pressure using the recommended ECM2 method. Equilibrium gas was removed, and then reinjected to the equilibrium oil until the original bubblepoint was reached. The resulting composition is quite accurate, as shown in **Table 9** (column D).

Having only a sample of the reservoir oil at 720 days and using the separator samples corresponding to this sample, a recombination is made to reach the original bubblepoint pressure. The resulting reservoir oil composition from this procedure (recommended when previously-depleted, currently-undersaturated oils are sampled) is shown in **Table 9** (column E). The oil is heavier than the original reservoir oil as seen in **Fig. 13**.

The separator recombination approach is acceptable for some previously-depleted, currently-undersaturated oils, but this example shows that the accuracy deteriorates for more volatile systems (compared with the MGC results). We also fear that the method may be inadequate for reservoirs that have reached far into depletion before being repressurized.

Application of ECM1 to Systems with Compositional Gradient

A valid question regarding the utility of the proposed ECM methods is whether they provide useful information for reservoir systems that exhibit compositional variation with depth. This problem has been studied for several reservoirs exhibiting compositional variation due to isothermal gravity/chemical equilibrium. All systems considered have a saturated gas-oil contact.

The short dashed lines in **Figs. 14-16** represent the actual compositional variation with depth calculated using the isothermal gravity/chemical equilibrium assumption.

Based on insitu, depth-specific compositions taken at equal distances above and below the GOC, the ECM1 procedure has been tested for three reservoir systems with greatly differing compositional gradients. The solid circles (connected by medium-dashed lines) represent the equilibrium compositions at GOC conditions resulting from the ECM1 procedure. These compositions clearly do not represent the true equilibrium compositions at the GOC.

Instead, we found for these three reservoir systems that ECM1-determined compositions give a good estimate of the depth-weighted average composition from the GOC to the points of sampling. The integrated depth-averaged compositions are shown as solid lines in **Figs. 14-16**). The ECM1-determined compositions give surprisingly accurate estimates for the depth-weighted average in the oil zone. Results in the gas zone are somewhat less accurate, but they should still be useful.

Further studies are needed to verify that ECM1-determined compositions in systems with compositional gradients *consistently* yield reasonable depth-weighted averages from the GOC to the point of sampling. For example, (1) when the reservoir gas and oil samples are not collected at equal depths away from the GOC, and (2) when reservoir samples already represent average compositions over a limited depth interval.

Separator Sampling

Traditional Sampling

Traditional separator samples are used for compositional analysis and PVT studies of gas condensate and oil reservoirs. Separator samples are also collected for gas injection studies requiring large sample volumes, and for special studies involving analysis of asphaltene precipitation, wax point, emulsions, hydrates, and corrosion.

Accuracy of separator gas and oil rates is typically 5% or better. Samples are collected simultaneously at the primary separator, using 20 l containers for the separator gas and 500 to 1000 ml containers for the separator oil. The gas sampling probe points downstream to ensure that only separator gas enters the sampler (*not* including liquid droplets that may be dispersed in the gas stream leaving the separator). A standard gas sample should therefore represent the actual separator gas composition when carryover exists.

Liquid Carryover in the Gas Well Stream

Gas condensates producing through a standard horizontal test separator may have some liquid leaving the separator as small droplets in the gas stream. Liquid "carryover" is most severe at high gas rates because the settling time is reduced, and coalescence processes in the separator are less efficient. Generally speaking, carryover is more important for leaner gas condensates because the total liquid "lost" due to carryover can be large relative to the total liquid content of the produced wellstream.

If carryover goes uncorrected in the recombination process, the result will be a wellstream composition that is always too lean. Carryover is identical to an erroneously-measured low oil rate. In fact, correction for carryover requires only a simple adjustment to the recombination GOR, as shown below.

We define carryover (δ) on a molar basis, $\delta=\Delta n_o/n_o$, where Δn_o is the moles of separator oil carried out of the separator in the gas stream, and n_o is the total moles of separator oil. The wellstream composition $\mathbf{z}$ entering the separator is given by $\mathbf{z}=\beta\mathbf{y}+(1-\beta)\mathbf{x}$, where β is the mole fraction of separator gas in the total wellstream, $\beta=n_g/(n_g+n_o)$, $\mathbf{y}$ is the composition of separator gas (obtained from a standard gas separator sample), and $\mathbf{x}$ is the composition of the separator oil. β is calculated from

$$\beta = \frac{\beta_{test} - \delta}{1 - \delta}$$
$$\beta_{test} = [1 + \frac{2130\rho_{osp}}{M_{osp}(R_{sp})_{test}}]^{-1} \quad (2)$$

where $(R_{sp})_{test}$ is the measured (erroneous) test GOR in scf/sep.bbl, ρ_{osp} is the separator oil density in lb/ft^3, and M_{osp} is the separator oil molecular weight. The separator GOR R_{sp} corrected for carryover is then given by

$$R_{sp} = (R_{sp})_{test} \frac{\beta_{test}^{-1} - 1}{\beta^{-1} - 1} \quad (3)$$

Effect of Carryover on ECM Procedure

Very Lean Gas (BO)

Fig. 17 shows production characteristics of a very lean saturated gas during a 2.5 day test. Producing GOR varies from 500 to 550 Mscf/STB during the test, compared with the insitu GOR of 445 Mscf/STB. The pressure drawdown is large (almost 2000 psi). Wellstream dewpoint remains constant at about 1600 psia which is substantially lower than the insitu dewpoint of 2275 psia. Sample 1 was taken after 12 hours of production.

The reservoir gas is underlain by an oil zone containing a low-GOR black oil. A very accurate sample of the original reservoir oil is obtained by recombining separator samples from an oil well test to the original bubblepoint.

The composition of Sample 1 is shown in **Table 10** (column B). This sample, when passed through a separator operating at 105°F and 375 psia produces the separator gas shown in **Table 10** (column C). Neither composition is accurate when compared with the original gas composition. The inaccuracies of these samples may be particularly important in the design of seabed transportation requirements (e.g. pigging requirements of the pipeline).

Sample 1 was mixed with the original reservoir oil using the ECM1 procedure. The resulting estimate of original reservoir gas is practically exact, as shown in **Table 10** (column D).

The separator gas from Sample 1, assuming 100% liquid carryover without correction, was mixed with the original reservoir oil using the ECM1 procedure. Again, the resulting estimate of original reservoir gas is almost exact as shown in **Table 10** (column E).

Medium Gas Condensate

A more extreme test of the effect that uncorrected carryover has on ECM results is given using the MGC gas which has a liquid yield of about 45 STB/MMscf. The high-drawdown (high-rate) DST 2 Sample 1 gas is used, where 20% carryover is assumed. **Table 11** gives the actual composition of Sample 1 (DST 2) in column B, together with the wellstream composition that would be incorrectly determined with 20% carryover (column C).

ECM1 results using gas Sample 1 (DST 2) and oil sample 1 (DST 3) with an oil volume ratio of 70% are shown in **Table 11** [column ECM(a)]. Results are excellent when compared with the original gas composition.

ECM1 results using uncorrected Sample 1 (DST 2) with 20% carryover and oil sample 1 (DST 3) with an oil volume ratio of 70% are also shown in **Table 11** [column ECM(b)]. Again, the results are excellent (only slightly different than using the correct Sample 1).

Table 12 gives the ECM1 oil compositions with and without correction for carryover. Results are excellent, with only a slight deterioration when carryover is not corrected.

In summary it appears that the ECM method is not dependent on reservoir gas samples being corrected for carryover. Given that larger carryover occurs only for lean condensates, and smaller carryover is expected for rich condensates, we conclude that the ECM method can be used with confidence even when uncorrected carryover exists. Obviously, however, we recommend that recombined gas samples be corrected if carryover has been quantified.

Isokinetic Sampling

In 1941, Buckley and Lightfoot[2] describe "isokinetic" wellstream sampling equipment and a miniature separator design used to make detailed compositional and PVT measurements on a gas condensate producing from a formation at 10,000 ft with reservoir pressure of 5055 psia and reservoir temperature of 178°F. Average liquid yield was about OGR=16 STB/MMscf, with a condensate gravity of 48 to 50°API.

One year later Flaitz and Parks give a detailed description of similar isokinetic sampling equipment for gas condensate wells. A wellhead mixture is sampled with a small-diameter (1/16 to 3/32 in) probe located in the center of the production tubing near the wellhead. The sample mixture enters the probe at a velocity equal to the average wellstream velocity. This "isokinetic" sampling rate ensures that the entrained liquid drops (assumed to be homogeneously distributed throughout the entire cross section of the tubing) enters the sample probe undisturbed. A miniature multistage separator with pressure and temperature control is used to analyze produced wellstream samples.

The Flaitz-Parks paper presents *detailed* comparisons of wellstream isokinetic samples with vertical separator (2.5 by 11 ft) samples for twelve condensate systems (oil-gas ratios ranging from 10 to 100 STB/MMscf). Recombined wellstream compositions are also compared for the two sampling methods. Results are quite impressive, though a clear increase in error was found with increasing OGR.

Perhaps the most impressive results were an extensive 18-month testing procedure where multi-well, rate-averaged isokinetic wellstream liquid yields were compared with actual liquid yields from a Gulf Coast recycling plant facility. Maximum deviation in liquid yields during the 18 months was 7%, and the average deviation was only 1%.

The Flaitz and Parks paper gives some theoretical analysis of the isokinetic wellstream procedure. Furthermore, several special field tests were conducted to study the effect of flow rate and probe diameter on sampling efficiency.

In 1953, Hoffman, et al.[5] used similar isokinetic wellstream equipment to conduct a study on reservoir compositions and equilibrium ratios of a saturated gas/oil system. To our knowledge, this paper is the most recent application of isokinetic wellstream sampling.

During the past 5 to 10 years, several oil companies and, subsequently, service companies have introduced isokinetic sampling technology for *separator gas streams* (not wellstream). The justification for isokinetic separator gas sampling has been to quantify liquid carryover in high-rate gas condensates. There does not appear to be other reasons for using isokinetic separator gas sampling, so the method is not a replacement for standard separator sampling.

In fact, standard separator samples must *also* be collected (and analyzed) to quantify carryover using the isokinetic method. This is at least the case using the "SAD" minimization method. This method calculates the carryover that minimizes the sum of absolute differences (SAD) between all components, $SAD=\sum_i |u_i^*-u_i|$, where u_i is the measured overall composition of the isokinetic sample and u_i^* is the calculated overall composition of a mixture with β moles of separator gas y_i and $\delta(1-\beta)$ moles of separator oil x_i, or $u_i^*=[\beta y_i+\delta(1-\beta)x_i]/[\beta+\delta(1-\beta)]$.

A fundamental problem with the SAD approach is that the overall composition of the isokinetic sample must be determined. This may be difficult. Current laboratory procedures heat the isokinetic gas container to about 100°C (at constant volume) before transferring the sample to a gas chromatograph. The assumption is that liquid carryover is *completely* revaporized during the heating process. Our experience is that this probably never occurs.

Fig. 18 shows the carryover liquid volume (as a percent of the sample container volume) for isokinetic gas samples from a lean gas condensate with an OGR of 18 STB/MMscf. The reservoir gas was passed through a separator operating at 105°F and 375 psia.

For varying amounts of carryover from 10 to 40%, isokinetic samples were created. The liquid volume of each isokinetic sample is plotted versus pressure in **Fig. 18**. The closed circles represent the condition after heating to 212°F at constant volume (note that pressure increases to about 500 psia for all samples). The numbers in parentheses (below the carryover values) are liquid volume percents at original separator conditions.

From **Fig. 18** it is obvious that the heating process does not revaporize liquid carryover for this relatively light condensate. In fact, elevated pressures greater than 2000 psia are required to completely revaporize the liquid at 212°F.

So, what is the error in carryover that would be calculated by using the equilibrium gas in an isokinetic sample container after heating (when only part of the liquid is vaporized)? This gas is what would be analyzed in the laboratory and defined as u_i in the SAD process of determining the carryover value. The SAD graphical minimum in **Fig. 19** gives a carryover value of 33% (instead of the correct value of 40%). Also note that the SAD function is not as well behaved; a better function for determining carryover by minimization would be the sum of squares (SSQ) function, also shown in **Fig. 19**.

In summary we can conclude that a simple heating procedure should not be used for trying to bring an isokinetic sample to single phase conditions.

The best method (most accurate and simplest procedure) for determining carryover from an isokinetic separator gas sample would be to measure, *onsite*, the physical volume of liquid carryover in the isokinetic container *at separator conditions*. Given the liquid carryover volume, test GOR can be corrected immediately without any compositional analysis. A simple onsite method for measuring liquid carryover volume needs to be developed.

However, we feel strongly that the best solution to the carryover problem is to produce gas wells at lower rates during sampling, thereby minimizing carryover. And finally, if an ECM method can be used, the effect of carryover is minimal.

Conclusions

1. A laboratory procedure (ECM1) is recommended for making up accurate samples of *original insitu* reservoir gas and reservoir oil in saturated reservoirs.
2. The traditional application of the ECM1 procedure uses separate reservoir oil and reservoir gas samples. A novel application of the ECM1 procedure uses separator samples collected during gas coning in an oil well test. Both applications yield very accurate results.
3. Because of the high accuracy obtained with the ECM procedures, lengthy stabilization periods are no longer needed to ensure that produced wellstreams are representative of insitu fluids. Consequently, time and expenses can be saved during testing (particularly for gas condensates).
4. The ECM1 procedure can be applied to reservoirs with vertical compositional gradients and a saturated GOC. The resulting ECM1 samples provide reasonable estimates of depth-averaged compositions.
5. For oil reservoirs depleting by solution gas drive, a slightly modified ECM procedure (ECM2) is proposed for obtaining accurate insitu-representative samples of the original reservoir oil. The method requires a current wellstream sample from the oil zone and an estimate of the original oil bubblepoint (the oil can be initially saturated *or* undersaturated).
6. For a depleted gas condensate *initially saturated with an underlying oil*, accurate insitu-representative samples of the original reservoir gas can be obtained using the ECM1 procedure. A currently-producing gas wellstream is mixed with a reservoir oil sample made up using the ECM2 procedure.
7. For oil reservoirs previously depleted by solution gas drive but currently undersaturated (e.g. following water flooding), reasonably accurate insitu composition of the original reservoir oil can be obtained by recombining currently producing separator samples in a ratio to obtain the original oil bubblepoint.
8. Results of the ECM1 procedure are only slightly affected by errors in recombination separator GOR (e.g. due to liquid carryover).

Nomenclature

B_{ob} Oil FVF at bubblepoint, RB/STB
B_{tb} Total gas-plus-oil FVF at bubblepoint, RB/STB
GOR Producing GOR, scf/STB
M_{osp} Separator oil molecular weight
n_g Moles of separator gas
n_o Moles of separator oil
Δn_o Moles of liquid (oil) carryover
p_b Bubblepoint pressure, psia
R_{sb} Solution GOR at bubblepoint, scf/STB
R_{sp} Separator GOR, scf/separator bbl
T Reservoir temperature, °F or °R
u Measured isokinetic sample overall molar composition
u^* Calculated isokinetic sample overall molar composition
V_g Reservoir gas volume, ft^3
V_o Reservoir oil volume, ft^3
V_t Total gas-plus-oil reservoir volume, ft^3
x Separator oil molar composition
y Separator gas molar composition
z Wellstream molar composition

Greek

β Gas mole fraction
γ_g Average surface gas specific gravity, air=1
γ_o STO specific gravity, water=1
δ Molar liquid carryover
ρ_{osp} Separator oil density, lb/ft^3

References

1. Whitson, C.H. and Belery, P.: "Compositional Gradients in Petroleum Reservoirs," paper SPE 28000 presented at the U. Tulsa/SPE Centennial Petroleum Engineering Symposium, Aug. 29-31, Tulsa.

2. Buckley, S.E. and Lightfoot, J.H.: "Effects of Pressure and Temperature on Condensation of Distillate from Natural Gas," *Trans.*, AIME (1941) **146**, 232-245.

3. Flaitz, J.M. and Parks, A.S.: "Sampling Gas-Condensate Wells," *Trans.*, AIME (1941) **146**, 13-27.

4. Weber, C.: "Testing and Sampling Methods Used on Condensate Wells," *Oil and Gas Journal* (Oct. 12, 1939).

5. Hoffmann, A.E., Crump, J.S., and Hocott, C.R.: "Equilibrium Constants for a Gas-Condensate System," *Trans.*, AIME (1953) **198**, 1-10.

6. McCain, W.D.J. and Alexander, R.A.: "Sampling Gas-Condensate Wells," *Society of Petroleum Engineers Journal* (August 1992) 358-362.

7. Reffstrup, J. and Olsen, H.: "Evaluation of PVT Data from Low Permeability Gas Condensate Reservoirs," *North Sea Oil and Gas Reservoirs - III*, Kluwer Academic Press, (1994) 289-296.

8. Standing, M.B.: *Volumetric and Phase Behavior of Oil Field Hydrocarbon Systems*, 8th printing, Society of Petroleum Engineers, Dallas (1977).

9. Glaso, O.: "Generalized Pressure-Volume-Temperature Correlations," *JPT* (Nov. 1980) 785-795.

10. McCain, W.D., Jr.: "Reservoir Fluid Property Correlations - State of the Art," *SPERE* (May 1991) **6**, No. 2, 266-272.

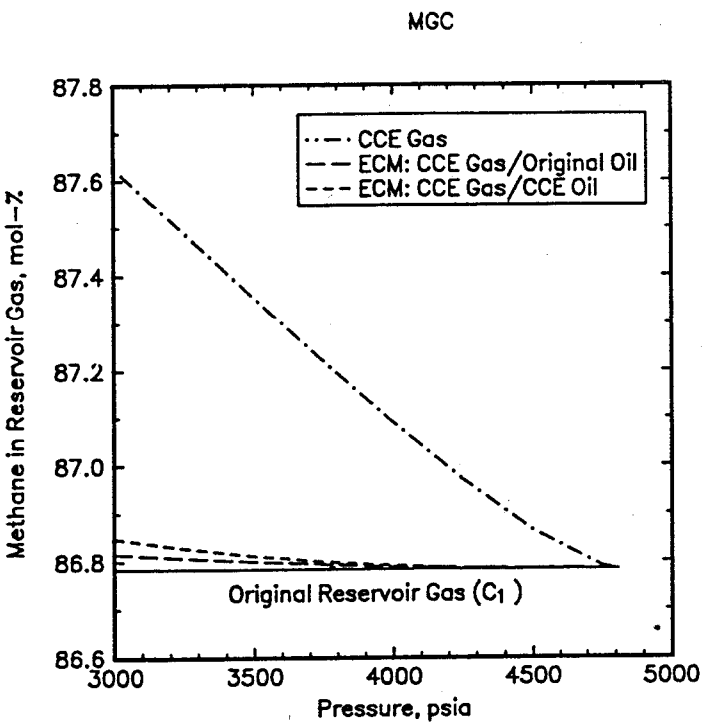

Fig. 1a ECM1 results for static PVT cell simulations using MGC reservoir. Methane molar composition in reservoir gas.

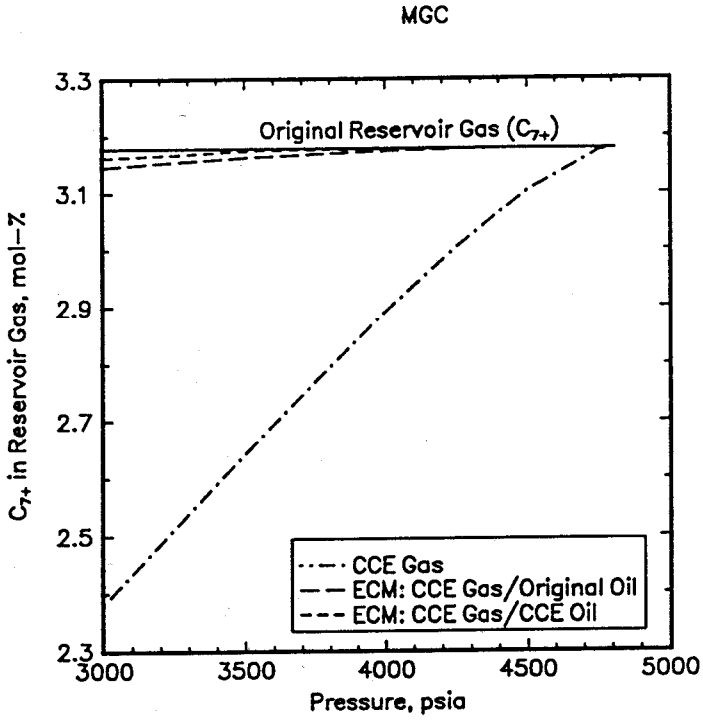

Fig. 1b ECM1 results for static PVT cell simulations using MGC reservoir. C_{7+} molar composition in reservoir gas.

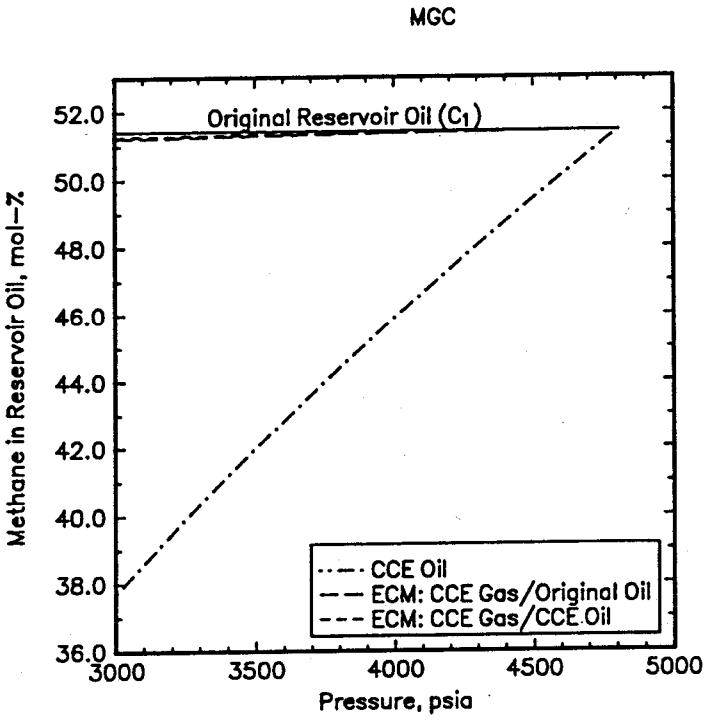

Fig. 1c ECM1 results for static PVT cell simulations using MGC reservoir. Methane molar composition in reservoir oil.

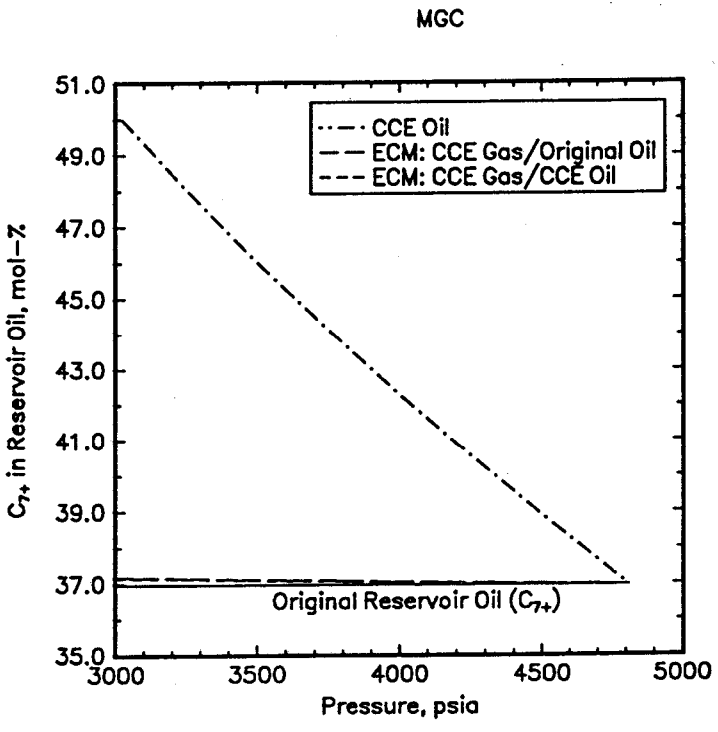

Fig. 1d ECM1 results for static PVT cell simulations using MGC reservoir. C_{7+} molar composition in reservoir oil.

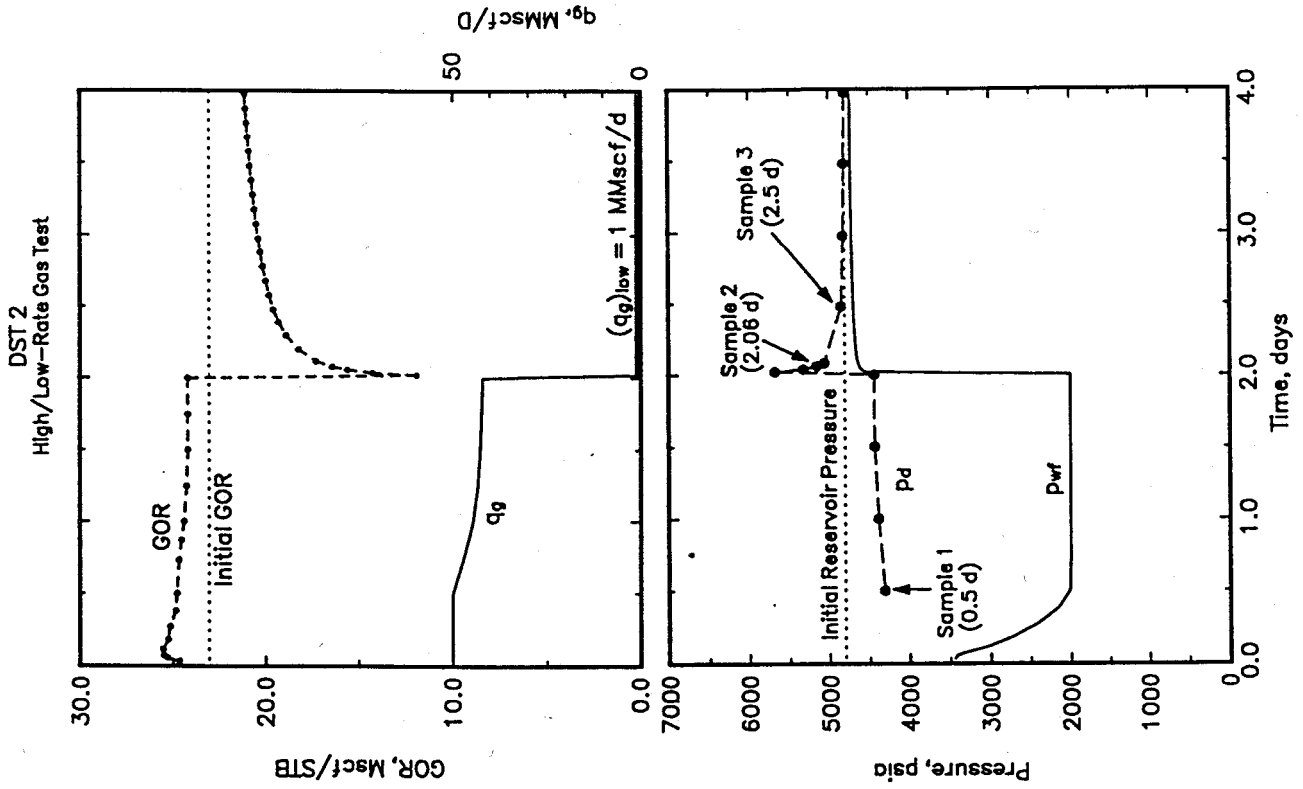

Fig. 3 Production performance during high/low-rate gas test DST 2, initially saturated MGC reservoir.

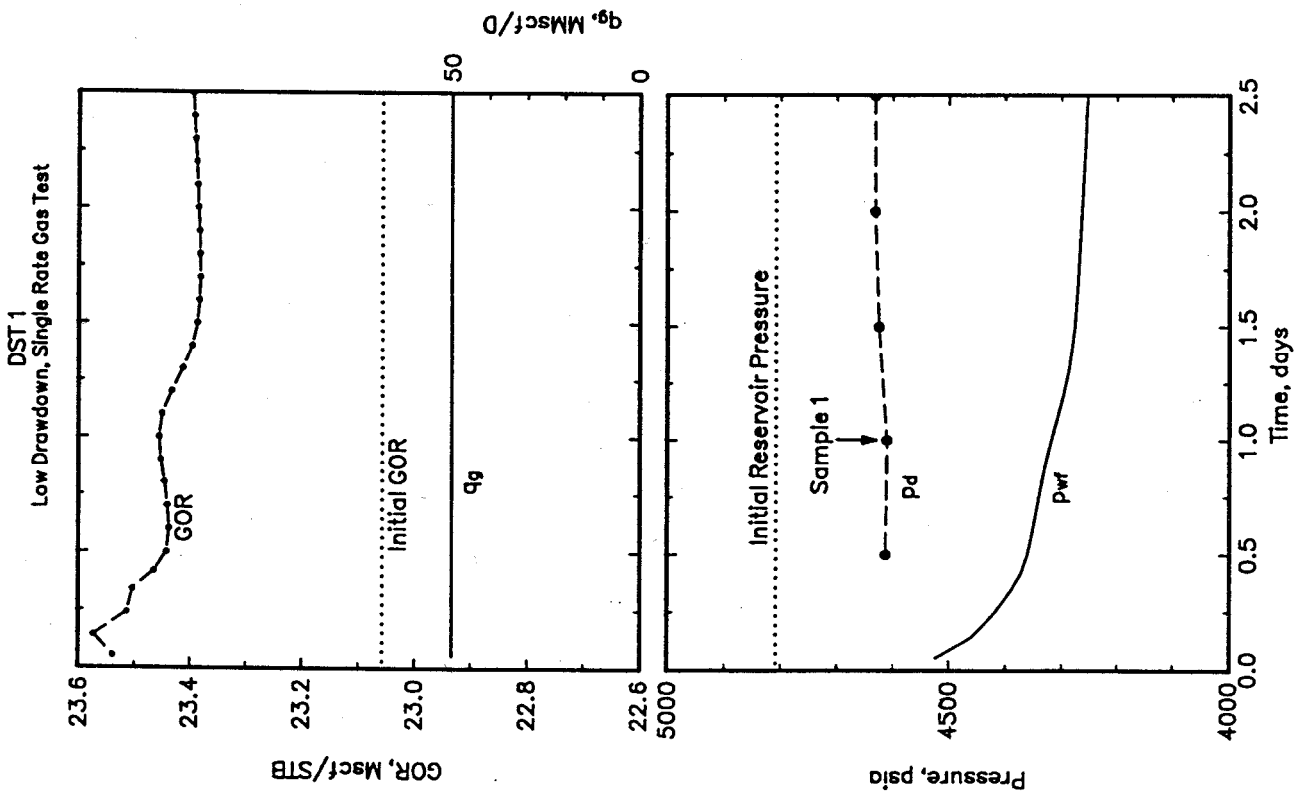

Fig. 2 Production performance during low-drawdown gas test DST 1, initially saturated MGC reservoir.

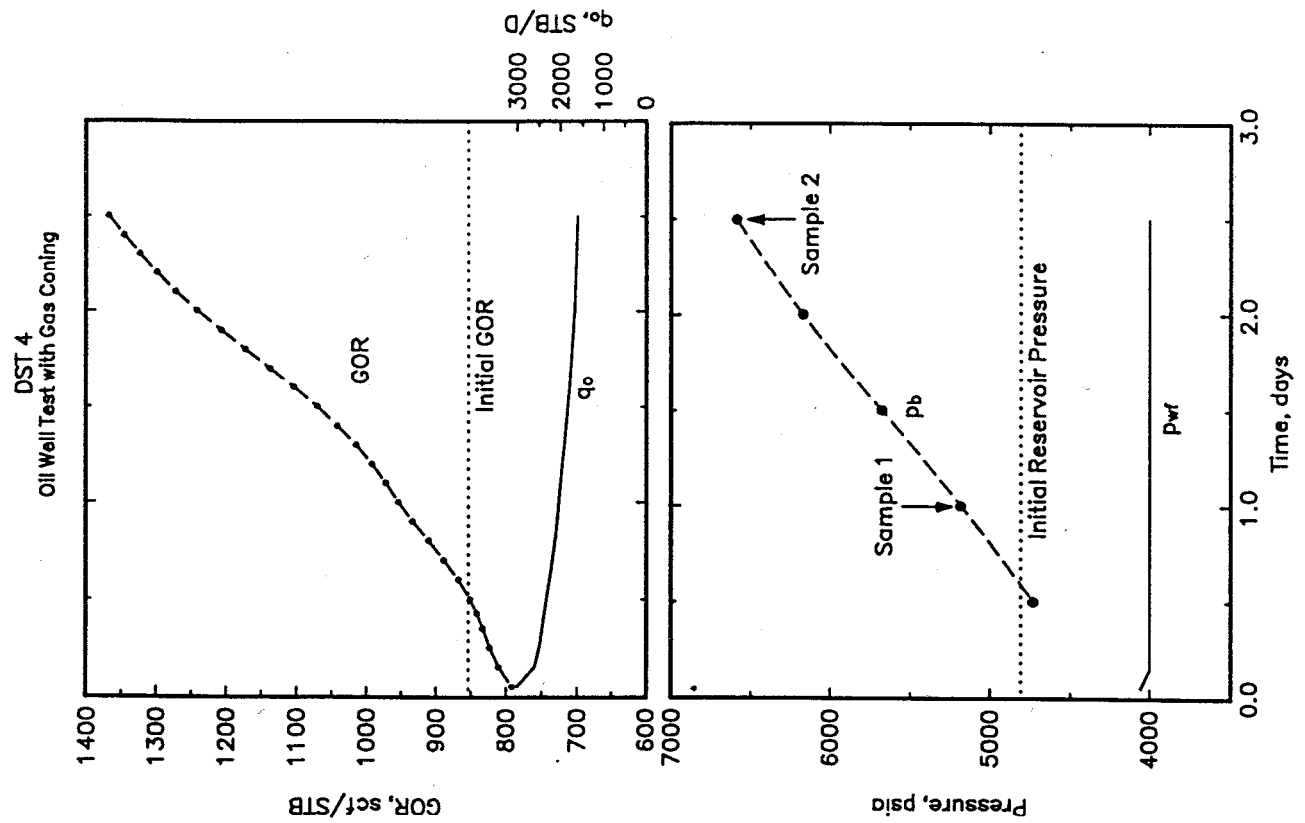

Fig. 5 Production performance during gas coning in oil test DST 4, initially saturated MGC reservoir.

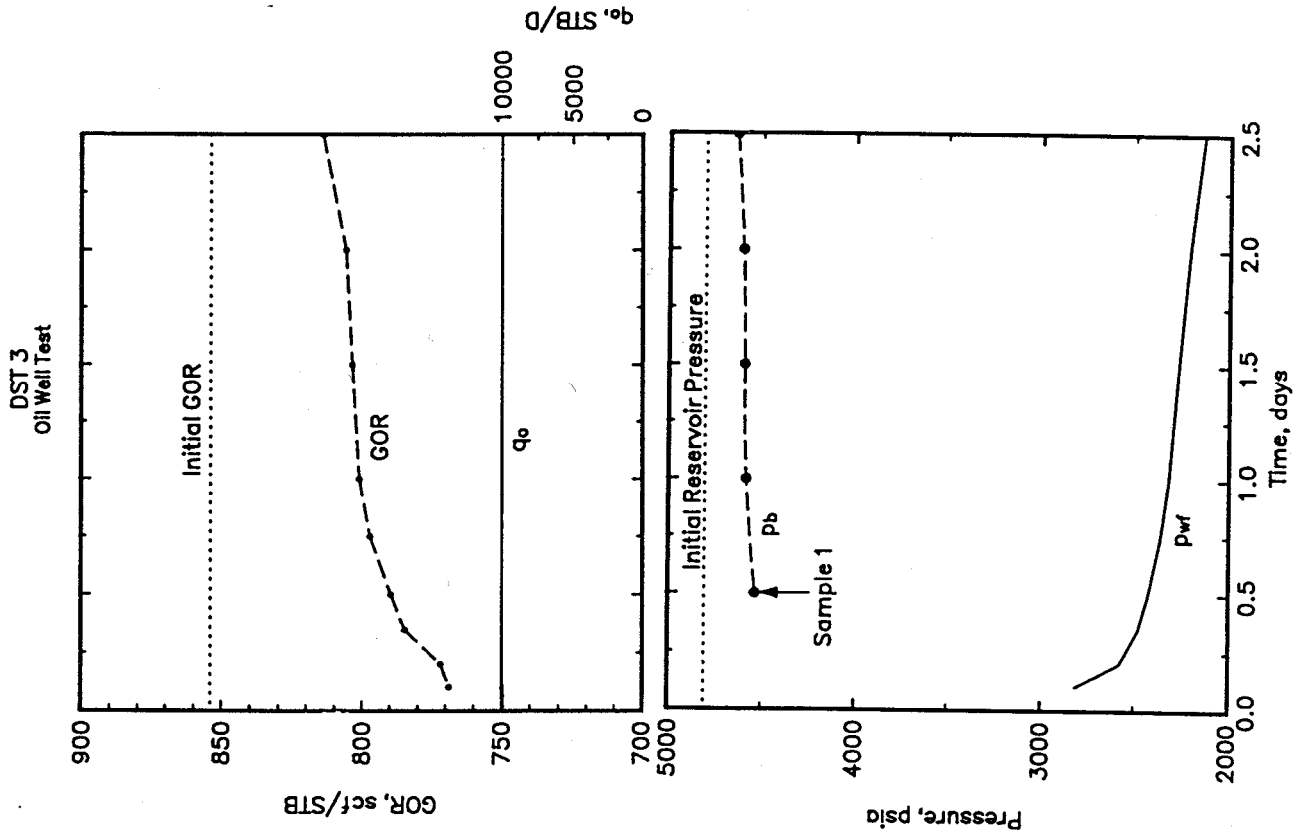

Fig. 4 Production performance during high-drawdown oil test DST 3, initially saturated MGC reservoir.

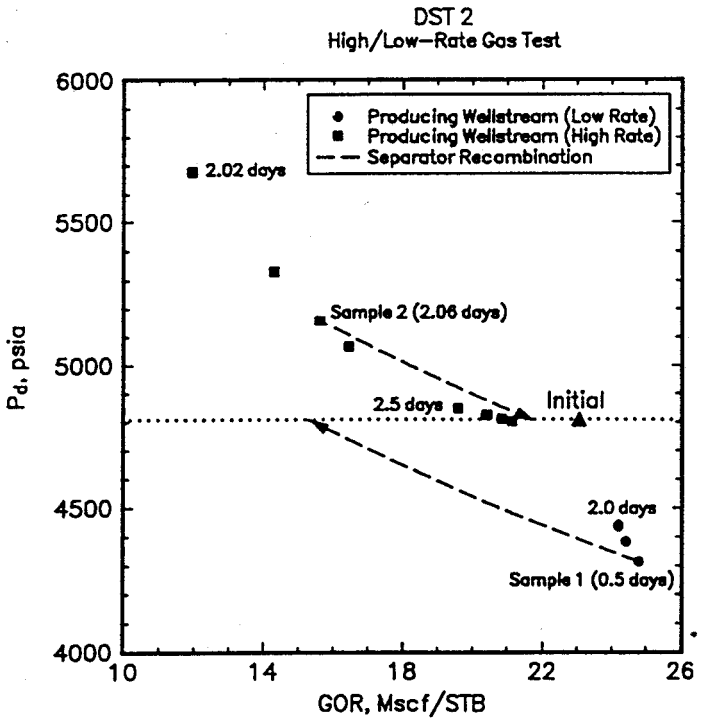

Fig. 6 Produced wellstream dewpoint vs. GOR behavior during high- and low-rates in gas test DST 2, initially saturated MGC reservoir.

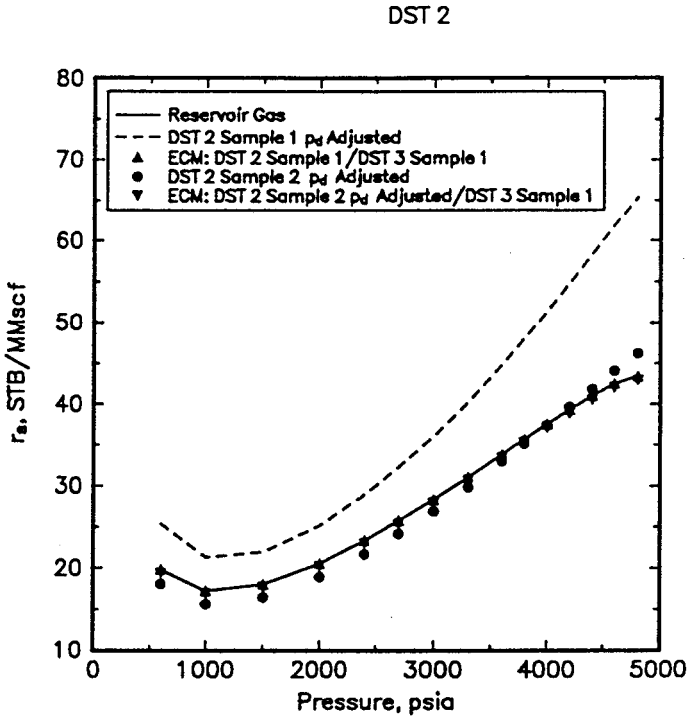

Fig. 7 Solution OGR of MGC insitu reservoir gas and various laboratory-prepared samples approximating the original reservoir gas.

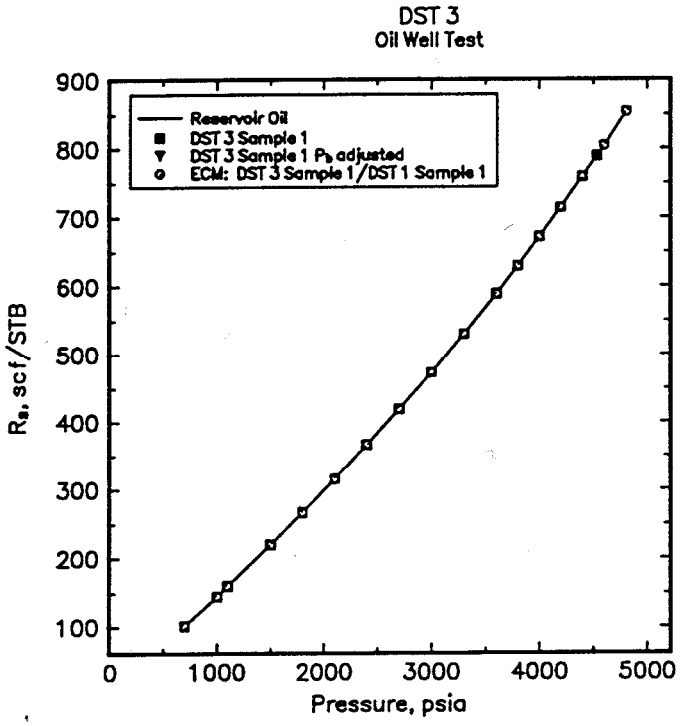

Fig. 8 Solution GOR of MGC insitu reservoir oil and various laboratory-prepared samples approximating the original reservoir oil.

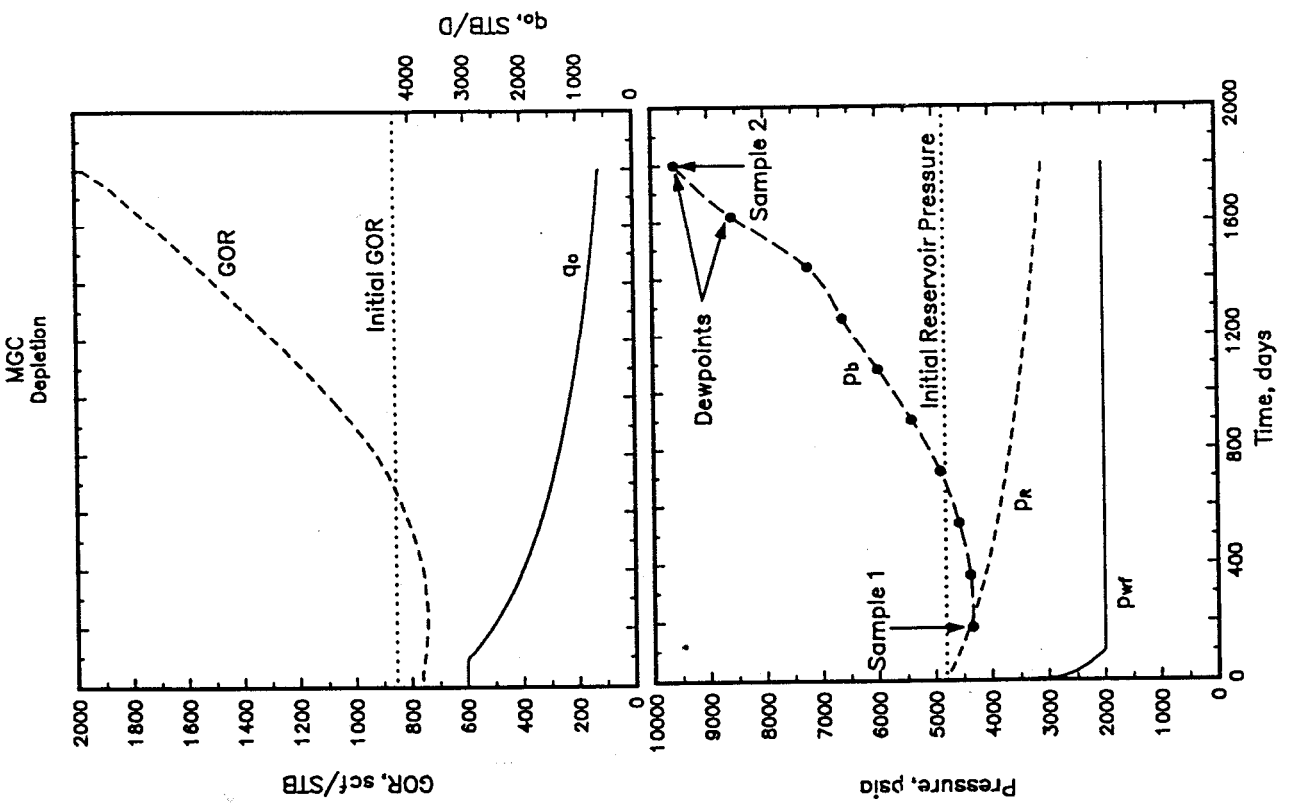

Fig. 10 Production performance during depletion of oil zone in initially-saturated MGC reservoir.

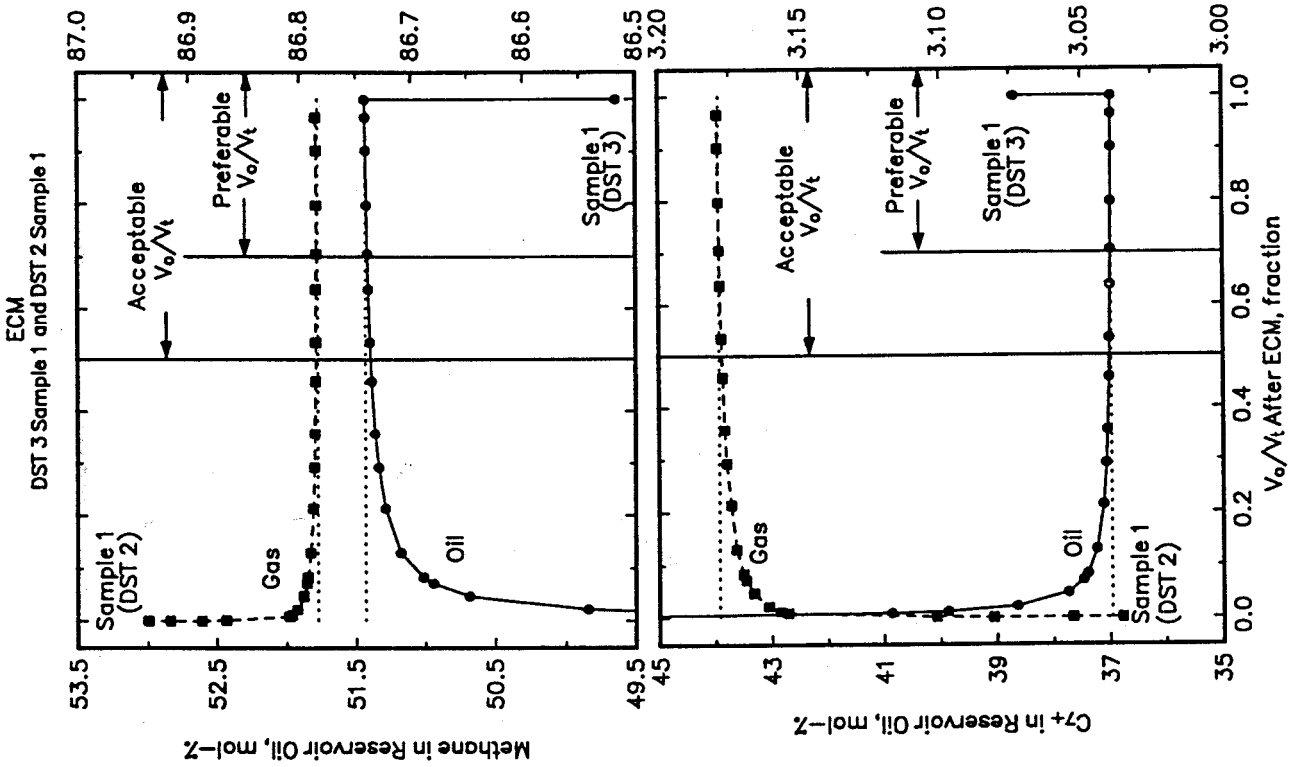

Fig. 9 Effect of oil volume ratio V_o/V_t on ECM1 results (methane and C_{7+} molar compositions) for MGC reservoir oil and gas. DST 2 Sample 1 and DST 3 Sample 1.

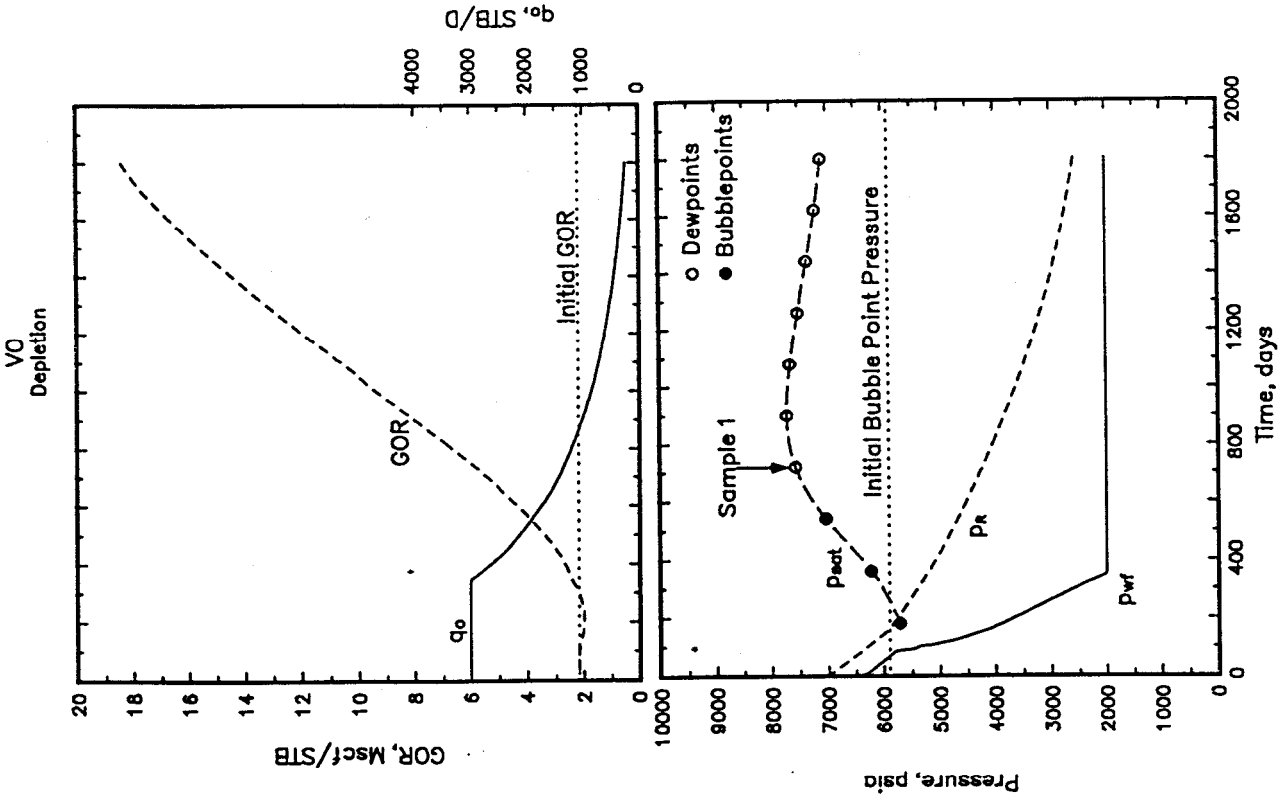

Fig. 12 Production performance during depletion of oil zone in initially-undersaturated VO reservoir.

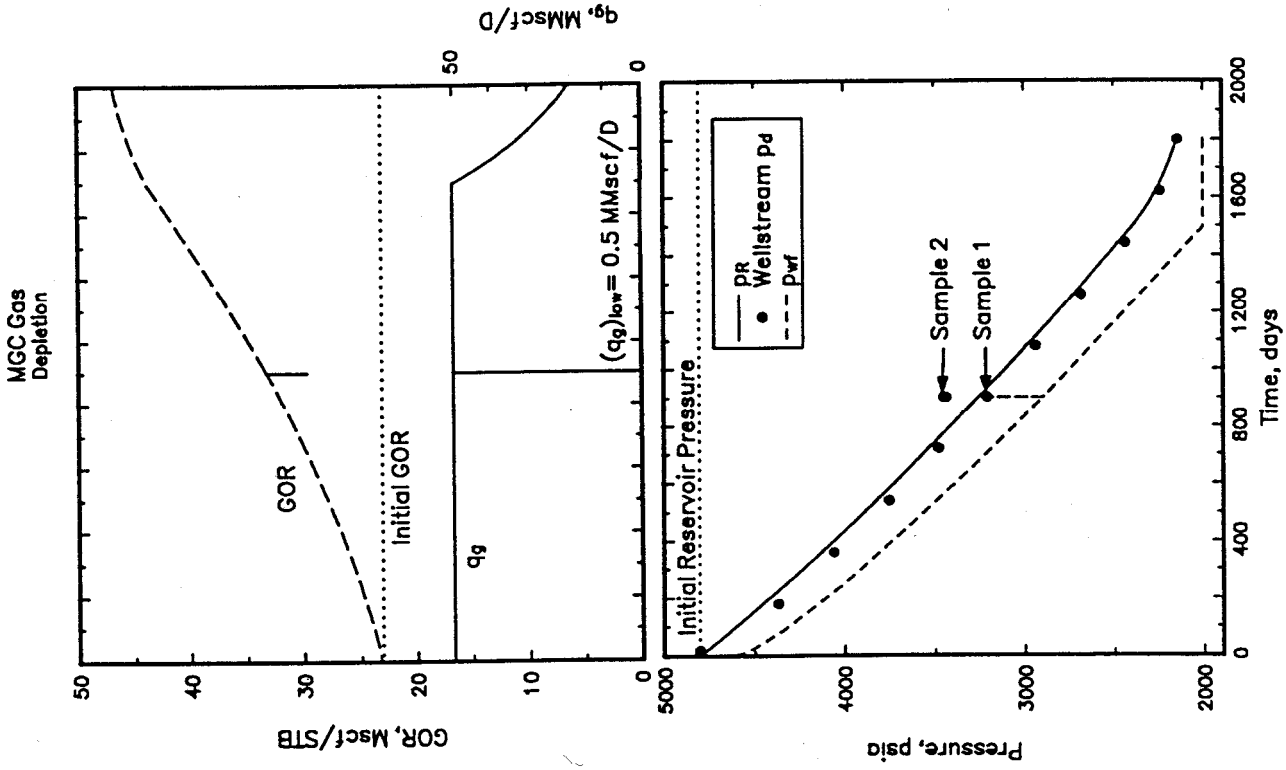

Fig. 11 Production performance during depletion of gas zone in initially-saturated MGC reservoir.

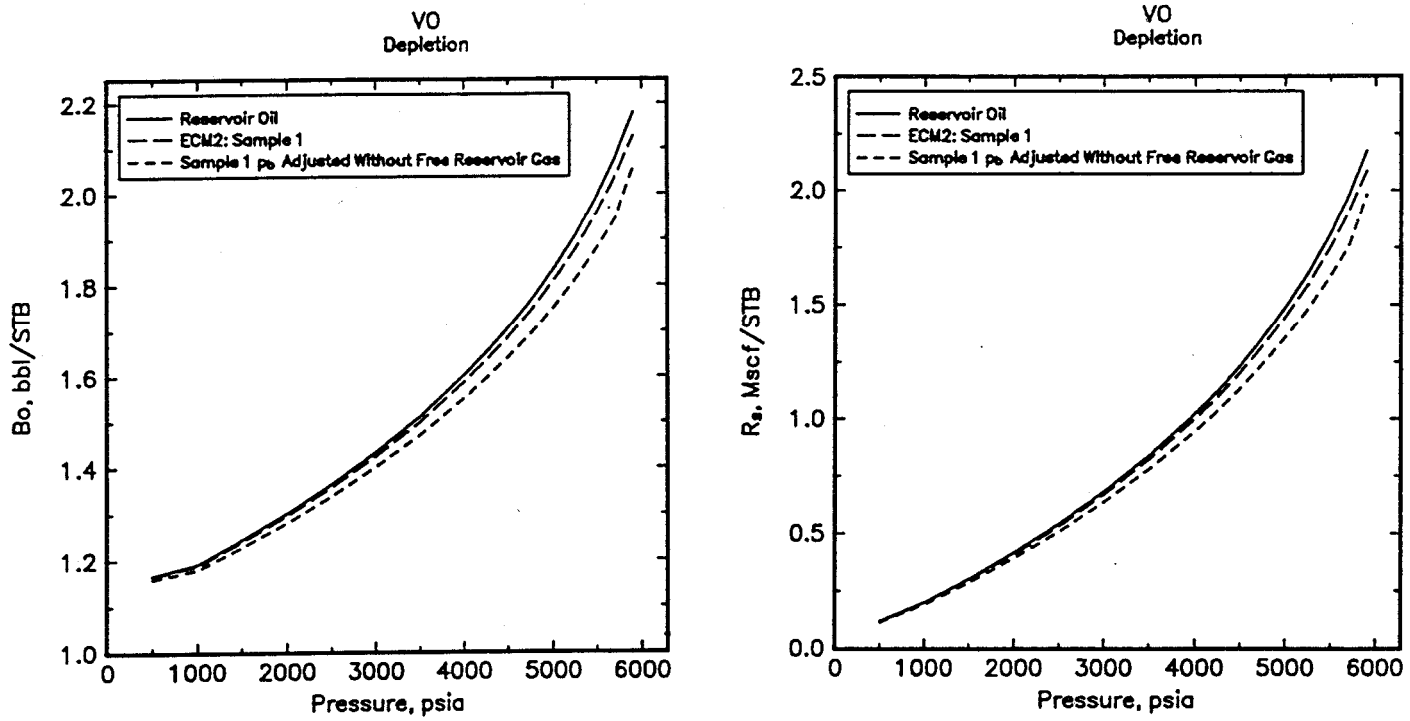

Fig. 13 Solution GOR and oil FVF of VO insitu reservoir oil and various laboratory-prepared samples approximating the original reservoir oil.

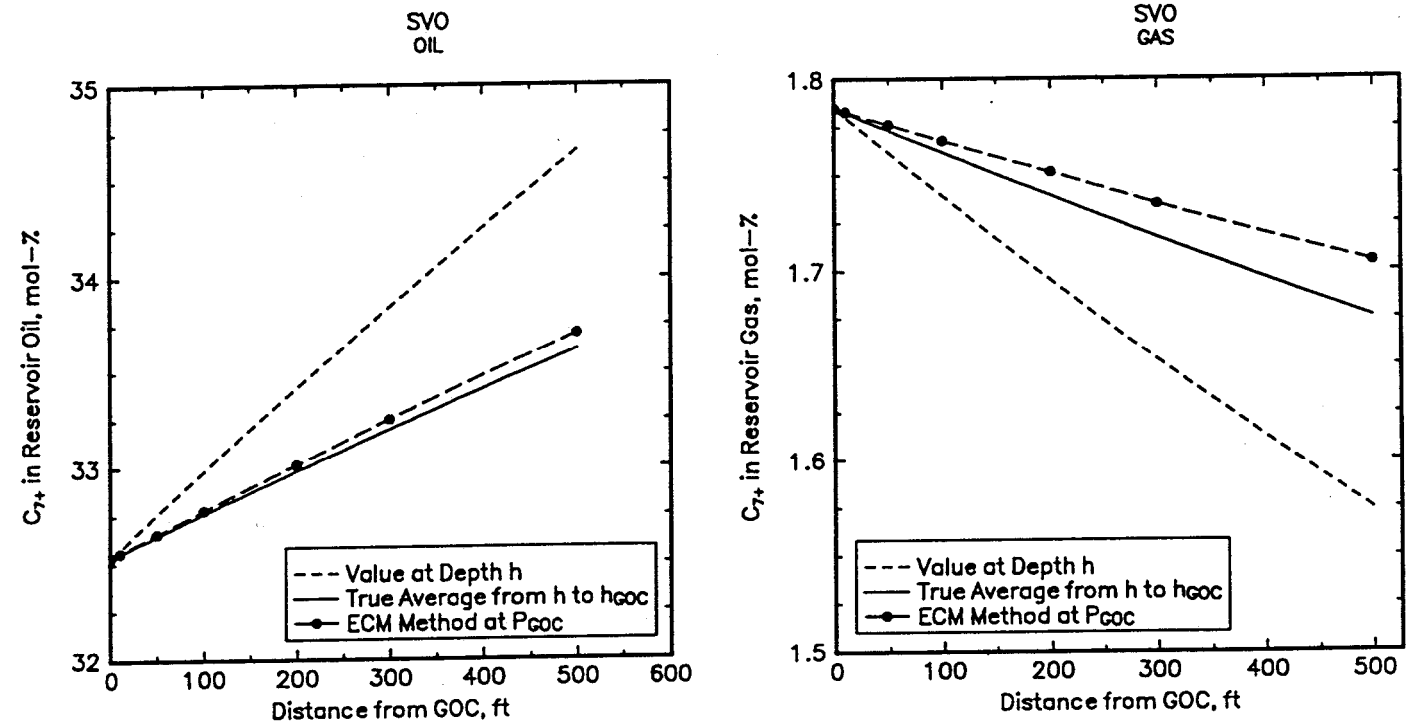

Fig. 14 ECM1 calculations (C_{7+} compositions) for SVO reservoir with vertical compositional gradient.

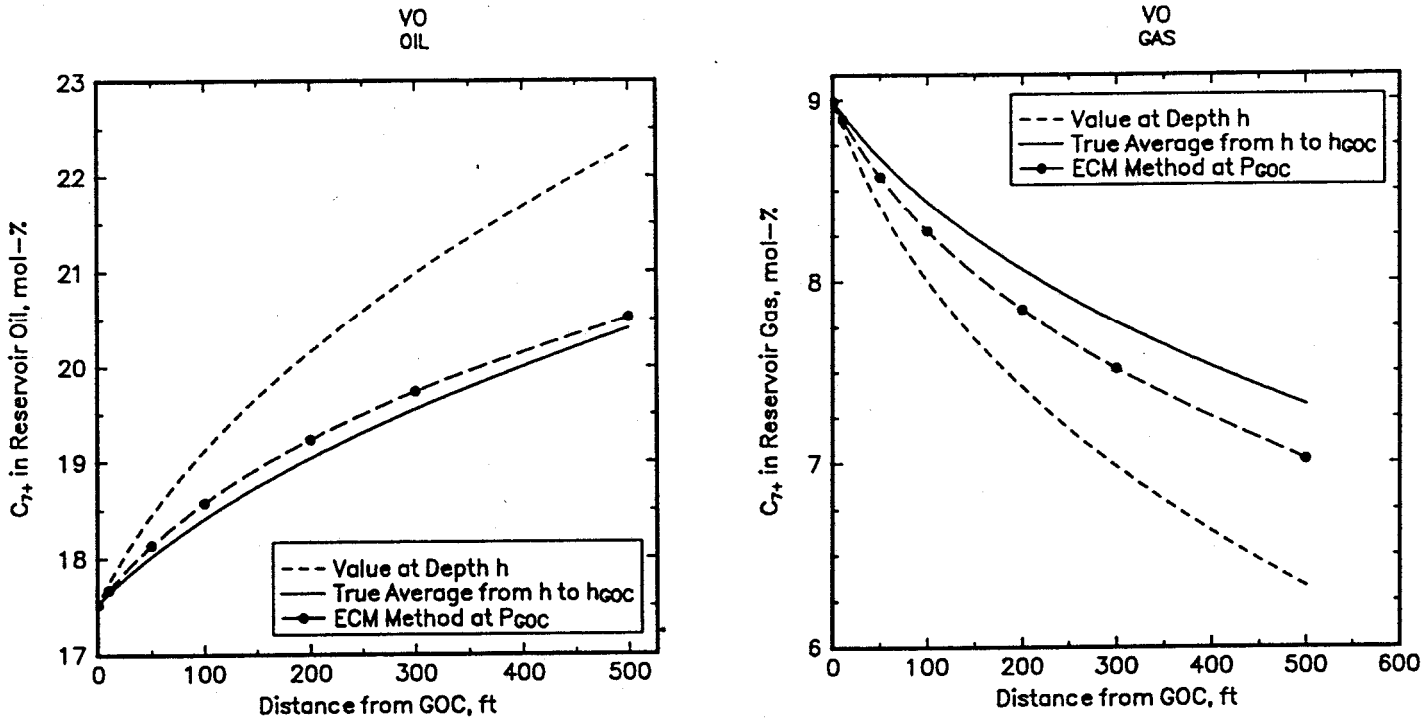

Fig. 15 ECM1 calculations (C_{7+} compositions) for the VO reservoir with vertical compositional gradient.

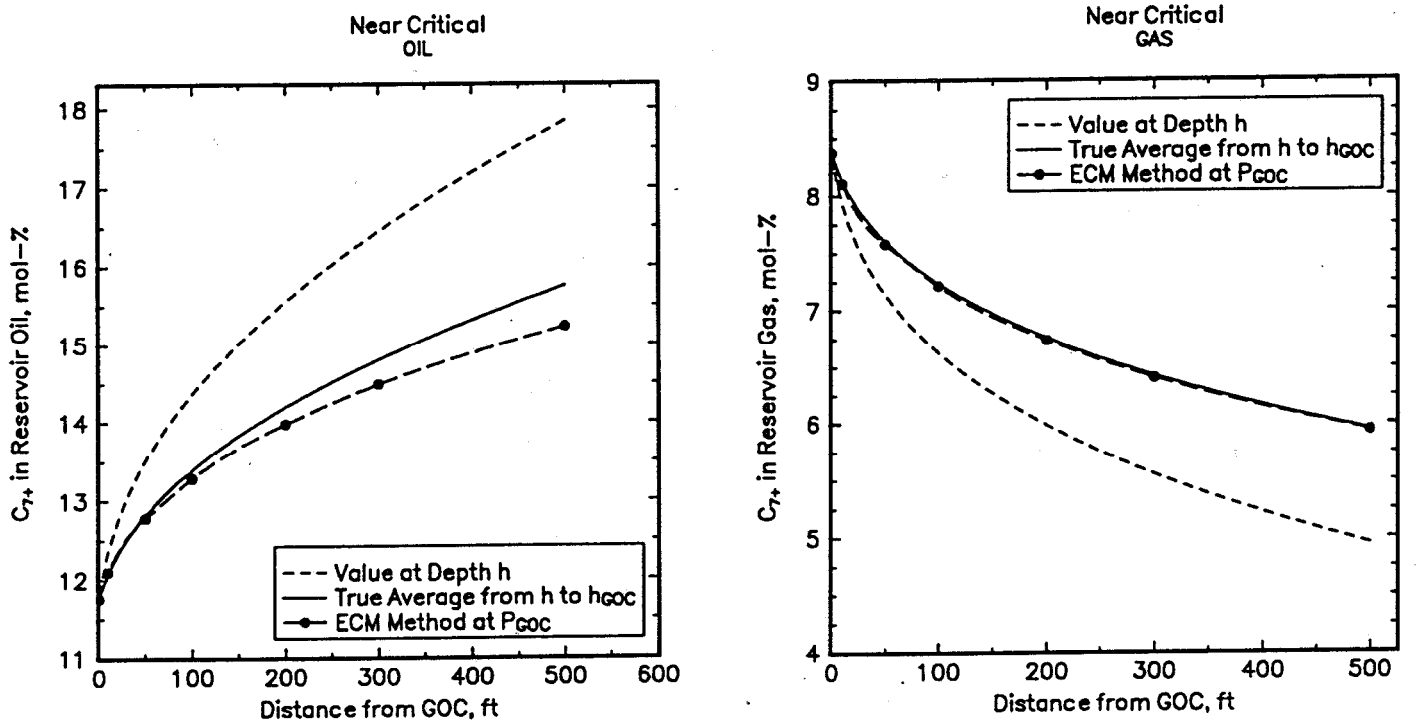

Fig. 16 ECM1 calculations (C_{7+} compositions) for the NCO reservoir with vertical compositional gradient.

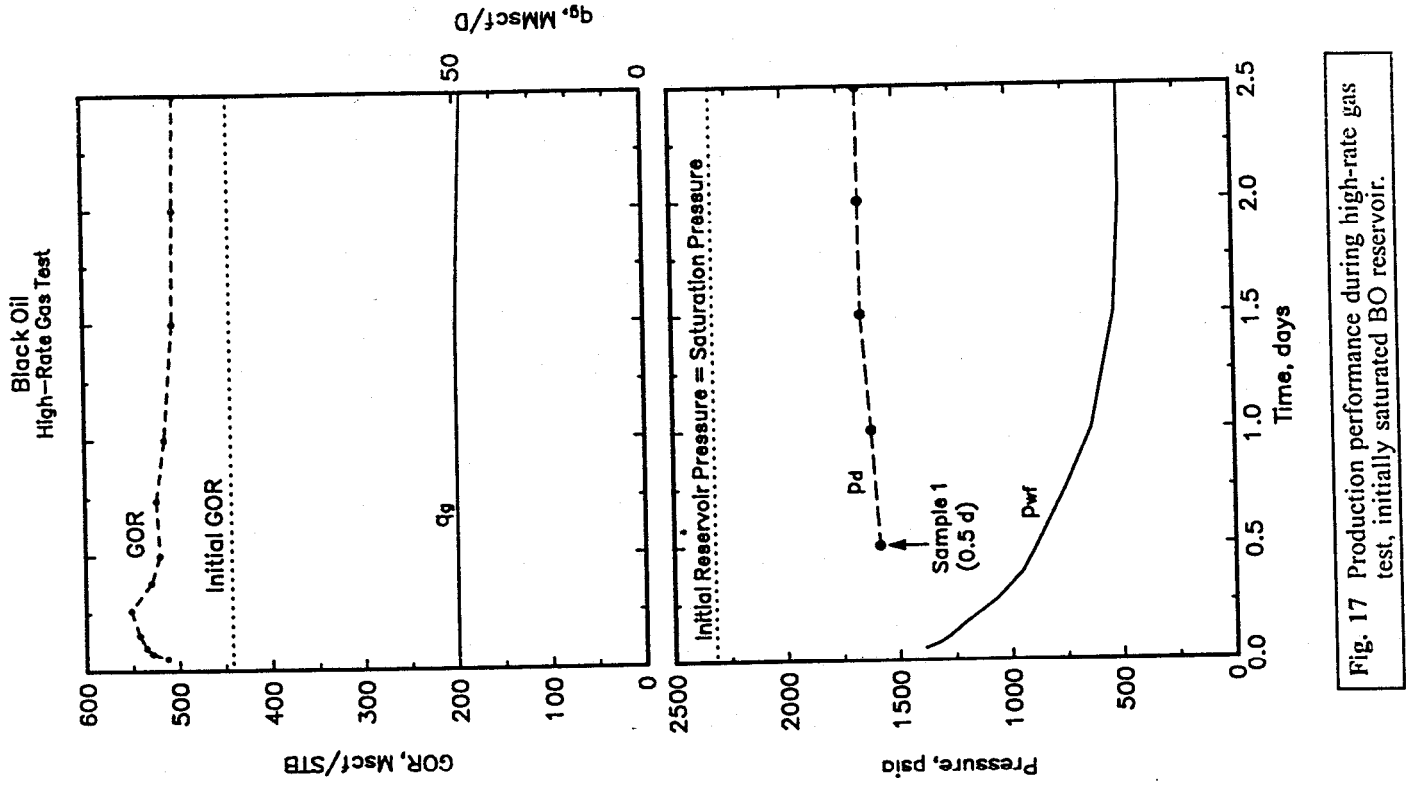

Fig. 17 Production performance during high-rate gas test, initially saturated BO reservoir.

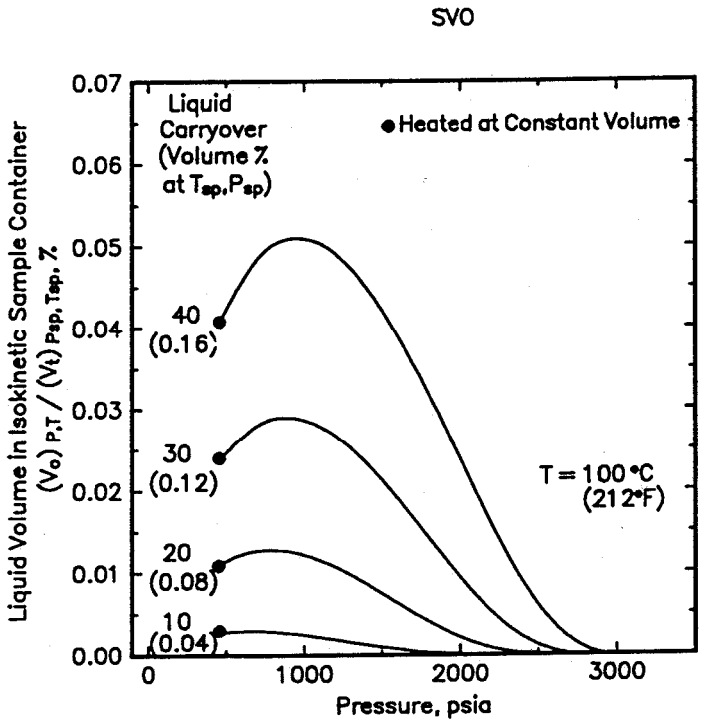

Fig. 18 Partial revaporization of isokinetic samples taken from separator gas stream of SVO insitu reservoir gas sample. Heated to 212°F.

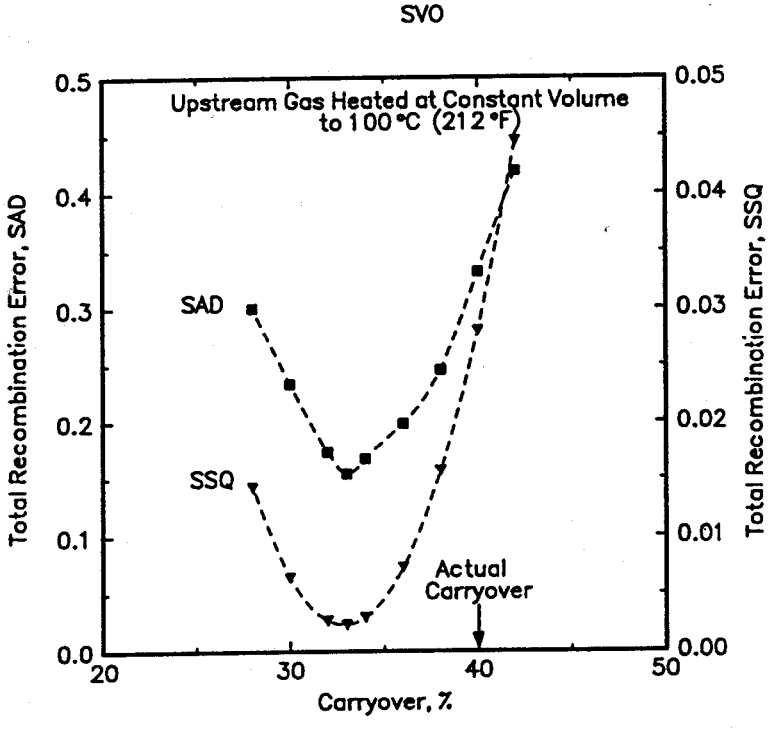

Fig. 19 Effect of incorrect sample taken from isokinetic container after heating (liquid carryover only partially revaporized).

TABLE 1

	Molar Composition of Reservoir Gas (DST 1 / DST 3 Initial Tests)				
	A	B	C	ECM(a)	ECM(b)
N2	0.755	0.756	0.750	0.756	0.750
CO2	3.615	3.615	3.592	3.614	3.634
C1	86.784	86.819	86.150	86.784	86.772
C2	2.578	2.578	2.568	2.578	2.595
C3	1.156	1.155	1.161	1.156	1.158
IC4	0.359	0.359	0.365	0.359	0.358
C4	0.565	0.565	0.579	0.565	0.563
IC5	0.293	0.293	0.309	0.294	0.292
C5	0.271	0.271	0.289	0.271	0.270
C6	0.444	0.443	0.496	0.444	0.441
C7+	3.178	3.146	3.742	3.179	3.168
C10+	1.336	1.311	1.583	1.336	1.334
C15+	0.330	0.315	0.381	0.330	0.330
C36+	0.013	0.011	0.013	0.013	0.013
	A Original Reservoir Gas B DST 1 Sample 1 C DST 1 Sample 1 Dewpoint Adjusted ECM1 using DST 1 Sample 1 Gas with Oils: (a) DST 3 Sample 1 (b) DST 3 Sample 1 Bubblepoint Adjusted				

TABLE 2

	Molar Composition of Reservoir Oil (DST 1 / DST 3 Initial Tests)				
	A	B	C	ECM(a)	ECM(b)
N2	0.33	0.309	0.321	0.330	0.327
CO2	2.950	2.915	2.990	2.949	2.965
C1	51.430	49.637	51.377	51.425	51.385
C2	2.650	2.653	2.689	2.649	2.667
C3	1.570	1.591	1.577	1.570	1.573
IC4	0.580	0.591	0.578	0.580	0.579
C4	1.010	1.033	1.004	1.010	1.007
IC5	0.630	0.647	0.624	0.630	0.626
C5	0.620	0.638	0.614	0.620	0.616
C6	1.270	1.312	1.258	1.270	1.262
C7+	36.960	38.675	36.970	36.966	36.992
C10+	27.810	29.152	27.862	27.814	27.872
C15+	16.850	17.685	16.903	16.851	16.908
C36+	3.032	3.184	3.044	3.033	3.045
	A Original Reservoir Oil B DST 3 Sample 1 C DST 3 Sample 1 Bubblepoint Adjusted ECM1 using DST 1 Sample 1 Gas with Oils: (a) DST 3 Sample 1 (b) DST 3 Sample 1 Bubblepoint Adjusted				

TABLE 3

	Molar Compositions of Reservoir Gas (DST 2 / DST 3 Initial Tests)									
	A	B	C	D	E	F	ECM(a)	ECM(b)	ECM(c)	ECM(d)
N2	0.755	0.757	0.740	0.745	0.756	0.750	0.755	0.759	0.758	0.756
CO2	3.615	3.618	3.555	3.562	3.605	3.600	3.615	3.593	3.609	3.610
C1	86.784	86.937	85.137	85.520	86.750	86.307	86.786	86.705	86.852	86.755
C2	2.578	2.578	2.550	2.557	2.576	2.576	2.578	2.562	2.575	2.575
C3	1.156	1.154	1.168	1.164	1.154	1.161	1.156	1.152	1.154	1.156
IC4	0.359	0.358	0.375	0.368	0.356	0.363	0.359	0.360	0.357	0.360
C4	0.565	0.563	0.602	0.584	0.558	0.573	0.565	0.567	0.561	0.566
IC5	0.293	0.292	0.336	0.311	0.283	0.300	0.293	0.296	0.288	0.294
C5	0.271	0.270	0.319	0.290	0.259	0.278	0.271	0.274	0.266	0.272
C6	0.444	0.440	0.583	0.496	0.409	0.461	0.444	0.453	0.431	0.447
C7+	3.178	3.036	4.635	4.402	3.294	3.631	3.177	3.277	3.149	3.210
C10+	1.336	1.228	1.942	2.118	1.552	1.640	1.335	1.380	1.341	1.351
C15+	0.330	0.270	0.428	0.559	0.409	0.430	0.330	0.334	0.330	0.332
C36+	0.013	0.006	0.010	0.013	0.010	0.010	0.013	0.013	0.013	0.013
	A Original Reservoir Gas B DST 2 Sample 1 C DST 2 Sample 1 Dewpoint Adjusted D DST 2 Sample 2 E DST 2 Sample 2 Dewpoint Adjusted F DST 2 Sample 3 ECM1 using DST 3 Sample 1 Oil with following Gases: (a) DST 2 Sample 1 (b) DST 2 Sample 2 (c) DST 2 Sample 2 Dewpoint Ajusted (d) DST 2 Sample 3									

TABLE 4

	Molar Composition of Reservoir Oil (DST 2 / DST 3 Initial Tests)					
	A	B	ECM(a)	ECM(b)	ECM(c)	ECM(d)
N2	0.330	0.309	0.330	0.335	0.331	0.331
CO2	2.950	2.915	2.948	2.941	2.946	2.949
C1	51.430	49.637	51.391	51.809	51.475	51.564
C2	2.650	2.653	2.649	2.635	2.649	2.648
C3	1.570	1.591	1.570	1.562	1.569	1.569
IC4	0.580	0.591	0.580	0.579	0.578	0.580
C4	1.010	1.033	1.010	1.008	1.004	1.010
IC5	0.630	0.647	0.630	0.632	0.621	0.631
C5	0.620	0.638	0.620	0.623	0.609	0.621
C6	1.270	1.312	1.270	1.284	1.237	1.273
C7+	36.960	38.675	37.001	36.591	36.983	36.825
C10+	27.810	29.152	27.846	27.310	27.957	27.642
C15+	16.850	17.685	16.879	16.197	16.870	16.629
C36+	3.032	3.184	3.043	2.854	3.012	2.962
	A Original Reservoir Oil B DST 3 Sample 1 ECM1 using DST 3 Sample 1 Oil with Gases: (a) DST 2 Sample 1 (b) DST 2 Sample 2 (c) DST 2 Sample 2 Dewpoint Ajusted (d) DST 2 Sample 3					

TABLE 5

	Molar Compositions of Reservoir Gas (DST 4 Initial Test with Coning)		
	A	ECM(a)	ECM(b)
N2	0.755	0.755	0.755
CO2	3.615	3.615	3.615
C1	86.784	86.784	86.784
C2	2.578	2.578	2.578
C3	1.156	1.156	1.156
iC4	0.359	0.359	0.359
C4	0.565	0.565	0.565
iC5	0.293	0.293	0.293
C5	0.271	0.271	0.271
C6	0.444	0.444	0.444
C7+	3.178	3.178	3.178
C10+	1.336	1.336	1.336
C15+	0.330	0.330	0.330
C36+	0.013	0.013	0.013
V_d/V_o %		95	78
	A Original Reservoir Gas ECM1 using Produced Wellstream (a) DST 4 Sample 1 (1.0 day) (b) DST 4 Sample 2 (2.5 days)		

TABLE 6

	Molar Composition of Reservoir Oil (DST 4 Initial Test with Coning)		
	A	ECM(a)	ECM(b)
N2	0.330	0.330	0.330
CO2	2.950	2.950	2.950
C1	51.430	51.429	51.428
C2	2.650	2.650	2.650
C3	1.570	1.570	1.570
iC4	0.580	0.580	0.580
C4	1.010	1.010	1.010
iC5	0.630	0.630	0.630
C5	0.620	0.620	0.620
C6	1.270	1.270	1.270
C7+	36.960	36.961	36.962
C10+	27.810	27.811	27.812
C15+	16.850	16.850	16.852
C36+	3.032	3.032	3.033
V_d/V_o %		95	78
	A Original Reservoir Oil ECM1 using Produced Wellstream (a) DST 4 Sample 1 (1.0 day) (b) DST 4 Sample 2 (2.5 days)		

TABLE 7

	Molar Composition of Reservoir Oil (MGC Depletion)					
	A	B	C	D	E	F
N2	0.330	0.315	0.369	0.307	0.329	0.272
CO2	2.950	3.017	2.759	3.066	2.958	3.205
C1	51.430	51.348	51.861	51.092	51.411	51.166
C2	2.650	2.716	2.416	2.750	2.659	2.896
C3	1.570	1.581	1.529	1.602	1.574	1.596
IC4	0.580	0.576	0.609	0.581	0.581	0.562
C4	1.010	1.000	1.085	1.009	1.011	0.970
IC5	0.630	0.620	0.706	0.620	0.630	0.596
C5	0.620	0.610	0.698	0.608	0.619	0.586
C6	1.270	1.250	1.422	1.231	1.267	1.207
C7+	36.960	36.968	36.547	37.134	36.960	36.946
C10+	27.810	27.887	26.952	28.182	27.826	28.007
C15+	16.850	16.928	16.141	17.288	16.872	17.049
C36+	3.032	3.049	2.894	3.142	3.037	3.073

A Original Reservoir Oil
B Sample 1 Bubblepoint Adjusted
C Sample 2 Bubblepoint Adjusted
D ECM1: Sample 2
E ECM2: Sample 2
F Undersaturated Sample Bubblepoint Adjusted

TABLE 8

	Molar Gas Composition (MGC Depletion)						
	A	B	C	D	E	F	G
N2	0.755	0.764	0.766	0.754	0.753	0.758	0.754
CO2	3.615	3.632	3.610	3.622	3.624	3.611	3.588
C1	86.784	87.529	87.325	86.805	86.775	86.805	86.342
C2	2.578	2.579	2.561	2.584	2.586	2.574	2.561
C3	1.156	1.147	1.141	1.158	1.159	1.154	1.154
IC4	0.359	0.354	0.354	0.359	0.360	0.359	0.361
C4	0.565	0.554	0.556	0.565	0.566	0.564	0.570
IC5	0.293	0.284	0.288	0.293	0.293	0.293	0.299
C5	0.271	0.262	0.266	0.270	0.271	0.271	0.278
C6	0.444	0.420	0.433	0.441	0.443	0.444	0.464
C7+	3.178	2.474	2.701	3.148	3.171	3.168	3.630
C10+	1.336	0.835	0.964	1.321	1.333	1.328	1.620
C15+	0.330	0.110	0.139	0.328	0.330	0.328	0.407
C36+	0.013	0.001	0.001	0.013	0.013	0.013	0.008

A Original Reservoir Gas
B Sample 1
C Sample 2
D ECM1: Sample 1 Gas/ECM2 Sample 2 Oil (V_g/V_l)= 0.5
E ECM1: Sample 1 Gas/ECM2 Sample 2 Oil (V_g/V_l)= 0.9
F ECM1: Sample 2 Gas/ECM2 Sample 2 Oil (V_g/V_l)= 0.5
G ECM2 (modified): Sample 2 Gas without reservoir oil

TABLE 9

	Molar Composition of Reservoir Oil (VO Depletion)				
	A	B	C	D	E
CO2	0.956	0.949	0.948	0.954	1.006
N2	0.231	0.261	0.204	0.228	0.194
C1	62.537	65.098	59.669	62.155	61.801
C2	7.933	7.815	7.677	7.913	8.309
C3	4.202	4.159	4.129	4.201	4.249
IC4	0.923	0.957	0.911	0.923	0.878
C4	2.101	2.214	2.086	2.103	1.968
IC5	0.762	0.850	0.759	0.763	0.685
C5	1.134	1.280	1.130	1.136	1.012
C6	1.694	1.931	1.690	1.696	1.510
F1	5.071	5.475	5.072	5.076	4.661
F2	5.242	4.600	5.255	5.252	5.246
F3	4.054	2.665	4.502	4.162	4.545
F4	2.194	1.217	3.866	2.380	2.721
F5	0.967	0.529	2.103	1.057	1.213
C7+	17.528	14.485	20.798	17.928	18.387

A Original Reservoir Oil
B Sample 1 Bubblepoint Adjustment
C ECM1 Sample 1
D ECM2 Sample 2
E Undersaturated Oil Bubblepoint Adjustment

TABLE 10

	Reservoir Gas Composition (BO Very Lean Gas Carryover)				
	A	B	C	D	E
N2	1.58246	1.58289	1.58583	1.58243	1.58173
CO2	0.59625	0.59634	0.59725	0.59626	0.59644
C1	92.69770	92.71723	92.87722	92.69767	92.69748
C2	3.66008	3.66010	3.66376	3.66014	3.66227
C3	0.38920	0.38907	0.38875	0.38921	0.38948
IC4	0.34046	0.34021	0.33887	0.34046	0.34061
C4	0.08571	0.08562	0.08508	0.08571	0.08574
IC5	0.11749	0.11726	0.11535	0.11748	0.11743
C5	0.02319	0.02314	0.02264	0.02319	0.02318
C6	0.12099	0.12042	0.11333	0.12098	0.12069
C7+	0.38652	0.36771	0.21192	0.38645	0.38496
F3+	0.13494	0.12021	0.03073	0.13490	0.13452
F8+	0.00008	0.00000	0.00000	0.00008	0.00008
	A Original Reservoir Gas B Gas Sample 1 C Separator Gas from Sample 1 D ECM1: Sample 1 / Original Reservoir Oil E ECM1: Separator Gas from Sample 1 / Original Reservoir Oil				

TABLE 11

	Reservoir Gas Composition (MGC DST 2 Carryover / DST 3)				
	A	B	C	ECM(a)	ECM(b)
N2	0.755	0.757	0.763	0.756	0.755
CO2	3.615	3.618	3.639	3.614	3.618
C1	86.784	86.937	87.551	86.785	86.825
C2	2.578	2.578	2.587	2.578	2.581
C3	1.156	1.154	1.149	1.156	1.156
IC4	0.359	0.358	0.352	0.359	0.358
C4	0.565	0.563	0.550	0.565	0.563
IC5	0.293	0.292	0.277	0.293	0.291
C5	0.271	0.270	0.253	0.271	0.269
C6	0.444	0.440	0.391	0.444	0.437
C7+	3.178	3.036	2.489	3.178	3.145
C10+	1.336	1.228	0.984	1.336	1.327
C15+	0.330	0.270	0.215	0.330	0.329
C36+	0.013	0.006	0.005	0.013	0.013
	A Original Reservoir Gas B DST 2 Sample 1 C DST 2 Sample 1 with 20 % Carryover ECM1 (V_o/V_t=0.7) using DST 3 Sample 1 Oil with Gases: (a) DST 2 Sample 1 (b) DST 2 Sample 1 with 20% Carryover				

TABLE 12

	Reservoir Oil Composition (MGC DST 2 Carryover / DST 3)		
	A	ECM(a)	ECM(b)
N2	0.330	0.330	0.329
CO2	2.950	2.949	2.951
C1	51.430	51.415	51.347
C2	2.650	2.649	2.653
C3	1.570	1.570	1.572
IC4	0.580	0.580	0.580
C4	1.010	1.010	1.008
IC5	0.630	0.630	0.627
C5	0.620	0.620	0.616
C6	1.270	1.270	1.255
C7+	36.960	36.977	37.063
C10+	27.810	27.823	27.988
C15+	16.850	16.860	17.018
C36+	3.032	3.036	3.070
	A Original Reservoir Oil ECM1 (V_o/V_t=0.7) using DST 3 Sample 1 Oil with Gases: (a) DST 2 Sample 1 (b) DST 2 Sample 1 with 20% Carryover		

Appendix B

Modeling Gas Condensate Well Deliverability (SPE 30714)

SPE 30714

Modeling Gas Condensate Well Deliverability

Ø. Fevang, SPE, and C.H. Whitson, SPE, U. Trondheim, NTH

This paper was prepared for presentation at the SPE Annual Technical Conference & Exhibition held in Dallas, U.S.A., 22-25 October, 1995.

Abstract

This paper gives an accurate method for modeling the deliverability of gas condensate wells. Well deliverability is calculated using a modified form of the Evinger-Muskat[1] pseudopressure (originally proposed for solution gas drive oil wells). The producing GOR is needed to calculate pseudopressure, together with PVT properties (black-oil or compositional), and gas-oil relative permeabilities. The proposed method is successfully tested for radial, vertically fractured, and horizontal wells.

Using the proposed deliverability model, we show that fine-grid single-well simulations can be reproduced almost exactly with a simple rate equation using pseudopressure. The key is knowing the producing GOR accurately. The effect of near-wellbore damage, vertical fracture, or flow improvement due to horizontal well trajectory is readily incorporated into the rate equation as a constant skin term.

The effect of gas-oil relative permeability is studied. We show that well deliverability impairment due to near-wellbore condensate "blockage" is only dependent on the relative permeabilities within the range defined by $1<k_{rg}/k_{ro}<50$. Usually this represents gas and oil relative permeabilities ranging from 0.05 to 0.3. Gas relative permeabilities at low oil saturations ($k_{rg}>0.3$) only affect deliverability for richer gas condensates (with maximum liquid dropout of 10% or greater).

A key observation and conclusion from this study is that critical oil saturation has *no* direct effect on well deliverability. We also show that IFT-dependence of relative permeability has little or no effect on gas condensate well performance (e.g. length of plateau production).

The most important application of this study is to provide a simple method for calculating bottomhole flowing pressure (BHFP) in coarse-grid models. We show that the proposed pseudopressure method is readily calculated for each well grid cell based only on grid cell pressure and producing GOR. Local grid refinement near wells is not necessary, and relatively large well grid cells can be used while still providing an accurate description of well deliverability.

Based on our analysis of the three basic flow regions of a gas condensate well, and the large effect of near-wellbore condensate blockage on well deliverability, we propose an experimental procedure for measuring relative permeabilities (specifically for modeling well deliverability).

Introduction

Calculation of gas condensate well deliverability has been a long-standing problem, without a simple solution. When BHFP drops below the dewpoint, a region of high condensate saturation buildups up near the wellbore, resulting in reduced gas permeability and lower gas deliverability. The effect of a condensate blockage region depends on relative permeability and PVT properties, and how the well is being produced.

Obviously, reduced gas deliverability due to condensate blockage is *only* important when the BHFP reaches a minimum (dictated by surface constraints) and the well is forced to go on decline.

Muskat[2] addresses the condensate blockage problem in his discussions of gas cycling, where he introduces a simple method for estimating the radius of condensate blockage as a function of time, gas rate, and reservoir rock and fluid properties. Fetkovich[3] uses Muskat's results to derive a rate- and time-dependent blockage skin for use in the standard gas rate equation.

Kniazeff and Naville[4] and Eilerts et al.[5,6] were the first to numerically model radial gas condensate well deliverability. These studies show radial saturation and pressure profiles as a function of time and other operational variables, confirming that condensate blockage reduces well deliverability. Kniazeff and Naville also study the effect of non-Darcy flow (in the gas phase) on well deliverability.

Gondouin et al.[7] make a significant contribution towards the fundamental understanding of gas condensate well deliverability. Through radial black-oil simulations, they extend the work by Kniazeff and Naville, showing the importance of

condensate blockage and non-Darcy flow effects on backpressure performance. They also give experimental procedures and measurements that quantify the effects of relative permeability and *multiphase* non-Darcy flow.

O'Dell and Miller[8] present the first gas rate equation using a pseudopressure function to describe the effect of condensate blockage. The equation is valid when (1) produced wellstream is the original reservoir gas, and (2) the blockage radius is relatively small (i.e. the reservoir pressure is significantly above the dewpoint). From their results, it is clear that well deliverability can be significantly reduced even for small regions of condensate blockage.

Fussell[9] presents EOS compositional simulations of radial gas condensate wells producing by pressure depletion below the dewpoint. He shows that the O'Dell-Miller equation (with a small correction to account for gas dissolved in the flowing oil phase) dramatically overpredicts the deliverability loss due to condensate blockage, compared with simulation results.

Jones and Raghavan[10,11] treat, for the most part, transient pressure behavior (drawdown and buildup) of radial wells. They use EOS compositional simulation with simple three-component (C_1-C_4-C_{10}) gas condensate mixtures. The key observation made concerning long-term ("boundary-dominated") well deliverability, is that the pseudopressure function presented by Fussell is accurate at all times during depletion. However, the integral must be evaluated using pressures and saturations known as a function of radius at a given time in depletion ("reservoir integral pseudopressure"). However, as they point out themselves, this isn't very helpful because they have to do compositional simulation to know the pressures and saturations at a given time in depletion. We show in this paper how to easily get the pressures and saturations from the instantaneous producing GOR (i.e. the producing wellstream composition).

Gas Condensate Rate Equation

The general volumetric rate equation for a gas condensate well of any geometry (e.g. radial, vertically fractured, or horizontal) is, for a compositional formulation,

$$q_g = C\left(\frac{RT_{sc}}{p_{sc}}\right)\beta_s \int_{p_{wf}}^{p_R}\left(\frac{\rho_o k_{ro}}{M_o u_o} + \frac{\rho_g k_{rg}}{M_g \mu_g}\right) dp \quad \cdots\cdots\cdots (1)$$

or in terms of black-oil PVT,

$$q_g = C \int_{p_{wf}}^{p_R}\left(\frac{k_{ro}}{B_o \mu_o} R_s + \frac{k_{rg}}{B_{gd} \mu_g}\right) dp \quad \cdots\cdots\cdots\cdots\cdots (2)$$

where

$$C = \frac{2\pi a_1 kh}{\ln(r_e/r_w) - 0.75 + s} \quad \cdots\cdots\cdots\cdots\cdots\cdots\cdots (3)$$

$a_1=1/(2\pi\cdot 141.2)$ for field units, and $a_1=1$ for pure SI units. The constant C includes basic reservoir properties such as permeability k, thickness h, drainage radius r_e, wellbore radius r_w, and other constants. Relative permeabilities k_{rg} and k_{ro} are defined relative to *absolute permeability*, and *not* relative to permeability at irreducible water saturation (this distinction is particularly important when correlating relative permeability data).

Skin s is a composite factor that includes non-ideal flow effects such as damage, stimulation, drainage geometry, and partial penetration. The traditional approach for estimating[12] or measuring[13] composite skin for a well producing single-phase fluid can be used to determine skin.

The condensate blockage effect is treated separately by the pseudopressure integral. We show that the pseudopressure integral, if evaluated properly, is for practical purposes independent of well geometry. This greatly simplifies the treatment of gas condensate well deliverability.

Flow Regions. An accurate yet simple model of a gas condensate well undergoing depletion consists of three regions:

Region 1: An inner near-wellbore region where both gas and oil flow simultaneously (at different velocities).

Region 2: A region of condensate buildup where only gas is flowing.

Region 3: A region containing single phase (original) reservoir gas.

For a given producing condition, one, two, or all three regions may exist. These three regions define pseudosteady-state flow conditions, meaning that they represent steady-state conditions at a given time but that the steady-state conditions change gradually during depletion.

Region 1. The *flowing* composition (GOR) within Region 1 is constant throughout. That means that the single-phase gas entering Region 1 has the same composition as the produced wellstream mixture. Conversely, if we know the producing wellstream, then we know the flowing composition within Region 1. Furthermore, the dewpoint of the producing wellstream mixture equals the reservoir pressure at the outer edge of Region 1.

Region 1 is the main source of deliverability loss in a gas condensate well. Gas relative permeability is reduced due to condensate buildup. The size of Region 1 increases with time. For steady-state conditions, the condensate saturation in Region 1 is determined (as a function of radius) *specifically* to ensure that all liquid that condenses from the single-phase gas entering Region 1 has sufficient mobility to flow through and out of Region 1 without any net accumulation.

Region 2. If it exists (as it usually does), Region 2 defines a region of net accumulation of condensate. Effectively, only gas is flowing in this region because oil mobility is zero (or very small). Condensate saturations in Region 2 are closely approximated by the liquid dropout curve from a constant volume depletion (CVD) experiment[14], corrected for water saturation.

The size of Region 2 is largest at early times just after the reservoir pressure drops below the dewpoint. It decreases in size with time because Region 1 is expanding. The size and importance of Region 2 is greater for lean gas condensates.

The main consequence of Region 2 is that producing wellstream composition (GOR) is leaner than calculated by a simple volumetric material balance (e.g. CVD measurements). Incorrect use of material balance GORs in the calculation of

the pseudopressure significantly overestimates deliverability loss in Region 1, especially at early times in depletion just after reservoir pressure drops below the dewpoint.

Region 3. Region 3 will always (and only) exist in a gas condensate reservoir that is currently undersaturated. The standard treatment[15] of single phase gas flow is used to quantify the contribution of Region 3 to well deliverability. Composition is constant in Region 3, equal to the original reservoir gas.

Coexistence of Flow Regions. If FBHP is less than the dewpoint, Region 1 will always exist (after a short transient required to build up the steady-state saturations in Region 1). Region 1 will not exist if FBHP is greater than the dewpoint.

Region 2 will always exist together with Region 1 after reservoir pressure drops below the dewpoint. In this case, Region 3 will not exist.

All three regions exist for reservoirs that are slightly undersaturated and FBHP is less than the dewpoint. Region 2 may "disappear" or have negligible effect for highly undersaturated reservoirs.

It is not possible for Regions 2 and 3 to exist in the absence of Region 1 (after steady-state conditions are reached).

For a very rich (near-critical) gas condensate, Region 1 may exist *throughout* the drainage area (in the absence of Regions 2 and 3), after reservoir pressure drops below the dewpoint.

Calculating Pseudopressure. Based on our observations of the three flow regions for many gas condensate systems, we have developed a simple method to accurately calculate the pseudopressure integral in Eqs. (1) and (2). The approach is an extension of the pseudopressure method proposed by Evinger and Muskat for solution gas drive oil wells.

First we break the pseudopressure integral into three parts, corresponding to the three flow regions discussed above.

$$\underline{\text{Total}} \qquad \Delta p_p = \int_{p_{wf}}^{p_R} \left(\frac{k_{rg}}{B_{gd}\mu_g} + \frac{k_{ro}}{B_o\mu_o}R_s\right) dp =$$

$$\underline{\text{Region 1}} \qquad \int_{p_{wf}}^{p^*} \left(\frac{k_{rg}}{B_{gd}\mu_g} + \frac{k_{ro}}{B_o\mu_o}R_s\right) dp \; + \qquad \ldots (4)$$

$$\underline{\text{Region 2}} \qquad \int_{p^*}^{p_d} \frac{k_{rg}}{B_{gd}\mu_g}\, dp \; +$$

$$\underline{\text{Region 3}} \qquad k_{rg}(S_{wi}) \int_{p_d}^{p_R} \frac{1}{B_{gd}\mu_g}\, dp$$

Given the producing GOR R_p, we know immediately p* because it equals the dewpoint of the producing wellstream. Using black-oil PVT, with r_s defined as the solution oil-gas ratio, we locate the pressure in the PVT table where $r_s=1/R_p$ and define this pressure as p*. In a compositional treatment the dewpoint of the producing wellstream composition is defined as p*. If $p^*>p_R$, then integration of the Region 1 integral should only be from p_{wf} to p_R; in this case, Regions 2 and 3 don't exist.

Region 1. The Region 1 pseudopressure integral is solved using the modified Evinger-Muskat approach. At pressures $p<p^*$ the PVT properties R_s, B_o, r_s, B_{gd}, μ_o, and μ_g are found directly. Next, the equation defining producing GOR[16]

$$R_p = R_s + \left(\frac{k_{rg}}{k_{ro}}\right)\left(\frac{\mu_o B_o}{\mu_g B_{gd}}\right)(1 - r_s R_p) \quad \ldots (5)$$

is used to calculate k_{rg}/k_{ro} as a function of pressure,

$$\frac{k_{rg}}{k_{ro}}(p) = \left(\frac{R_p - R_s}{1 - r_s R_p}\right)\frac{\mu_g B_{gd}}{\mu_o B_o} \quad \ldots (6)$$

where PVT properties are known as a function of pressure. It is readily shown that Eq. (6) can be expressed in terms of the oil relative volume of the flowing gas during a constant composition expansion, $V_{roCCE}=V_o/(V_g+V_o)$,

$$\frac{k_{rg}}{k_{ro}}(p) = \left(\frac{1}{V_{roCCE}} - 1\right)\frac{\mu_g}{\mu_o} \quad \ldots (7)$$

From Eqs. (6) and (7), V_{roCCE} can be expressed in terms of black-oil PVT properties, for any producing GOR R_p,

$$V_{roCCE}(p) = \left[1 + \left(\frac{R_p - R_s}{1 - r_s R_p}\right)\frac{B_{gd}}{B_o}\right]^{-1} \quad \ldots (8)$$

As shown by Evinger and Muskat, relative permeabilities k_{rg} and k_{ro} can be expressed directly as a function of the ratio k_{rg}/k_{ro} (when both phases are mobile). This means that we can evaluate k_{rg} and k_{ro} directly as a function of pressure in the Region 1 pseudopressure integral, $k_{rg}(p) = f[k_{rg}/k_{ro}(p)]$ and $k_{ro}(p) = f[k_{rg}/k_{ro}(p)]$, using Eq. (6).

Region 2. When Region 2 exists ($p^*<p_R$), the Region 2 integral is evaluated using $k_{rg}(S_o)$, where S_o is estimated as a function of pressure from CVD relative oil volumes $V_{roCVD}(p)=V_o(p)/V_d$, yielding $S_o(p)=[V_{roCVD}(p)](1-S_w)$. If V_{roCVD} values are not known for the black-oil PVT data set, they can be calculated using the following equations:

$$(V_{roCVD})_k = \frac{N_{k-1} - G_{k-1}(r_s)_k}{1 - (r_s R_s)_k}(B_o)_k$$

$$N_{k-1} = \left(\frac{V_{roCVD}}{B_o} + \frac{1 - V_{roCVD}}{B_{gd}} r_s\right)_{k-1} \quad \ldots (9)$$

$$G_{k-1} = \left(\frac{V_{roCVD}}{B_o} R_s + \frac{1 - V_{roCVD}}{B_{gd}}\right)_{k-1}$$

where k represents the current pressure, k-1 represents the previous pressure, and $(V_{roCVD})_0 = 0$.

Region 3. Only PVT properties are found in the Region 3 integral, where the traditional single-phase gas pseudopressure function can be used.

Verification of Proposed Pseudopressure Approach

To illustrate the proposed method for determining gas rate from Eq. (2), with pseudopressure calculated using the

proposed method outlined above, we have simulated several examples. We use two gas condensate fluids with radial, vertically fractured, and horizontal well geometries.

The two fluids are: *Rich Gas A*, an undersaturated gas condensate with 175 STB/MMscf and a maximum CVD liquid dropout of 23%; and *Lean Gas B*, a slightly undersaturated gas condensate with 45 STB/MMscf and a maximum CVD liquid dropout of 2%. PVT properties[14] for the two fluids are shown in **Figs. 1-4**. The reservoir properties and numerical grids are given in **Tables 1 and 2**. The gas/oil relative permeability data are calculated using a Corey equation.[17] Set A curves are shown in **Fig. 5**, and unless otherwise state, these curves are used in all calculations.

Compositional vs. Black-Oil PVT Formulation. Coats[18] presents radial well simulations that show a modified black-oil PVT formulation gives the same results as a fully compositional EOS PVT formulation. Results are given for a rich gas condensate producing on decline for 8 years. The EOS characterization uses seven components with one C_{7+} fraction.

Results from this example should probably be used with caution. A serious limitation is that only one C_{7+} fraction is used. With a more detailed C_{7+} split, oil viscosity differences between black-oil and compositional formulations often yield noticeable differences in well deliverability.

The problem is illustrated in **Fig. 6** where oil viscosity is plotted versus pressure. The solid line represents black-oil data, and the symbols represent results taken from compositional simulation of Rich Gas A. The figure shows that oil viscosities can change significantly during depletion.

Because the oil mobility required to flow condensed oil in Region 1 is basically fixed, a lower oil viscosity in the compositional simulations (particularly near the wellbore) results in a lower oil relative permeability and lower oil saturation than in the black-oil simulations; lower oil saturation results in higher gas relative permeability and better well deliverability for the compositional simulations (**Fig. 7**).

This problem can be improved using a modified $\mu_o(p)$ relationship in the black-oil simulator. The dashed line in **Fig. 6** passes through the "important" compositional results (data at pressures lower than the point where μ_o reaches a minimum). This same trend can be determined using a PVT simulator. When the modified $\mu_o(p)$ relation is used in black-oil reservoir simulation, well performance is closer to compositional results (dashed line in Fig. 7).

Pseudopressure Calculations. Gas rate is calculated with the *"Proposed Method"* for determining pseudopressure in Eq. (2), using the same black-oil PVT data as used in the simulation; the producing GOR, BHFP, and average reservoir pressure, as a function of time, are taken from the simulator.

Gas rate is also calculated using the same pseudopressure function, but with producing GOR set equal to $1/r_s$, evaluated at p_R; once again, the BHFP and average reservoir pressure, as a function of time, are taken from the simulator. This approach is equivalent to using a material balance based on a simple CVD depletion process (*"CVD MB Method"*), which also implies that Region 2 doesn't exist.

Radial Well - Lean Gas B. The Lean Gas B production forecast for a radial well is shown in **Fig. 8**, with simulated black-oil results shown as symbols. The solid line represents gas rate calculated with the Proposed Method to evaluate the pseudopressure (using R_p, p_R, and p_{wf} from the simulator). The PI constant C in Eq. (2) is calculated from Eq. (3) with s=0. Results are excellent.

The dashed line represents gas rate calculated with the same pseudopressure function [Eq. (2)], also using p_R and p_{wf} from the simulator, but using $R_p=1/r_s$ (with r_s evaluated at p_R). Results are poor, with well deliverability highly underestimated. The dot-dashed line uses the same CVD MB Method but with $p_{wf} = p_{wfmin} = 1500$ psia for all times.

The difference in rates calculated with the Proposed Method and the CVD MB Method is largest at early times. The reason is that Region 2 is largest at early times, decreasing in size with time.

Radial Well - Rich Gas A. The same radial well simulation is run with Rich Gas A. Results are given in **Fig. 9**, where the Proposed Method for evaluating pseudopressure reproduces the simulated results almost exactly. The simplified CVD MB Method gives good results for only a short time while the reservoir is still sufficiently undersaturated that producing GOR equals the initial solution GOR ($1/r_{si}$). As soon as R_p deviates from $1/r_s(p_R)$, the CVD MB Method starts to overestimate deliverability loss.

Vertically Fractured Well - Rich Gas A. A vertical fracture was simulated using the 2D cartesian grid given in Table 3 (420 grid cells). Results are plotted as symbols in **Fig. 10**.

Before making calculations with Eq. (2), the productivity index C had to be determined. We simulated the well with single-phase gas at high pressure (10,000 psia) to back-calculate C from pseudosteady state pressure performance. Using the Proposed Method for calculating pseudopressure, we obtained the rates given by a solid line in Fig. 10. The results are very accurate, with only slight deviation at late times.

Calculations based on the CVD MB Method with $R_p=1/r_s(p_R)$ underpredicts well deliverability at all times. Again, the largest deviations occur when Region 2 is largest (1-3 years).

Horizontal Well - Rich Gas A. A horizontal well was simulated using the 3D cartesian grid given in Table 3 (2223 grid cells). Results are given as symbols in **Fig. 11**.

Before making calculations with Eq. (2), the productivity index C had to be determined. We simulated the well with single-phase gas at high pressure (10,000 psia) to back-calculate C from pseudosteady state pressure performance. Using the Proposed Method for calculating pseudopressure, results are very accurate throughout the 20 year production period (solid line in Fig. 11).

Calculations based on the CVD MB Method with $R_p=1/r_s(p_R)$ underpredicts well deliverability at all times. The largest deviations occur when Region 2 has most effect (1-3 years).

Note that the well deliverability of a well with a 50-foot vertical fracture half-length is the same as the deliverability of a 1000-foot horizontal well! This result is for a typical k_v/k_h ratio of 0.1. Using $k_v/k_h=1$, the plateau period increases from 3.0 to 9.5 years. This extreme sensitivity to k_v/k_h does not exist for vertically fractured wells, and if horizontal wells are being considered in the development of a gas condensate reservoir, the k_v/k_h ratio should be determine with certainty to avoid overly optimistic production forecasts.

Application to Coarse-Grid Field Models

The main conclusion from the comparisons above is that the Proposed Method for calculating the gas rate pseudopressure function for a gas condensate well is accurate as long as the producing GOR is known accurately, independent of well geometry and production mode. Given this observation, we decided to evaluate the accuracy of producing GORs predicted by coarse-grid simulations.

Results show that coarse-grid GORs are generally very accurate. Consequently, the Proposed Method for calculating pseudopressure function of a gas condensate well can be used to accurately convert coarse grid cell pressures to BHFPs (individually for each well grid cell).

Conversion from grid cell pressure to BHFP for a gas well is usually made with the radial flow equation and a well index J, where $p_{wf} = p_{grid} - q_g/J$, with J given by

$$J = C\frac{k_{rg}}{\mu_g B_{gd}} \quad \ldots\ldots\ldots\ldots\ldots\ldots\ldots\ldots\ldots\ldots\ldots\ldots (10)$$

where k_{rg}, μ_g, and B_{gd} are evaluated at conditions in the well grid cell. Our proposal is simply to replace the $k_{rg}/\mu_g B_{gd}$ term with the pseudopressure integral defined in Eqs. (2) and (4), evaluating the integral from p_{wf} to p_{grid}.

Although Peaceman's equation(s)[19] can be used to calculate J (or C), we consistently found that it was better to determine the well index using results from single-phase simulations with a fine grid.

In a simulator, all PVT and relative permeability properties are available in each grid cell. For the sake of efficiency, the pseudopressure function Δp_p can be calculated during initialization for several producing GORs, and then stored as a three-dimensional table $\Delta p_p(p_{wf},p_{grid},R_p)$. Conceivably a different Δp_p function needs to be generated for all PVT/relative permeability regions. In the most general case, Δp_p can be stored as a four-dimensional table to handle changing water saturations, $\Delta p_p(p_{wf},p_{grid},R_p,S_w)$.

We wanted to test the proposed application using a commercial reservoir simulator. Intera's ECL100 was used, but because we did not have access to source code, it was necessary to incorporate the pseudopressure table as a "pseudo" tubing table. First we introduced an "infinite" well index J so that the model-calculated BHFP equals the well-grid-cell pressure. The pseudo-tubing table then converts this (well-grid-cell) pressure to actual BHFP [using Eq. (2)], based on gas rate and producing GOR.

The pseudo-tubing table approach can be used as a general solution to problems where the well produces from layers that are in vertical communication (i.e. experiencing reservoir crossflow). However, the approach is not recommended for wells producing from layered no-crossflow systems. The best general solution is to have the well pseudopressure tables generated at initialization, so that any grid cell that becomes a well grid will automatically have the multiphase pseudopressure method available.

Coarse Radial Grid. The size of the first grid cell in a radial simulation can be important in modeling well deliverability of gas condensates. This is shown in **Fig. 12**, where Lean Gas B is used with a first-grid cell radius of 100 ft (versus 0.7 ft in the fine-grid simulation); the remaining grids are spaced logarithmically. The plateau period is more than doubled from 2.5 for the fine-grid simulation to 6.25 years for the coarse grid simulation. Even for an 18 ft inner radius, the plateau period is overpredicted by more than one year.

Using the multiphase pseudopressure method (based on a pseudo-tubing curve), the correct plateau period of 2.5 years is predicted and the rate-time performance overlays the fine-grid simulation results. Using the same coarse radial grid (r_1=100 ft) and Rich Gas A, the proposed pseudoporessure method again predicts the rate-time performance accurately (**Fig. 13**).

Coarse Cartesian Grid. Using a coarse cartesian grid with a 200x200 ft well grid cell, the proposed method was compared with the fine-grid radial simulation for Lean Gas B. Results are shown in **Fig. 14**, where the rate-time performance is accurately calculated using the coarse grid pseudopressure method. Note that the standard well treatment [Eq. (10)] results in a plateau of 6 years compared with the correct plateau of 2.5 years.

Using a coarse cartesian grid with a 500x500 ft well grid cell, the proposed method was compared with 2D fine-grid simulation results of a vertically fractured well using Rich Gas A. **Fig. 15** shows that the rate-time performance is accurately calculated using the coarse grid pseudopressure method. The standard well treatment results in a plateau of 6 years compared with the correct plateau of 3 years.

Using a coarse cartesian grid with 333x333x25 ft well grid cells, the proposed method was compared with fine-grid 3D horizontal well simulation results for Rich Gas A. Results are shown in **Fig. 16**, where the rate-time performance is accurately calculated using the coarse grid pseudopressure method. The standard well treatment results in a plateau of almost 6 years compared with the correct plateau of 3 years.

Discussion of Coarse Grid Pseudopressure Method. We have shown that local grid refinement in gas condensate wells is not necessary. The only limitation of the pseudopressure approach is that producing GOR from the coarse grid model is reasonably accurate (compared with fine grid simulation).

Effectively, Region 2 is eliminated *in the well grid cell* using this approach. Surrounding grid cells, however, automatically treat the Region 2 pressures losses. The more important Region 1 behavior is treated accurately in the well grid cell. However, if the size of the well grid cell becomes too large, Region 1 pressure losses will be overestimated and calculated well deliverability underestimated. In the limit of one grid cell describing the entire drainage area, this method becomes equivalent to the CVD MB Method, which always underestimates well deliverability.

Deciding an appropriate well grid size will depend on (1) the leanness of the gas condensate, (2) the minimum well plateau length, and (3) the degree of undersaturation. Smaller well grids are needed for lean gas condensates, short plateau periods, and initially saturated fluids. In other words, a saturated lean gas condensate that goes on decline immediately will require the smallest well grid size.

A few sensitivity cases can be run to determine the required well grid size for a given gas condensate reservoir. These cases should evaluate wells producing at the maximum expected rate (dictated by equipment constraints such as tubing diameter and erosional velocity). A case with initial pressure equal to the dewpoint should be used, even for highly undersaturated reservoirs, to evaluate a "late" well being drilled after depletion to the dewpoint.

Relative Permeability Effects

Primary Functional Relationship $k_{rg} = f(k_{rg}/k_{ro})$. The deliverability loss due to condensate blockage is dictated by the Region 1 contribution to the pseudopressure integral. This contribution is solved by finding the relationship between k_{rg} and the ratio k_{rg}/k_{ro}. **Fig. 17** shows a plot of k_{rg} vs. k_{rg}/k_{ro} based on the Corey equation for different pore size distribution parameters λ.

The relevant range of k_{rg}/k_{ro} found in Region 1 can be calculated directly from PVT properties and Eq. (6) as a function of pressure, from the dewpoint pressure *of the flowing mixture* (wellstream) to any lower pressure.

Calculation of $k_{rg}/k_{ro}(p)$ from Eq. (7) can be done readily with a PVT simulator. Results for both Gases A and B are shown in Figs. **18**-**19**, together with plots of $V_{roCCE}(p)$. The $k_{rg}/k_{ro}(p)$ plot defines the lower range of relative permeabilities of interest. The upper limit on relevant k_{rg}/k_{ro} ranges from 10 for rich condensates to about 50 for lean condensates. Accordingly, the range of relative permeabilities to be measured in the laboratory are defined from the $k_{rg}/k_{ro}(p)$ plot (Appendix A).

Returning to Fig. 17 (k_{rg} vs. k_{rg}/k_{ro}), we show for different gas condensate fluids the practical range of k_{rg}/k_{ro} existing in Region 1. An upper limit of 50 will practically apply for all gas condensates because (1) the k_{rg} value is relatively high at $k_{rg}/k_{ro}>50$, (2) only a small pressure interval just below the wellstream dewpoint experiences this range of k_{rg}/k_{ro} (at the outer edge of Region 1), and (3) if k_{rg} vs. k_{rg}/k_{ro} is well defined experimentally at $k_{rg}/k_{ro}<50$, then the extrapolation to higher k_{rg}/k_{ro} values is trivial.

To illustrate the importance of the k_{rg} vs. k_{rg}/k_{ro} relationship for well deliverability, we first simulated a radial well for Rich Gas A using relative permeability Set B (shown as solid lines in **Figs. 20**-**21**).

For this relatively rich fluid we assume that the relevant range of relative permeabilities in Region 1 is limited by $k_{rg}/k_{ro}<10$. We then made a second radial simulation using a second set of relative permeabilities (Set B') with an identical $k_{rg} = f(k_{rg}/k_{ro})$ relationship for all saturations (**Fig. 22**), but with completely different $k_{rg}(S_g)$ and $k_{ro}(S_g)$ curves in the range $k_{rg}/k_{ro}<10$ (Figs. 20 and 21).

Simulations of rate-time performance using relative permeability Sets B and B' are shown in **Fig. 23**. The well performs identically, for practical purposes, with both sets of relative permeabilities. These results are *not* a special case, but they are generally true for all gas condensate reservoirs. k_{rg} vs. k_{rg}/k_{ro} *is* the fundamental relative permeability relationship dictating Region 1 behavior and well deliverability, not k_{rg} and k_{ro} as a function of saturation.

Critical Oil Saturation. It has been suggested that S_{oc} is an important parameter in defining relative permeabilities of gas condensates. The only reason this claim can be made is that S_{oc} has been used in parametric equations where effective oil saturation S_o^* is normalized with S_{oc}, e.g.

$$k_{ro} = (S_{o*})^2 \left(\frac{S_o}{1-S_{wi}}\right)^{(2+\lambda)/\lambda} \quad \ldots\ldots\ldots\ldots\ldots\ldots (11)$$

$$S_{o*} = \frac{S_o - S_{oc}}{1 - S_{wi} - S_{oc}}$$

When this is done, a change in S_{oc} affects k_{ro}, and consequently k_{rg}/k_{ro}, at *all* saturations. The result is a totally different $k_{rg} = f(k_{rg}/k_{ro})$ relationship, even though $k_{rg}(S_g)$ is unchanged.

In the absence of relative permeability data, or if available data are questionable, it is a bad idea to make "sensitivity" studies of relative permeability using S_{oc} as a parameter in a general correlation. Instead, the $k_{rg}=f(k_{rg}/k_{ro})$ relationship (in the range $1<k_{rg}/k_{ro}<50$) should be varied systematically, for example using pore size distribution λ in the Corey equation. If S_{oc} *is* used as a parameter in sensitivity studies, the effect it has on well deliverability should be recognized as the effect S_{oc} has on the $k_{rg} = f(k_{rg}/k_{ro})$ relationship, and not on k_{ro} or k_{rg} values near S_{oc}.

Because Region 1 flow behavior dictates well deliverability loss due to condensate blockage, and because oil saturation, oil relative permeability, and oil mobility are all at a maximum in Region 1, the low-oil-saturation relative permeabilities (near S_{oc}) are irrelevant to condensate blockage.

For richer condensates, Region 2 may have oil saturations somewhat greater than S_{oc}. Even so, the oil relative permeability in this saturation region is irrelevant because oil mobility is practically zero. Furthermore, gas relative permeability at low oil saturations is not affected directly by S_{oc}.

To illustrate the insignificance of S_{oc}, Rich Gas A was simulated with radial and vertically fractured well geometries using Set A relative permeabilities (S_{oc}=10%). Rate-time performance for the two wells are shown as solid lines in **Fig. 24**.

For this fluid, the important region of k_{rg}/k_{ro} is less than 10 for most of depletion. Based on this observation, we modified the k_{ro} curve at saturations where k_{rg}/k_{ro} is greater than 10 (low S_o values). Extrapolations of k_{ro} using S_{oc}=0% and S_{oc}=20% are shown in **Fig. 25**. As seen in Fig. 24, the simulated rate-time performance is practically identical for S_{oc}=0% and 20%, compared with the base case using S_{oc}=10%.

We also ran simulations at lower BHFP (250 psia) to see if low oil saturations in Region 1 due to vaporization would result in significant differences in well deliverability for the three oil relative permeability curves with different S_{oc} values. As seen in **Fig. 26**, the effect is very small.

Gas-Oil Interfacial Tension. Probably the most misleading and deceptive concept put forth by earlier publications on gas condensates is the importance of gas-oil IFT on relative permeabilities. Many workers have discussed the potential effect, functional dependence, and methods for measuring the IFT effect on relative permeabilities. But no one has yet shown that reservoir performance is significantly altered by "straightened-line" relative permeabilities due to low IFTs.

The two reservoir mechanisms that are affected by relative permeabilities in gas condensate reservoirs are (1) well deliverability and (2) gravity segregation of condensate that theoretically can occur in high-permeability or fractured reservoirs.

The physics of IFT effect on relative permeabilities is not well understood. Measurements quantifying the effect in a systematic way are lacking, and the data available are not reliable enough to build a theoretical (or empirical) model for predicting the effect. The existing conceptual model states that IFTs must be lower than a "threshold" IFT σ^* before relative permeabilities are affected. Furthermore, as IFT approaches zero the relative permeabilities approach straight lines with zero residual saturations. The model is given by

$$k_r = F\,k_{r,\text{Immiscible}} + (1-F)\,k_{r,\text{Miscible}}$$

$$S_r = F\,S_{r,\text{Immiscible}}$$

$$k_{r,\text{Miscible}} = (S-S_r)/(1-S_{wi}-S_r) \qquad \cdots\cdots\cdots (12)$$

$$F = \left(\frac{\sigma}{\sigma^*}\right)^n \;,\; \sigma<\sigma^* \;;\; F = 1 \;,\; \sigma\geq\sigma^*$$

Recent measurements indicate that σ^* ranges from 0.1 to 0.3 mN/m. Exponent n=0.1 is recommended, though this is based more on physical intuition than experimental evidence.

In this paper we deal mostly with the potential effect of IFT on well deliverability. We also have studied gravity segregation, with the following observations: (1) segregation is negligible unless permeability is high (> 1000 md) and near-straight-line relative permeability curves exist, (2) the low-IFT period just below the dewpoint (with near-straight-line curves) is short-lived, (3) IFTs exceeding the "threshold" IFT (ranging from 0.1 to 0.3 mN/m) exist during the major part of depletion even for near-critical systems (see **Fig. 27**); IFT effect on relative permeability is nonexistent for IFTs exceeding the threshold IFT.

Consequently, we do not see how it is possible to develop significant condensate accumulations by gravity segregation. Our simulations indicate that such accumulations do not develop unless straight-line curves are used throughout depletion, and physically this can only be expected in a single-porosity fractured reservoir (where relative permeabilities are basically independent of IFT!). Finally, even if some segregation does occur, it is difficult to conceptualize a reservoir development strategy that would be economically competitive with gas cycling. Blue sky!

Concerning the effect of IFT on well deliverability, we have made the following observations (which are supported by simulations presented below): (1) Gas condensate reservoirs will generally never experience IFTs lower than threshold IFTs of 0.1 to 0.3 mN/m in near-wellbore Region 1, *when BHFP reaches a minimum and the well goes on decline.* (2) Low IFT in Region 2 and the resulting improvement in gas relative permeability has only a minor effect (if any) on deliverability.

Simulation of a "worst" case using Rich Gas A is given for radial and vertically fractured wells. The IFT model given by Eq. (12) uses Set A "Immiscible" relative permeability curves, σ^*=0.3 mN/m, and n=0.1. Simulated rate-time performance is shown in **Figs. 28-29**, indicating relatively little effect of IFT-corrected relative permeabilities on well deliverability. Absolutely no effect of IFT on well deliverability is found for Lean Gas B, because $\sigma>\sigma^*$ at all $p<p_d$ (Fig. 27).

The potential effect of IFT on well deliverability will be greatest for rich, near-critical fluids producing on decline initially (no plateau). However, for this type of low-permeability well the IFT effect on relative permeabilities will be only one of several major uncertainties (absolute permeability, fracture length, rock relative permeabilities, and oil viscosity). Practically, it will be impossible to separate IFT effects from these other effects, and it also will be difficult to "sell" the optimistic effect of low IFTs to project economics when the IFT/relative permeability phenomena is so poorly understood.

Velocity/IFT Effect. Schulte[20] (and coworkers) at Shell have questioned the validity of using only IFT effect on relative permeabilities for gas condensate systems. They present arguments that indicate an additional improvement in k_{rg} (in addition to low IFT) that might be expected due to high velocities (i.e. pressure drops) experienced near the wellbore. Effectively, they claim that the capillary number (given by the ratio of viscous to capillary forces) should be the correlating parameter instead of IFT (capillarity) alone. Some of their results are to be presented at the 1995 Annual SPE Technical Conference & Exhibition[21].

Subsequently, Henderson et al.[22] provided experimental results of velocity and velocity/IFT effects on relative permeability using Berea sandstone for a five-component

synthetic gas condensate mixture. The two systems used had IFTs of 0.05 and 0.4 mN/m with flowing velocities ranging from 3 to 120 ft/D (10^{-5} m/s to $4 \cdot 10^{-4}$ m/s). The experiments combined a stabilized steady-state flow test followed by interpretation of an unsteady-state flow test.

Fig. 30 shows a plot of the 0.4 mN/m data plotted as k_{rg} vs. k_{rg}/k_{ro} (the 0.05 mN/m data are totally irrelevant to well deliverability). The curve is shifted to higher k_{rg} values at higher velocities, without changing the shape of the curve significantly. Unfortunately, 0.4 mN/m is probably the smallest IFT that can ever be expected in Region 1 (when a well is approaching the minimum BHFP). The net effect of high velocities at more relevant (higher) IFTs has yet to be studied experimentally; we suspect that the effect may "disappear" at higher IFTs (found in most of Region 1), as mentioned by Henderson et al.

Fig. 31 plots k_{rg} (at $k_{rg}/k_{ro}=10$) vs. capillary number N_c ($N_c = \mu_g v_s/\sigma$, where v_s is gas pore velocity) for the six velocity/IFT conditions reported. A clear trend of increasing k_{rg} with N_c is seen. However, the practical range of N_c expected in Region 1 (when a well is approaching the minimum BHFP) is less than about $5 \cdot 10^{-5}$.

The actual profile of N_c in Region 1 needs to be studied in more detail. We suspect note that this profile will be very different in radial and vertically fractured wells. If N_c is small enough (e.g. $<10^{-5}$) in a significant portion of Region 1, then the net IFT/velocity effect on well deliverability is probably small.

Furthermore, near the wellbore where velocity is highest, any positive effect that a high N_c value might have on "Darcy" relative permeability (k_{rg}) may be offset by non-Darcy flow effects. We estimate that Henderson et al.'s highest-velocity data are just on the limit of Darcy flow (based on a Reynold's number of about 0.5 to 1, as defined by Muskat[2,12]).

Conclusions

1. Gas condensate wells producing with BHFP below the dewpoint have up to three flow regions. *Region 1* has a constant flowing composition (GOR) where both gas and oil flow simultaneously. Most of the deliverability loss is caused by reduced gas permeability in Region 1. *Region 2* is where condensate accumulates but has no mobility. *Region 3* is the outer region where reservoir pressure is greater than the dewpoint and only gas flows.

2. Gas well deliverability can be accurately determined using a simple rate equation, Eq. (1) or Eq. (2). The multiphase pseudopressure function is easily calculated from producing GOR (composition) and PVT properties. The effect of reduced gas permeability (condensate blockage) is incorporated in the pseudopressure function. All other well terms (well geometry, damage skin, etc.) are accounted for in the "productivity" constant C. The method is shown to work for radial, vertically fractured, and horizontal wells.

3. The multiphase pseudopressure function is calculated in three parts, based on the three flow regions. Region 1 pseudopressure is calculated using the Evinger-Muskat approach, modified for gas condensate systems. Region 2 uses the $k_{rg}(S_o)$ relationship, and $S_o(p)$ estimated from the liquid dropout curve from a CVD experiment. Region 3 pseudopressure is the same as for single phase gas.

4. Local grid refinement is not needed for gas condensate wells in full-field models. The proposed pseudopressure method calculates well deliverability accurately in coarse grid models, without any near-well grid refinement. Examples are given for radial, vertically fractured, and horizontal wells.

5. The primary relative permeability relationship affecting condensate blockage (in Region 1), and thus the primary cause of reduced well deliverability, is k_{rg} as a function of k_{rg}/k_{ro}. Saturation does not enter the calculation.

6. Critical oil saturation S_{oc} has no effect on gas condensate well deliverability.

7. Gas-oil interfacial tension has little effect on gas condensate well deliverability (unless a physically questionable model is used for the dependence of relative permeability on IFT).

8. An experimental procedure is recommended for obtaining the key relative permeability data needed to properly model gas condensate well deliverability.

9. Deliverability of horizontal gas condensate wells is strongly affected by the k_v/k_h ratio. Severe deliverability loss is shown even for a normal k_v/k_h ratio of 0.1, compared with the performance of the same horizontal well with $k_v/k_h=1$.

Nomenclature

B_{gd} = dry gas FVF, RB/scf or m^3/m^3
B_o = oil FVF, RB/STB or m^3/m^3
C = gas rate constant
F = IFT correlating parameter
G = Current surface gas in place in CVD cell, scf or m^3
h = reservoir thickness, ft or m
J = productivity index, scf/D/psi or $m^3/s/Pa$
k = absolute permeability, md (μm^2)
k_r = relative permeability (generic)
k_{rg} = gas relative permeability
k_{ro} = oil relative permeability
k_v/k_h = vertical-to-horizontal permeability ratio
L = core length, ft or m
M_g = gas molecular weight
M_o = oil molecular weight
n = exponent in IFT correction
N = Current STO in place in CVD cell, STB or m^3
N_c = Dimensionless viscous-to-capillary number
p = pressure, psia or Pa
p* = pressure at outer boundary of Region 1, psia or Pa
p_d = dewpoint pressure, psia or Pa
Δp = total pressure drop (across core), psi or Pa
Δp_p = total pseudopressure, psi/cp or 1/s
p_R = average reservoir pressure, psia or Pa
p_{sc} = standard condition pressure, psia or Pa
p_{wf} = wellbore flowing pressure, psia or Pa
q_g = surface gas rate, scf/D or m^3/s
$q_{g,core}$ = gas flow rate at core conditions, ft^3/D or m^3/s
$q_{o,core}$ = oil flow rate at core conditions, ft^3/D or m^3/s
q_{inj} = pump injection rate, ft^3/D or m^3/s

r_e = external drainage radius, ft or m
r_s = solution OGR, STB/scf or m^3/m^3
r_w = wellbore radius, ft
R = gas constant
R_p = producing GOR, scf/STB or m^3/m^3
R_s = solution GOR, scf/STB or m^3/m^3
s = skin factor
S* = normalized saturation
S_g = gas saturation
S_o = oil saturation
S_{oc} = critical oil saturation
S_r = residual saturation (generic)
S_w = water saturation
S_{wi} = irreducible water saturation
T = reservoir temperature, ^oR or K
T_{sc} = standard condition temperature, ^oR or K
V_d = dewpoint volume, ft^3 or m^3
V_{ro} = CCE oil relative volume, $V_o/(V_g+V_o)$
V_{ro} = CVD oil relative volume, V_o/V_d
V_{rt} = CCE total relative volume, $(V_g+V_o)/V_d$
v_s = pore velocity = $v/[\phi(1-S_{wi})]$, ft/D or m/s

β_s = surface gas mole fraction in wellstream
λ = Corey pore size distribution factor
μ_g = gas viscosity, cp or Pa·s
μ_o = oil viscosity, cp or Pa·s
ρ_g = gas density, lb/ft^3 or kg/m^3
ρ_o = oil density, lb/ft^3 or kg/m^3
σ = gas-oil IFT, dynes/cm or N/m
σ^* = threshold gas-oil IFT, dynes/cm or N/m
ϕ = porosity

References

1. Evinger, H.H. and Muskat, M.: "Calculation of Theoretical Productivity Factor," *Trans.*, AIME (1942) **146**, 126-139.
2. Muskat, M.: *Physical Principles of Oil Production*, McGraw-Hill Book Company, Inc. (1949).
3. Fetkovich, M.J.: "The Isochronal Testing of Oil Wells," paper SPE 4529 presented at the 1973 SPE Annual Technical Conference and Exhibition, Las Vegas, Sept. 30-Oct. 3.
4. Kniazeff, V.J. and Naville, S.A.: "Two-Phase Flow of Volatile Hydrocarbons," *SPEJ* (March 1965) 37-44; *Trans.*, AIME, **234**.
5. Eilerts, C.K., Sumner, E.F., and Potts, N.L.: "Integration of Partial Differential Equation for Transient Radial Flow of Gas-Condensate Fluids in Porous Structures," *SPEJ* (June 1965) 141-152.
6. Eilerts, C.K. and Sumner, E.R.: "Integration of Partial Differential Equations for Multicomponent, Two-Phase Transient Radial Flow," *SPEJ* (June 1967) 125-135.
7. Gondouin, M., Iffly, R., and Husson, J.: "An Attempt to Predict the Time Dependence of Well Deliverability in Gas Condensate Fields," *SPEJ* (June 1967) 112-124; *Trans.*, AIME, **240**.
8. O'Dell, H.G. and Miller, R.N.: "Successfully Cycling a Low Permeability, High-Yield Gas Condensate Reservoir," *JPT* (Jan. 1967) 41-47; *Trans.*, AIME, **240**.
9. Fussell, D.D.: "Single-Well Performance Predictions for Gas Condensate Reservoirs," *JPT* (July 1973) 258-268, 860-870; *Trans.*, AIME, **255**.
10. Jones, J.R. and Raghavan, R.: "Interpretation of Flowing Well Response in Gas Condensate Wells," paper SPE 14204 presented at the 1985 SPE Annual Technical Conference and Exhibition, Las Vegas, Sept. 22-25.
11. Jones, J.R., Vo, D.T., and Raghavan, R.: "Interpretation of Pressure Buildup Responses in Gas Condensate Wells," paper SPE 15535 presented at the 1986 SPE Annual Technical Conference and Exhibition, New Orleans, Oct. 5-8.
12. Golan, M. and Whitson, C.H.: *Well Performance*, 2nd ed., Prentice-Hall (1986).
13. Earlougher, R.C., Jr.: *Advances in Well Test Analysis*, Monograph, SPE, Dallas (1977).
14. Whitson, C.H. and Torp, S.B.: "Evaluating Constant Volume Depletion Data," *JPT* (March 1983) 610-620; *Trans.*, AIME, **275**.
15. Al-Hussainy, R., Ramey, H.J., Jr., and Crawford, P.B.: "The Flow of Real Gases Through Porous Media," *JPT* (May 1966) 624.
16. Fetkovich, M.D., Guerrero, E.T., Fetkovich, M.J., and Thomas, L.K.: "Oil and Gas Relative Permeabilities Determined From Rate-Time Performance Data," paper SPE 15431 presented at the 1986 SPE Annual Technical Conference and Exhibition, New Orleans, Oct. 5-8.
17. Standing, M.B.: "Notes on Relative Permeability Relationshops," *Proc.*, University of Trondheim, NTH, Norway (1975) .
18. Coats, K.H.: "Simulation of Gas Condensate Reservoir Performance," *JPT* (Oct. 1985) 1870-1886.
19. Peaceman, D.W.: "Interpretation of Well Block Pressures in Numerical Reservoir Simulation," *SPEJ* (1978) 183-194; *Trans.*, AIME 253, .
20. Schulte, A.: "Simulation Mechanisms of Well Impairment Due to Condensate Dropout," SPE Forum Series in Europe, Gas Condensate Reservoirs, Seefeld, Austria (1994).
21. Boom, W., *et al.*: "Experimental Evidence for Improved Condensate Mobility at Near Wellbore Flow Conditions," paper SPE 30766, presented at the 1995 SPE Annual Technical Conference & Exhibition, Oct. 22-25, Dallas.
22. Henderson, G.D., Danesh, A., Tehrani, D., and Peden, J.M.: "The Effect of Velocity and Interfacial Tension on the Relative Permeability of Gas Condensate Fluids in the Wellbore Region," Paper Presented at the 8th European IOR Symposium (May 15-17, 1995), Vienna.
23. Chierici, G.L.: "Novel Relation for Drainage and Imbibition Relative Permeabilities," *Society of Petroleum Engineers Journal* (June 1984) 275-276.

Appendix A.
Measuring Gas Condensate Relative Permeabilities

Based on the simulation work presented in this paper, we have established an experimental procedure for measuring the *key relative permeability data needed for well deliverability*. The most important data (and easiest to measure) is $k_{rg} = f(k_{rg}/k_{ro})$. We recommend that this relation always be determined accurately for k_{rg}/k_{ro} values ranging from a maximum of k_{rg}/k_{ro}=50, to a minimum calculated by PVT calculations using Eq. (7) (based on the original reservoir mixture, $R_p=1/r_{si}$).

For Region 2 calculations, it may also be useful to know $k_{rg} = f(S_o)$ at low oil saturations defined by the CVD liquid dropout curve. This data is usually only needed for richer gas condensates where maximum liquid dropout is greater than

about 10%. For leaner systems, the reduction in k_{rg} in Region 2 is negligible, and experimental determination of $k_{rg}(S_o)$ at low oil saturations has little value.

Steady-State Flow (Region 1): $k_{rg} = f(k_{rg}/k_{ro})$. In Region 1, flow near the wellbore is a steady-state process where, at any radius, the mixture entering a volume element ΔV is the same mixture leaving the volume. Practically, a core plug can be considered as such a volume element. Our procedure is based on conducting core plug flow tests that are representative of conditions in Region 1 throughout depletion.

At least five or six steady state points should be measured to define the $k_{rg} = f(k_{rg}/k_{ro})$ relation. Flowing conditions of these data are determined using the PVT-derived plot of $k_{rg}/k_{ro}(p)$ from Eq. (7) [using equally spaced $\log(k_{rg}/k_{ro})$ values], evaluated at the minimum BHFP. An example is shown in **Fig. 32** for Lean Gas B.

The first data is measured using original reservoir fluid. This mixture is flowed through the core at a pressure equal to minimum FBHP until steady state conditions are reached. The pressure drop across the core is used to calculate phase mobilities using

$$k_{rg} = q_{g,core} \frac{L}{kA\Delta p} \mu_g \quad \text{or} \quad k_{rg} = q_{o,core} \frac{L}{kA\Delta p} \mu_o \qquad \text{(A-1)}$$

$$q_{g,core} = q_{inj}(1 - V_{ro,core}) \frac{V_{rt,core}}{V_{rt,inj}} \quad \text{or} \quad q_{o,core} = q_{inj} V_{ro,core} \frac{V_{rt,core}}{V_{rt,inj}} \qquad \text{(A-2)}$$

where $V_{ro}=V_o/(V_g+V_o)$ and $V_{rt}=(V_g+V_o)/V_d$ are relative volumes from a CCE test of the flowing reservoir mixture. Subscript "core" indicates the quantity is evaluated at the pressure in the core, and "inj" indicates the quantity is evaluated at the pressure of the injection pump; core and pump temperatures are assumed equal in Eqs. (A-2).

The entire system pressure is brought to a pressure significantly above the original dewpoint. Gas is circulated until the original permeability is obtained, thereby ensuring the original reservoir mixture is contained throughout the system.

The entire system pressure is lowered by removing gas from the system. This results in a depleted reservoir gas (similar to that obtained from a CVD process). This gas mixture is flowed through the core at minimum FBHP until steady state conditions are reached.

Another depletion of the system is made, and the resulting reservoir gas is flowed through the core at minimum FBHP until steady state conditions are reached.

This process is continued until a reservoir gas with $k_{rg}/k_{ro}=50$ is reached in the core (at minimum FBHP). The system "depletion" pressure of this last data is known from calculations made earlier using Eq. (7).

A plot is made of k_{rg} vs. k_{rg}/k_{ro} using a semilog scale. The relation describing these data are the key to accurate description of well deliverability.

Several steady state points can be measured for a given reservoir gas mixture (if sufficient sample is available). For example, injection rate can be varied to study velocity effects, and to minimize end effects. Flow tests at core pressures greater than minimum BHFP can also be made, e.g. to study the potential effect of IFT on relative permeability (i.e. on the k_{rg} vs. k_{rg}/k_{ro} relationship).

Saturation Measurement for Steady State Test. Although saturations do not need to be measured for each steady state test, we do recommend measuring oil saturation for one test, and preferably the final test. This additional data will help convert the $k_{rg} = f(k_{rg}/k_{ro})$ function to a saturation-dependent relation that can be input to a simulator.

After reaching steady state conditions with the final reservoir gas mixture, flow is stopped. The receiving container is brought to minimum BHFP and the condensed oil is removed temporarily from the system. The remaining gas in the receiving container is compressed to a high pressure, and connected with the core. The compressed gas is used to displace the core at elevated pressure into a second receiving container.

After sufficient displacement at high pressure, flow is stopped, the second receiving container is disconnected from the core and brought to minimum FBHP. Oil volume is measured, where this volume is easily shown to equal the average core oil saturation times pore volume.

Equilibrium Gas Flow (Region 2): $k_{rg} = f(S_o)$. For richer gas condensates, the deliverability loss due to condensate accumulation in Region 2 can also be significant. Here we need to quantify k_{rg} as a function of saturation directly. The procedure recommended for measuring $k_{rg}(S_o)$ uses a CVD type process. At each depletion stage, the *entire* system (core and containers) is brought to equilibrium by removing gas from the system.

At each depletion pressure, equilibrium gas is flowed through the core and pressure drop is measured. k_{rg} is calculated from Eq. (A-1), and saturation is taken from the CVD liquid dropout curve, $S_o=V_{roCVD}(1-S_{wi})$. Measurements are made at decreasing pressures until the maximum liquid dropout occurs, or until oil flow is observed. A sight glass downstream to the core holder is used to detect oil flowing from the core.

Should relative permeabilities be affected by IFT at the higher pressures, this effect is automatically included in the $k_{rg}(S_o)$ measurements.

Fitting Measured Data to Relative Permeability Model. The measured data must be converted into a form that can be used in reservoir simulation, namely k_{rg} and k_{ro} as functions of saturation(s). This conversion process is readily automated by fitting the parameters in a relative permeability model (Corey[17], Chierici,[23] etc.) to the steady-state k_{rg} vs. k_{rg}/k_{ro} data, and the available saturation data from one or more of the steady state tests.

TABLE 1 -- RESERVOIR PROPERTIES USED IN SIMULATIONS

Water Compressibility, psi^{-1}	$2.67 \cdot 10^{-6}$
Rock Compressibility, psi^{-1}	$5.00 \cdot 10^{-6}$
Reservoir Height h, ft	200
Porosity ϕ, %	30
Absolute (horizontal) Permeability k, md	6
Relative Permeability at S_{wi}	0.8
Irreducible Water Saturation S_{wi}, %	25
Reservoir Area, acres	650
Gas Plateau Rate, MMscf/D	40
Minimum BHFP p_{wfmin}, psia	1500

TABLE 2 -- KEY RESERVOIR FLUID PROPERTIES

	Rich Gas A	Lean Gas B
Initial Reservoir Pressure, psia	6500	5500
Initial Reservoir Temperature, ^oF	266	315
Dewpoint Pressure, psia	5900	5400
Maximum CVD Liquid Dropout V_{roCVD}, %	24	2
Initial Solution OGR r_{si}, STB/MMscf	175	45
STO API Gravity, ^oAPI	55	45

Separator conditions. Stage 1 p = 375 psia and T = 108^{o}F, Stage 2 p = 14.7 psia and T = 60^{o}F.

TABLE 3 -- NUMERICAL MODEL GRID DATA.

Grid Description		Grid Dimension, ft
Radial Well Grid		
Radial coordinates. Total radius r_e = 3000 ft. Skin s = 0 in Eq. (3), used in Eqs. (1)-(2).		0.53 0.89 1.39 2.15 3.35 5.20 8.07 12.53 19.46 30.23 36.94 72.9 113.2 175.01 273.01 423.97 658.41 1022.49 1587.88 2465.9
Vertically Fractured Well Grid		
Cartesian coordinates. One quarter of the well simulated. Equal model width and length of 2658.5 ft. Fracture grid k = 10,000 md. Skin s = -4 in Eq. (3), used in Eqs. (1)-(2).	Δx	2*15 7*10 2*50 3*100 100 100 15*137.2
	Δy	3 0.83 1.53 2.81 5.15 9.44 17.31 58.24 106.82 195.92 359.34 659.06 1207.8
Horizontal Well Grid		
Cartesian coordinates. One eighth of the well simulated (1/2 reservoir height and 1/4 area). Equal model width and length of 2658.5; model height of 100 ft. Skin s = -4 in Eq. (3), used in Eqs. (1)-(2).	Δx	100 2*50 8*10 2*100 2*200 300 400 500 458
	Δy	3 0.83 1.53 2.81 5.15 9.44 17.31 58.24 106.82 195.92 359.34 659.06 1207.8
	Δz	3 0.83 1.53 2.81 5.15 9.44 17.31 31.75 28.18

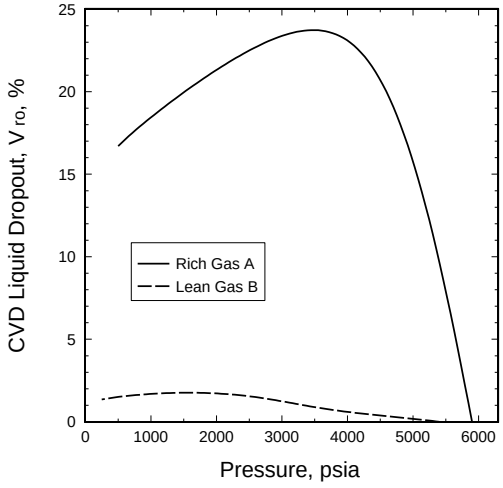

Fig. 1--CVD liquid dropout curves for reservoir fluids Rich Gas A and Lean Gas B.

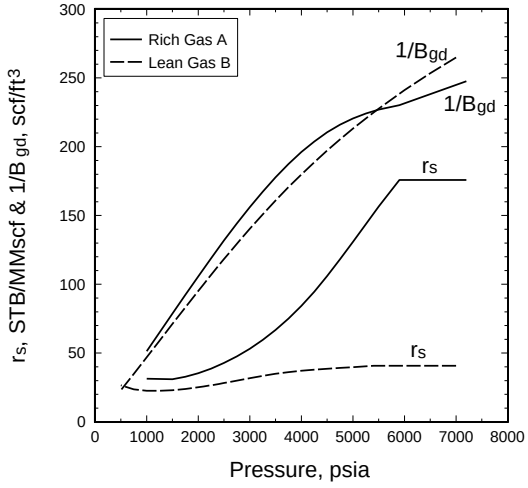

Fig. 2--Black-oil PVT data for Rich Gas A and Lean Gas B. Gas phase properties r_s and B_{gd}.

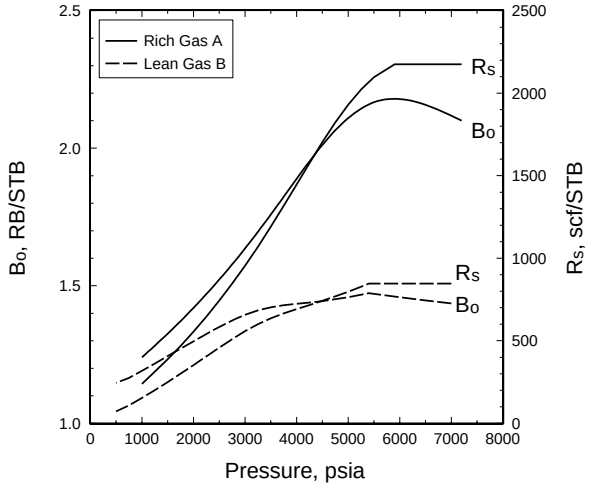

Fig. 3--Black-oil PVT data for Rich Gas A and Lean Gas B. Oil phase properties R_s and B_o.

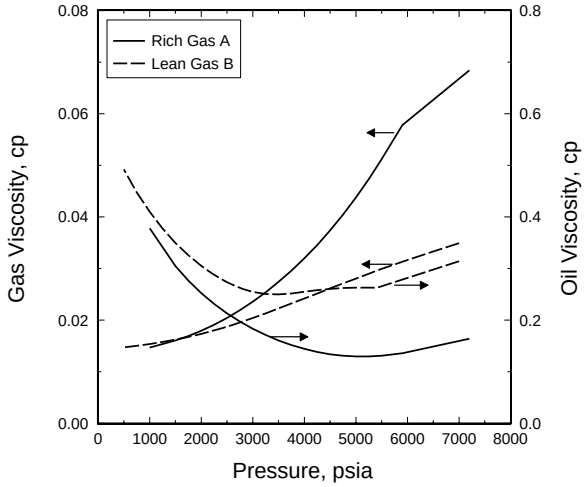

Fig. 4--Black-oil PVT data for Rich Gas A and Lean Gas B. Gas and oil phase viscosities.

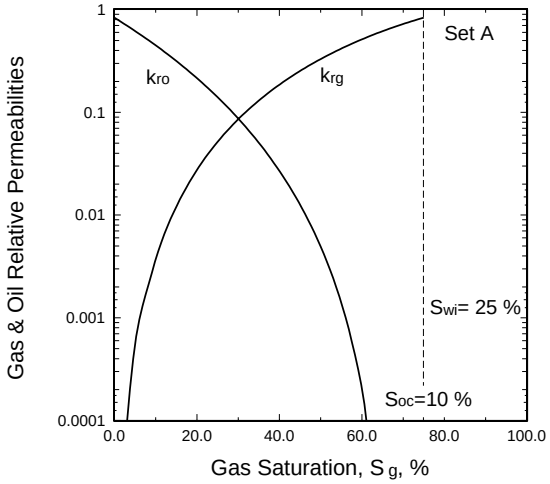

Fig. 5--Set A gas and oil relative permeability curves used in simulations.

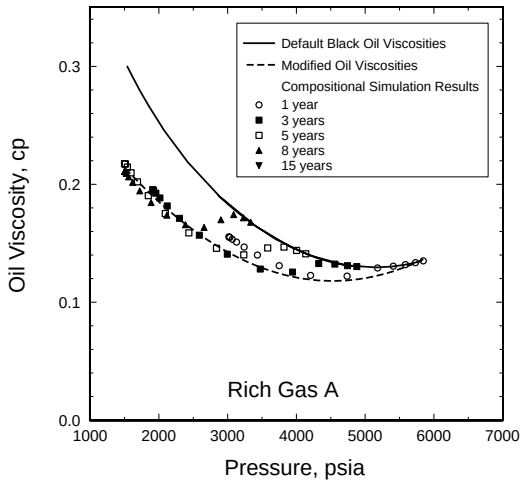

Fig. 6--Changing oil viscosities as a function of pressure for black-oil and compositional PVT models.

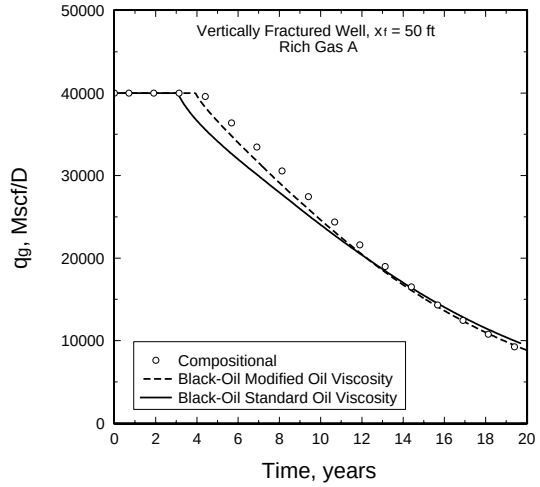

Fig. 7--Effect of oil viscosity on well deliverability for black-oil and compositional simulations of a vertically fractured well with Rich Gas A.

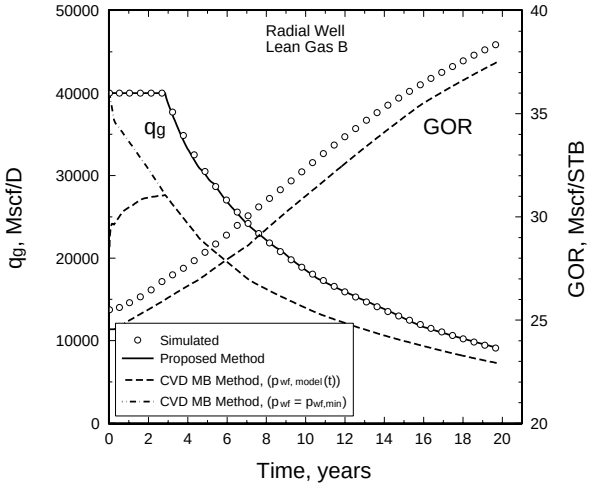

Fig. 8--Well performance for a radial well with Lean Gas B. Comparison of fine-grid simulation with proposed pseudopressure method (and with approximate CVD MB method).

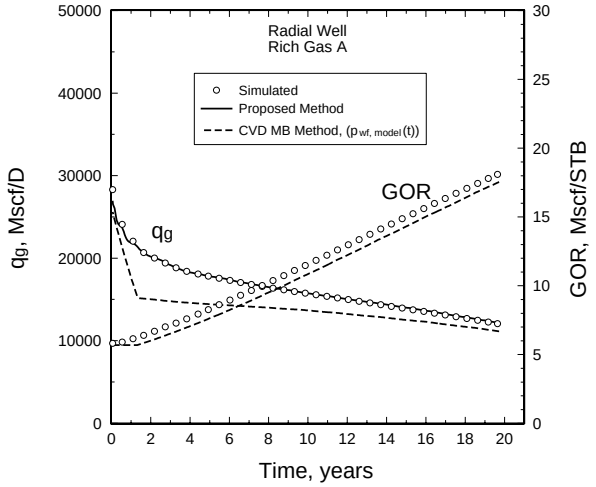

Fig. 9--Well performance for a radial well with Rich Gas A. Comparison of fine-grid simulation with proposed pseudopressure method (and with approximate CVD MB method).

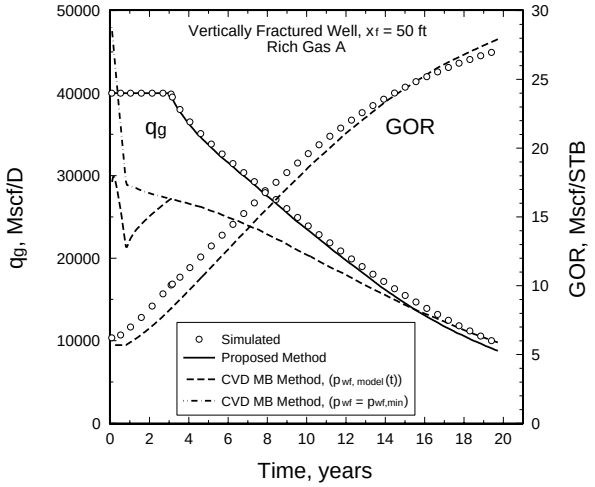

Fig. 10--Well performance for a vertically fractured well with Rich Gas A. Comparison of fine-grid simulation with proposed pseudopressure method (and with approximate CVD MB method).

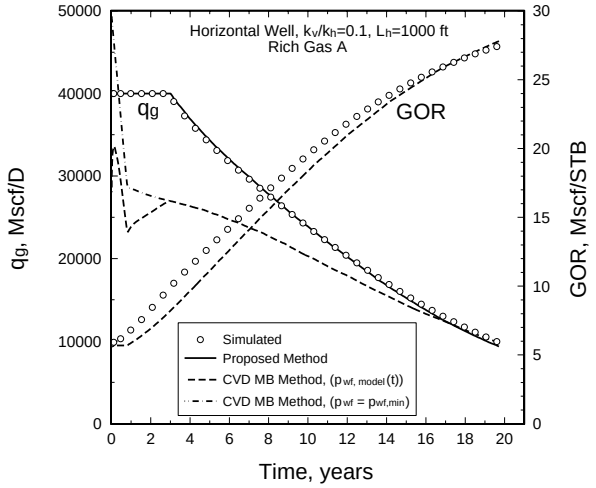

Fig. 11--Well performance for a horizontal well (k_v/k_h=0.1) with Rich Gas A. Comparison of fine-grid simulation with proposed pseudopressure method (and with approximate CVD MB method).

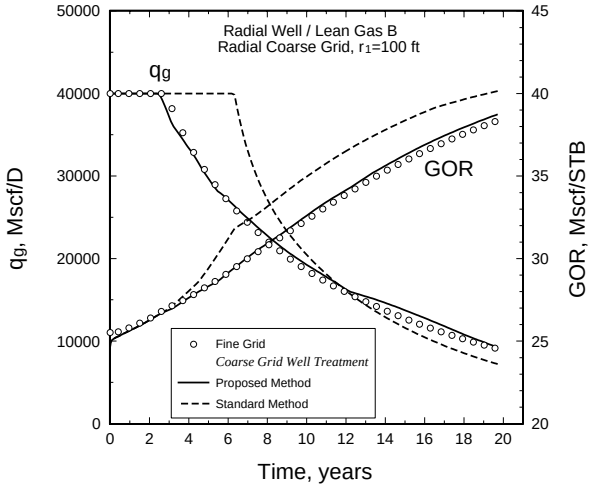

Fig. 12--Well performance for a radial well with Lean Gas B. Comparison of fine-grid simulation with radial coarse-grid simulation using proposed pseudopressure method for calculating well BHFP.

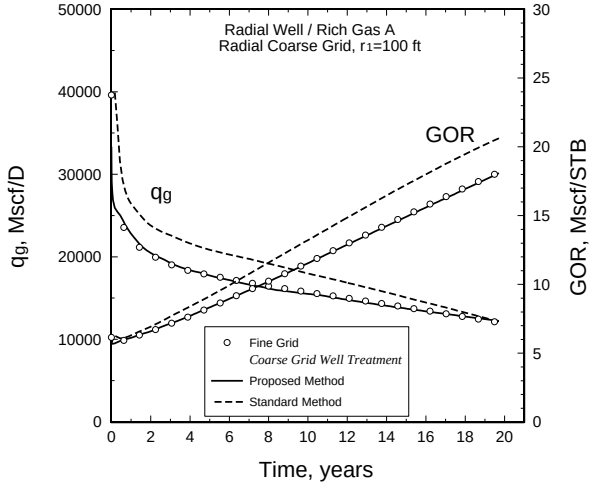

Fig. 13--Well performance for a radial well with Rich Gas A. Comparison of fine-grid simulation with radial coarse-grid simulation using proposed pseudopressure method for calculating well BHFP.

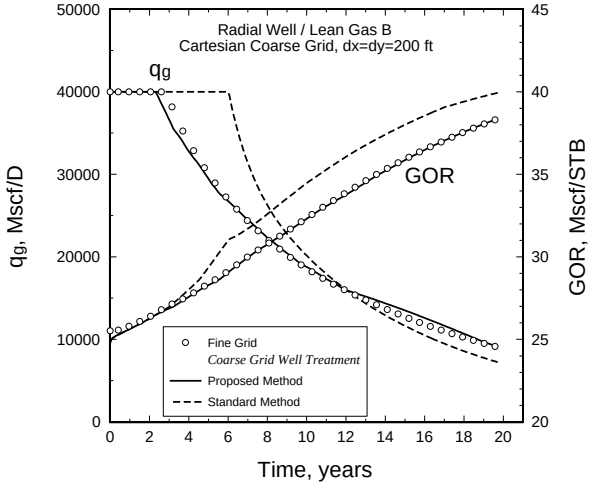

Fig. 14--Well performance for a radial well with Lean Gas B. Comparison of fine-grid simulation with cartesian coarse-grid simulation using proposed pseudopressure method for calculating well BHFP.

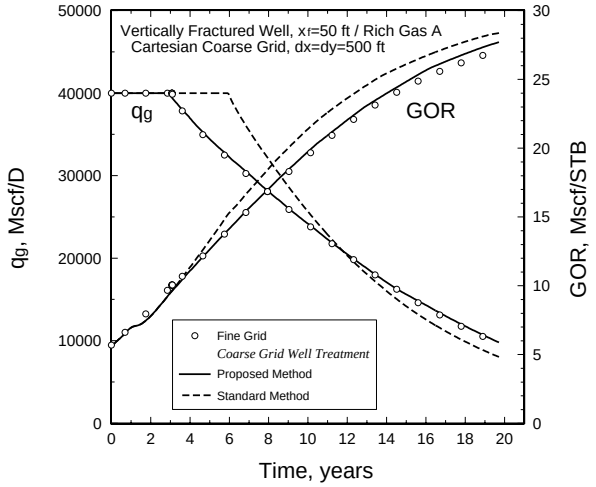

Fig. 15--Well performance for a vertically fractured well with Rich Gas A. Comparison of fine-grid simulation with cartesian coarse-grid simulation using proposed pseudopressure method for calculating well BHFP.

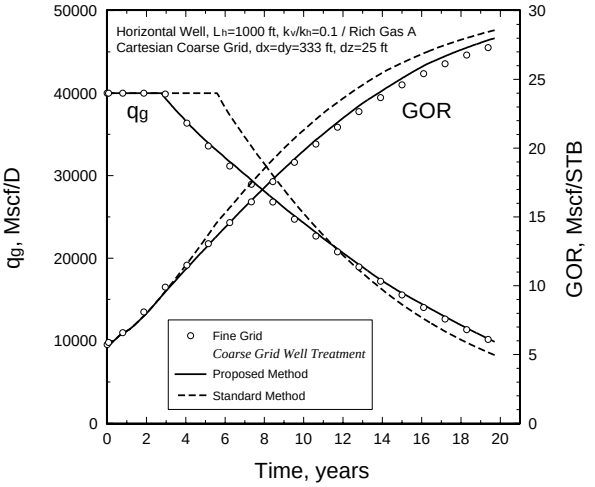

Fig. 16--Well performance for a horizontal well with Rich Gas A. Comparison of fine-grid simulation with coarse-grid simulation using proposed pseudopressure method for calculating well BHFP.

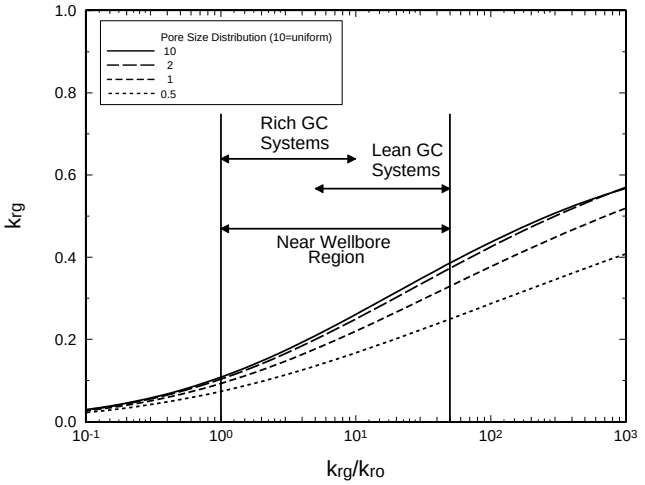

Fig. 17--Generalized k_{rg} vs. k_{rg}/k_{ro} plot based on the Corey relative permeability model. Important range of k_{rg}/k_{ro} in near-wellbore Region 1 is defined.

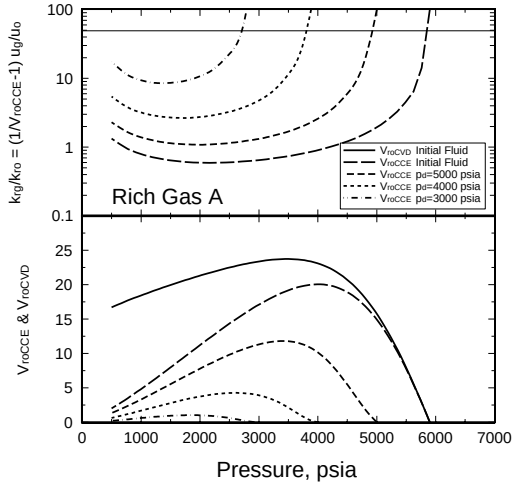

Fig. 18--Diagnostic plots for Rich Gas A showing the variation of k_{rg}/k_{ro} (in Region 1) and CCE oil relative volume as a function of pressure during depletion.

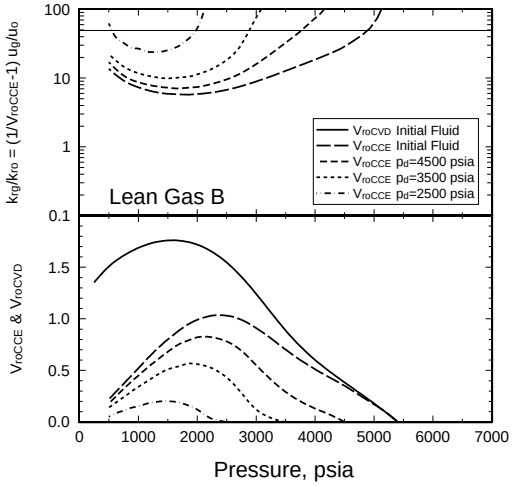

Fig. 19--Diagnostic plots for Lean Gas B showing the variation of k_{rg}/k_{ro} (in Region 1) and CCE oil relative volume as a function of pressure during depletion.

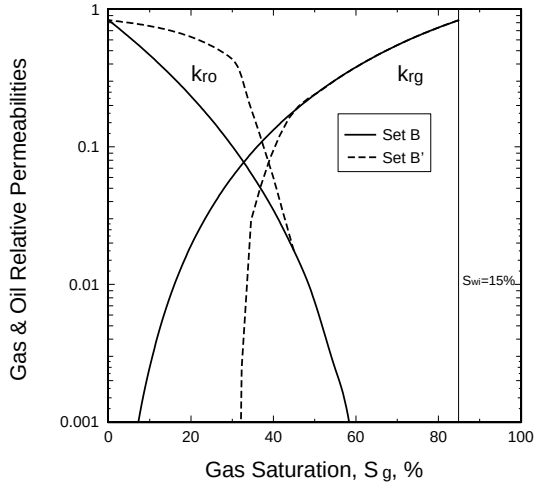

Fig. 20--Two sets of gas/oil relative permeability curves that have identical $k_{rg} = f(k_{rg}/k_{ro})$ relationships.

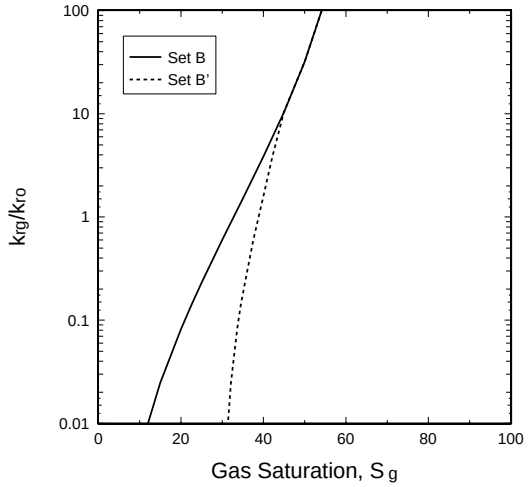

Fig. 21--k_{rg}/k_{ro} vs. S_g for two sets of gas/oil relative permeability curves that have identical $k_{rg} = f(k_{rg}/k_{ro})$ relationships.

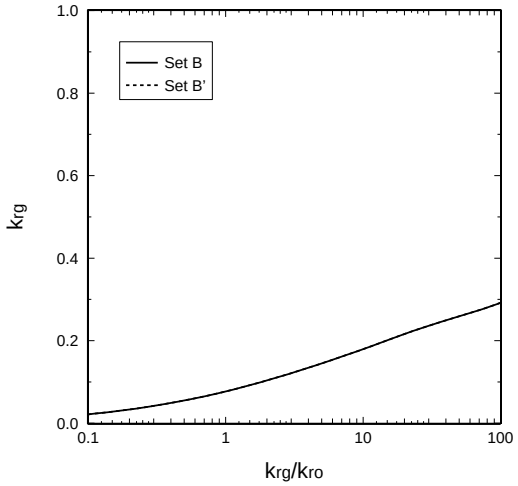

Fig. 22-- Identical $k_{rg} = f(k_{rg}/k_{ro})$ relationship for two completely different sets of $k_{rg}(S_g)$ and $k_{ro}(S_g)$ curves.

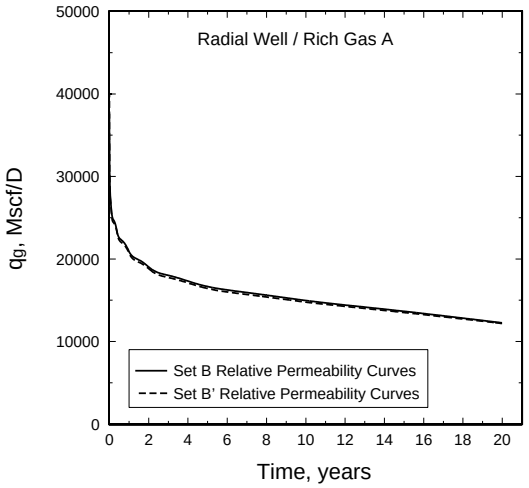

Fig. 23--Rate-time performance of a radial well with Rich Gas A, based on fine-grid simulations using two dramatically different sets of gas/oil relative permeabilities (see Fig. 20).

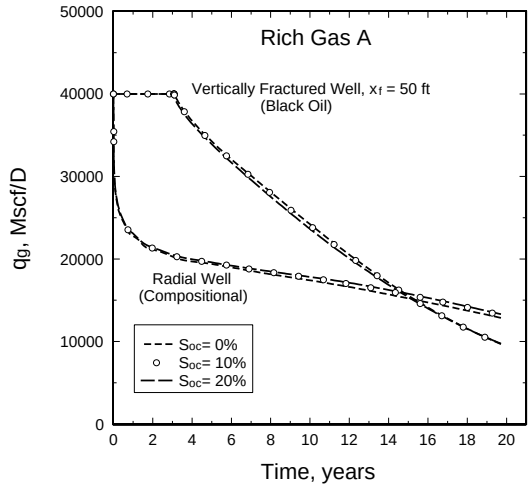

Fig. 24--Rate-time performance of radial and vertically-fractured wells with Rich Gas A, showing the insensitivity of well performance to critical oil saturation S_{oc} (see Fig. 25).

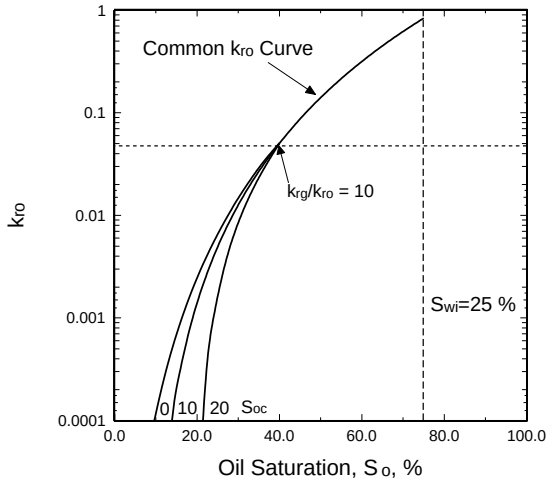

Fig. 25--Variation of k_{ro} curve as a function of oil saturation used in simulations. $k_{ro}(S_o)$ is *unaltered* for $k_{rg}/k_{ro}<10$ ($k_{ro}>0.05$).

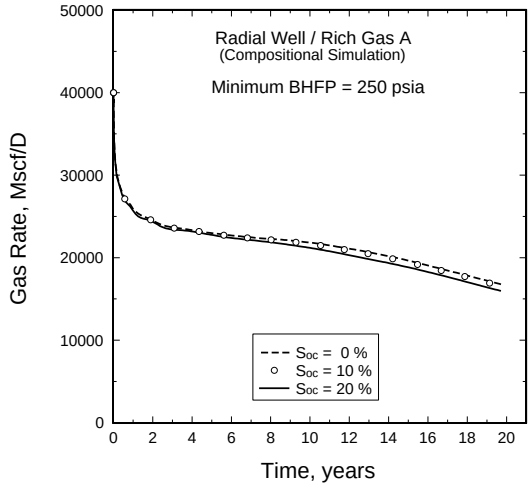

Fig. 26--Rate-time performance of radial well with Rich Gas A, showing the insensitivity of well performance to critical oil saturation S_{oc} (see Fig. 25).

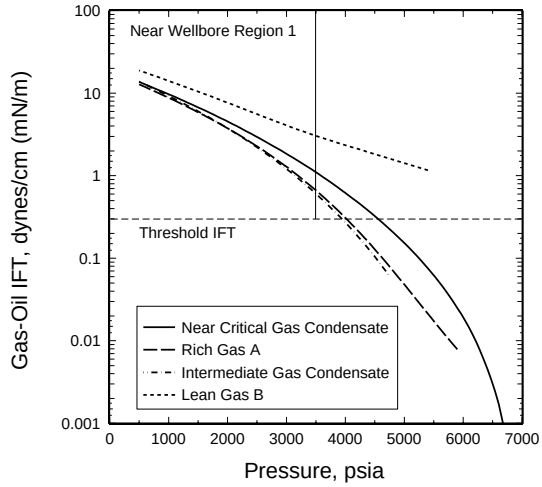

Fig. 27--General pressure dependence of gas-oil IFT for different gas condensate systems.

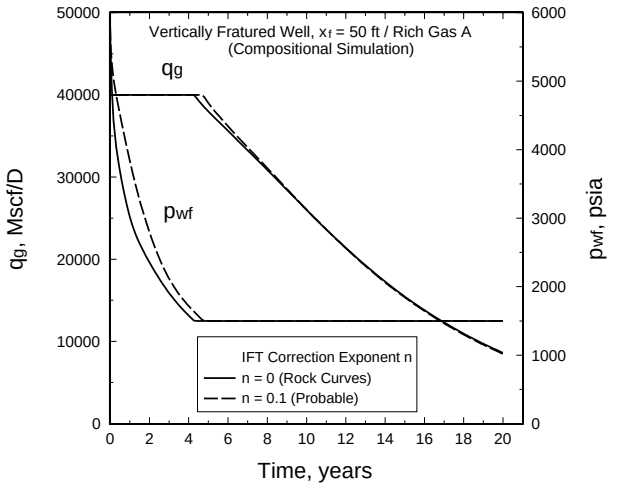

Fig. 28--Well performance of a vertically fractured well with Rich Gas A, based on fine-grid compositional simulations with and without IFT corrections to relative permeability.

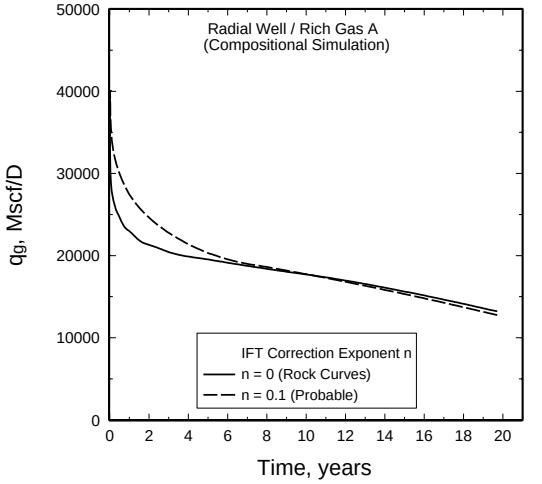

Fig. 29--Well performance of a radial well with Rich Gas A, based on fine-grid compositional simulations with and without IFT corrections to relative permeability.

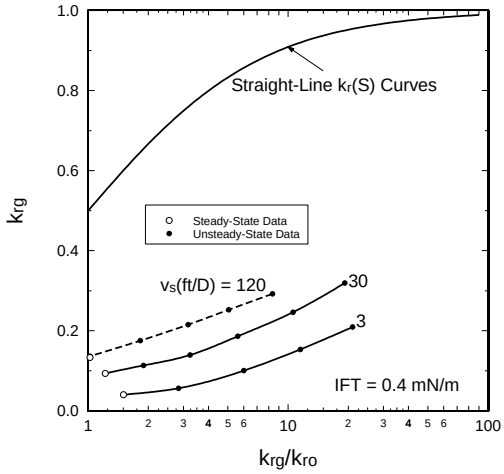

Fig. 30--Velocity effects on $k_{rg} = f(k_{rg}/k_{ro})$ relationship for a Berea sandstone and synthetic gas condensate mixture at IFT of 0.4 mN/m. Data taken from Henderson et al.

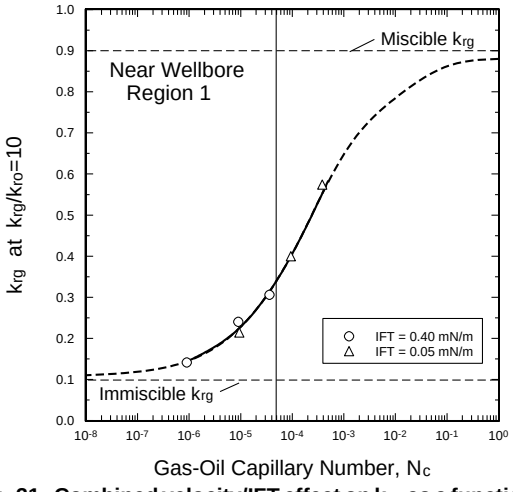

Fig. 31--Combined velocity/IFT effect on k_{rg} as a function of gas/oil capillary number for data presented by Henderson et al.

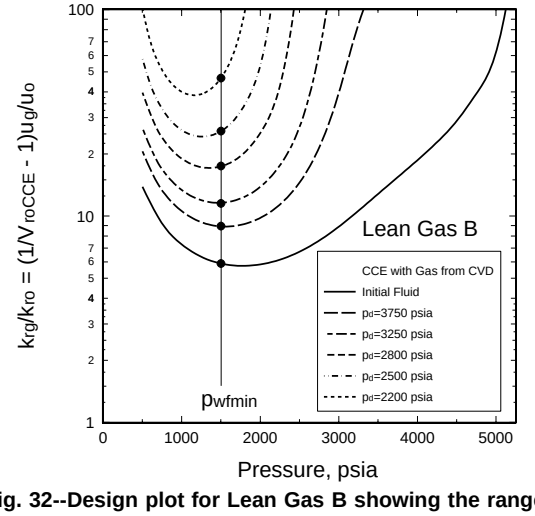

Fig. 32--Design plot for Lean Gas B showing the range of k_{rg}/k_{ro} values that should be measured experimentally for accurate modeling of well deliverability.